NUMERICAL MODELLING OF PIPELINE AND RISER SEABED INTERACTION

by

© Xiaoyu Dong

A Thesis submitted to the

School of Graduate Studies

in partial fulfillment of the requirements for the degree of

Doctor of Philosophy

Faculty of Engineering and Applied Science

Memorial University of Newfoundland

May 2020

St. John's Newfoundland Canada

ABSTRACT

Subsea risers and pipelines are widely used in offshore industries especially for the production of oil and gas resources. Due to complex subsea environment, a variety of risks are challenging the operation or serviceability life of subsea pipelines and risers. Subsea riser and pipeline-seabed interaction are proven to have significant effect on its performance. This interaction can be modeled by two main approaches, beam-spring, and continuum approach. Beam-spring model provided the most efficient and economical way to estimate the response of soil. While with more explorations in fields, more sophisticated and accurate models are required and thus continuum models are developed to give more details on the soil behavior around the pipe.

Two challenging topics in pipeline and riser seabed interaction were selected,

1- the effect of riser-seabed interaction on fatigue life in touchdown zone,

2- the effect of trenching/backfilling on lateral response of buried pipelines.

The first one was modelled by beam-spring approach and the second one investigated by continuum approach. The abstracts of the conducted research works are independently discussed below:

A.1. Part I Pipeline-Seabed Interaction

Subsea pipelines are often protected by burying in the subsea trenches to mitigate the effects of the functional and environmental loads. Depending on the trenching methodology (pre-lay or post-lay trenching), trenching and laying the pipeline may take place at the same time or in a different period of time. Using the excavated material for backfilling of the pipeline is a common practice and a cost-effective solution. Depending on trenching methodology, construction strategy, and environmental loads, the backfilling material may experience different degrees of remolding resulting in a softer material with a range of shear strengths. The difference between the stiffness of the backfill and native material affects the soil failure

mechanisms under the lateral pipeline displacement. The relative displacement between the pipeline and the surrounding soil that may occur due to the ground movements, faults, slope instabilities, ice gouging, etc. exerts forces on the pipeline. The amplitude of these forces on the pipeline depends on several parameters, including the submerged weight of the mobilized backfilling and native soil, the horizontal component of shearing resistance offered by interacted soil, and the suction behind the pipe. And the load-displacement curve becomes important in terms of the design of the embedded pipelines. Under different circumstances, trenched pipelines might be displaced at different velocities (could be from millimeters per year to very high), resulting in different drainage conditions (including undrained condition, partially drained condition, and drained condition). Partially drainage condition in pipe-soil interaction has been a very challenging topic since it requires a coupled analysis with the pore fluid pressure to explore the induced excess pore pressure which affects the responses of the pipe, internal soil deformation, and also the failure mechanism in the soil. However, most of the published works only explored the undrained condition of soil.

These parameters in turn depend on several parameters such as the properties of the backfill and the native soil, trench geometry, burial depth and confining pressure, pipeline roughness, pipeline size, loading rate (drained/undrained), soil stress history, the backfill extent of consolidation, and the over-consolidation ratio (OCR) of native soil . In this thesis, a coupled large deformation finite element (LDFE) model using re-meshing and interpolation technique with small strain (RITSS) was developed to give prediction of the pipeline force-displacement response together with the computation of the induced excess pore pressure within large deformations. This coupled LDFE model was proven to have advantages in modelling pipe-soil interaction under drained and partially drained conditions using the ABAQUS built-in coupled pore fluid pressure method, which cannot work with the popular existing LDFE

method such as Coupled Eulerian Lagrangian (CEL) method. And the LDFE model was proved to be a strong tool for comprehensive investigation of the progressive failure mechanisms around the pipeline considering the varying pipeline-backfill-trench interaction effects.

A.2. Part II Riser-Seabed Interaction

Steel catenary risers (SCR) are popular amongst the riser families because of their lower cost and technical advantages such as applicability in a wider range of sizes and water depths. The survey results obtained by remote operating vehicles (ROV) have proved the complex non-linear seabed response to riser fluctuations in the touchdown zone (TDZ), where SCR penetrates into the seabed and cyclically creates trenches often with several diameters deep. The oscillatory motions of SCR in the touchdown zone result in a complex riser interaction mechanism with surrounding media including fluid and soil. Some of the influential parameters contributing to these non-linear hysteretic interactions are: soil stiffness degradation under cyclic loads and riser penetration into the seabed, mobilization of suction force within uplift motions of riser, trench base softening and damping, erosive mechanism by water velocity field around the SCR in TDZ and consequent variation of flow pattern of displaced water, the riser dynamics influenced by internal multi-phase flow regimes and also vessel motions (velocity and frequencies), and vortex-induced vibration (VIV).

The existing non-linear hysteretic riser-seabed interaction models have been verified in wave-induced fatigue assessment. However, the effect of non-linear seabed interaction on the riser fatigue under riser vibrations has never been examined. In this work, the performance of the non-linear hysteretic models was investigated in slug-induced fatigue damages in touchdown zone which is a key contributor to fatigue damage. For this purpose, first the nodal and global performance of the most popular models was comprehensively examined, and its pros and cons were thus explored. Then an advanced and novel model was developed to simulate the riser

slugging and slug-induced fatigue, which has never been done in the past due to extreme complexity. This model was incorporated into slug-induced fatigue analysis and it was indicated that the model was applicable to these type of analysis with acceptable level of accuracies. The research work showed that the slug-induced vibrations can combine with the wave-induced oscillations and create critical case scenarios. Therefore, it is critical to consider the combined effects of slugging and wave in riser fatigue analysis and fill the knowledge gap.

STATEMENT OF AUTHORSHIP

Among the outcomes of this work, I as the main author and Dr. Hodjat Shiri as my supervisor, are the authors of the published papers and submitted manuscripts shown as below:

- Dong, X., and Shiri, H., 2020. A coupled LDFE model for analysis on large lateral displacement of trenched pipeline. Submitted as journal manuscript.
- Dong, X., and Shiri, H., 2019. Performance of non-linear seabed interaction models for steel catenary risers, part II: global response. Applied Ocean Research 82, 158-174.
- Dong, X., and Shiri, H., 2019. The influence of nonlinear hysteretic seabed interaction on slug-induced stress oscillations in steel catenary risers. Applied Ocean Research 82, 175-190.
- Dong, X., and Shiri, H., 2018. Performance of non-linear seabed interaction models for steel catenary risers, part I: Nodal response. Ocean Engineering 154, 153-166.
- Dong, X., and Shiri, H., 2019. The influence of slug characteristics on oscillation of steel catenary risers in the non-linear hysteretic seabed. GeoSt.John's2019, St. John's, NL, Canada, September 2019.
- Dong, X., and Shiri, H., 2018. Nonlinear hysteretic seabed response to vibrations of slugging steel catenary risers. GeoEdmonton 2018， Edmonton, Alberta, Canada, September 2018.

Also, I went for visiting study in Center for Offshore Foundation Systems in University of Western Australia (UWA) with financial support via Mitacs Globalink program from Jul 2018 to Apr 2019. During the visiting, I weekly proposed and emailed summary reports to my home supervisor and host supervisor to get them update well on time, which clearly presented the recent week progress by clarifying the completed tasks, problems to be solved, and possible solutions to be tried. Significant help on theoretical, numerical, and experimental knowledge

were provided both by my home and host supervisors, Dr. Hodjat Shiri at Memorial University and Prof. Mark Randolph in UWA through weekly meetings and discussions. Besides, with Dr. Randolph's introduction, I had the chance to work closely with his post-doc student, Dr. Wangcheng Zhang, who gave me excellent instructions regarding the application of remeshing and interpolation technique with small strain (RITSS) in ABAQUS. We altogether used the coupled pore pressure method to develop the coupled large displacement finite element (LDFE) model of embedded pipeline in uniform seabed, which enabled us to explore the induced excess pore pressure in soil and the soil resistances with pipe laterally pulled at different velocities (which induced different drainage conditions). Besides, we developed an LDFE model for the lateral displacement of a trenched pipeline with a modified Tresca material considering the soil softening. The outcome of this collaboration is:

- Dong, X., Zhang, W., Shiri, H., and Randolph, M.F., 2020. Large Deformation Coupled Analysis of Embedded Pipeline – Soil Lateral Interaction. Submitted as journal manuscript.
- Dong, X., Shiri, H., Zhang, W., and Randolph, M.F., 2020. A 2D RITSS method for Lateral Large Deformation Analysis of trenched pipeline. Submitted as journal manuscript.
- Dong, X., Shiri, H., Zhang, W., and Randolph, M.F., 2020. Large deformation analysis of lateral pipeline-backfill-trench interaction by remeshing and interpolation technique with small strain model (RITSS). 4th International Symposium on Frontiers in Offshore Geotechnics, Austin, Texas, August 2020.

ACKNOWLEDGMENT

First, I would like to thank my supervisor, Dr. Hodjat Shiri, who provided me excellent opportunities to join his research team and took part in this challenging research topic. I am grateful for his unconditional support, keen supervision, and indispensable guide during the whole period of the research. And special thanks to Prof. Mark Randolph and Dr. Wangcheng Zhang for their explicit instructions during my visiting study in Center for Offshore Foundation Systems (COFS) in the University of Western Australia. Also, I would like to sincerely acknowledge Dr. Rocco Lagioia and Dr. Andrea Panteghini for their valuable help on the user-coded Modified Cam-Clay model.

I gratefully acknowledge the financial support of the Wood Group PLC, which established a Research Chair program in Arctic and Harsh Environment Engineering at Memorial University of Newfoundland, the "Natural Science and Engineering Research Council of Canada (NSERC)" through "CRD" program, and the "Newfoundland Research and Development Corporation (RDC) (now TCII)" through "Ignite" and "Collaborative Research and Developments Grants (CRD)", and Mitacs through "Globalink" program for funding this project. Special thanks are extended to School of Graduate Studies (SGS), and Faculty of Engineering and Applied Science at Memorial University for providing financial supports and excellent resources to conduct this research project.

Last but not least, many thanks to my parents (Zhuxue Ma and Baoke Dong), who warmly encouraged me during my studies. This work could never be completed without their unconditional love and support.

Contents

List of Figures

List of Tables

List of Abbreviations and Symbols

Abbreviations

CEL	Coupled Eulerian-Lagrangian
DISP	User-defined boundary condition subroutine in ABAQUS
DOF	Degree of Freedom
DLOAD	Distributed Load subroutine in ABAQUS
MC	Mohr-Coulomb
MCC	Modified Cam-Clay
MPC	Multi-points Constraints subroutine in ABAQUS
LDFE	Large Deformation Finite Element
OCR	Over-Consolidation Ratio
RITSS	Re-meshing and Interpolation technique with Small Strain
SCR	Steel Catenary Riser
TDP	Touchdown Point
TDZ	Touchdown Zone
UEL	User-defined element subroutine in ABAQUS

English Symbols

A^i	Array of the derivatives
B_p	Hardening parameter
C_A	Added mass coefficient
C_D	Drag coefficient
C_I	Inertia coefficient

c_v	Coefficient of vertical consolidation
D	Pipe diameter
D_o	Outer diameter
E	Young's modulus of the soil skeleton
E_s	Compression modulus of soil
f_{slug}	Slug frequency
f_{suc}	Suction ratio
H	Burial depth
H_{IP}	Hyperbolic factor
h_{soil}	Height of the soil body
Δh	Characteristic element size near the disturbance
I	Second moment of area
G	Elastic shear modulus
k	Soil permeability
K_0	Coefficient of earth pressure at rest
K_{max}	Normalized maximum stiffness parameter
L_{slug}	Slug length
m	Inverse slope of the S-N curve
M	Slope of the critical state line in $p-q$ space
m_s	In service submerged weight
m_v	Coefficient of volume compressibility
n	Flow index
N	Number of cycles until failure

N_c	Soil bearing factor
n_i	Number of stress cycles in stress block i over the design life
N_i	Number of stress cycles to failure for the constant stress range i
p	Mean pressure
p'	Mean effective stress
p_0	Overburden pressure
p_c	Yield stress in isotropic compression controlling the size of the yield curve
$P_u(z)$	Ultimate penetration resistance
q	Equivalent von Mises stress
s	Total consolidation settlement at the soil surface
s_t	Consolidation settlement
s_u	Undrained shear strength
s_{u0}	Mudline shear strength
s_{u_b}	Average backfill soil undrained shear strength
s_{u_s}	Average seabed soil undrained shear strength
T_v	Time factor
U_t	Degree of consolidation
V	Normalized velocity
v	Moving velocity of the pipe
v_{ref}	Reference velocity
v_{slug}	Flow velocity
W	Trench width

Greek Symbols

γ	Effective unit soil weight
$\dot{\gamma}$	Strain rate
γ^e	Elastic shear strain
γ^p	Accumulated plastic shear strain
γ_r^p	Value of γ^p to reduce the shear strength from peak to residual
$\dot{\gamma}_{ref}$	Reference strain rate
γ_w	Specific weight of the permeating fluid
δ	Pipe displacement
δ^p	Accumulated plastic shear displacement ($\delta^p = \gamma^p s$)
δ_r^p	Residual plastic shear displacement
ε_v^p	Plastic volumetric strain
$d\varepsilon_{q\theta}^p$	Total plastic deviatoric strain increment
ζ	Non-dimensional penetration
η	Dimensionless viscosity coefficient
λ_{suc}	Suction decay parameter
λ_{rep}	Repenetration parameter
ν	Poisson's ratio
ξ	Constitutive parameter used for coupling the hardening associated to plastic deviatoric strain
ρ	Shear strength gradient
ρ_s	Steel density
ρ_{slug}	Slug density

ρ_{bubble}	Bubble density
σ	Stress tensor
$\Delta\sigma_f$	Factored stress variation range in MPa
τ_p	Peak shear strength
τ_r	Residual shear strength

PART I: LATEARL PIPELINE-BACKFILL-TRENCH INTERACTION

Chapter 1

Introduction

1.1. Background

Since the thesis is paper-based, each chapter has its own introduction. However, a summary of the introductions from Chapter 3 to Chapter 5 was brought as Chapter 1.

Lateral interaction between trenched pipeline and seabed is among the most challenging structure-soil interaction problems in offshore geotechnics. It is very important regarding the estimation of soil resistance which can be significantly dependent on the trench geometry, soil stiffness and interaction rates. Subsea pipelines are often protected by burying inside the subsea trenches to mitigate the effects of the functional and environmental loads. Using the excavated material for backfilling of the pipeline is a common practice and a cost-effective solution. Depending on trenching methodology, construction strategy, and environmental loads, the backfilling material may experience different degrees of remolding resulting in a softer material with a range of shear strengths. The difference between the stiffness of the backfill and native material affects the soil failure mechanisms under the lateral pipeline displacement. The relative displacement between the pipeline and the surrounding soil that may occur due to the ground movements, faults, slope instabilities, ice gouging, etc. exerts forces on the pipeline. The amplitude of these forces and the force-displacement response of the pipeline depend on several parameters including the submerged weight of the mobilized backfilling and native soil, the horizontal component of shearing resistance offered by interacted soil, and the suction behind the pipe. These parameters in turn depend on several parameters such as the properties of the backfill and the native soil, trench geometry, burial depth and confining pressure, pipeline roughness, pipeline size, loading rate (drained/undrained), soil stress history, the backfill extent of consolidation, and the over-consolidation ratio (OCR) of native soil.

1.2. Motivation

As shown in Figure 1-1, subsea pipeline are usually embedded in the trench backfilled with pre-excavated materials. And those trenched pipelines may undergo large lateral displacements due to the environmental, operational and accidental loads. The displacement could be caused by ground movement (see Figure 1-1), ice gouging, landslide, drag anchors etc.

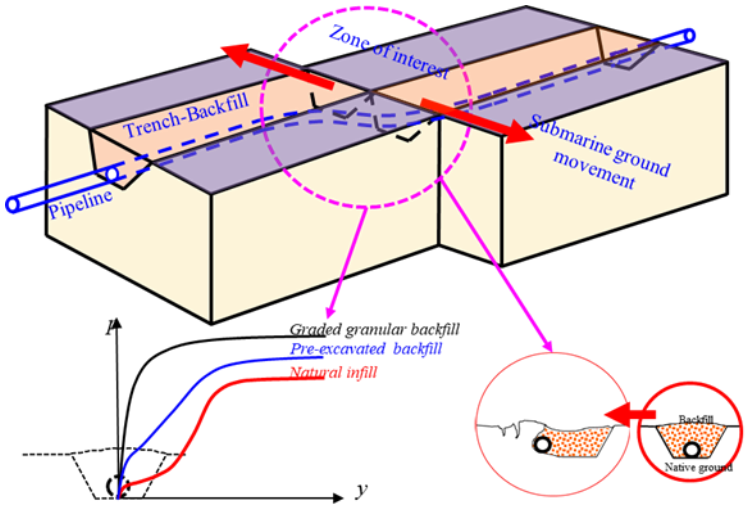

Figure 1-1. The trenched pipeline to submarine ground movement (Kianian and Shiri, 2019)

The lateral soil resistance against largely displaced pipe is proved to be significantly affected by the difference between the stiffness of the backfill soil and native ground soil, and this is getting back to the interaction between the pipeline-backfill and trench (Paulin 1998, C-CORE report 2003). There are a number of theoretical and experimental models availabe to predict the ultimate lateral resistance or force-displacement (p-y) curves of moving structures (Edgers and Karlsrud 1982; Rizkalla and Mclntyre 1991; Merifield 2001; Klar and Randolph 2008), while very few are specific to pipeline-soil interactions (Poorooshasb et al. 1994; Paulin 1998; Oliveira et al. 2010). Large discrepancies are observed in the recommendations provided by different design codes and the empirical equations proposed in some previous studies for

calculation of the ultimate lateral resistance and the p-y response (Paulin 1998, ALA 2001, PRCI 2009, Rajah et al. 2014, Pike 2016). The simplified assumptions, which ignore the effect of pipeline-backfill-trench interaction, and inherent differences in the frameworks of the studies conducted, are the main sources of the observed discrepancies.

Besides, the models proposed for prediction of lateral pipeline response in fine-grained material use the undrained shear strength as the key soil strength parameter, which may not be appropriate for slower loading rates where consolidation may occur (Hsu, 1993; Paulin, 1998; C-CORE report, 2003).

It becomes challenging to make assumptions and to identify the range of assumptions. In order to make more accurate prediction on the pipeline force-displacement response within large deformations, a comprehensive investigation is needed to explore the progressive failure mechanisms around the pipeline considering the penetration rates (particularly in drained and partially drained conditions) and the varying pipeline-backfill-trench interaction effects.

Part I aims at developing strong tools for comprehensively analyzing the consolidation effects and trench effects for laterally displaced pipelines.

1.3. Organization of the Thesis

This thesis is a paper-based thesis which is divided into two parts.

The part I includes chapters from chapter 1 to chapter 6 (with appendix A). Chapter 1 is the introduction which discusses the topic of the Part I: Pipeline-seabed interaction. Chapter 2 includes the literature review which focus on the pipeline-seabed interaction problem and the previous studies in this area and the related implications for buried pipeline and the seabed soil. Recent discoveries in this area and different methods of modeling pipeline-seabed interaction have been reviewed. Chapter 3 is presented with a submitted journal manuscript, which incorporated consolidation effects into large deformation finite element analysis for laterally displaced pipeline embedded in soil. An advanced coupled Large Deformation Finite Element

(LDFE) model (coupling of porous medium and the fluids in the medium) was developed and verified against published centrifuge test results. A comprehensive parametric study was conducted to show the influence of interaction rates and consolidation effects on the failure mechanisms of soil and responses of embedded pipeline during its large lateral displacement. Chapter 4 is presented with a submitted journal manuscript, which discussed the LDFE model developed for pipeline-backfill-trench interaction. The model is capable of producing a clear view of failure mechanisms of the soil during the large lateral displacement of the trenched pipeline. Re-meshing and Interpolation Technique with Small-Strain (RITSS) analysis was conducted in the developed LDFE model to overcome the mesh distortion problem (which is quite common in the conventional modelling with Lagrangian mesh). And one of the most popular method for large deformation problem, coupled Eulerian-Lagrangian method (CEL) was adopted to produce results and serve as comparisons. The failure mechanisms in soil for trenched pipe with deep burial and shallow burial were examined respectively using the developed LDFE model and CEL model. And the comprehensive pipeline-backfill-trench interaction was discussed. Chapter 5 is presented with a manuscript submitted to journal, which explored the consolidation effects and trench effects at the same time. The model is capable of producing a clear view of failure mechanisms and induced excess pore pressure in the soil during the large lateral displacement of the trenched pipeline. This is the first-time excess pore pressure being analyzed together with the responses of trenched pipeline. The failure mechanisms in soil for trenched pipe with deep burial and shallow burial were examined respectively using the developed coupled LDFE model. Chapter 6 summarizes the key conclusions obtained in Part I and sheds lights on the future studies, followed by Appendix A, which is a summary of the Chapter 3 and Chapter 4 and accepted in 4th International Symposium on Frontiers in Offshore Geotechnics (ISFOG) 2020.

The part II includes chapters from Chapter 7 to Chapter 12 (with Appendix B and Appendix C). Chapter 7 is the introduction which discusses the topic of the Part II: Riser-seabed interaction. Chapter 8 includes the literature review which explored the riser-seabed interaction problem and the previous related research works. Chapter 9 is presented with a journal paper which was published in Ocean Engineering. The nodal performance of a popular non-linear hysteretic riser-seabed interaction model has been comprehensively studied through developing a global numerical riser model in ABAQUS and a user-defined subroutine (UEL). The studied non-linear seabed model showed a dominantly strong nodal performance. However, nodal response violations were frequently observed in proximity of trench bottom towards the vessel, which is the most fatigue prone section of SCR in the touchdown zone. Chapter 10 is presented with a journal paper which was published in Applied Ocean Research. This is a sister journal paper to chapter 9 which continued the comprehensive study on the popular non-linear seabed model. The results showed a strong global performance of the non-linear seabed model in the touchdown area. However, over-estimations were observed due to incapability of the model in explicit modelling the trench and updating the lowering elevation of the mudline inside the trench. Variation of the model parameters showed significant impact on migration of touchdown point and the peak responses as well. It was also noticed that the model response is violated, when extreme values of re-penetration offset parameter is used for automative trench creation. Chapter 11 is presented with a journal paper which was published in Applied Ocean Research. It investigated the influence of nonlinear hysteretic riser-seabed interaction on slug-induced stress oscillations in the touchdown zone of steel catenary risers (SCRs) that had never been studied before. An advanced numerical model was developed in ABAQUS using the distributed loads and moving tie constraints to model the moving slugs. A user-defined element (UEL) and a subroutine called DISP were coded to model the nonlinear hysteretic riser-seabed interaction and the complex vessel excitations under the environmental

loads. It was observed that the cyclic soil stiffness degradation might have a significant impact on the slug-induced cross-sectional stress oscillations and consequently the fatigue. Chapter 12 briefly collected the key conclusions obtained in Part II and recommended potential aspects for further explorations and future studies, followed by Appendix B and Appendix C, which summarized and compensated details of the Chapter 11 and were published in GeoEdmonton 2018 and GeoSt.John's 2019.

1.4. Key objectives

The main research objectives of this research work are given below:

- Part I: Pipeline-Seabed Interaction
    - To explore the consolidation effects on lateral p-y response of buried pipe with different interaction rates (i.e. resulting in different drainage conditions).
    - To develop a strong numerical tool which is capable of conducting coupled analysis to explicitly show the induced excess pore pressure and failure mechanisms in soil.
    - To examine the influences of several key parameters on lateral pipeline response are investigated including backfilling properties, trench geometry, and burial depth.
    - To simulate the consolidation effects in pipeline-backfill-trench interaction by developing a model to perform coupled analysis of trenched pipeline.
- Part II: Riser-Seabed Interaction
    - Develop a global numerical riser model in ABAQUS and a user defined subroutine (UEL) to investigate:
        - The nodal performance of the R-Q model, hysteretic non-linear force-penetration curves including cyclic soil stiffness degradation.
        - The global performance of the R-Q model, the resultant longitudinal and transverse force, moment and stress profiles, fatigue damage.
        - The R-Q model capability in simulation of trench formation.

- Develop an advanced model to:
    - simulate the slug-induced vibration and resultant fatigue damage in the presence of non-linear hysteretic seabed.
    - Investigate the combined effect of wave and slug-induced vibrations and fatigue and trenching process.
    - Examine the performance of R-Q model under slug-induced vibrations.

1.5. Thesis outcomes

The research work provided new reliable/useful information and data on the subsea pipeline-seabed and riser-seabed interaction. It is expected that such a research investigation offers effective tips/guidelines to deal with pipeline-seabed interaction caused by pipe large lateral deformation and riser-seabed interaction caused by riser vibrations.

The outputs of my research work have been published in /submitted to ISI journals (with a high impact factor) and presented in Canadian conferences, as listed below:

- Pipeline-seabed interaction
    - Dong, X., and Shiri, H., 2020. A coupled LDFE model for analysis on large lateral displacement of trenched pipeline. Submitted as journal manuscript.
    - Dong, X., Zhang, W., Shiri, H., and Randolph, M.F., 2020. Large Deformation Coupled Analysis of Embedded Pipeline – Soil Lateral Interaction. Submitted as journal manuscript.
    - Dong, X., Shiri, H., Zhang, W., and Randolph, M.F., 2020. A 2D RITSS method for Lateral Large Deformation Analysis of trenched pipeline. Submitted as journal manuscript.
    - Dong, X., Shiri, H., Zhang, W., and Randolph, M.F., 2020. Large deformation analysis of lateral pipeline-backfill-trench interaction by remeshing and

interpolation technique with small strain model (RITSS). 4th International Symposium on Frontiers in Offshore Geotechnics, Austin, Texas, August 2020.

- Riser-seabed interaction
    - Dong, X., and Shiri, H., 2019. Performance of non-linear seabed interaction models for steel catenary risers, part II: global response. Applied Ocean Research 82, 158-174.
    - Dong, X., and Shiri, H., 2019. The influence of nonlinear hysteretic seabed interaction on slug-induced stress oscillations in steel catenary risers. Applied Ocean Research 82, 175-190.
    - Dong, X., and Shiri, H., 2018. Performance of non-linear seabed interaction models for steel catenary risers, part I: Nodal response. Ocean Engineering 154, 153-166.
    - Dong, X., and Shiri, H., 2019. The influence of slug characteristics on oscillation of steel catenary risers in the non-linear hysteretic seabed. GeoSt.John's2019, St. John's, NL, Canada, September 2019.
    - Dong, X., and Shiri, H., 2018. Nonlinear hysteretic seabed response to vibrations of slugging steel catenary risers. GeoEdmonton 2018, Edmonton, Alberta, Canada, September 2018.
- Other contributions
    - Akpan, E., Dong, X., Moharrami, M.J., and Shiri, H., 2019. Analytical Modeling of Well-Conductor Seabed Interaction in Complex Layered Soil in Newfoundland Offshore. GeoSt.John's2019, St. John's, NL, Canada, September 2019. (additional contribution to the drilling riser seabed interaction.)
    - Akpan, E., Dong, X., Moharrami, M.J., and Shiri, H., 2019. Analytical Assessment of the Drilling Risers Stability in Newfoundland Deep Offshore. GeoSt.John's2019,

St. John's, NL, Canada, September 2019. (additional contribution to the drilling riser seabed interaction.)

References

ALA. Guidelines for the design of buried steel pipe. In ASCE, 2005.

C-CORE, Honeggerm, D., D.G. Honegger Consulting, 2003. Extended Model for Pipe Soil Interaction.

Edgers, L., Karlsrud, K., 1982. Soil flows generated by submarine slides - case studies and con-sequences. In Third International Conference on the Behaviour of OffShore Structures. pp. 425–437.

Hsu, T., 1993. Rate effect on lateral soil restraint of pipelines. Soils and Foundations, vol. 33(4), pp. 159-169.

Kianian, M., Shiri, H., 2019. The influence of pipeline-trenchbed interaction intensity on lateral soil resistance and failure mechanisms. International Journal of Geotechnical Engineering.

Klar, A., Randolph, M.F., 2008. Upper-bound and load–displacement solutions for laterally loaded piles in clays based on energy minimization. Géotechnique, 58(10): 815–820.

Merifield, R.S., Sloan, S.W., Yu, H.S., 2001. Stability of plate anchors in undrained clay. Géotechnique, 51(2): 141–153.

Oliveira, J.R.M.S., Almeida, M.S.S., Almeida, M.C.F., Borges, R.G., 2010. Physical Modeling of Lateral Clay-Pipe Interaction. Journal of Geotechnical and Geoenvironmental Engineer-ing, 136(2010): 950–956.

Paulin, M., 1998. An investigation into pipelines subjected to lateral soil loading. Memorial University of Newfoundland, St. John’s, Canada.

Pike, K. 2016. Physical and numerical modeling of pipe/soil interaction events for large deformation geohazards. Memorial University of Newfoundland, St. John’s, Canada.

Poorooshasb, F., Paulin, M., Rizkalla, M., Clark, J., 1994. Centrifuge modeling of laterally loaded pipelines. Transportation research record, 33–40.

PRCI. 2009. Guidelines for constructing natural gas and liquid hydrocarbon pipelines through areas prone to landslide and subsidence hazards. In Pipeline Research Council International.

Rajah, S., Shumaker, S., Bardakjian, H., Botteicher, B., Bushdiecker, K., Conner, R., Cox, A., Fisher, C., LeBlanc, J., McCabe, M.W., Walker, R., and Whidden, W. 2014. Soil parameters for assessing axial and transverse behavior of restrained pipelines—Part 2: Transverse behavior. In Pipelines 2014: From Underground to the Forefront of Innovation and Sustainability. ASCE, Portland. pp. 1849–1863.

Rizkalla, M., Mclntyre, M.B., 1991. A Special Pipeline Design for Unstable Slopes. Proceedings, Pipeline Engineering 1991, 14th Annual Energy-Sources Technology Conference and Exhibition, Houston, ASME, Vol. 34, pp. 69-74.

Chapter 2

Literature Review

2.1. Overview

Since the thesis is paper based, each chapter has its own literature review. However, a summary of literature review in chapters from Chapter 3 to Chapter 5 was brought as Chapter 2.

2.2. Literature review

2.2.1. Pipeline seabed interaction

Subsea pipelines are widely used in offshore field developments either laid on the seabed or buried beneath backfilled materials. Pipelines may undergo large lateral displacements due to environmental, operational and accidental loads. The lateral soil resistance against a moving pipe significantly depends on the relative moving rate between the pipe and soil ground and drainage condition (Hsu, 1993; Paulin, 1998; C-CORE report, 2003).

2.2.1.1. Consolidation effects

In practice, the undrained shear strength of the cohesive soil is usually considered as a key design parameter, assuming a sufficiently high loading velocity that does not allow for dissipation of the excess pore pressure. However, some published studies reported that the lateral resistance of cohesive soil may be increased by reducing the loading velocity that may happen with gentle ground movement, ice gouging, etc. (Paulin, 1998; Bemben and Myers, 1974; Kim et al., 2006; Kim, 2005; Randolph and Hope, 2004; Roy et al., 1982). In these occasions, accurate predictions of the lateral *p-y* response of the pipe need proper incorporation of the coupled analysis considering excess pore pressure generation and dissipation, in addition to the large deformation that a moving pipe involves. Some large deformation numerical methods have been proposed to incorporate coupled consolidation analyses (Chaterjee et al., 2012b; Ragni et al., 2016; Wang and Bienen, 2015).

2.2.1.2. Trench effects

In practice, the pipeline-soil interaction response is generally idealized by defining a set of the specialized beam and spring elements (ALA, 2005), where the behaviour of springs are expressed by bilinear or hyperbolic functions (ALA, 2005; PRCI, 2009). However, large discrepancies are observed in the recommendations provided by different design codes and the empirical equations proposed in some previous studies for calculation of the ultimate lateral resistance and also the p-y response (ALA, 2005; PRCI, 2009; Paulin, 1998; Rajah, 2014; Pike, 2016). The simplified assumptions ignoring the effect of pipeline-backfill-trench interaction and resulting in discrepancies.

There are a number of theoretical and experimental models availabe to predict the ultimate lateral resistance or force-displacement (p-y) curves of moving structures (Mackenzie, 1955; Tschebotarioff, 1973; Luscher et al., 1979; Rowe and Davis, 1982; Das et al., 1985, 1987; Rizkalla and Mclntyre, 1991; Ranjani et al., 1993; Merifield et al., 2001; Klar and Randolph, 2008). While limited models are based on pipelines lateral interaction (Paulin, 1998; Oliveira et al., 2010; Poorooshasb et al., 1994).

Besides, the influence of different stiffness between the backfilling and native material on lateral p-y response of the pipeline is rarely considered in the proposed models and design codes, while the limited published works have proven the significant influence of relative backfill-trench stiffness on lateral pipe response.

2.2.1.3. Progress in physical modelling

Paulin (1998) conducted a series of lateral pipeline-soil interaction centrifuge tests in clay to study the effects of trench width, burial depth, interaction rate, backfill properties, and stress history of the soil on force-displacement curves. This technique provided some qualitative information about the failure mechanisms, but lack of direct visualization and seemed to be less reliable due to the technique limitation. Kianian et al. (2018) conducted series of centrifuge

tests to overcome the shortcomings of the project performed by Paulin (1998). The progressive and interactive failure mechanisms were explicitly obtained by using a transparent acrylic sheet, digital cameras, and particle image velocimetry (PIV).

Since test in clay is extremely costly and time-consuming for the soil consolidation and soil preparation, only limited number of published research works were published with physical tests modeling the pipeline-backfill-trench interaction (Paulin, 1998; Kianian et al., 1998; C-CORE report, 2003). Besides, limited number of numerical studies were published with modeling the pipeline-backfill-trench interaction because of the complexities in model configuration and overdistorsion in conventional Lagrangian meshes with large deformation problem (Phillips et al., 2004; Kouretzis et al., 2013; Chaloulos et al., 2015). However, these studies with numerical model lack accurately calibration due to the limitations in the observation of the failure mechanisms.

2.2.1.4. Progress in numerical modelling

The Remeshing and Interpolation Technique with Small Strain (RITSS) (Hu and Randolph, 1998) was proved to be an efficient and advanced method in solving the large deformation offshore problems. The RITSS method has been successfully used in the past for the rate-dependent modeling of the partially embedded pipes (Chaterjee et al., 2012a, 2012b, 2012c; Barbosa-Cruz and Randolph, 2005; Wang et al., 2010c; Zhou et al., 2008; Ullah et al., 2018) and some of the other large deformation geotechnical problems (Zhang et al., 2015; Zhang et al., 2018; Ragni et al., 2016; Song et al., 2008; Wang and Bienen, 2014; Wang et al., 2013; Wang et al., 2010a; Wang et al., 2006) for its advantage in avoiding over distortion of meshes (Yu et al., 2008; Zhou and Randolph, 2006; Hu and Randolph, 2002; Randolph et al., 2008; Song et al., 2008; Wang et al., 2010b). The RITSS method (Hu and Randolph, 1998) enables solving large deformation problems by dividing the large deformation into a series of small deformation increments, followed by remeshing and interpolation of solution variables from

the old to new meshes. The RITSS method was originally proposed by Hu and Randolph (1998) using an in-house Fortran package, and extended by Wang et al. (2015, 2018) with performing efficient Lagrangian calculations at a commercial package ABAQUS though retaining interpolation algorithms in Fortran. The interpolation scheme was simplified with minimal coding by adopting the mesh-to-mesh solution mapping method built-in ABAQUS by Tian et al. (2014).

The literature review shows the empirical and analytical solutions, physical modeling, laboratory testing, and numerical methods. The knowledge gap to be filled by this research is clarified, and numerical models developed to facilitate filling this knowledge gap are to be presented in the following Chapters in the PART I of the thesis. Reliability on progressing finite element procedures to model the complicated, nonlinear coupled pipeline seabed interaction requires a deep understanding of parameters affecting soil constitutive model and behavior, coupled pore fluid pressure and failure mechanisms during the large lateral displacement of embedded pipeline.

Part I of the thesis (Chapter3, Chapter 4, and Chapter 5) focuses on the influence of the consolidation effects and trench effects on the soil resistance during the large lateral displacement of pipe.

References

ALA. In ASCE, 2005. Guidelines for the design of buried steel pipe.

Barbosa-Cruz, E.R., Randolph, M.F., 2005. Bearing capacity and large penetration of a cylindrical object at shallow embedment. Proc. Int. Symp. on. Frontiers in Offshore Geotechnics-ISFOG, Perth, Australia.

Bemben, S., Myers, H., 1974. The influence of rate of penetration on static cone resistance in Connecticut river valley varved clay. In Proc., European Symp. on Penetration Testing, vol. 2, no. 2: National Swedish Council for Building Research Stockholm, pp. 33-43.

Bhushan, K., Haley, S.C., Fong, P.T., 1979. Lateral Load Tests on Drilled Piers in Stiff Clays ASCE. Journal of the Geotechnical Engineering Division, ASCE, 105(GT8): 969–985.

C-CORE, Honeggerm, D., D.G. Honegger Consulting, 2003. Extended Model for Pipe Soil Interaction.

Chatterjee, S., Randolph, M.F., White, D., 2012a. The effects of penetration rate and strain softening on the vertical penetration resistance of seabed pipelines. Géotechnique, vol. 62, no. 7, p. 573.

Chatterjee, S., White, D., Randolph, M.F., 2012b. Numerical simulations of pipe-soil interaction during large lateral movements on clay. Géotechnique, vol. 62, no. 8, p. 693.

Chatterjee, S., Yan, Y., Randolph, M., White, D., 2012c. Elastoplastic consolidation beneath shallowly embedded offshore pipelines. Géotechnique Letters, vol. 2, no. 2, pp. 73-79.

Chaloulos, Y., Bouckovalas, G., Zervos, S., Zampos, A. 2015. Lateral soil-pipeline interaction in sand backfill: effect of trench dimension, Computers and Geotechnics, 69 (2015) 442-451.

Das, B.M., Moreno, R., Dallo, K., 1985. Ultimate pullout capacity of shallow vertical anchors in clay. Soils and Foundations, 25(2): 148–152.

Edgers, L., Karlsrud, K., 1982. Soil flows generated by submarine slides - case studies and con-sequences. In Third International Conference on the Behaviour of OffShore Structures. pp. 425–437.

Hansen, J.B., 1948. The Stabilizing Effect of Piles in Clay. In CN Post No. 3, Christiani and Nielson, Copenhagen, Denmark, November. pp. 14–15.

Hansen, J.B., Christensen, N.H., 1961. The ultimate resistance of rigid piles against transversal forces. Geoteknisk Institut, Copenhagen.

Hsu, T., 1993. Rate effect on lateral soil restraint of pipelines. Soils and Foundations, vol. 33, no. 4, pp. 159-169.

Hu, Y., Randolph, M.F., 1998. A practical numerical approach for large deformation problems in soil. Int. J. Numer. Analyt. Meth. Geomech., vol. 22, pp. 327-350.

Hu, Y., Randolph, M.F., 2002. Bearing Capacity of Caisson Foundations on Normally Consolidated Clay. Soils and Foundations, Japanese Geotechnical Soiciety, vol. 42, no. 5, pp. 71-77.

Kianian, M., Esmaeilzadeh, M., Shiri, H., 2018. Lateral Response of Trenched Pipelines to Large Deformations in Clay. Offshore Technology Conference, OTC2018, Houston, TX, US, OTC-28842-MS.

Kim, K.K., Prezzi, M., Salgado, R., 2006. Interpretation of cone penetration tests in cohesive soils.

Kim, T., 2005. Dissipation of pore water pressure due to piezocone penetration in OC clay. Ph. D. dissertation, Korea Univ., Seoul, Korea.

Klar, A., Randolph, M.F., 2008. Upper-bound and load–displacement solutions for laterally loaded piles in clays based on energy minimization. Géotechnique, 58(10): 815–820.

Kouretzis, G., Sheng, D., Sloan, S., 2013. Sand-pipeline-trench lateral interaction effects for shallow buried pipelines, Computers and Geotechnics, 54 (2013) 53-59.

Luscher, U., Thomas, H.P., Maple, J.A., 1979. Pipe-Soil Interaction. Trans-Alaska Pipeline. In Pipelines in Adverse Environments: A State of the Art. ASCE. pp. 486–502.

Mackenzie, T.R., 1955. Strength of Deadman Anchors in Clay. M.Sc. Thesis, Princeton University, Princeton, USA.

Merifield, R.S., Sloan, S.W., Yu, H.S., 2001. Stability of plate anchors in undrained clay. Géotechnique, 51(2): 141–153.

Oliveira, J.R.M.S., Almeida, M.S.S., Almeida, M.C.F., Borges, R.G., 2010. Physical Modeling of Lateral Clay-Pipe Interaction. Journal of Geotechnical and Geoenvironmental Engineer-ing, 136(2010): 950–956.

Paulin, M., 1998. An investigation into pipelines subjected to lateral soil loading. Memorial University of Newfoundland, St. John's, Canada.

Phillips, R., Nobahar, A., Zhou, J., 2004, Trench effects on pipe-soil interaction, Proceeding of International Pipeline Conference, Calgary, Alberta, Canada, IPC2004-141.

Pike, K., 2016. Physical and numerical modeling of pipe/soil interaction events for large deformation geohazards. Memorial University of Newfoundland, St. John's, Canada.

Poorooshasb, F., Paulin, M., Rizkalla, M., Clark, J., 1994. Centrifuge modeling of laterally loaded pipelines. Transportation research record, 33–40.

Poulos, H.G., 1995. Design of Reinforcing Piles to Increase Slope Stability. Canadian Geotech-nical Journal, 32(5): 808–818.

PRCI. 2009. Guidelines for constructing natural gas and liquid hydrocarbon pipelines through areas prone to landslide and subsidence hazards. In Pipeline Research Council International.

Ragni, R., Wang, D., Mašín, D., Bienen, B., Cassidy, M.J., Stanier, S.A., 2016. Numerical modelling of the effects of consolidation on jack-up spudcan penetration. Computers and Geotechnics, vol. 78, pp. 25-37.

Rajah, S., Shumaker, S., Bardakjian, H., Botteicher, B., Bushdiecker, K., Conner, R., Cox, A., Fisher, C., LeBlanc, J., McCabe, M.W., Walker, R., Whidden, W., 2014. Soil parameters for assessing axial and transverse behavior of restrained pipelines—Part 2: Transverse behavior. In Pipelines 2014: From Underground to the Forefront of Innovation and Sustainability. ASCE, Portland. pp. 1849–1863.

Randolph, M.F., Hope, S., 2004. Effect of cone velocity on cone resistance and excess pore pressures. Engineering Practice and Performance of Soft Deposits, Osaka, Japan, pp. 147-152.

Randolph, M.F., Wang, D., Zhou, H., Hossain, M., Hu, Y., 2008. Large deformation finite element analysis for offshore applications. In 12th International Conference of International Association for Computer Methods and Advances in Geomechanics (IACMAG), Goa, India, pp. 1-6.

Ranjani, B.B., Robertson, P.K., Morgenstern, N.R., 1993. A Simplified Method for Pipelines Subject to Transverse Soil Movements Proceedings, vol. V, pp. 157-165. In 12th Offshore Mechanics and Arctic Engineering Symposium.

Reese, L.C., Welch, R.C., 1975. Lateral Loading of Deep Foundations in Stiff Clay. Journal of the Geotechnical Engineering Division, 101(7): 633–649.

Rizkalla, M., Mclntyre, M.B., 1991. A Special Pipeline Design for Unstable Slopes. Proceedings, Pipeline Engineering 1991, 14th Annual Energy-Sources Technology Conference and Exhibition, Houston, ASME, Vol. 34, pp. 69-74.

Rowe, R.K., Davis, E.H., 1982. The Behaviour of Anchor Plates in Clay. Geotechnique, 32(1): 9–23.

Roy, M., Tremblay, M., Tavenas, F., Rochelle, P. L., 1982. Development of pore pressures in quasi-static penetration tests in sensitive clay. Canadian Geotechnical Journal, vol. 19, no. 2, pp. 124-138.

Song, Z., Hu, Y., Randolph, M.F., 2008. Numerical simulation of vertical pullout of plate anchors in clay. Journal of geotechnical and geoenvironmental engineering, vol. 134, no. 6, pp. 866-875.

Tian, Y., Cassidy, M.J., Randolph, M.F., Wang, D., Gaudin, C., 2014. A simple implementation of RITSS and its application in large deformation analysis. Computers and Geotechnics, vol. 56, pp. 160-167.

Tschebotarioff, G.P, 1973. Foundations, Retaining and Earth Structures. McGraw-Hill Book Company, New York, 642p.

Ullah, S.N., Hou, L.F., Satchithananthan, U., Chen, Z., Gu, H., 2018. A 3D RITSS approach for total stress and coupled-flow large deformation problems using ABAQUS. Computers and Geotechnics, vol. 99, pp. 203-215.

Wang, D., Bienen, B., 2014. Coupled large deformation consolidation analysis of a spudcan footing penetrating into kaolin clay. In Computer Methods and Recent Advances in Geomechanics: Proceedings of the 14th International Conference of International Association for Computer Methods and Recent Advances in Geomechanics, 2014 (IACMAG 2014), 2015: Taylor & Francis Books Ltd, pp. 877-882.

Wang, D., Gaudin, C., Randolph, M.F., 2013. Large deformation finite element analysis investigating the performance of anchor keying flap. Ocean Engineering, vol. 59, pp. 107-116.

Wang, D., Hu, Y., Jin, X., 2006. Two-dimensional large deformation finite element analysis for the pulling-up of plate anchor. China Ocean Engineering, vol. 20, no. 2, pp. 269-278.

Wang, D., Hu, Y., Randolph, M.F., 2010a. Three-dimensional large deformation finite element analysis of plate anchors in uniform clay. J. Geotech. Geoenviron. Engi ASCE 136, vol. 2, pp. 355–365.

Wang, D., Hu, Y., Randolph, M.F., 2010b. Keying of rectangular plate anchors in normally consolidated clays. Journal of Geotechnical and Geoenvironmental Engineering, vol. 137, no. 12, pp. 1244-1253.

Wang, D., White, D.J., Randolph, M.F., 2010c. Large-deformation finite element analysis of pipe penetration and large-amplitude lateral displacement. Canadian Geotechnical Journal, vol. 47, no. 8, pp. 842-856.

Yu, L., Liu, J., Kong, X., Hu, Y., 2008. Three-dimensional RITSS large displacement finite element method for penetration of foundations into soil. Computers and Geotechnics, vol. 35, no. 3, pp. 372-382.

Zhang, W., Wang, D., Randolph, M.F., Puzrin, A., 2015. Catastrophic failure in planar landslides with a fully softened weak zone. Géotechnique, vol. 65, pp. 755-769.

Zhang, W., Randolph, M.F., Puzrin, A., Wang, D., 2018. Transition from shear band propagation to global slab failure in submarine landslides. Canadian Geotechnical Journal, vol. 56.

Zhou, H., Randolph, M.F., 2006. Large deformation analysis of suction caisson installation in clay. Canadian Geotechnical Journal, vol. 43, no. 12, pp. 1344-1357.

Zhou, H., White, D.J., Randolph, M.F., 2008. Physical and numerical simulation of shallow penetration of a cylindrical object into soft clay. in GeoCongress 2008: Characterization, Monitoring, and Modeling of GeoSystems, pp. 108-117.

Chapter 3

Large Deformation Coupled Analysis of Embedded Pipeline – Soil Lateral Interaction

Xiaoyu Dong[1], Wangcheng Zhang[2], Hodjat Shiri[3], Mark F. Randolph[4]

1: Department of Civil
Engineering, Memorial University of Newfoundland
e-mail: xiaoyu.dong@mun.ca

2: Oceans Graduate School,
the University of Western Australia
e-mail: wangcheng.zhang@uwa.edu.au

3: Department of Civil
Engineering, Memorial University of Newfoundland
e-mail: hshiri@mun.ca

4: Oceans Graduate School,
the University of Western Australia
e-mail: mark.randolph@uwa.edu.au

This chapter is submitted as a journal manuscript.

.

Abstract

Subsea pipelines buried in the seabed may undergo large lateral displacements under environmental, operational, and accidental loads at different interaction rates and hence different drainage conditions. The undrained shear strength is commonly used in practice to assess the pipe-soil interaction assuming a sufficiently high interaction rate. This approach neglects the consolidation effects and the rate-dependent response of the soil, and significantly underestimates the lateral resistance against the pipeline moving with a low velocity. In this study, a coupled large deformation finite element (LDFE) framework was developed via a remeshing and interpolation technique with small strain (RITSS). Modified Cam-Clay (MCC) model with efficient numerical integration is used. The proposed coupled LDFE framework is verified against existing physical and numerical results. Effects of the interaction rate and hence drainage condition on the embedded pipe-soil lateral responses, excess pore pressure generation and dissipation, and failure mechanisms are discussed.

Keywords: Pipeline, Pipeline-soil interaction, Offshore Engineering, Numerical modeling, Coupled analysis

3.1. Introduction

Subsea pipelines are widely used in offshore field developments either laid on the seabed or buried beneath backfilled materials. Pipelines may undergo large lateral displacements due to environmental, operational and accidental loads. The lateral soil resistance against a moving pipe depends significantly on the relative displacement rate between the pipe and soil ground and drainage condition (Hsu, 1993; Paulin, 1998; C-CORE report, 2003). In practice, the undrained shear strength of the cohesive soil is usually considered as a key design parameter, assuming a sufficiently high loading velocity that does not allow dissipation of the excess pore pressures. However, some published studies reported that the lateral resistance of cohesive soil may be increased at low displacement rates such as may occur with gentle ground movement, ice gouging, etc. (Bemben and Myers, 1974; Roy et al., 1982; Paulin, 1998; Randolph and Hope, 2004; Kim et al., 2006). For such applications, accurate prediction of the lateral p-y response of the pipe needs proper incorporation of coupled analyses considering excess pore pressure generation and dissipation, in addition to the large deformation that a moving pipe involves.

Some large deformation numerical methods have been proposed to incorporate coupled consolidation analyses (Chatterjee et al., 2012; Wang and Bienen, 2015; Ragni et al., 2016). In this study, the Remeshing and Interpolation Technique with Small Strain (RITSS) (Hu and Randolph, 1998) was adopted to conduct the large deformation coupled consolidation analysis of a buried pipeline with different lateral displacement rates. The RITSS method has been used successfully in the past for the rate-dependent modeling of partially embedded pipes (Barbosa-Cruz and Randolph, 2005; Zhou et al., 2008; Wang et al., 2010; Chatterjee et al., 2012a, 2012b, 2012c; Yllah et al., 2018) and some other large deformation geotechnical problems (Wang et al, 2006, 2010, 2013; Song et al., 2008; Wang and Bienen, 2015; Zhang et al., 2015, 2018; Ragni et al., 2016), because of its ability to avoid over distortion of meshes (Hu and Randolph,

2002; Zhou and Randolph, 2006; Randolph et al., 2008; Song et al., 2008; Yu et al., 2008; Wang et al., 2010). The RITSS method (Hu and Randolph, 1998) enables analysis of large deformation problems by dividing the whole displacement into a series of small deformation increments, followed by remeshing and interpolation of solution variables from the old to new meshes. The RITSS method was originally proposed by Hu and Randolph (1998) using an in-house Fortran package, and extended by Zhang et al. (2015, 2018) who performed efficient Lagrangian calculations in a commercial package ABAQUS incorporating bespoke interpolation algorithms in Fortran. The interpolation scheme was simplified by Tian et al. (2014), with minimal coding by adopting the mesh-to-mesh solution mapping method built into ABAQUS.

The paper presents a series of large deformation finite element (LDFE) analyses undertaken to understand the failure mechanisms and soil resistance during lateral pipe displacement under different drainage conditions. The numerical results are compared with published experimental and numerical studies (Paulin, 1998; C-CORE report, 2003). A parametric study was performed with respect to the influence of the drainage conditions on failure mechanisms and lateral resistance.

3.2. Methodology

3.2.1. Overall framework and techniques of coupled LDFE analysis

The flowchart of the RITSS procedure used in the study for coupled LDFE analyses considering soil consolidation is summarized in Figure 3-1. Overall, a large-deformation analysis is accomplished by dividing the whole analysis into a series of small strain increments. The domain is remeshed periodically, with material and stress parameters interpolated from old deformed to newly generated meshes. The results are then post-processed by extraction of the required information (field properties and boundaries etc.) from the deformed meshes. The process is repeated until the ultimate displacement (or deformation) is achieved.

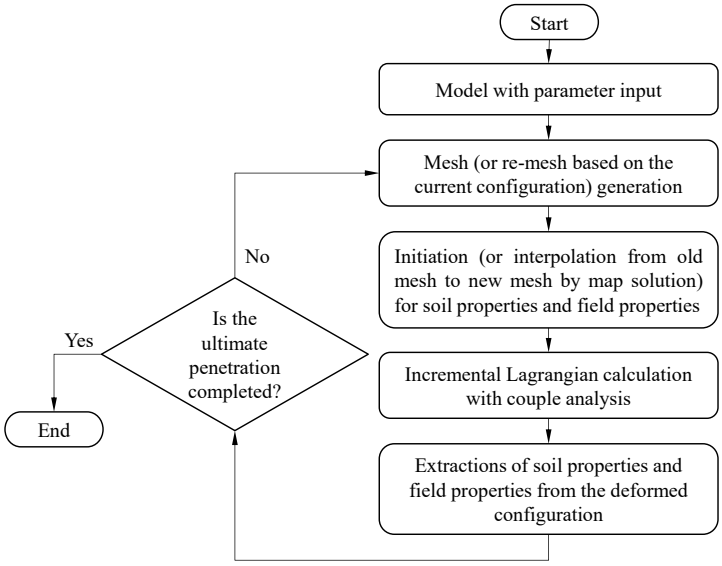

Figure 3-1. Schematic flowcharts for framework

The RITSS framework consists of five main modules: parameter input, mesh (remesh) generation, interpolation of soil and field properties, Lagrangian calculation and extraction of soil and field properties. A main Python code is used to invoke all modules. The interpolation module (of soil and field properties from old to new meshes) using a mapping solution technique and the Lagrangian calculation module are accomplished within the commercial platform ABAQUS with light coding, while other modules are similar to those for a standard small strain finite element analysis. In every analysis increment, small strain is guaranteed by ensuring the maximum value of the Equivalent Plastic Strain (PEEQ) is less than 1%, to maintain numerical accuracy. Some special techniques and tips are necessary to incorporate a coupled consolidation analysis into the RITSS method.

The map solution technique (or mesh-to-mesh solution mapping) in ABAQUS is such that information associated with nodal and integration points in the new meshes can be interpolated from nodal properties in old meshes (Dassault Systemes Simulia Corp., 2017). The interpolation of nodal solution variables is straightforward, while integration point variables in old meshes have to be extrapolated from the integration points to the nodes of each element.

To incorporate the consolidation analysis into the RITSS with ABAQUS-based solution mapping, the introduction of a dummy job is necessary in each increment to keep the calculation loop working when using the Modified Cam-Clay (MCC) model built into ABAQUS. One limitation of the mesh-to-mesh solution mapping in ABAQUS/Standard is that it ignores all initial conditions specified in the input file (except for temperature for a pure stress-displacement analysis). On the other hand, implementation of the ABAQUS built-in MCC model requires non-zero initial normal stress (a kind of initial condition that is deleted during mesh-to-mesh solution mapping). To solve this dilemma, remeshing and interpolation of soil and field properties are undertaken exclusively by a dummy job with an infinitesimal time step. Note that the user-defined MCC model that was eventually used in this study does not suffer from this problem.

The displacement boundary conditions can be carried over directly from the old meshes to the new meshes. The force boundary conditions (e.g. reaction force), however, had to be tracked and transferred by a separate Python file to keep the same conditions in effect as at the last increment from the old job. The transfer and interpolation of force boundary conditions have not been considered in previous studies using RITSS; however, their absence was found to result in potential numerical inaccuracy and non-convergence issues.

In the soil consolidation analysis, an implicit method was used iteratively to solve excess pore fluid pressures and effective stresses in the soil. The accuracy of the time integration for the consolidation step is controlled by the maximum allowable pore pressure change per time step; the value adopted was increased as much as possible without compromising convergence of the calculation (Dassault Systemes Simulia Corp., 2017). Besides, the initial time step Δt (s) is determined by:

$$\Delta t \geq \frac{\gamma_w}{6Ek}(\Delta h)^2 \tag{3-1}$$

where Δh (m) is the characteristic element size near the disturbance (e.g. the drainage surface in the study), E (Pa) is the elastic modulus of the soil skeleton, k (m/s) is the soil permeability, and γ_w (N/m^3) is the specific weight of the permeating fluid.

3.2.2. Constitutive model

A Cam-Clay type of constitutive model with strain hardening was used in the coupled LDFE analysis to conduct tests with different drainage conditions. The model was that proposed by Lagioia and Nova (1995), originally with incorporation of non-zero 'cohesion' or cementing, as an improved model compared with that proposed by Nova (1992).

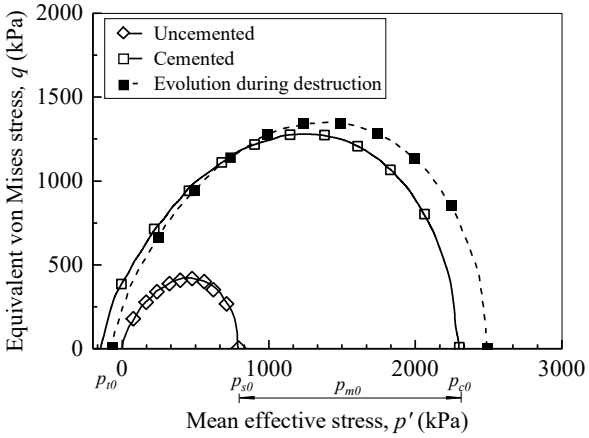

Figure 3-2. Initial yield surface and evolution (Lagioia and Nova, 1995)

As shown in Figure 3-2, the evolving yield surface size is controlled by p_c, which is given by

$$p_c = p_s + p_m + p_t \tag{3-2}$$

where hidden variables (p_s, p_t, p_m) depend on the plastic history of the material during hardening, and are given by

$$p_s = p_{s0} \cdot \exp\left[\frac{\varepsilon_v^p + \xi \int (d\varepsilon_{q\theta}^p)}{B_p}\right] \tag{3-3}$$

$$p_m = p_{m0} \cdot \exp\left[-\rho_m \left(\int |d\varepsilon_v^p|\right)^3\right] \tag{3-4}$$

$$p_t = p_{t0} \cdot \exp\left[-\rho_t \left(\int |d\varepsilon_v^p|\right)\right] \tag{3-5}$$

respectively, where p_{s0}, p_{m0} and p_{t0} ·are initial hidden variables, ε_v^p is the plastic volumetric strain, ξ is the constitutive parameter used for coupling the hardening associated with plastic

deviatoric strain, $d\varepsilon_{q\theta}^{p}$ is the total plastic deviatoric strain increment, B_p is the hardening parameter, ρ_m and p_t control the speed at which the *e*-ln(*p*') curve rejoins that of the uncemented soil.

In the present study, initial cementation was not considered, so that $p_c = p_s$. Ignoring the deviatoric strain induced hardening, the evolution law of hidden variables can be simplified to:

$$p_c = p_{c0} \cdot \exp\left(\frac{\varepsilon_v^p}{B_p}\right) \tag{3–6}$$

with the initial yield surface size controlled by p_{c0} (Panteghini and Lagioia, 2018a). B_p represents the slope of the $\varepsilon_v^p - \ln p'$ curve (Lagioia and Nova, 1995) and can be related to the conventional MCC parameters by (detailed in the Appendix):

$$B_p = \frac{d\varepsilon_v^p}{d\ln p'} = \frac{\lambda - \kappa}{(1 + e_0)} \tag{3–7}$$

where λ is the slope of the isotropic compression of the virgin material, κ is the slope of the unloading-reloading line in the specific volume versus the natural logarithm of the virgin material, e_0 is the initial void ratio. Linear elasticity was considered in alignment with the work by Lagioia and Nova (1995).

Panteghini and Lagioia (2018a, 2018b) recently improved the numerical integration efficiency for this MCC type constitutive model with considerations of full convexity and double homothety. For the elliptical yield surface used in present study, the new expression is given by:

$$f(p, q, p_c) = \sqrt{\left(\frac{\bar{p}}{p_c/2}\right)^2 + \left(\frac{q}{Mp_c/2}\right)^2} - 1 = 0 \tag{3–8}$$

where p is the mean pressure, $(\bar{p} = p - p_c/2\,, q)$ is the coordinate system moved in the center of the ellipse, q is the equivalent von Mises stress, M is the slope of the critical state line in $p - q$ space. The Matsuoka-Nakai failure criterion, with an associated flow rule, was considered for the three-dimensional yield surface.

Panteghini and Lagioia have published several papers introducing their convexification technique (e.g. Panteghini and Lagioia, 2018a). As mentioned in the paper, a full convexity is important for viscoplastic models, where stress points outside the yield surface are in general admissible. They have proposed the method to convexify the yield and plastic potential surfaces in the published paper. The yield function is equivalently formulated in terms of invariants associated to the relative cylindrical coordinate system in the principle stress space (details could be found in Lagioia and Panteghini, 2016; Panteghini and Lagioia, 2018a). Using a particular instance of this formulation, which is based on a separate definition of the curves resulting from a section of the surface with a meridional and with a deviatoric plane. This particular instance includes a shape function, which describes the curve resulting from a deviatoric section of the surface. With a generalized form, different set of parameters can be used to represent for different shapes. More details about the constitutive model can be found in Panteghini and Lagioia (2018a) and Lagioia and Panteghini (2016).

3.2.3. Verifications with 1D Terzaghi consolidation

In order to verify the developed LDFE framework for a coupled consolidation analysis, the one dimensional (1D) Terzaghi consolidation problem was solved using the proposed framework, comparing the results with standard small-strain and finite-strain finite element analyses, and the analytical solution from Terzaghi's 1D consolidation theory (Terzaghi et al., 1996). Verification model is set up according to the Terzaghi Consolidation Problem in ABAQUS Benchmarks manual (Dassault Systemes Simulia Corp., 2017).

Actually here the 1D consolidation is not aimed at checking the plasticity of the constitutive model (because its performance has already been examined and published in Panteghini and Lagioia 2018a), here we only use the elasticity and check the incorporation of the coupled pore pressure analysis. Therefore, the pre-consolidation stress is set very large. This verification case was made according to the ABAQUS Benchmarks manual, 1.14.1 The

Terzaghi Consolidation Problem, there they also obtained soil settles ~60% to 75% of its height. The only goal here is to benchmark the coupled model in simulating the excess pore pressure.

The model used for verification is shown in Figure 3-3. The submerged soil unit weight was considered, leading to solutions for the effective stress and excess pore pressure profiles directly. The soil ground was assumed to be 10 m high and 1 m wide, with the FE model comprising ten CPE4P elements arranged in a single column (see Figure 3-3).

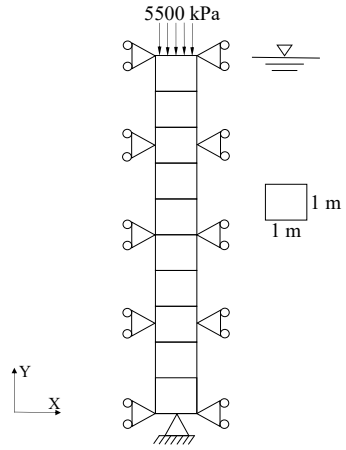

Figure 3-3. One dimensional consolidation test example.

The LDFE coupled consolidation analysis consisted of 100 small deformation increments with time for each increment being 7×10^5 s. Two reference cases were conducted with one using a single job finite-strain analysis (strains measured from the current configuration) and the other using a single job small-strain analysis (strains measured from the initial configuration). In these two FE analyses, the transient analysis considering the wetting liquid continuity was carried out using the consolidation soil step (Dassault Systemes Simulia Corp., 2017; Panteghini and Lagioia, 2018a).

Table 3-1. Parameters in 1D consolidation verification.

Properties	Symbol	Value	Unit
Permeability of soil	k_v	10^{-9}	m/s
Specific weight of pore fluid	γ_w	10	kN/m^3
Young's modulus of soil	E	5500	kPa
Poisson's ratio	υ	0.3	-
1D compression modulus of soil	E_s	7404	kPa
Height of soil body	h_{soil}	10	m
Surface pressure	q	5500	kPa
Initial void ratio	e_0	1.1	-
Effective unit soil weight	γ	8	kN/m^3
Hardening parameter	B_p	0.085	-
Size of the initial yield surface	p_{c0}	5800	kPa
Coefficient of vertical consolidation (elastic)	c_v	4.58×10^{-9}	m^2/s

The material properties and loading conditions are summarized in Table 3-1. The initial yield surface was set large enough ($p_{c0} = 5800$ kPa) to make the linear elasticity of soil play the main role and hence an easy comparison.

The time factor T_v is calculated as:

$$T_v = \frac{c_v t}{h_{soil}^2} = \frac{kE_s}{\gamma_w h_{soil}^2} t \tag{3-9}$$

where c_v is the coefficient of vertical consolidation, t is the consolidation time, h_{soil} is the height of the soil body, k is the permeability of soil, γ_w is the specific weight of pore fluid and E_s is the 1D compression modulus of soil given by:

$$E = E_s \frac{(1-\nu)}{(1+\nu)(1-2\nu)} \tag{3-10}$$

where ν is Poisson's ratio.

Consolidation settlement s_t at the soil surface is calculated as:

$$s_t = s \cdot U_t = m_v p_0 h_{soil} \left[1 - \frac{8}{\pi^2} \sum_{m=1}^{\infty} \left(\frac{1}{m^2} \cdot e^{\frac{-m^2\pi^2 T_v}{4}} \right)\right], m = 1,3,5,7,\cdots \tag{3-11}$$

where s is the total consolidation settlement at the soil surface, U_t is the degree of consolidation, p_0 is the overburden pressure, m_v is the coefficient of volume compressibility. Degree of consolidation, U_t, is calculated as:

$$U_t = 1 - \frac{8}{\pi^2} \sum_{m=1}^{\infty} \left(\frac{1}{m^2} \cdot e^{\frac{-m^2 \pi^2 T_v}{4}} \right), m = 1,3,5,7,\cdots \quad (3\text{-}12)$$

Pore pressure u at the bottom of soil ($z = h_{soil}$) is calculated as:

$$u = u_0 \frac{4}{\pi^2} \sum_{m=1}^{\infty} \left[\frac{1}{m} \cdot \sin\left(\frac{m\pi z}{2h_{soil}} \right) \cdot e^{\frac{-(m^2 \pi^2 T_v)}{4}} \right], m = 1,3,5,7,\cdots \quad (3\text{-}13)$$

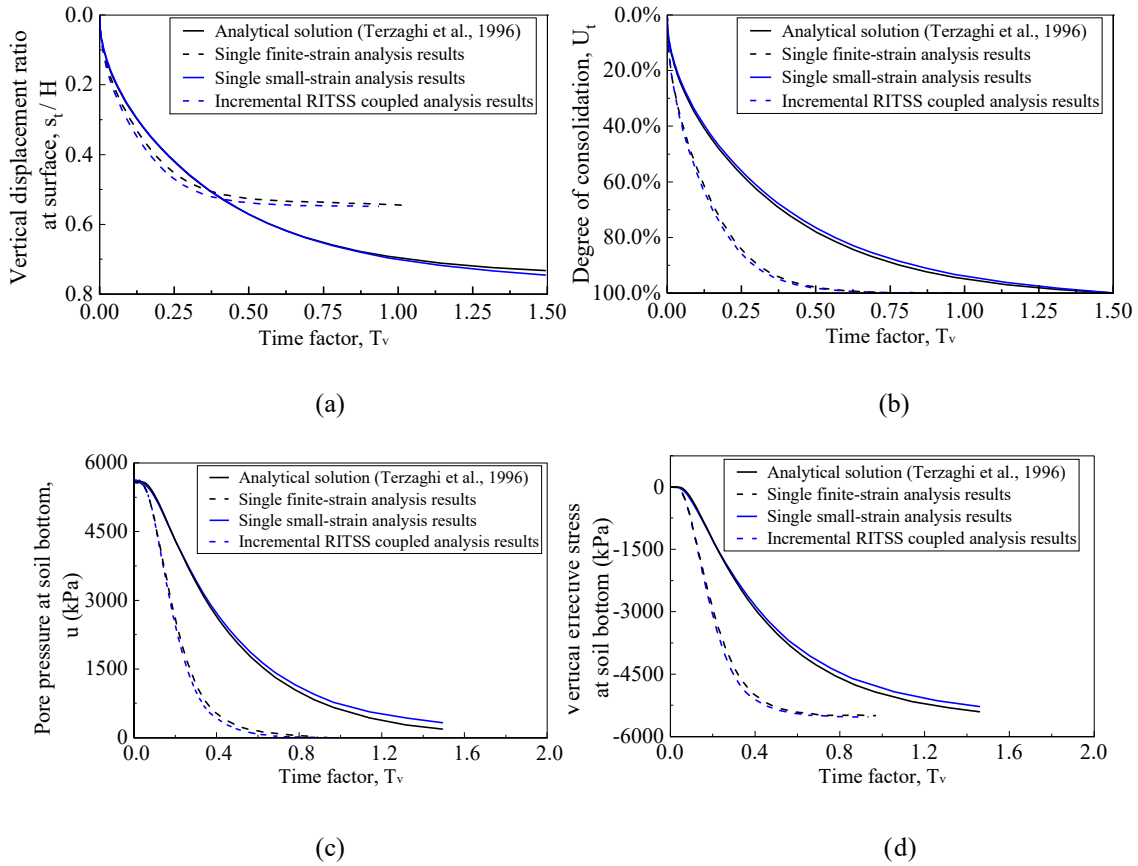

Figure 3-4. 1D Consolidation results with elastic soil model.

Figure 3-4 shows the comparisons among the analytical and numerical solutions. As expected, the results of the small-strain analysis matched the analytical solution well due to the closer basis of assumptions (i.e. infinitesimal strain theory with strains calculated based on the initial configuration). Large displacements would invalidate the fundamental assumptions and result in a level of inaccuracy in the solutions. Incorporation of finite-strain theory, by which strains are based on the current configuration, resulted in faster consolidation (due to the reduction in drainage distance) but smaller ultimate accumulated settlement (see Figure 3-4 a and Figure 3-4 b). The updated configuration in the LDFE method enables it to reflect the finite strain effects (deviation less than 1.2% in Figure 3-4a, less than 0.5% in Figure 3-4c and d), even though small strain analysis is adopted in each increment. Regarding the pore pressure and vertical effective stress at the bottom of the model, the LDFE analysis using the RITSS procedure

produced very close results to the finite-strain analysis (See Figure 3-4 c and Figure 3-4 d), validating its accuracy.

3.3. Large deformation coupled consolidation analysis of pipe-soil interaction

The LDFE framework considering soil consolidation was used to analyse buried pipe-soil interactions with large lateral displacements and different drainage conditions. Since clay sample preparation and consolidation are rather time-consuming and the pipeline-backfill-trench interaction is highly complicated, there is a paucity of relevant physical tests on which to draw for comparisons.

Results from two centrifuge model tests (C-CORE Report, 2003) were selected for numerical model benchmarking. The tests were carried out under 50g acceleration with a model pipeline of 19 mm in diameter (D) and 25 mm in length, corresponding to a prototype pipeline of 0.95 m in diameter and 12.5 m in length. The pipeline was buried at a depth (from the ground surface to the pipeline centre) of H = 1.5 D and 3.0 D respectively. Soils used in the centrifuge test were a mixture of 50% (by weight) speswhite kaolin clay and 50% Sil-CoSil silt. The soil sample was consolidated to a vertical stress of 400 kPa to obtain an undrained shear strength of 40 kPa and the two tests were performed by displacement control with pipe moving rates of 0.5 and 0.7 mm/s respectively (C-CORE Report, 2003), which are sufficient to satisfy near undrained conditions with $c_v = 0.38$ mm^2/s (Paulin et al., 1998a, 1998b). The two centrifuge tests were also modelled numerically in C-CORE Report (2003) using conventional finite element analysis, where over-distorted meshes were observed and expected to introduce inaccuracy to the modelling. For the LDFE analyses here, permeability of the soil was taken as 10^{-10} m/s, consistent with the published numerical work (C-CORE Report, 2003). In the following, the lateral p-y response and failure mechanisms of the buried pipeline will be discussed under different displacement rates and thereby different drainage conditions.

3.3.1. Numerical details

The numerical model for the LDFE coupled consolidation analyses of pipe-soil interactions is shown in Figure 3-5. To enable direct comparison between numerical and physical tests, the dimensions of the numerical model were set identical to the prototype simulated in the two centrifuge tests. Two different burial depth ratios (H/D of 1.5 and 3.0) were selected with the same penetration velocity of pipe (0.5 mm/s as described in C-CORE Report (2003)).

Table 3-2. Parameters used for numerical model in Section 3.

Properties		Symbol	Value				Unit
Specific weight of pore fluid		γ_w	10				kN/m^3
Effective unit soil weight		γ	7.5				kN/m^3
Pipe diameter		D	0.95				m
Young's modulus of soil		E	5000				kPa
Poisson's ratio		υ	0.3				-
Initial void ratio		e_0	1.5				-
Coefficient of earth pressure at rest		K_0	0.65				-
Permeability of soil		k_v	10^{-10}				m/s
Hardening parameter		B_p	0.064				-
Size of the initial yield surface		p_{c0}	177				kPa
Slope of CSL		M_{tc}	0.77				-
Triaxial compression conditions frictional angle		ϕ_{tc}	0.35				rad
Plane strain conditions frictional angle		ϕ_{ps}	0.39				rad
Coefficient of vertical consolidation (Elastic)		$c_{v,elastic}$	4.16×10^{-8}				m^2/s
Properties		Symbol	H/D=1.5		H/D=3.0		-
			Pipe centre	Pipe bottom	Pipe centre	Pipe bottom	-
Triaxial compression (see appendix, equation (3-A.26) – equation (3-A.35), Wroth 1984)	Mean effective stress	p'	8.25	11.00	16.50	19.25	kPa
	Over Consolidated Ratio	OCR	21.45	16.09	10.73	9.19	-
	Equivalent stress	q	3.66	4.87	7.31	8.53	kPa
	Stress ratio	η	0.44	0.44	0.44	0.44	-

	parameter	Λ	0.97	0.96	0.94	0.93	-
	Equivalent undrained shear strength (NC)	$s_{u,tc,NC}$	2.14	2.87	4.34	5.08	kPa
	Equivalent undrained shear strength (OC) (using $s_{u,OC} = s_{u,NC}(OCR)^{\Lambda}$)	$s_{u,tc,OC}$	41.95	41.37	40.53	40.23	kPa
	coefficient of volume compressibility	m_v	0.0080	0.0061	0.0041	0.0036	m^2/kN
	Coefficient of vertical consolidation	c_v	1.24×10^{-9}	1.64×10^{-9}	2.41×10^{-9}	2.79×10^{-9}	m^2/s
Compression under plane strain condition (see appendix, equation (3-A.36) – equation (3-A.45), Wroth 1984)	Mean effective stress	s'	8.86	11.81	17.72	20.67	kPa
	Over Consolidated Ratio	OCR	19.98	14.98	9.99	8.56	-
	Equivalent stress	t	1.83	2.44	3.66	4.26	kPa
	Stress ratio	θ	0.21	0.21	0.21	0.21	-
	parameter	Λ	0.97	0.96	0.94	0.93	-
	Equivalent undrained shear strength (NC)	$s_{u,ps,NC}$	2.22	2.97	4.50	5.27	kPa
	Equivalent undrained shear strength (OC) (using $s_{u,OC} = s_{u,NC}(OCR)^{\Lambda}$)	$s_{u,ps,OC}$	40.28	39.72	38.94	38.68	kPa
	coefficient of volume compressibility	m_v	0.0075	0.0057	0.0039	0.0034	m^2/kN
	Coefficient of vertical consolidation	c_v	1.33×10^{-9}	1.75×10^{-9}	2.58×10^{-9}	2.98×10^{-9}	m^2/s
Numerical model for plane strain value of $s_{u,ps}$	Equivalent undrained shear strength (NC)	$s_{u,ps,numerical,NC}$	2.18	3.16	4.82	5.64	kPa
	Equivalent undrained shear strength (OC) (using $s_{u,OC} = s_{u,NC}(OCR)^{\Lambda}$)	$s_{u,ps,numerical,OC}$	39.58	42.24	41.75	41.41	kPa
Note.							

The initial stress state at burial depth (p', q) and (s', t) are computed according to equations in appendix and are used as input for calculation in the study cases. $\eta = \frac{q}{p'}$, $\theta = \frac{t}{s'}$, $\Lambda = 1 - \frac{\kappa}{\lambda}$ where $\kappa = \frac{p'(1+e_0)3(1-2\nu)}{E}$ and $\lambda = B_p(1+e_0) + \kappa$ (see Appendix).

$s_{u,NC}$ is calculated by equation (3-A.45). And $c_{v,elastic}$ is calculated by equation (3-15) ignoring the plastic part.

$s_{u,NC,numerical}$ is obtained from the plane strain compression test as described in Appendix.

As given in Table 3-2, other parameters in the numerical modelling were determined in accordance with the physical tests described in C-CORE Report (2003). The initial value of Λ is computed and presented in the table (around 0.95), which seems larger than the typical value (0.8). Since in the model, the Λ is not a constant value, it will change with p'. When the pipe starts moving, the p' of soil will be influenced and Λ will therefore change.

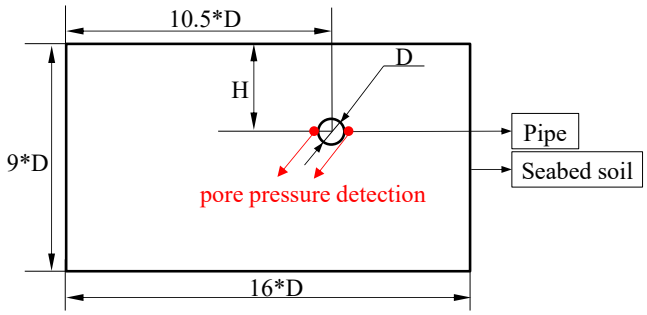

(a)

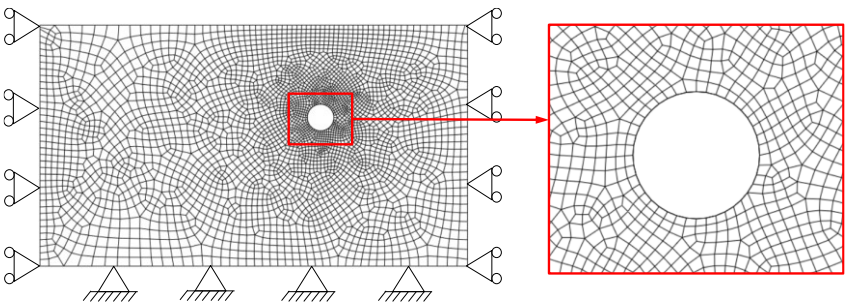

(b)

Figure 3-5. Configuration of buried pipe.

Figure 3-5 b shows details of the mesh, with the soil domain modeled using 4-node bilinear displacement and pore pressure plane strain elements (CPE4P) and the pipe by rigid wire elements (R2D2). The bottom boundary was fixed and the side boundaries were restrained

against displacement perpendicular to the respective sides. The contact surfaces of the pipe and soil ground were tied together. During the consolidation soil step, the excess pore pressure at the top surface of the soil ground was set to zero to allow full drainage.

3.3.2. Numerical results and comparisons

Figure 3-6 shows the numerical predictions in terms of the soil resistances against the pipe at different displacements, compared with the results from the centrifuge tests, previous numerical modelling in C-CORE Report (2003), and recommended values by PRCI (Honegger and Nyman, 2001) and ASCE (1984) guidelines (which were presented in C-CORE Report (2003)). In Figure 3-6, the soil resistance is observed to increase slightly over large pipe displacements, indicating hardening behaviour, for the deeper case, while staying constant for the shallow embedment.

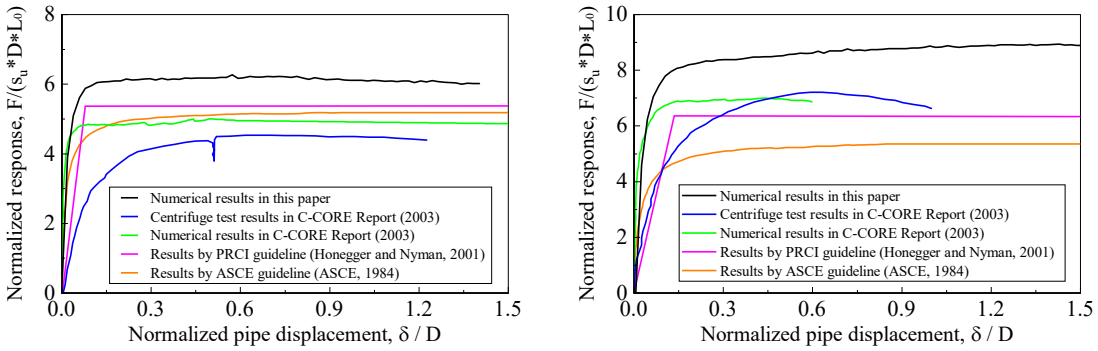

(a) H / D = 1.5, shallow burial case (b) H / D = 3.0, deep burial case

Figure 3-6. Load-displacement responses comparing LDFE results with published experimental and numerical data.

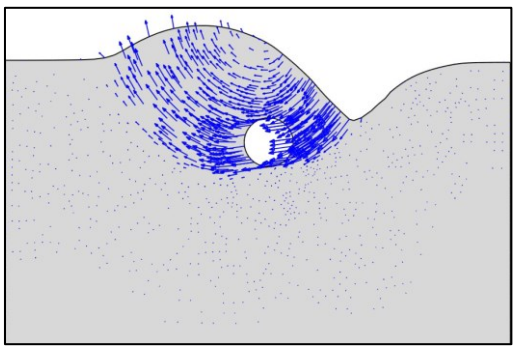

Figure 3-7. Soil deformations for H/D = 1.5.

As shown in Figure 3-7, the laterally displaced pipe pushes the soil to form an elevated surface ahead of the pipe and trough behind, resulting in extra soil weight in front of, and reduced soil weight behind, the pipe. This will tend to increase resistance, particularly for the shallower embedment case, though this may be partly offset by the reducing length of the failure surface. There may also by slight increases in resistance attributable to consolidation, noting that, just as for piezocone dissipation tests, the operative consolidation coefficient is likely 3 to 5 times higher than the oedometer value of 0.38 mm^2/s, particularly as the soil is heavily overconsolidated (Mahmoodzadeh et al., 2014). Assuming the same degree of 'hardening' (due to consolidation) for both embedments, the rising resistance for the deeper embedment is consistent with a reduced effect of the geometry changes observed in Figure 3-7 (see also, later, Figure 3-9).

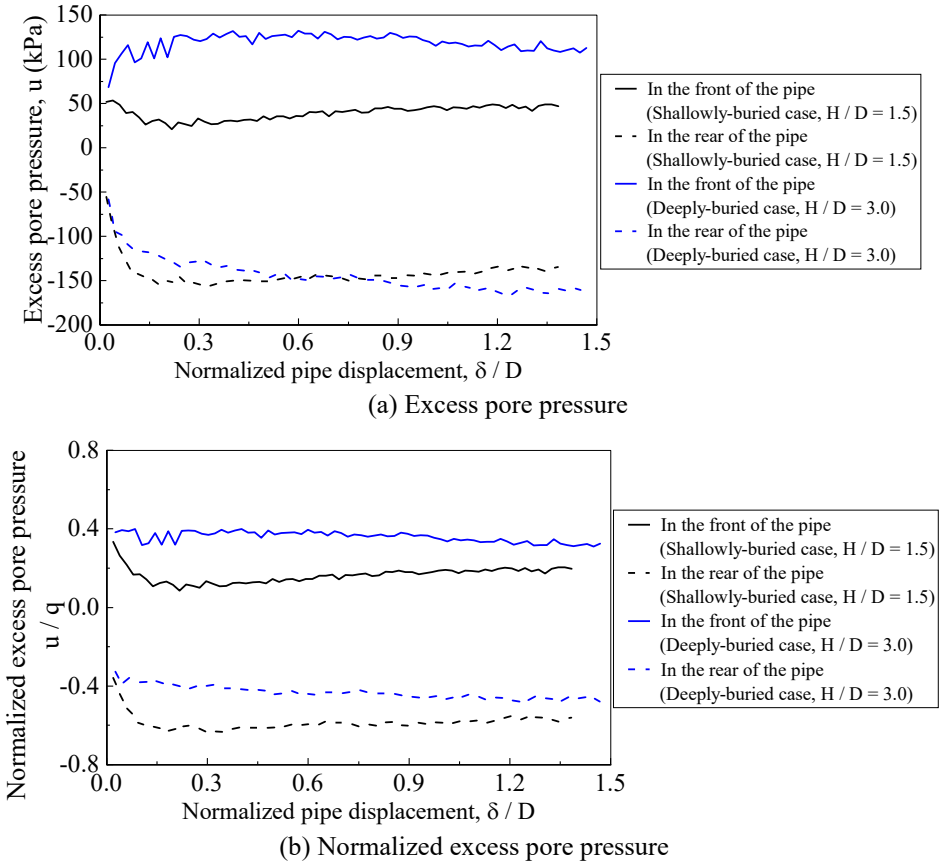

(a) Excess pore pressure

(b) Normalized excess pore pressure

Figure 3-8. Computed excess pore pressures in front and at the rear of the pipe.

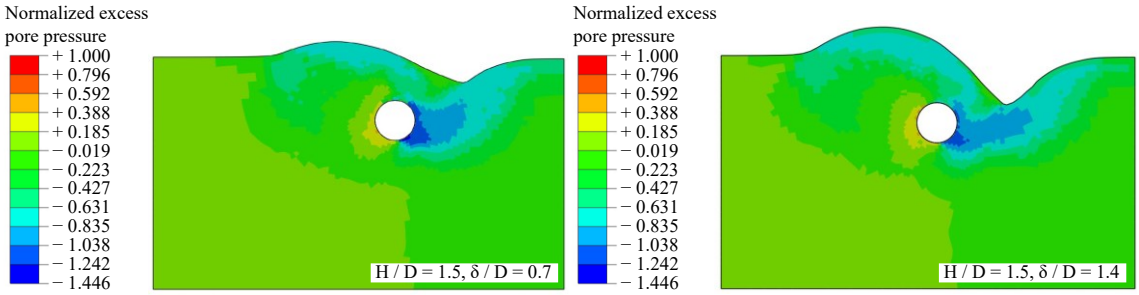

(a) H / D = 1.5, pipe moved by 0.7 D

(b) H / D = 1.5, pipe moved by 1.4 D

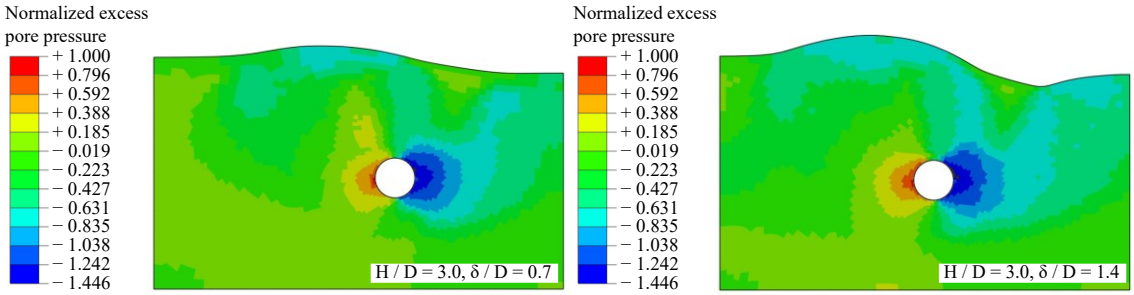

(c) H / D = 3.0, pipe moved by 0.7 D

(d) H / D = 3.0, pipe moved by 1.4 D

Figure 3-9. Normalized excess pore pressure (normalized by excess pore pressure in front of the pipe).

Figure 3-8 a plots the induced excess pore pressures in front and the rear of the pipe, while Figure 3-8 b plots the normalized excess pore pressure with respect to the soil resistance on the pipe as shown in Figure 3-6. With increasing pipe displacement, the normalized excess pore pressures both in front and at the rear of the pipe decrease slightly for the deeply buried case (H/D = 3.0), while increase slightly for the shallowly buried case (H/D = 1.5) (see Figure 3-8). The differences are affected by (a) different changes in soil weight above the pile (greater for the shallower embedment); and (b) slight reductions due to consolidation.

Figure 3-9 shows contours of excess pore pressure induced at two pipe displacements (0.7 D and 1.4 D respectively) for both cases. Comparing Figure 3-9 a and Figure 3-9 b, the distribution of excess pore pressure induced behind the pipe is more significantly affected by

the proximity of the deformed soil surface in the shallowly buried case. The change in excess pore pressure in front of the pipe due to soil heave is also more significant in the shallowly buried case than in the deeply buried case.

3.4. Discussions on effects on drainage condition on pipe-soil interaction

In Section 3, the coupled LDFE framework presented was verified against published data from physical and numerical modelling (C-CORE Report, 2003). In this section, a parametric study is presented and discussed with respect to the influence of drainage conditions on the pipe-soil response, excess pore pressure generation and dissipation, and soil failure mechanisms.

The moving velocity of the pipe, v, can be normalised as

$$V = v \cdot D/c_v \tag{3-14}$$

where c_v is the coefficient of vertical consolidation and given by:

$$c_v = k/(\gamma_w \cdot m_v) \tag{3-15}$$

where m_v is the coefficient of volume compressibility given by (see Appendix):

$$m_v = \frac{1}{K} + B_p \cdot \frac{1}{p'} \tag{3-16}$$

where the mean effective stress p' is obtained from stress tensors at the initial burial depth of the pipe. The undrained shear strength (s_u) of soils with the MCC model may be calculated as (Chai and Carter, 2011):

$$s_u = \frac{p'}{2^{1+\Lambda}} M \left(\frac{M^2+\eta^2}{M^2}\right)^{\Lambda} (OCR)^{\Lambda} \tag{3-17}$$

where parameter Λ is given by $\Lambda = 1 - \frac{\kappa}{\lambda}$, η is the stress ratio q/p and OCR is the over-consolidation ratio of the soil. Details of the computation of undrained shear strength with triaxial compression and plane strain conditions can be found in the appendix.

The geometry of the model is the same as that shown in Figure 3-5, with parameters given in Table 3-4.

Drainage condition can be assessed empirically based on the material coefficient of consolidation and pipe moving rate, with criteria proposed by e.g. House et al. (2001), Randolph and Hope (2004), Lehane et al. (2009). Generally, undrained conditions are maintained when V (based on the oedometer c_v, even though the operative consolidation coefficient may be higher) exceeds about 30, while fully drained conditions is achieved when V is smaller than about 0.10 (in House et al. (2001)) or 0.05 (in Lehane et al. (2009)). Between these limits, partially drained conditions pertain. Some caution is needed with respect to strain rate effects, which are present in the experimental results referred to above but are not modelled here numerically. Without strain rate effects, the undrained limit for V will tend to increase slightly.

A comprehensive parametric study was conducted with respect to pile displacement rate and burial depth ratio, with properties and results summarized in Table 3-3.

Table 3-3. Case studies map.

Burial depth ratio	H/D=1.5			H/D=2.0			H/D=3.0			H/D=3.5		
Displacement rate v (m/s)	Case study	Normalized velocity V	Drainage condition	Case study	Normalized velocity V	Drainage condition	Case study	Normalized velocity V	Drainage condition	Case study	Normalized velocity V	Drainage condition
1.0×10^{-6}	C-1	714	U	C-14	543	U	C-27	368	U	C-40	319	U
5.0×10^{-7}	C-2	357	U	C-15	271	U	C-28	184	U	C-41	159	U
1.0×10^{-7}	C-3	71	U	C-16	54.3	U	C-29	37	U	C-42	32	U
5.0×10^{-8}	C-4	36	U	C-17	27.1	U	C-30	18.4	U	C-43	15.9	U
1.0×10^{-8}	C-5	7.1	P	C-18	5.43	P	C-31	3.7	P	C-44	3.2	P
5.0×10^{-9}	C-6	3.6	P	C-19	2.71	P	C-32	1.8	P	C-45	1.59	P
2.5×10^{-9}	C-7	1.8	P	C-20	1.36	P	C-33	0.92	P	C-46	0.80	P
1.0×10^{-9}	C-8	0.71	P	C-21	0.54	P	C-34	0.37	P	C-47	0.32	P
7.5×10^{-10}	C-9	0.54	P	C-22	0.41	P	C-35	0.28	P	C-48	0.24	P
5.0×10^{-10}	C-10	0.36	P	C-23	0.27	P	C-36	0.18	P	C-49	0.159	P
2.5×10^{-10}	C-11	0.18	P	C-24	0.13	P	C-37	0.09	D	C-50	0.080	D
1.0×10^{-10}	C-12	0.071	D	C-25	0.054	D	C-38	0.037	D	C-51	0.032	D
5.0×10^{-11}	C-13	0.036	D	C-26	0.027	D	C-39	0.018	D	C-52	0.016	D
Note: For drainage conditions, U represents for undrained conditions, P represents for partially drained conditions, and D represents for drained conditions.												

Table 3-4. Parameters used for test example.

Properties		Symbol	Value								Unit
Specific weight of pore fluid		γ_w	10								kN/m^3
Effective unit soil weight		γ	7.5								kN/m^3
Pipe diameter		D	0.95								m
Young's modulus of soil		E	5000								kPa
Poisson's ratio		υ	0.3								-
Initial void ratio		e_0	1.5								-
Coefficient of earth pressure at rest		K_0	0.65								-
Slope of CSL		M_{tc}	0.77								-
Permeability of soil		k_v	10^{-10}								m/s
Properties (*H* refers to the distance from soil surface to pipe centre, while *w* refers to the distance from soil surface to pipe bottom)		Symbol	*H/D*=1.5, *w/D*=2.0		*H/D*=2.0 *w/D*=2.5		*H/D*=3.0, *w/D*=3.5		*H/D*=3.5, *w/D*=4.0		-
			Pipe centre	Pipe bottom	Pipe centre	Pipe bottom	Pipe centre	Pipe bottom	Pipe centre	Pipe bottom	
	Mean effective stress	p'	8.25	11.00		13.75	16.50	19.25		22.00	kPa
	Equivalent stress	q	3.65	4.87		6.09	7.31	8.53		9.75	kPa
	Effective vertical stress	σ_{v0}'	10.69	14.25		17.81	21.38	24.94		28.50	kPa
	Stress ratio	η	0.44	0.44		0.44	0.44	0.44		0.44	-

Triaxial compression (see appendix, equation (3-A.26) – equation (3-A.35), Wroth 1984)	parameter	Λ	0.97	0.96	0.95	0.94	0.93	0.92	-
	Equivalent undrained shear strength	$s_{u,tc}$	2.14	2.87	3.60	4.34	5.08	5.82	kPa
	coefficient of volume compressibility	m_v	0.0080	0.0061	0.0049	0.0041	0.0036	0.0032	m^2/kN
	Coefficient of vertical consolidation	c_v	1.24×10^{-9}	1.64×10^{-9}	2.03×10^{-9}	2.41×10^{-9}	2.79×10^{-9}	3.16×10^{-9}	m^2/s
Compression under plane strain condition (see appendix, equation (3-A.36) – equation (3-	Mean effective stress	s'	8.86	11.81	14.77	17.72	20.67	23.63	kPa
	Equivalent stress	t	1.83	2.44	3.05	3.66	4.26	4.87	kPa
	Effective vertical stress	σ'_{v0}	10.69	14.25	17.81	21.38	24.94	28.50	kPa
	Stress ratio	θ	0.21	0.21	0.21	0.21	0.21	0.21	-
	parameter	Λ	0.97	0.96	0.95	0.94	0.93	0.92	-
	Equivalent undrained shear strength	$s_{u,ps}$	2.22	2.97	3.73	4.50	5.27	6.04	kPa
	coefficient of volume compressibility	m_v	0.0075	0.0057	0.0046	0.0039	0.0034	0.0030	m^2/kN

A.45), Wroth 1984)	Coefficient of vertical consolidation	c_v	1.33×10^{-9}	1.75×10^{-9}	2.17×10^{-9}	2.58×10^{-9}	2.98×10^{-9}	3.37×10^{-9}	m^2/s
Numerical model for plane strain value of $s_{u,ps}$	Equivalent undrained shear strength	$s_{u,ps,numerical,N}$	2.18	3.16	3.97	4.80	5.64	6.48	kPa

Note.

The initial stress state at burial depth (p' , q) and (s' , t) are computed according to equations in appendix and are used as input for calculation in the study cases. $\eta = \frac{q}{p'}$, $\theta = \frac{t}{s'}$, $\Lambda = 1 - \frac{\kappa}{\lambda}$ where $\kappa = \frac{p'(1+e_0)3(1-2\nu)}{E}$ and $\lambda = B_p(1+e_0) + \kappa$ (see Appendix).

$s_{u,NC}$ is calculated by equation (3-A.45). And $c_{v,elastic}$ is calculated by equation (3-15) ignoring the plastic part.

$s_{u,NC,numerical}$ is obtained from the plane strain compression test as described in Appendix.

3.4.1. P-y response

Figure 3-10 gives the lateral resistance, F, normalised by product of $s_u D L_0$ (where pipe length $L_0 = 1$ m for the plane strain conditions considered here), against normalized lateral displacement δ/D, under different drainage conditions and different burial depth ratios. The equivalent undrained shear strength s_u used in Figure 3-10 is $s_{u,ps}$ with the properties listed in Table 3-4 (see Appendix for the computation of $s_{u,ps}$, the value of $s_{u,tc}$ and $s_{u,ps,numerical}$ are listed as well for reference).

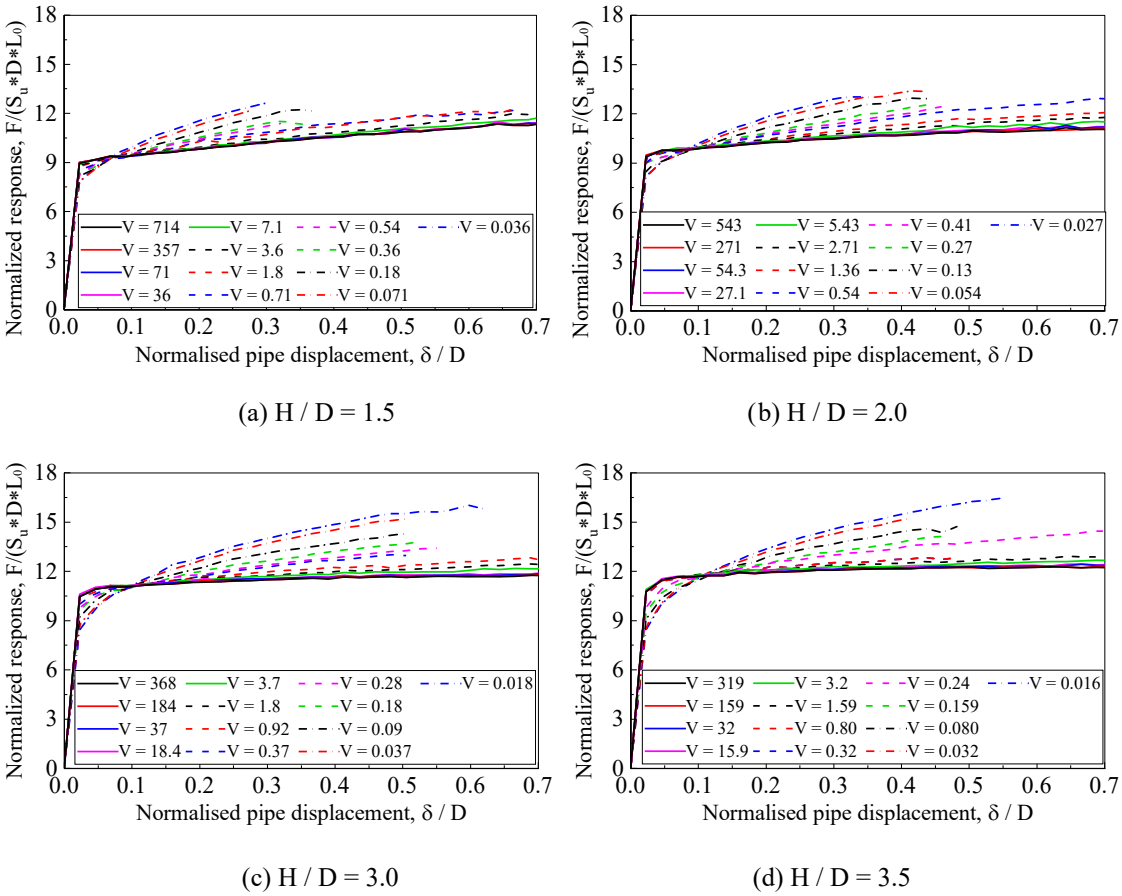

(a) H / D = 1.5

(b) H / D = 2.0

(c) H / D = 3.0

(d) H / D = 3.5

Figure 3-10. Normalized response under different drainage conditions.

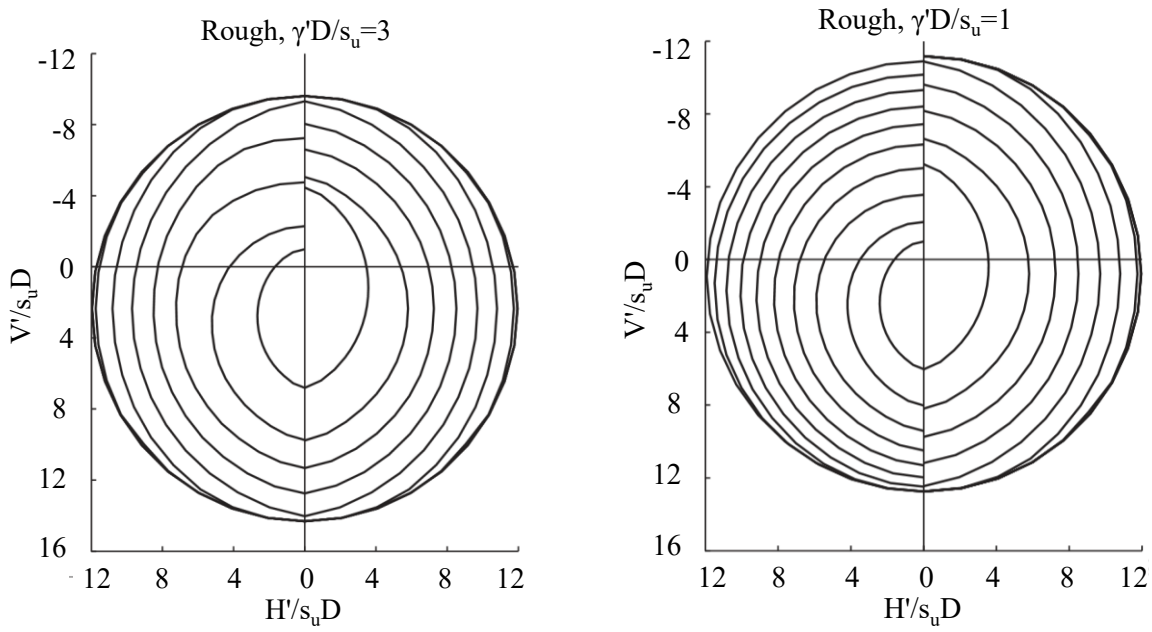

(a) $\gamma' D/s_u$=3 (b) $\gamma' D/s_u$=1

Figure 3-11. V-H failure envelopes for pipes in soil with uniform s_u in Martin and White (2012) (from inside to outside, embedment *w/D* = 0.5 to 5 at intervals of 0.5).

Under undrained conditions, the soil resistance levels off with increasing pipe moving displacement for the deepest embedment case, with the ultimate bearing capacity coefficient a bit higher than the results in Martin and White (2012) (i.e., approximately 10.91 in Figure 3-10 a versus 8.57 in Figure 3-11a for *w/D*=2.0, 11.02 in Figure 3-10 b versus 9.58 in Figure 3-11 a for *w/D*=2.5, 11.79 in Figure 3-10 c versus 11.83 in Figure 3-11 a for *w/D*=3.5; 12.23 in Figure 3-10 d versus 11.72 in Figure 3-11 b for *w/D*=4.0). However, the resistance keeps increasing for the shallowest embedment, reflecting the significant soil heave at the ground surface and noting that the effect of out of balance soil weight will be much more pronounced for these normally consolidated conditions

compared with the heavily over consolidated case considered in Figure 3-6. For cases with partially or fully drained conditions, however, hardening with increasing pipe displacement is evident due to increasing effective stresses and soil strength ahead of the pipe.

The ultimate capacity, for consistency taken at a pipe displacement of $\delta/D = 0.3$, may be plotted as a function of the normalised velocity $V = vD/c_{v0}$ (where c_{v0} is the initial consolidation coefficient – see Table 3-4).

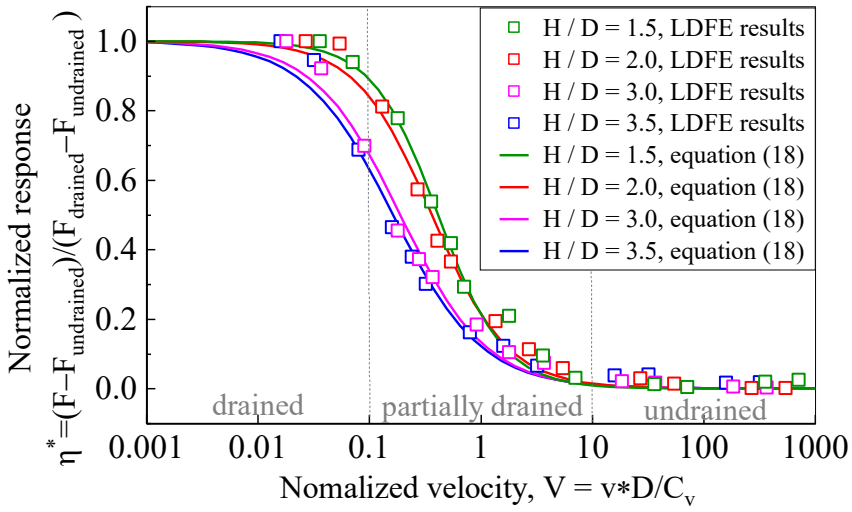

Figure 3-12. Normalized response ratios under different drainage conditions (based on responses at $\delta / D = 0.31$).

Figure 3-12 shows the resulting normalized ultimate resistances as a function of normalized velocity for the different depth ratios considered, together with fitted backbone curves. The normalized ultimate resistances increase with the burial depth ratio and decreasing normalised velocity, with the transition from undrained to partially drained conditions occurring at approximately similar normalized velocity of $V \sim 10$ for each burial depth.

However, the transition to fully drained conditions occurs at a lower normalized velocity for the two deepest embedment.

It is convenient to normalize the ultimate resistance with respect to the two limits under undrained and drained conditions according to

$$\frac{F - F_{undrained}}{F_{drained} - F_{undrained}} = \eta^* = \frac{1}{1 + (V/V_{50})^c} \quad (3\text{-}18)$$

where V_{50} is the normalized velocity for midway between the drained and undrained limits and c is a power that controls the abruptness of the transition. The actual resistance may then be expressed as

$$F = F_{undrained} + \eta^*(F_{drained} - F_{undrained}) \quad (3\text{-}19)$$

The finite element data in Figure 3-12 have been fitted by functions for η^* at each embedment depth, with best-fit values of V_{50} and c listed in Table 3-5. As noted above, V_{50} tends to decrease, while c tends to reduce (less abrupt transition), with increasing burial depth ratio of pipe (H/D).

Table 3-5. Curve fitting in Figure 3-12.

Coefficients in curves fitting		Burial depth ratio			
		H/D=1.5	H/D=2	H/D=3	H/D=3.5
$\eta^* = \frac{F - F_{undrained}}{F_{drained} - F_{undrained}} = f_1(V)$	V_{50}	0.4143	0.3643	0.1902	0.1636
Equation (18) for curve fitting: $f_1(V) = \frac{1}{1 + (V/V_{50})^c}$ (see Figure 3-12)	c	1.476	1.285	1.127	1.091

3.4.2. Failure mechanisms

The excess pore pressure (normalized by pressure on pipe $q = F/DL_0$) induced in the front and rear of the pipe under different drainage conditions are shown in Figure 3-13.

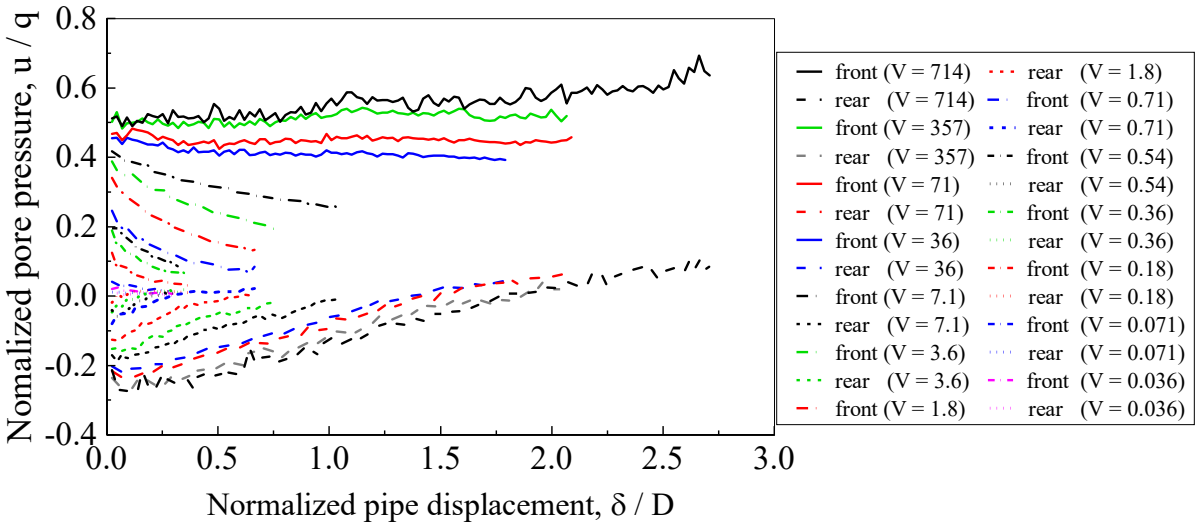

(a) H / D = 1.5

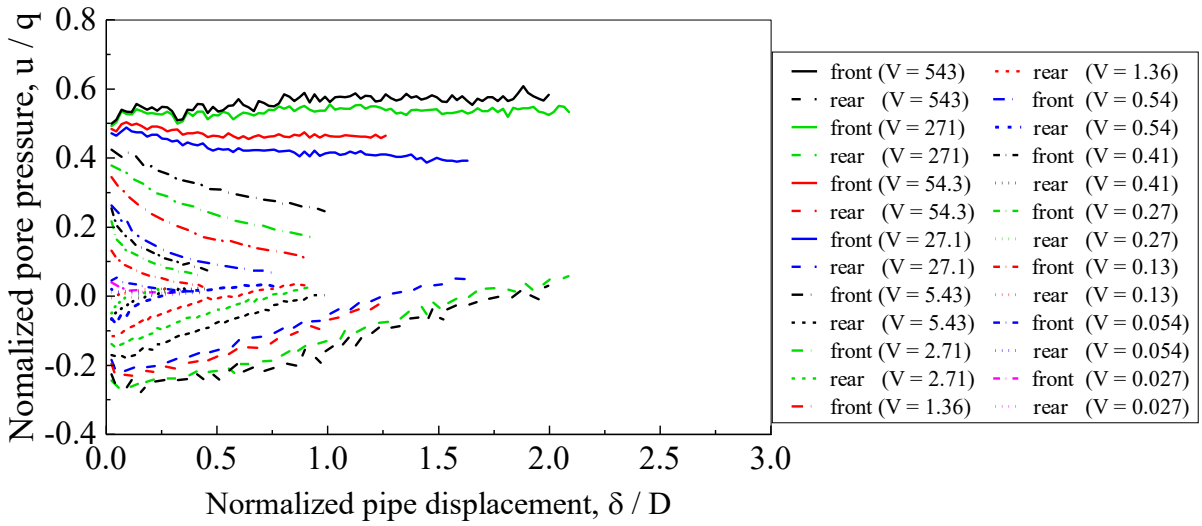

(b) H / D = 2.0

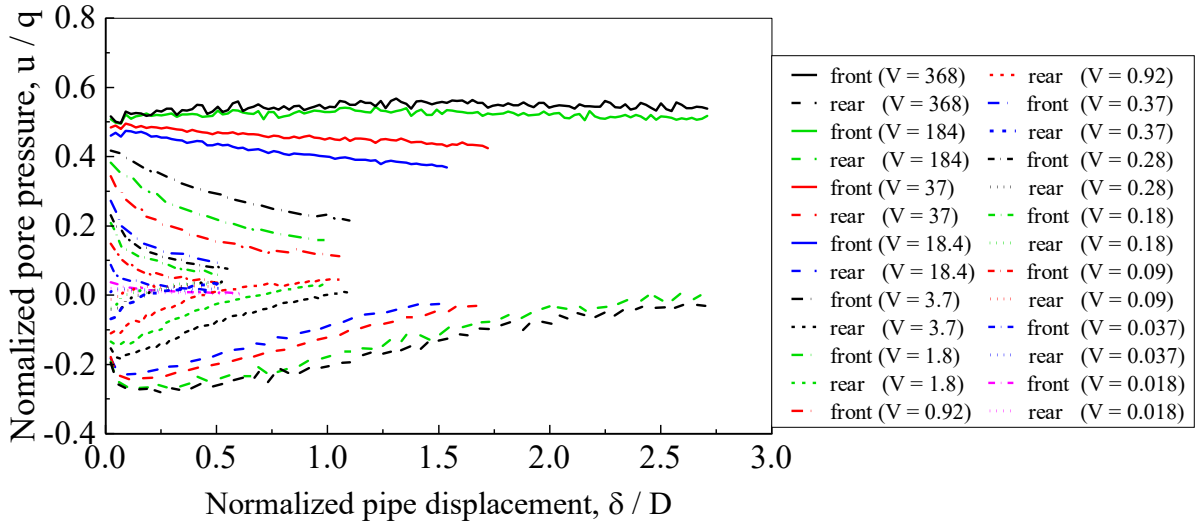

(c) H / D = 3.0

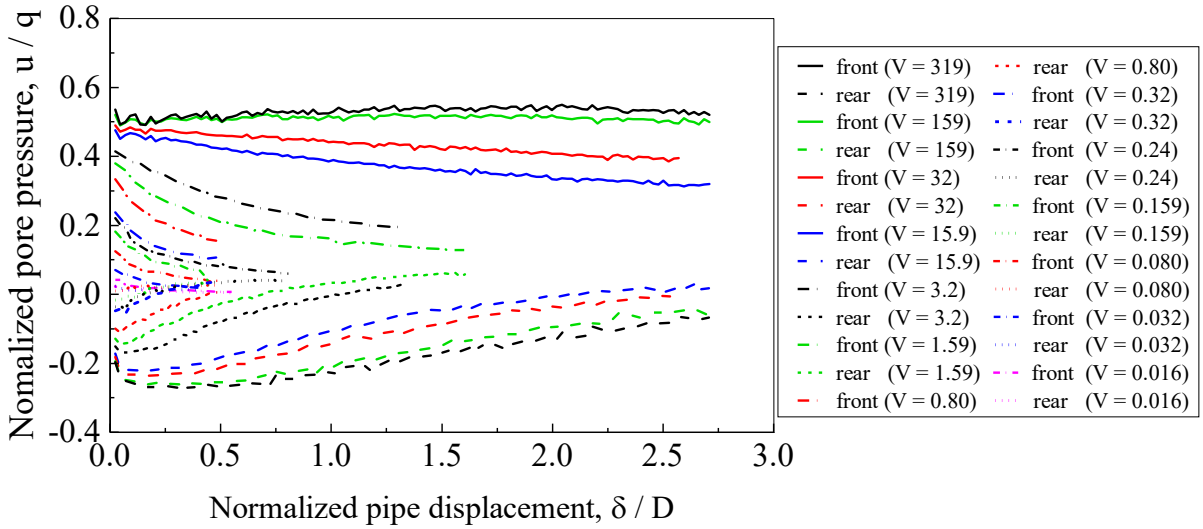

(d) H / D = 3.5

Figure 3-13. Normalized excess pore pressure induced in the front and in the rear of the pipe in tests under different drainage conditions.

Negative excess pore pressure is induced in the rear of the pipe reflecting suction resistance on the pipe. However, the magnitude of induced excess pore pressures in the rear of the

pipe is much lower than that in front of the pipe. Also, it may be observed that the magnitude of the excess pore pressures in front of the pipe remains almost constant with increasing pipe displacement for fully undrained conditions (V greater than 100); however, in the rear of the pipe, the magnitude of negative excess pore pressures decreases with increasing pipe displacement, even for undrained conditions. This may be attributed to the increasing proximity of the permeable soil surface in the rear of the pipe, which reduces the drainage path and hence allows drainage. This is more pronounced for the shallower embedment cases.

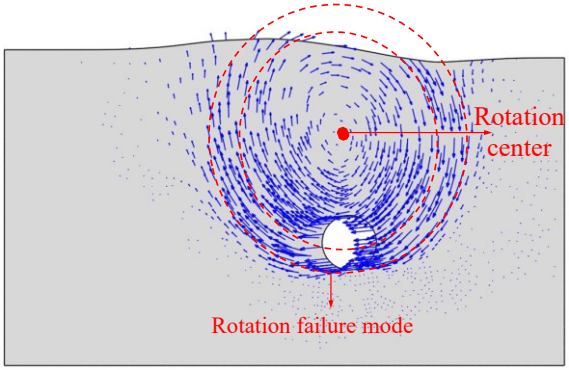

(a) Undrained condition (V = 319, δ / D = 0.31)

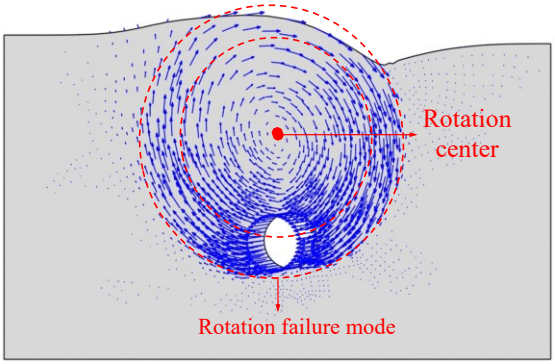

(b) Undrained condition (V = 319, δ / D = 1.41)

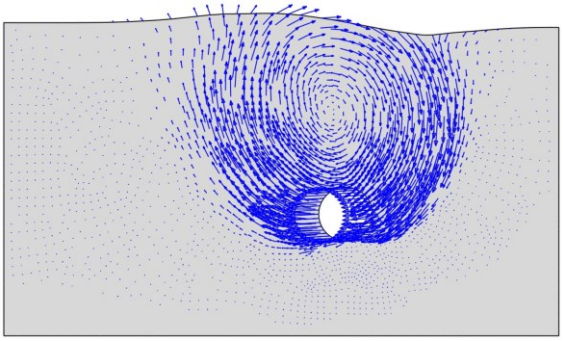

(c) Partially drained condition (V = 3.2, δ / D = 0.31)

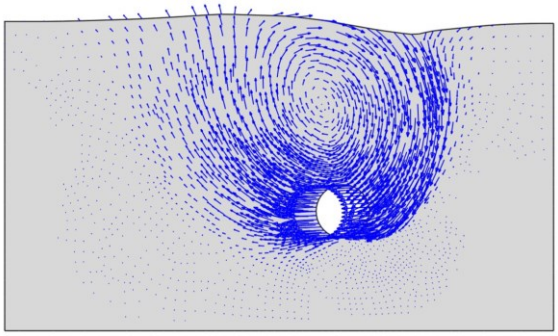

(d) Partially drained condition (V = 0.32, δ / D = 0.31)

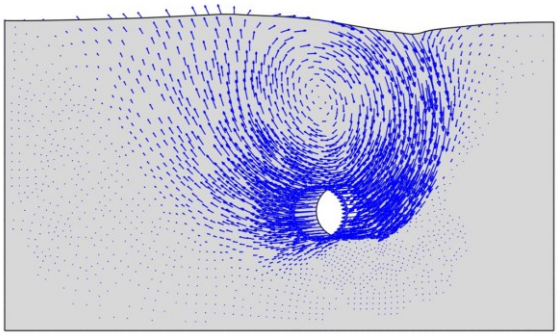

(e) Partially drained condition (V = 0.159, δ / D = 0.31)

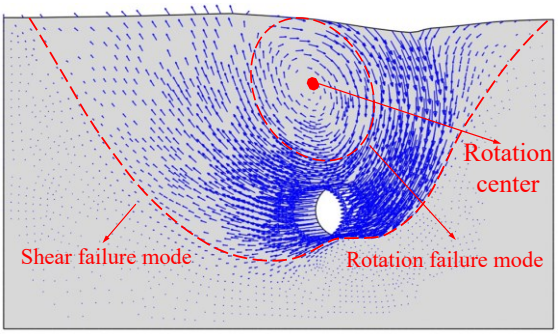

(f) Drained condition (V = 0.016, δ / D = 0.31)

Figure 3-14. Comparisons among displacement vectors under different interaction rates (burial depth ratio H/D = 3.5).

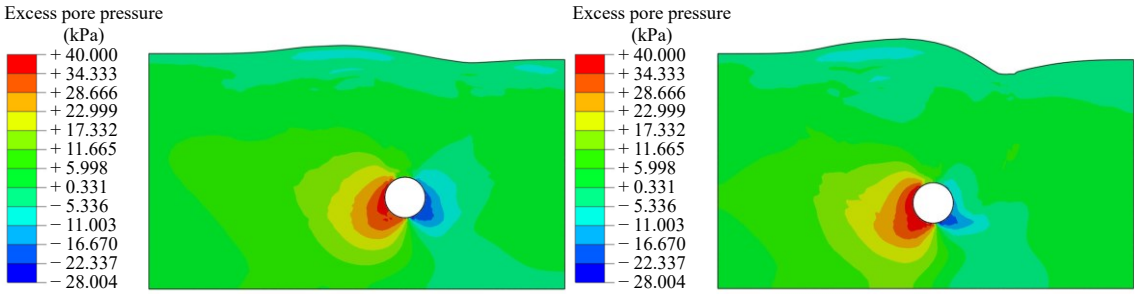

(a) Undrained condition (V = 319, δ / D = 0.31) (b) Undrained condition (V = 319, δ / D = 1.41)

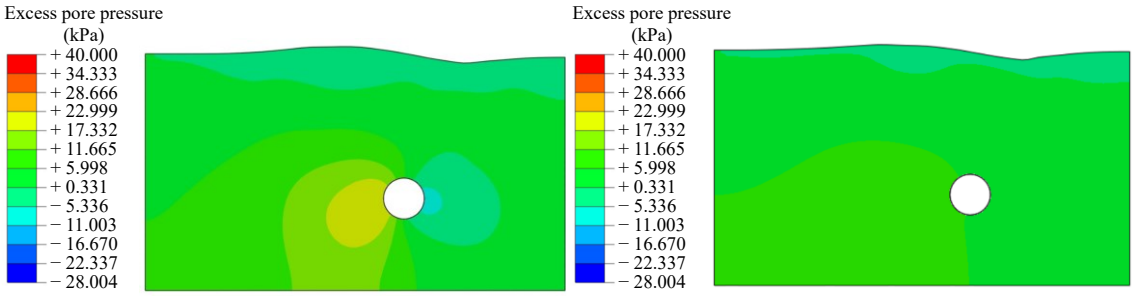

(c) Partially drained condition (V = 3.2, δ / D = 0.31) (d) Partially drained condition (V = 0.32, δ / D = 0.31)

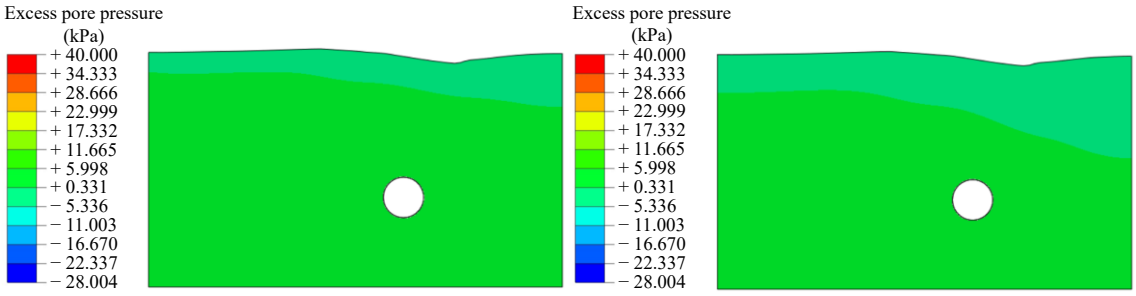

(e) Partially drained condition (V = 0.159, δ / D = 0.31) (f) Drained condition (V = 0.016, δ / D = 0.31)

Figure 3-15. Induced excess pore pressure under different interaction rates.

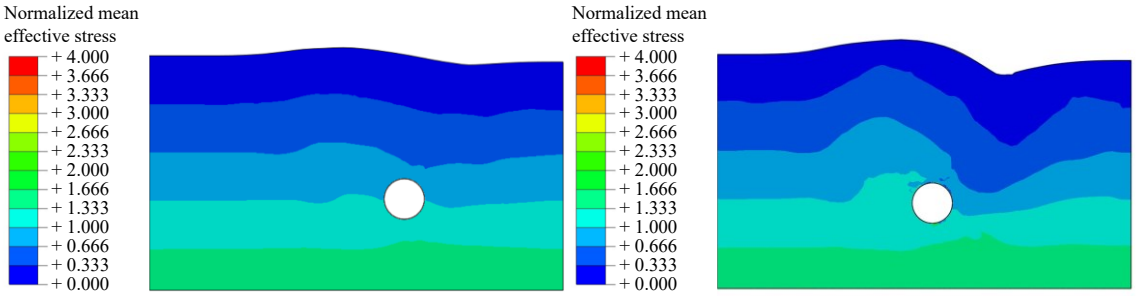

(a) Undrained condition (V = 319, δ / D = 0.31) (b) Undrained condition (V = 319, δ / D = 1.41)

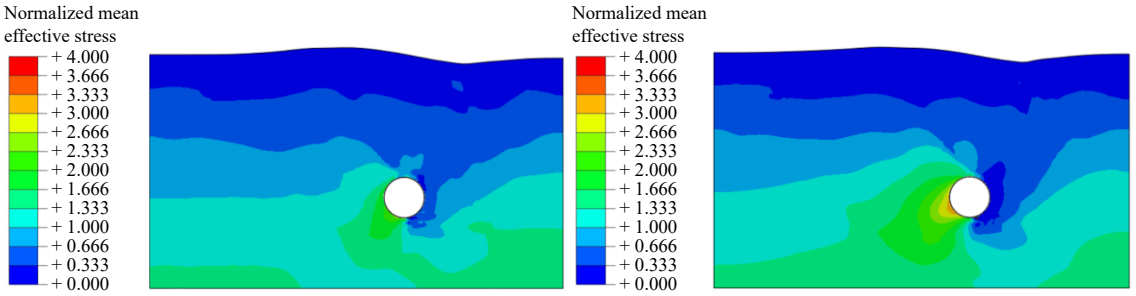

(c) Partially drained condition (V = 3.2, δ / D = 0.31) (d) Partially drained condition (V = 0.32, δ / D = 0.31)

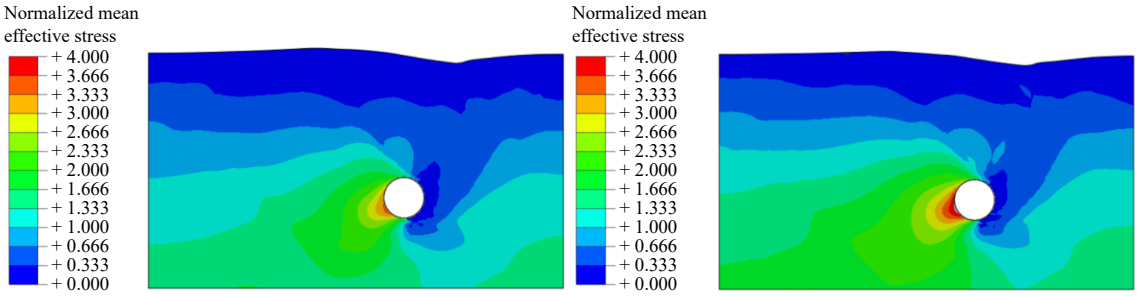

(e) Partially drained condition (V = 0.159, δ / D = 0.31) (f) Drained condition (V = 0.016, δ / D = 0.31)

Figure 3-16. Normalized mean effective stress (normalized by initial mean effective stress in front of the pipe) under different interaction rates.

Fields of displacement vectors, normalized excess pore pressures, and normalized mean effective stress (normalized by the initial mean effective stress in front of the pipe) are

shown in Figure 3-14, Figure 3-15 and Figure 3-16, respectively, for all cases of different pipe displacement rates.

The heave in front of the pipe and depression in the rear of the pipe become more significant with increasing pipe displacement rate. From Figure 3-14, two distinct failure types may be observed: for undrained with high pipe moving rates (V=319, H/D=3.5) and the partial drainage conditions (V=3.2, H/D=3.5), rotational failure dominates with the rotation centre of displacement vectors located above the pipe forming a vortex (as shown in Figure 3-14a and Figure 3-14b); for drained conditions with low pipe moving rates (V=0.016, H/D=3.5), active and passive shear failures to the soil surface are also apparent, in addition to the rotation failure mode (as shown in Figure 3-14f), which extends the deformed soil body markedly. The transition of the failure modes from undrained (Figure 3-14a) to drained (Figure 3-14f) conditions may be observed in the sub-plots for partially drained conditions (from Figure 3-14b to Figure 3-14e). Also, with further penetration of pipe and soil heave in front of the pipe, the rotational failure mode becomes more significant (compare Figure 3-14a and Figure 3-14b).

Excess pore pressures induced by displacement of the pipe are shown in Figure 3-15. While the interaction rates decrease from undrained condition with high pipe moving rates (V=319, H/D=3.5) to drained condition with low pipe moving rates (V=0.016, H/D=3.5), the excess pore pressure in the rear of the displaced pipe becomes less significant.

As shown in Figure 3-16f with low pipe moving rates (V=0.016, H/D=3.5), high mean effective stress at front of (lower side) the pipe was observed, while low mean effective stress shown behind (upper side) the pipe.

3.5. Conclusions

Two-dimensional coupled large deformation finite element (LDFE) analyses using the remeshing and interpolation technique with small strain were conducted to observe failure mechanisms and soil responses resulting from lateral displacement of a pre-buried pipe at different depth ratios and different displacement rates. A Modified Cam-clay model developed by Lagioia and Nova (1995) and improved by Panteghini and Lagioia (2018a, 2018b) was incorporated into the LDFE analysis, with an advanced integration scheme. The coupled LDFE framework developed, working with the MCC model (Lagioia and Nova, 1995; Panteghini and Lagioia,2018a, 2018b), was verified through a simple one-dimensional consolidation analysis. The LDFE model was then applied to the large lateral displacement of a buried pipe in clay to investigate the effect of partial consolidation conditions on the lateral force-displacement response and failure mechanisms. The predicted load-displacement curves from the coupled LDFE analyses match well with the centrifuge test. Following key observations were made:

- Under undrained conditions, the soil resistance quickly levels off with the increase of pipe displacement for deeply buried case with the ultimate bearing capacity coefficient being around 10.0; while it keeps growing in shallowly buried case due to the significant soil heave at the ground surface. For cases with partially or fully drained conditions, however, hardening phenomenon is obvious with the increase of pipe displacement due to the dissipation of excess pore pressure. The ultimate resistance in test under drained conditions is observed to be larger than the ultimate load obtained in tests with same configurations under undrained conditions.

- Different failure mechanisms were observed between tests with different drainage conditions. For the cases with undrained condition (i.e. high interaction rates), rotation failure mode is dominant with the rotation centre of displacement vectors located above the pipe forming a vortex. For drained conditions with low pipe moving rates, shear failure mode occurs which greatly extends the deformed soil body, in addition to the rotation failure mode. Cases with partial drainage conditions are in the transition with respect to the formation of shear failure mode.
- The different magnitudes in the increase of mean effective stress at front of the pipe from the same initial value under different drainage conditions were in good accordance with the induced excess pore pressure obtained. In drained condition, the interaction rate was slow enough to let the excess pore pressure fully dissipated and stress was taken mainly by the soil skeleton. While in undrained conditions, it has the highest magnitude of excess pore pressure and lowest increase in mean effective stress in front of the pipe.

It is worth mentioning that subsea pipelines are usually trenched and buried in shallow waters for physical protection against the environmental, operational, and accidental loads. The different stiffness of the pre-excavated backfilling material and the native ground could have a significant impact on the failure mechanisms of the surrounding soil and consequently on the lateral soil resistance. This challenging area needs further investigations that are currently going on by the authors through the incorporation of the developed LDFE framework into the large deformation analysis of lateral pipeline-backfill-trench interaction.

3.6. Acknowledgments

The authors gratefully acknowledge Dr. Rocco Lagioia and Dr. Andrea Panteghini for their valuable help on the user-coded Modified Cam-Clay model. And the authors sincerely acknowledge the financial support of "Wood Group," that established a Research Chair program in Arctic and Harsh Environment Engineering at Memorial University of Newfoundland, the "Natural Science and Engineering Research Council of Canada (NSERC)", and the "Newfoundland Research and Development Corporation (RDC) (now InnovateNL)" through "Collaborative Research and Developments Grants (CRD)". Also, the Authors acknowledge the visiting research funding provided by Mitacs through Globalink program and also the Center of Offshore Foundation Systems and the University of Western Australia for providing the visiting opportunity and collaboration. Special thanks are also extended to Memorial University for providing excellent resources to conduct this research.

3.7. Appendix

3.7.1. Determination of $\mathbf{m_v}$ and $\mathbf{B_p}$

Hardening parameter B_p is defined as the slope of $\ln(p') - \varepsilon_v^p$ curve (Lagioia and Nova, 1995) (where ε_v^p is the plastic volumetric strain and p' is the mean effective stress), which is given by:

$$B_p = \frac{\partial \varepsilon_v^p}{\partial p'} \cdot p' \tag{3−A.1}$$

The bulk modulus K is calculated as:

$$\frac{1}{K} = \frac{\partial \varepsilon_v^e}{\partial p'} = \frac{\partial e}{(1+e_0)} \cdot \frac{1}{\partial p'} \rightarrow \frac{\partial e}{\partial p'} = \frac{1+e_0}{K} \tag{3−A.2}$$

where ε_v^e is the elastic volumetric strain and e_0 is the initial void ratio. The coefficient of volume compressibility is calculated as:

$$m_v = \frac{\partial \varepsilon_v}{\partial p'} = \frac{\partial \varepsilon_v^e}{\partial p'} + \frac{\partial \varepsilon_v^p}{\partial p'} \tag{3−A.3}$$

where the total volumetric strain ε_v consists of the elastic volumetric strain ε_v^e and plastic volumetric strain ε_v^p. Substituting (3-A.1) and (3-A.2) into (3-A.3) gives

$$m_v = \frac{B_p}{p'} + \frac{1}{K} \tag{3−A.4}$$

For conventional MCC model, the slope of the swelling line, κ, is calculated as:

$$\kappa = \frac{\partial e}{\partial p'} \cdot p' \tag{3−A.5}$$

where e is the void ratio. The slope of the normal consolidation line, λ, is calculated as:

$$\lambda = \frac{\partial e_y}{\partial p'} \cdot p' \tag{3−A.6}$$

where e_y is the void ratio in the current yield state.

Substituting (3-A.2) into (3-A.5) gives

$$\frac{\kappa}{p'} = \frac{1 + e_0}{K} \tag{3−A.7}$$

which relates the slope of welling line κ to the bulk modulus K.

Considering $\frac{\partial \varepsilon_v}{\partial p'} = \frac{\partial e_y}{(1+e_0)} \cdot \frac{1}{\partial p'}$ and equations (3-A.1) to (3-A.3) and (3-A.7), (3-A.6) can be re-written as

$$\frac{\lambda}{p'} = \frac{1 + e_0}{K} + \frac{(1 + e_0)B_p}{p'} \rightarrow B_p = \frac{\lambda - \kappa}{(1 + e_0)} \tag{3−A.8}$$

3.7.2. Determination of s_u

3.7.2.1. Theoretical Value

The yield function of the constitutive model is defined in terms of stress invariants. It is a generalized form of the Modified Cam Clay model by retaining its mathematical advantages. The new characteristic of the proposed yield function is to provide a wide range of choices of shapes. One additional parameter introduced for defining the meridional section shape makes it convenient to control the relative position of the normal compression and critical state lines. In the deviatoric plane the function is chosen to be the exact shape of the classical failure criterion, i.e. Matsuoka-Nakai criterion is used here.

The calculation of undrained shear strength under triaxial compression and plane strain conditions was published by Wroth (1984) and the key points were briefly summarized in this appendix.

To relate the plane strain conditions friction angle ϕ_{ps} and the triaxial compression conditions friction angle ϕ_{tc}, Satake (1982) shown that ϕ_{ps} is the maximum value among all possible ϕ providing using the Matsuoka-Nakai criterion with an associated flow rule. By finding the maximum value of the ratio σ_1'/σ_3' (i.e., the maximum value of ϕ) for one octahedral plane, it can be shown that ϕ_{ps} ($\equiv \phi_{max}$) can be expressed by

$$\sec^2\phi_{ps} + \sec\phi_{ps} = 2\sec^2\phi_{tc} \qquad (3\text{−A.9})$$

The relationships of equations (3-A.10) can be approximated for engineering purposes by linear relationships

$$8\phi_{ps}^{\circ} \approx 9\phi_{tc}^{\circ} \qquad (3\text{−A.10})$$

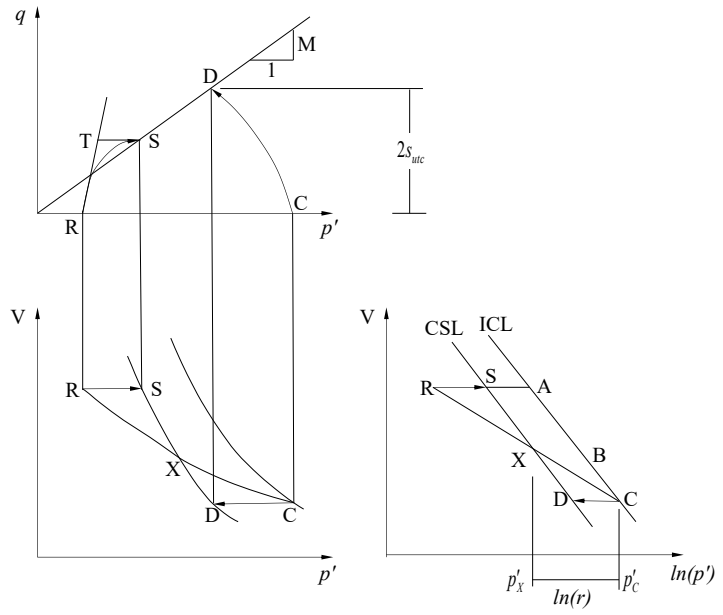

(a) Isotropically consolidated soil

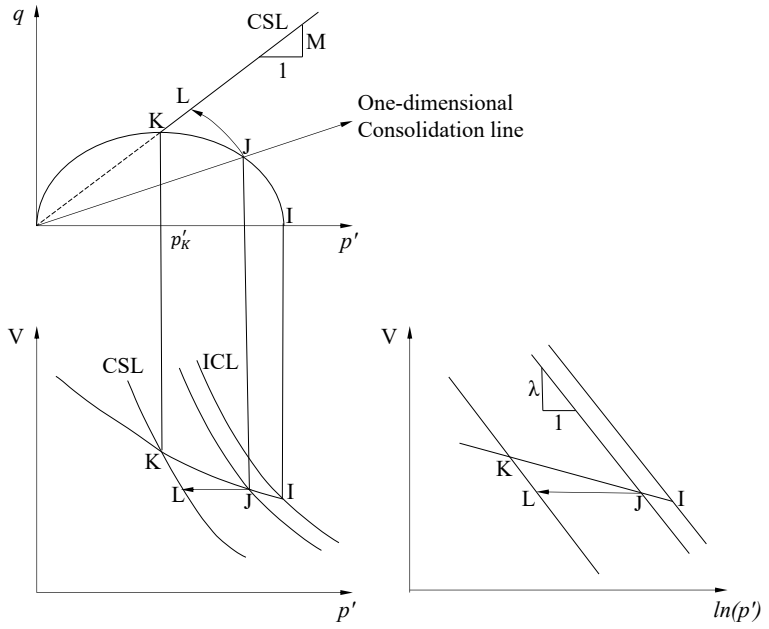

(b) One-dimensionally consolidated soil

Figure 3-A.1. Theoretical expressions for undrained shear strength in triaxial compression tests (Wroth, 1984).

The undrained triaxial compression tests are represented in Figure 3-A.. Point C represents for the initially normally consolidated soil and it undergoes the effective stress path CD during the triaxial compression. Point R represents the over-consolidated soil and follows the path RS during the triaxial compression. Point D and point S are the undrained failure points on the critical state line (CSL) for point C and R respectively. The CSL line is assumed to be parallel to the isotropic normal consolidation line (ICL) in the semi log-plot. Assuming point C and point R lie on the same swelling line CXR.

The over consolidation ratio (OCR) is represented by:

$$OCR = p'_C/p'_R \tag{3−A.11}$$

'Spacing ratio' r of the ICL and CSL is

$$r = p'_C/p'_X \tag{3−A.12}$$

And for modified Cam clay model, $r = 2$.

Since points A and C lie on the normal consolidation line,

$$V_A - V_C = \lambda \ln(p'_C/p'_A) \tag{3−A.13}$$

Points R and C lie on a swelling line (SL)

$$V_R - V_C = \kappa \ln(p'_C/p'_R) = \kappa \ln OCR \tag{3−A.14}$$

Since $V_R \equiv V_A$, equation (3-A.14) can be changed to

$$\lambda \ln(p'_C/p'_A) = \kappa \ln OCR \tag{3−A.15}$$

Points S and X lie on the CSL, so

$$\lambda \ln(p'_X/p'_S) = \kappa \ln(p'_X/p'_R) \tag{3−A.16}$$

Subtraction of both sides from $\lambda \ln(p'_X/p'_R)$

$$\lambda \ln(p'_S/p'_R) = (\lambda - \kappa)\ln(p'_X/p'_R) \quad (3\text{–A.17})$$

That is

$$\lambda \ln(p'_S/p'_R) = (\lambda - \kappa)\ln(OCR/r) \quad (3\text{–A.18})$$

i.e.

$$\Lambda = \frac{\lambda - \kappa}{\lambda} \quad (3\text{–A.19})$$

$$\frac{p'_S}{p'_R} = \left(\frac{OCR}{r}\right)^{\Lambda} \quad (3\text{–A.20})$$

The undrained shear strength in compression is half of the deviator stress at failure

$$s_{u,tc} = \frac{1}{2} q_S = \frac{1}{2} M p'_S \quad (3\text{–A.21})$$

Where for triaxial compression

$$M = \frac{6\sin\phi_{tc}}{3 - \sin\phi_{tc}} \quad (3\text{–A.22})$$

Substituting for p'_S with equation (3-A.12) gives

$$\frac{s_{u,tc}}{p'_R} = \frac{M}{2}\left(\frac{OCR}{r}\right)^{\Lambda} \quad (3\text{–A.23})$$

The expression is valid for specimens that have been isotopically consolidated. At the start of the compression test $\sigma'_{v0} \equiv p'_R$. Then

$$\frac{s_{u,tc}}{\sigma'_{v0}} = \frac{M}{2}\left(\frac{OCR}{r}\right)^{\Lambda} \quad (3\text{–A.24})$$

Besides, for isotopically normally consolidated clay tested in plane strain conditions the undrained strength ratio would be

$$\frac{s_{u,ps}}{\sigma'_{v0}} = \sin\phi_{ps}\left(\frac{1}{2}\right)^{\Lambda} \quad (3\text{–A.25})$$

For one dimensional consolidated soil under compression tests, its undrained shear strength can be derived as from equation (3-A.26) to equation (3-A.35).

Equation of the MCC elliptical yield envelope is

$$q^2 + M^2 p'^2 = 2M^2 p'_K p' \tag{3−A.26}$$

When the specimen is normally consolidated at state J and the coefficient of earth pressure at rest is given by

$$K_0 \approx 1 - \sin\phi_{tc} \tag{3−A.27}$$

The ratio of stresses at J is calculated as

$$\eta_J = \frac{q_J}{p'_J} = \frac{3(1-K_0)}{1+2K_0} = \frac{3\sin\phi_{tc}}{3-2\sin\phi_{tc}} \tag{3−A.28}$$

Since point J lie on the yield envelope and therefore satisfy equation (3-A.26)

$$\left(\eta_J^2 + M^2\right) p'^2_J = 2M^2 p'_K p'_J \tag{3−A.29}$$

An undrained compression test will bring the specimen to failure at point L on the CSL at the same specific volume, thus

$$s_{u,tc} = \frac{1}{2} q_L = \frac{M}{2} p'_L \tag{3−A.30}$$

Like equation (3-A.20)

$$\frac{p'_L}{p'_J} = \left(\frac{p'_K}{p'_J}\right)^{\Lambda} \tag{3−A.31}$$

According to equation (3-A.29)

$$\frac{p'_K}{p'_J} = \frac{\eta_J^2 + M^2}{2M^2} \tag{3−A.32}$$

According to equation (3-A.22) and (3-A.28)

$$\frac{\eta_J}{M} = \frac{3\sin\phi_{tc}}{3-2\sin\phi_{tc}} \frac{3-\sin\phi_{tc}}{6\sin\phi_{tc}} = \frac{3-\sin\phi_{tc}}{2(3-2\sin\phi_{tc})} \tag{3−A.33}$$

Besides

$$\frac{p'_J}{\sigma'_{1J}} = \frac{1+2K_0}{3} = \frac{3-2\sin\phi_{tc}}{3} \tag{3−A.34}$$

Therefore

$$\begin{aligned}
\frac{s_{u,tc}}{\sigma'_{1J}} &= \frac{s_{u,tc}}{p'_L}\frac{p'_L}{p'_J}\frac{p'_J}{\sigma'_{1J}} = \frac{\frac{M}{2}p'_L}{p'_L}\left(\frac{p'_K}{p'_J}\right)^{\Lambda}\frac{3-2\sin\phi_{tc}}{3} \\
&= \frac{M}{2}\left(\frac{\eta_J^2+M^2}{2M^2}\right)^{\Lambda}\frac{3-2\sin\phi_{tc}}{3} \\
&= \frac{M}{2}\left[\frac{1}{2}\left(\frac{\eta_J}{M}\right)^2+\frac{1}{2}\right]^{\Lambda}\frac{3-2\sin\phi_{tc}}{3} \\
&= \frac{1}{2}\frac{6\sin\phi_{tc}}{3-\sin\phi_{tc}}\left\{\frac{1}{2}\left[\frac{3-\sin\phi_{tc}}{2(3-2\sin\phi_{tc})}\right]^2+\frac{1}{2}\right\}^{\Lambda}\frac{3-2\sin\phi_{tc}}{3} \\
&= \frac{\sin\phi_{tc}(3-2\sin\phi_{tc})}{3-\sin\phi_{tc}}\left\{\frac{1}{8}\left(\frac{3-\sin\phi_{tc}}{3-2\sin\phi_{tc}}\right)^2+\frac{1}{2}\right\}^{\Lambda}
\end{aligned} \tag{3−A.35}$$

And the compression test carried out under plane strain condition can be explored similarly (see from equation (3-A.36) to (3-A.45)). Stress variables p' and q are replaced by $s' = \frac{1}{2}(\sigma'_1+\sigma'_3)$ and $t = \frac{1}{2}(\sigma'_1-\sigma'_3)$, and ϕ_{tc} replaced by ϕ_{ps} for failure condition. The approximation of $K_0 \approx 1-\sin\phi_{tc}$ is used here.

Thus, we have the ratio of stresses calculated as

$$\theta_J = \frac{t_J}{s'_J} = \frac{1-K_0}{1+K_0} = \frac{\sin\phi_{tc}}{2-\sin\phi_{tc}} \tag{3−A.36}$$

For elementary tests (triaxial or plane strain)

$$\frac{\sigma_1 - \sigma_3}{2} = \frac{\sigma_1 + \sigma_3}{2}\sin\phi \tag{3−A.37}$$

Since J lies on the yield envelope

$$\left(\theta_J^2 + m^2\right)s_J'^2 = 2m^2 s_K' s_J' \tag{3−A.38}$$

Where

$$m = \sin\phi_{ps} \tag{3−A.39}$$

and

$$s_{u,ps} = t_L = m s_L' \tag{3−A.40}$$

Like equation (3-A.31)

$$\frac{s_L^{'}}{s_J^{'}} = \left(\frac{s_K^{'}}{s_J^{'}}\right)^{\Lambda} \tag{3−A.41}$$

From equation (3-A.38)

$$\frac{s_K'}{s_J'} = \frac{\theta_J^2 + m^2}{2m^2} \tag{3−A.42}$$

Combine equation (3-A.36) and equation (3-A.39)

$$\frac{\theta_J}{m} = \frac{\frac{\sin\phi_{tc}}{2 - \sin\phi_{tc}}}{\sin\phi_{ps}} = \frac{\sin\phi_{tc}}{\sin\phi_{ps}(2 - \sin\phi_{tc})} \tag{3−A.43}$$

Besides

$$\frac{s_J'}{\sigma_{1J}'} = \frac{1 + K_0}{2} = \frac{2 - \sin\phi_{tc}}{2} \tag{3−A.44}$$

Therefore

$$\frac{s_{u,ps}}{\sigma_{1J}^{'}} = \frac{s_{u,ps}}{s_L^{'}}\frac{s_L^{'}}{s_J^{'}}\frac{s_J^{'}}{\sigma_{1J}^{'}} = \frac{ms_L^{'}}{s_L^{'}}\left(\frac{s_K^{'}}{s_J^{'}}\right)^{\Lambda}\frac{2-\sin\phi_{tc}}{2}$$

$$= m\left(\frac{\theta_J^2+m^2}{2m^2}\right)^{\Lambda}\frac{2-\sin\phi_{tc}}{2} = m\left[\frac{1}{2}\left(\frac{\theta_J}{m}\right)^2+\frac{1}{2}\right]^{\Lambda}\frac{2-\sin\phi_{tc}}{2} \quad (3\text{–A.45})$$

$$= \sin\phi_{ps}\left\{\frac{1}{2}\left[\frac{\sin\phi_{tc}}{\sin\phi_{ps}(2-\sin\phi_{tc})}\right]^2+\frac{1}{2}\right\}^{\Lambda}\frac{2-\sin\phi_{tc}}{2}$$

$$= \frac{\sin\phi_{ps}(2-\sin\phi_{tc})}{2}\left\{\frac{1}{2}\left[\frac{\sin\phi_{tc}}{\sin\phi_{ps}(2-\sin\phi_{tc})}\right]^2+\frac{1}{2}\right\}^{\Lambda}$$

3.7.2.2. Numerical Value

As shown in Figure 3-A.2, an element compression test was modelled under plane strain condition to estimate the plane strain value of the undrained shear strength of the soil. Soil properties were listed in Table 3-4.

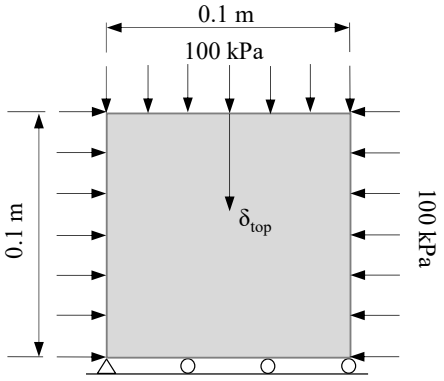

Figure 3-A.2. Element plane strain compression test.

The element (0.1 m × 0.1 m) chosen to be tested was CPE8RP (an 8-node plane strain quadrilateral, biquadratic displacement, bilinear pore pressure, reduced integration). The

bottom of the finite element mesh was on rollers, simulating the frictionless interface between the soil and the bottom surface of the plane strain test apparatus. A uniform downward displacement was applied slowly on the top surface of the mesh (strain-controlled shear test). All edges were impermeable during the analysis, representing for the undrained test. A single increment of analysis in which the confining pressure was applied at the top surface and the sides of the mesh (e.g., 100 kPa). During Step-1, to make sure that equilibrium is satisfied within the element, the geostatic stress was assigned for the element, and the magnitude of the geostatic stress was determined by the burial depth it represented for. Step-2 was a shearing step in which the top edge of the element was forced to displace downward (δ_p) at a small rate.

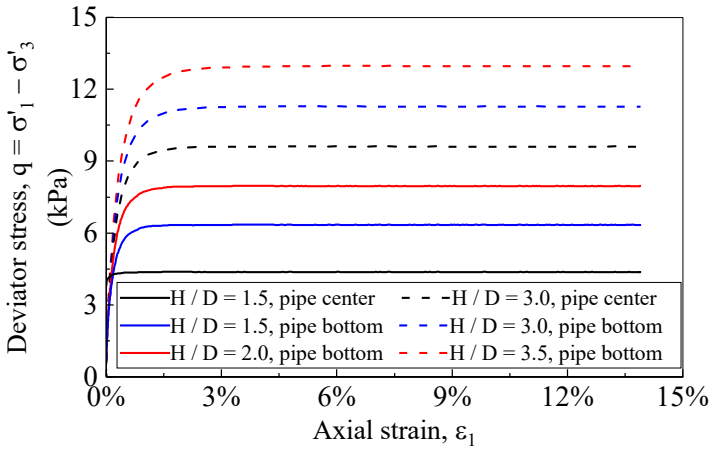

Figure 3-A.3. Deviator stress versus strain in the plane strain compression test.

The deviator stress versus strain in the element test was plotted in Figure 3-A.3. And the value of s_u under different burial depths were obtained from

$$s_u = \frac{q_f}{2} \qquad (3\text{−A.46})$$

Where q_f is the maximum deviator stress shown in Figure 3-A.3.

s_u under different burial depths were calculated by equation (3-A.46) and summarized in Table 3-4.

References

ASCE, 1984. Guidelines for the seismic design of oil and gas pipeline systems. American Society of Civil Engineers, Committee on Gas and Liquid Fuel Lifelines, Technical Council on Lifeline Earthquake Engineering, ASCE, New York.

Barbosa-Cruz ER, and Randolph, M.F., 2005. Bearing capacity and large penetration of a cylindrical object at shallow embedment. In *Proc. Int. Symp. on. Frontiers in Offshore Geotechnics-ISFOG*, Perth, Australia.

Bemben, S., and Myers, H., 1974. The influence of rate of penetration on static cone resistance in Connecticut river valley varved clay. In *Proceedings of the European* Symp*. on Penetration Testing*, National Swedish Council for Building Research Stockholm, vol. 2(2), pp.33-43.

C-CORE, Honeggerm, D., D.G. Honegger Consulting, 2003. Extended Model for Pipe Soil Interaction.

Chai, J., and Carter, J.P., 2011. Deformation analysis in soft ground improvement. Geotechnical, geological, and earthquake engineering, vol. 18. Springer Science & Business Media.

Chatterjee, S., Randolph, M.F., and White D., 2012. The effects of penetration rate and strain softening on the vertical penetration resistance of seabed pipelines. Géotechnique, vol. 62(7), pp.573-582.

Chatterjee, S., White, D., and Randolph, M.F., 2012. Numerical simulations of pipe-soil interaction during large lateral movements on clay. Géotechnique, vol. 62(8), pp. 693-705.

Chatterjee, S., Yan, Y., Randolph, M.F., and White, D., 2012. Elastoplastic consolidation beneath shallowly embedded offshore pipelines. Géotechnique Letters, vol. 2(2), pp. 73-79.

Dassault Systemes Simulia Corp., 2017. Abaqus version 6.17 documentation. Providence, RI, USA.

Honegger, D.G., and Nyman, D.J., 2001. Manual for the seismic design and assessment of natural gas transmission pipelines. Pipeline Research Council International (PRCI), Project PR-268-9823.

House, A.R., Oliveira, J.R.M.S., and Randolph, M.F., 2001. Evaluating the Coefficient of Consolidation using Penetration Tests. International Journal of Physical Modelling in Geotechnics, vol.3, pp.17-26.

Hsu, T., 1993. Rate effect on lateral soil restraint of pipelines. Soils and Foundations, vol. 33(4), pp. 159-169.

Hu, Y., and Randolph, M.F., 1998. A practical numerical approach for large deformation problems in soil. Int. J. Numer. Analyt. Meth. Geomech, vol.22, pp. 327-350.

Hu, Y., and Randolph, M.F., 2002. Bearing Capacity of Caisson Foundations on Normally Consolidated Clay. Soils and Foundations, vol.42(5), pp. 71-77.

Kim, K.K., Prezzi, M., and Salgado, R., 2006. Interpretation of cone penetration tests in cohesive soils. Joint Transportation Research Program, Indiana Department of Transportation and Purdue University, West Lafayette, Indiana.

Kim, T., 2005. Dissipation of pore water pressure due to piezocone penetration in OC clay. Ph. D. dissertation, Korea University, Seoul, Korea.

Lagioia, R., and Nova, R., 1995. An experimental and theoretical study of the behaviour of a calcarenite in triaxial compression. Géotechnique, vol. 45(4), pp. 633-648.

Lagioia, R., and Panteghini, A., 2016. On the existence of a unique class of yield and failure criteria comprising Tresca, von Mises, DruckerPrager, MohrCoulomb, GalileoRankine, MatsuokaNakai and LadeDuncan. In *Proceedings of the Royal Society A: Mathematical, Physical and Engineering Sciences*.

Lehane, B.M., O'Loughlin, C.D., Gaudin, C., and Randolph, M.F., 2009. Rate effects on penetrometer resistance in kaolin. Géotechnique, vol. 41(1), pp. 41-52.

Mahmoodzadeh, H., Randolph, M.F., and Wang, D., 2014. Numerical simulation of piezocone dissipation test in clays. Géotechnique, vol. 64(8), pp. 657–666.

Martin, C.M., and White, D.J., 2012. Limit analysis of the undrained bearing capacity of offshore pipelines. Géotechnique, vol. 62(9), vol. 847-863.

Nova, R., 1992. Mathematical modelling of natural and engineered geomaterials. General lecture 1st E.C.S.M. Munchen, Eur. J. Mech. A/Solids, pp. 135-154.

Panteghini, A., and Lagioia, R., 2018a. An approach for providing quasi‐convexity to yield functions and a generalized implicit integration scheme for isotropic constitutive models based on 2 unknowns. International Journal for Numerical and Analytical Methods in Geomechanics, vol. 42(6), pp. 829-855.

Panteghini, A., and Lagioia, R., 2018b. An extended modified Cam-Clay yield surface for arbitrary meridional and deviatoric shapes retaining full convexity and double homothety. Géotechnique, vol. 68(7), pp. 590-601.

Paulin, M., 1998. An investigation into pipelines subjected to lateral soil loading. Ph.D. thesis, Memorial University of Newfoundland.

Paulin, M.J., Phillips, R., Clark, J.I., and Boivin, R., 1998a. An experimental investigation into lateral pipeline/soil interaction – phase II. Centrifuge 98 – *Proceedings of the International Conference Centrifuge 98*.

Paulin, M.J., Phillips, R., Clark, J.I., Trigg, A., and Konuk, I., 1998b. A full-scale investigation into pipeline/soil interaction. In *Proceedings of 1998 International Pipeline Conference*, ASME, Calgary, AB, vol. 2, pp. 779-787.

Ragni, R., Wang, D., Mašín, D., Bienen, B., Cassidy, M.J., and Stanier, S.A., 2016. Numerical modelling of the effects of consolidation on jack-up spudcan penetration. Computers and Geotechnics, vol. 78, pp. 25-37.

Randolph, M.F., and Hope, S., 2004. Effect of cone velocity on cone resistance and excess pore pressures. Engineering Practice and Performance of Soft Deposits, Osaka, Japan, pp. 147-152.

Randolph, M.F., Wang, D., Zhou, H., Hossain, M., and Hu, Y., 2008. Large deformation finite element analysis for offshore applications. In *12th International Conference of International Association for Computer Methods and Advances in Geomechanics (IACMAG)*, Goa, India, Oct, pp. 1-6.

Roy, M., Tremblay, M., Tavenas, F., and Rochelle, P.L., 1982. Development of pore pressures in quasi-static penetration tests in sensitive clay. Canadian Geotechnical Journal, vol. 19(2), vol. 124-138.

Satake, M., 1982. On equivalent Mohr's circle for granular materials. Report No. R-205, University of New South Wales.

Song, Z., Hu, Y., and Randolph, M.F., 2008. Numerical simulation of vertical pullout of plate anchors in clay. Journal of geotechnical and geoenvironmental engineering, vol. 134(6), pp. 866-875.

Terzaghi, K., Peck, R.B., and Mesri, G., 1996. Soil mechanics in engineering practice. John Wiley & Sons.

Tian, Y., Cassidy, M.J., Randolph, M.F., Wang, D., and Gaudin, C., 2014. A simple implementation of RITSS and its application in large deformation analysis. Computers and Geotechnics, vol. 56, pp.160-167.

Ullah, S.N., Hou, L.F., Satchithananthan, U., Chen, Z., and Gu, H., 2018. A 3D RITSS approach for total stress and coupled-flow large deformation problems using ABAQUS. Computers and Geotechnics, vol. 99, pp. 203-215.

Wang, D., and Bienen, B., 2015. Coupled large deformation consolidation analysis of a spudcan footing penetrating into kaolin clay. Computer Methods and Recent Advances in Geomechanics: *Proceedings of the 14th International Conference of International Association for Computer Methods and Recent Advances in Geomechanics*, 2014 (IACMAG 2014), 2015: Taylor & Francis Books Ltd, pp. 877-882.

Wang, D., Gaudin, C., and Randolph, M.F., 2013. Large deformation finite element analysis investigating the performance of anchor keying flap. Ocean Engineering, vol. 59, pp. 107-116.

Wang, D., Hu, Y., and Jin, X., 2006. Two-dimensional large deformation finite element analysis for the pulling-up of plate anchor. China Ocean Engineering, vol. 20(2), pp. 269-278.

Wang, D., Hu, Y., and Randolph, M.F., 2010. Keying of rectangular plate anchors in normally consolidated clays. Journal of Geotechnical and Geoenvironmental Engineering, vol. 137(12), pp. 1244-1253.

Wang, D., Hu, Y., and Randolph, M.F., 2010. Three-dimensional large deformation finite element analysis of plate anchors in uniform clay. J. Geotech. Geoenviron. Engng ASCE, vol. 136(2), pp. 355–365.

Wang, D., White, D.J., and Randolph, M.F., 2010. Large-deformation finite element analysis of pipe penetration and large-amplitude lateral displacement. Canadian Geotechnical Journal, vol. 47(8), pp. 842-856.

Wroth, C.P., 1984. The interpretation of in situ soil tests. Géotechnique, vol. 34(4), pp. 449-489.

Yu, L., Liu, J., Kong, X., and Hu, Y., 2008. Three-dimensional RITSS large displacement finite element method for penetration of foundations into soil. Computers and Geotechnics, vol. 35(3), pp. 372-382.

Zhang, W., Wang, D., Randolph, M.F., and Puzrin, A., 2015. Catastrophic failure in planar landslides with a fully softened weak zone. Géotechnique, vol. 65, pp. 755-769.

Zhang, W., Randolph, M.F., Puzrin, A., and Wang, D., 2018. Transition from shear band propagation to global slab failure in submarine landslides. Canadian Geotechnical Journal, vol. 56.

Zhou, H., White, D., and Randolph, M.F., 2008. Physical and numerical simulation of shallow penetration of a cylindrical object into soft clay. In GeoCongress 2008: Characterization, Monitoring, and Modeling of GeoSystems, 2008, pp. 108-117.

Zhou, H., and Randolph, M.F., 2006. Large deformation analysis of suction caisson installation in clay. Canadian Geotechnical Journal, vol. 43(12), pp. 1344-1357.

Chapter 4

A 2D RITSS model for analysis on large lateral displacement of trenched pipeline

Xiaoyu Dong[1], Hodjat Shiri[2], Wangcheng Zhang[3], Mark F. Randolph[4]

1: Department of Civil
Engineering, Memorial University of Newfoundland
e-mail: xiaoyu.dong@mun.ca

2: Department of Civil
Engineering, Memorial University of Newfoundland
e-mail: hshiri@mun.ca

3: Oceans Graduate School,
the University of Western Australia
e-mail: wangcheng.zhang@uwa.edu.au

4: Oceans Graduate School,
the University of Western Australia
e-mail: mark.randolph@uwa.edu.au

This chapter is submitted as a journal manuscript.

.

Abstract

Offshore pipelines have been widely used for transportation of oil, gas and water. Trenching and backfilling are one of the effective ways for protecting subsea pipelines. However, due to complex subsea environments, large lateral displacement of trenched pipelines may still be induced by ground movement, landslides, ice gouging and etc. While the pipeline experiences large lateral displacement, failure mechanisms in the soil and load-displacement response of the pipeline will be significantly affected by many factors, including trench geometry, burial depth, backfilling material. However, the difference in strength between native ground and backfilling material has not attracted enough attention and therefore has not been covered thoroughly in design codes. In this chapter, a 2D RITSS framework with a modified Tresca model considering strain-softening effects and a CEL model were developed in ABAQUS respectively to examine the pipeline-backfill-trench effects. The numerical results showed close prediction to the centrifuge test results and the developed 2D RITSS model showed great advantages in assuring calculation accuracy and tracking detailed failure mechanisms in large deformation finite element analysis.

Keywords: RITSS, LDFE, CEL, Numerical modeling, Lateral pipeline-backfill-trench interaction

4.1. Introduction

Subsea pipelines in shallow waters are often protected by burying inside subsea trenches to mitigate the impacts from the functional and environmental loads. Using excavated materials as backfilling is a common practice and a cost-effective solution. Depending on trenching methodology, construction strategy, and environmental loads, backfilling materials may experience more or less remouldingmaking them distinct from the 3surrounding native soils. The difference between the stiffness of the backfill and native material affects the failure mechanisms of soils subjected to lateral pipeline movement (Paulin 1998).

The relative displacement between the pipeline and the surrounding soils that may occur due to the ground movements, faults, slope instabilities, ice gouging, etc. exerts forces on the pipeline. The amplitude of these forces and the force-displacement response of the pipeline depend on the backfill and native soil properties, trench geometry, pipeline burial depth, pipeline roughness, pipeline size and loading rate (related to drained/undrained conditions) etc. (Hsu, 1993; Paulin, 1998; C-CORE report, 2003). In practice, the pipeline-soil interaction is commonly idealized as a set of the specialized beam and spring elements (ALA 2005), where the mechanical behaviours of springs are expressed by bilinear or hyperbolic functions (ALA 2005; PRCI 2009), despite of the existence of the trench and the difference in backfill and native soils. However, large discrepancies in terms of the ultimate lateral resistance and the p-y response have been recognised in different design codes and empirical equations (Paulin 1998; ALA 2005; PRCI 2009; Rajah et al. 2014; Pike 2016), partly resulted from the inconsideration of the effect of pipeline-backfill-trench interactions.

There are a number of theoretical and experimental models availabe to predict the ultimate lateral resistance or force-displacement (p-y) curves of moving structures (Hansen 1948; Mackenzie 1955; Poulos 1995; Hansen and Christensen 1961; Tschebotarioff 1973; Reese and Welch 1975; Bhushan 1979; Luscher et al. 1979; Edgers and Karlsrud 1982; Rowe and Davis 1982; Das et al. 1985; Das et al. 1987; Rizkalla and Mclntyre 1991; Ranjani 1993; Merifield 2001; ALA 2005; Klar and Randolph 2008), while very few of them are specific to pipeline-soil interactions (Poorooshasb et al. 1994; Paulin 1998; Oliveira et al. 2010).

The influence of different stiffness between the backfilling and native materials on lateral p-y response of the pipeline has been rarely considered in the existing design codes and analytical frameworks, though it has been widely identified in many physical modelling tests (e.g. in Paulin 1998; C-CORE Report 2003; Kianian et al. 2018). Paulin (1998) conducted a series of centrifuge tests on pipeline – clayey soil lateral interactions with the focus on the effects of trench width, burial depth, interaction rate, backfill properties, and stress history on the pipeline-soil response. This study has attempted to qualitatively address the failure mechanism, which is though plausible without satisfactory visualization techniques then. It has been later improved in Kianian et al. (2018) through a similar set of centrifuge tests, where progressive and interactive failure mechanisms were visualised with the adis of transparent acrylic sheet, digital cameras, and particle image velocimetry (PIV) tecnique.

Since test in clay is extremely costly and time-consuming considering the soil consolidation during sample preparation, only limited number of physical modelling tests of the pipeline-backfill-trench interaction were reported (Paulin 1998; C-CORE Report 2003; Kianian et al. 2018). The failure mechnisms and p-y curves of pipeline subjected to

lateral movement have neither been comprehensively understood through numerical modelling due to the complex configurations and large deformation involved (Phillips et al. 2004; Kouretzis et al. 2013; Chaloulos et al. 2015).

The current study aims to numerically investigate the failure mechanism and p-y response of pipeline during the pipeline-backfill-trench lateral interaction using a large deformation finite element method, termed remeshing and interpolation technique with small strain (RITSS, Hu and Randolph 1998). It has shown advantages and accuracy in modelling large deformation geotechnical problems (Yu et al. 2008; Wang et al. 2010; Tian et al. 2014; Ragni et al. 2016; Ullah et al. 2018). A modified Tresca model (Zhang et al. 2015, 2018) accounting for strain softening and rate effect was used in the study to consider different properties of backfill and native soils. The numerical results were compared with the published experimental work (Paulin 1998; C-CORE Report 2003) and the existing design codes (ASCE 1984).

4.2. Methodology

The study first attempts to numerically replicate the physical modelling tests in centrifuge by Paulin (1998). The testing set-up, pipeline geometry and soil properties are brefely introduced here. The physical model was scaled at 1:50 in the centrifuge, with the model pipeline set as 19 mm in diameter (corresponding to a prototype value of 0.95 m) The model trench was 50 mm in width which corresponds to 2.5 m in prototype. Different cover depths were used in the tests, namely 16 mm and 65 mm (corresponding to prototype value of 0.8 m and 3.25 m) respectively. The silty clay used in the tests was a mixture by weight of speswhite kaolin clay (50%) and Sil-Co-Sil silt (50%), andpreconsolidated to 400 kPa to reach a desired undrained shear strength around 40 kPa. During the tests, the trenched

pipe was pulled at a minimal speed of 0.5 to 0.7 mm/s to ensure undrained conditions roughly (Paulin 1998).

4.2.1. Numerical details

The flowchart of numerical procedure and coding packages are briefly shown in Figure 4-1. Overall, the large deformation is divided into a series of incremental jobs with small strain increments. The calculation solutions are interpolated from old mesh to new mesh by map solution technique to ensure the whole problem is solved with high-quality meshes throughout the entire analysis.

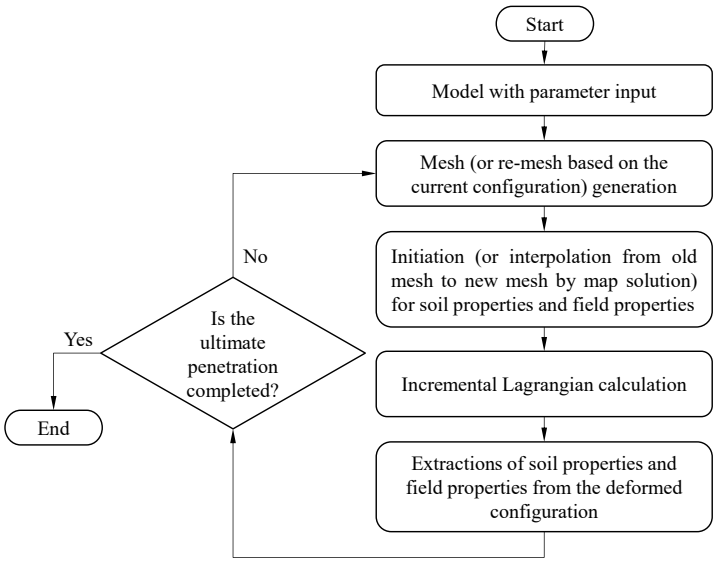

Figure 4-1. Overall scheme of calculation loop.

A main python code was developed to periodically execute the pre-processing, interpolation, Lagrangian calculation and post-processing of the results for each small stain increment, until the whole analysis is finished upon target lateral displacement of pipeline. Interpolation module (of soil and field properties from old to new meshes) by map solution technology and Lagrangian calculation are implemented in ABAQUS with light coding

(ABAQUS analysis User's Manual 2017); while pre-processing and post-processing modules are coded externally for small strain analysis.

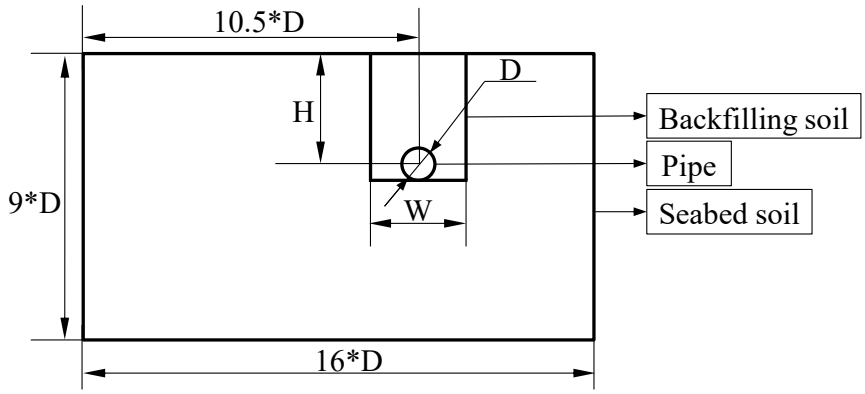

(a)

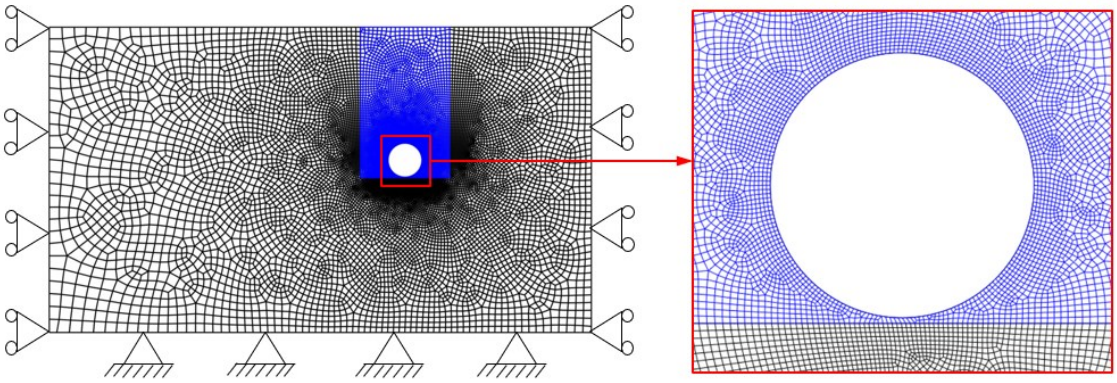

(b)

Figure 4-2. Configuration of trenched pipe.

Figure 4-2 shows the numerical model of prototype at the initial state, constituting of three components: pipe, backfilling material, and native soil. The pipe is laid on the bottom of the trench surrounded by backfilling soils. Trench geometries and backfilling material properties are various among different cases as will be discussed in detail later. The soil domain was modeled by using 4-node bilinear plane strain elements (CPE4), with details

shown in Figure 2b. Rigid wire elements (R2D2) were used to model the pipe of a 0.95 m diameter. The bottom boundary was fixed, while the side boundaries were restrained against displacement perpendicular to the respective sides.

First, a geostatic step was set to achieve the desired gravity stress level in the soil ground. Then, the deformed boundary nodes were extracted from the old job and used to sketch the geometry parts in the new job with the deformed configuration. In each new incremental job, two analysis steps were included. The first step was used to transfer field properties such as stresses, material properties, etc. from the old mesh through the map solution technique available in ABAQUS, with a minimal time step (=1s). Note that the reaction forces on boundary nodes (including the pipe) were not considered in the map solution technique, which was improved in the current study by customizing the command *CLOAD in ABAQUS/Standard. If the reaction forces have not been correctly transferred to the new mesh, a sharp increase or decrease in stresses near the boundary (and the pipe) may occur in our trial simulations, potentially resulting in non-convergence. In the second step the pipeline was displaced by a required incremental magnitude.

In addition, an analysis with the Coupled Eulerian – Lagragian (CEL) technique (which is available in the ABAQUS) with the same model and soil properties was conducted for comparison.

4.2.2. Soil properties

The strain softening and rate effect were considered in the numerical analysis with a modified Tresca model following Zhang et al. (2015, 2018). It was implemented using a USDFLD subroutine for the implicit analysis in the LDFE model and a VUSDFLD subroutine for explicit analysis in the CEL model.

The undrained shear strength considering strain softening and rate effect are calculated by (Zhang et al. 2018)

$$\tau = \max\left[\tau_p + (\tau_r - \tau_p)\frac{\gamma^p}{\gamma_r^p}, \gamma_r\right]\left[1 + \eta\left(\frac{\dot{\gamma}}{\dot{\gamma}_{ref}}\right)^n\right] \quad (4\text{-}1)$$

where

τ_p is the peak shear strength

τ_r is the residual shear strength

η is the dimensionless viscosity coefficient

n is the flow index

γ^p is the accumulated plastic shear strain

γ_r^p is the value of γ^p to reduce the shear strength from peak to residual

$\dot{\gamma}$ is the shear strain rate

$\dot{\gamma}_{ref}$ is the reference strain rate

Thickness of shear band is approximate to one layer of elements (Zhang et al. 2018). Mesh dependency can be therefore avoided by using fixed pairs of γ_r^p and s (e.g. $\gamma_r^p s = 0.2$ m in this study, where s is the element size) or $\dot{\gamma}_{ref}$ and s (e.g. $\dot{\gamma}_{ref} s = 1.0$ m/s in this study). And sensitivity of soil is used as 5.

4.2.3. Boundary splitting scheme

While the pipe is moved from the trench into the native ground, the original backfilling material in front of the pipe will be squeezed up or down and the fore part of pipe tends to get in contact with the native ground directly (see Figure 4-3). This requires for a specific boundary splitting scheme considered in our framework to achieve the large lateral displacement of the trenched pipeline. In the boundary splitting scheme, the original

backfilling soil-seabed soil interface is split to give rise to the new interface between pipe and seabed soil.

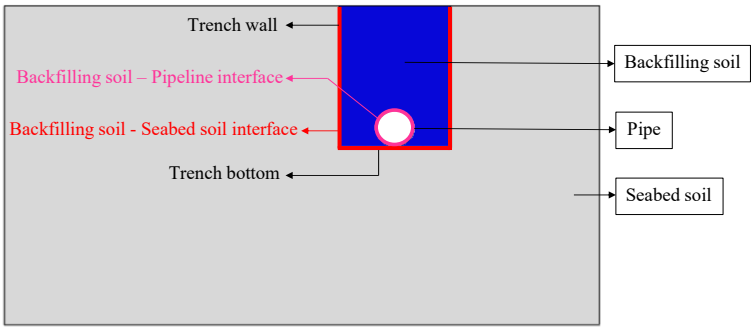

(a) initial configuration

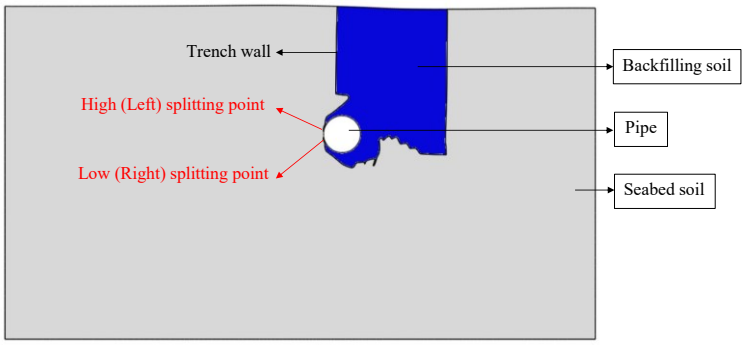

(b) pipeline reaches the trench wall

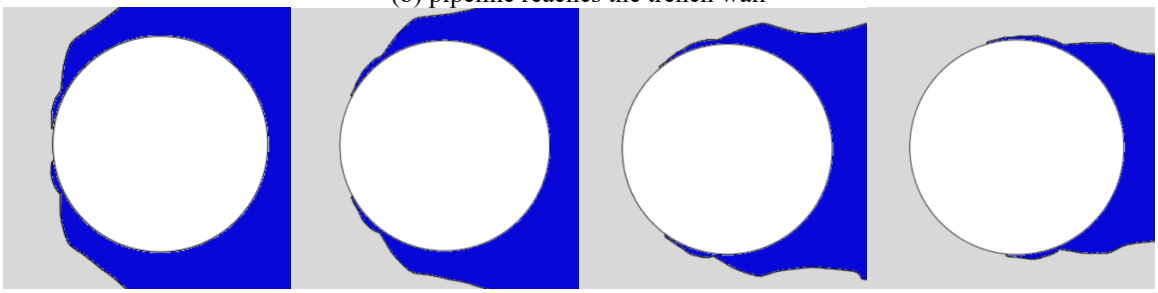

(c) splitting of the original backfilling soil-seabed soil interface

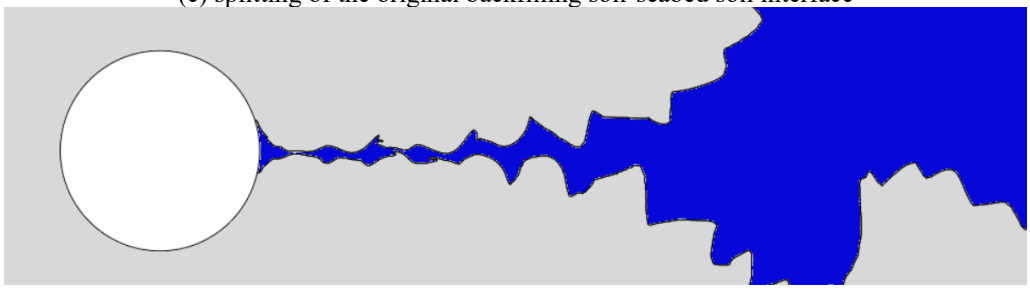

(d) pipeline displaced laterally by long distance (up to 4D)

Figure 4-3. Test for boundary splitting scheme.

4.3. Large deformation analysis of pipe-soil interaction

4.3.1. Pipe embedded in homogenous seabed

Uniform strength without softening and rate effectwas considered in both the trench and native ground for benchmarking the RITSS model.

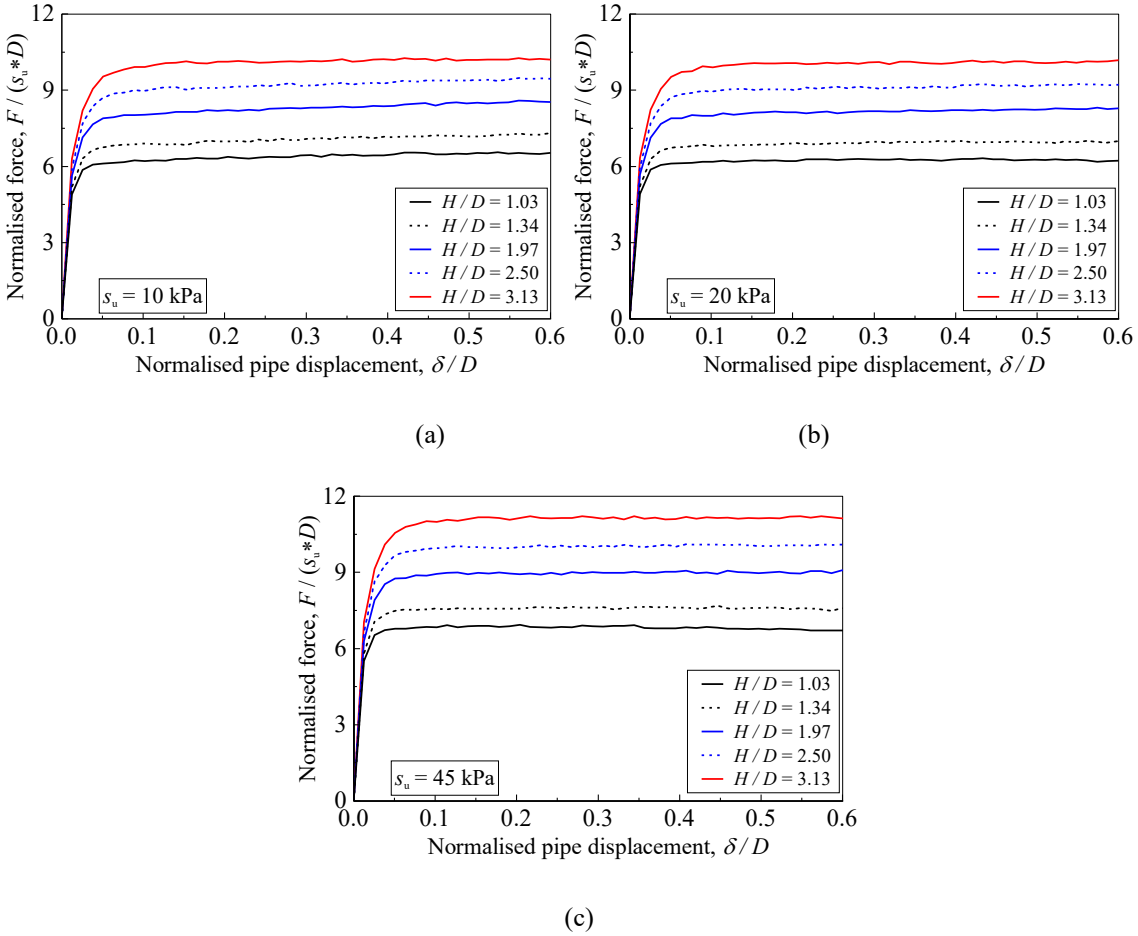

Figure 4-4. Load-displacement curves predicted by total stress analysis framework with Tresca material.

Responses of pipe with different burial depths and undrained shear strengths of seabed soils were examined (see Figure 4-4). Soil properties are listed in Table 4-6. The bearing capacity factor (F_{ult}/s_uD) at different burial depth ratios were plotted in Figure 4-5.

As shown in Figure 4-4, with the same burial depth ratio, larger responses could be observed in soil with larger cohesion. Soil resistance also increases with the increase of burial depth ratio.

Table 4-6. Benchmark case for RITSS model: pipe embedded in homogenous seabed (C-CORE report, 2003)

Properties	Symbol	Unit	Value
Strength parameters	s_u	kPa	10, 20, 45
Young's modulus of soil	E	kPa	$400s_u$
Burial depth ratio	H/D	-	1.03, 1.34, 1.97, 2.50, 3.13
Submerged unit weight of soil	γ_y'	kN/m^3	7.5
Pipe diameter	D	m	0.95

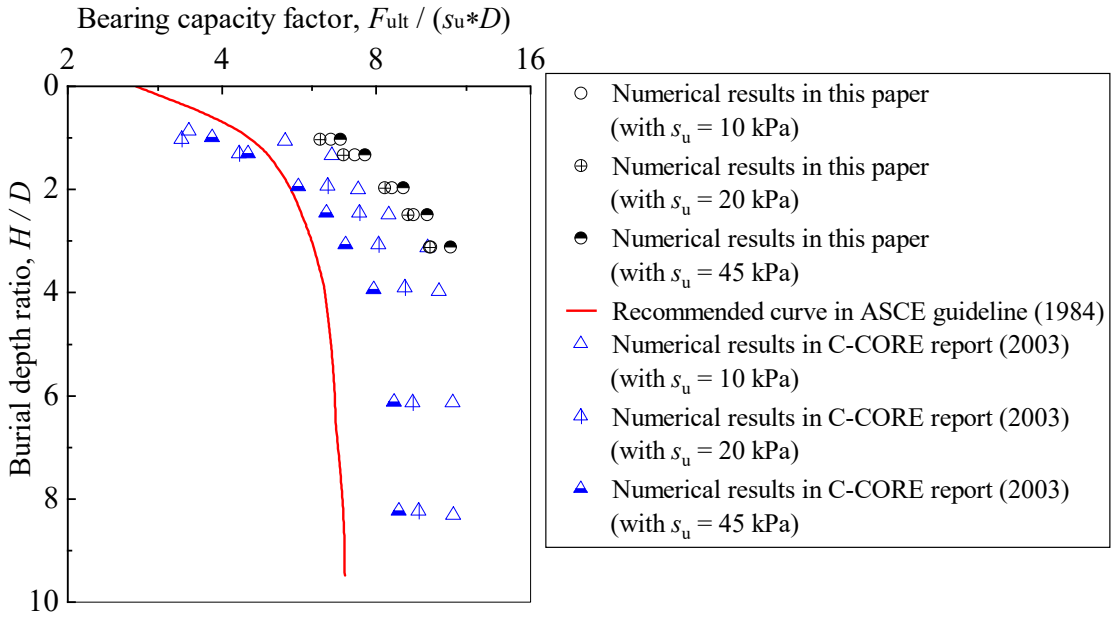

Figure 4-5. Effects of burial depth on bearing capacity factor.

As shown in Figure 4-5, the predicted curves show larger bearing capacity factors than the recommended value in ASCE guideline (1984) but are quite close to the published numerical work (C-CORE Report 2003). The effects of cohesion of soil on bearing capacity factors were relatively small.

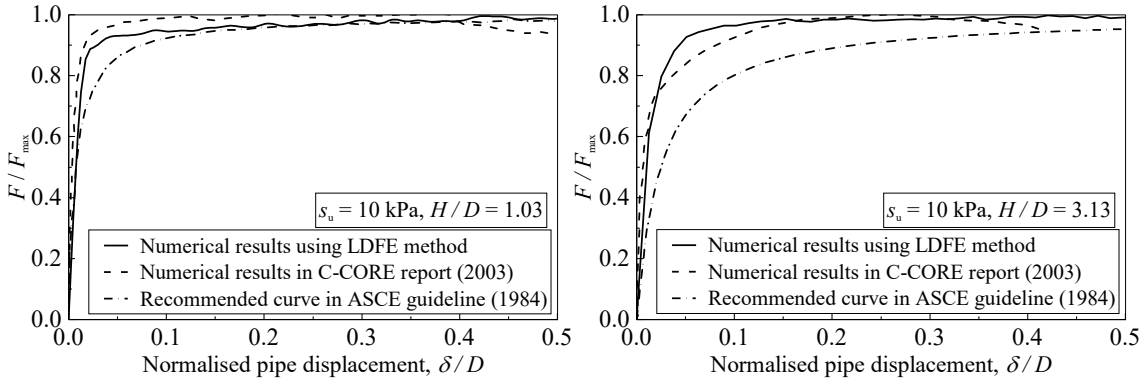

(a) Shallow burial (b) Deep burial

Figure 4-6. Comparison of calculated load-displacement curves and recommendations.

The normalized load-displacement curves from the current LDFE numerical analysis are presented in Figure 4-6 and compared to the ASCE guidelines (1984) and published numerical work (C-CORE Report 2003). The stiffness resulted from the numerical modelling is larger than the recommended value in ASCE guidelines at the starting stage of the displacement of pipe but matches well with the recommendation in later stage.

Compared with the recommended curves in ASCE guidelines (1984) and published numerical work (C-CORE Report 2003), the predicted responses by developed 2D RITSS framework with Tresca material are in accordance with the recommendations and showed only slight differences in some cases (see Figure 4-6 b).

4.3.2. Trenched pipeline

As briefly introduced at the beginning of Section 2, the configurations of numerical model for trenched pipelines were set based on the two centrifuge tests conducted by Paulin (1998). One is set for shallowly buried pipe, the other is set for deeply buried pipe. The parameters were given in Table 4-7.

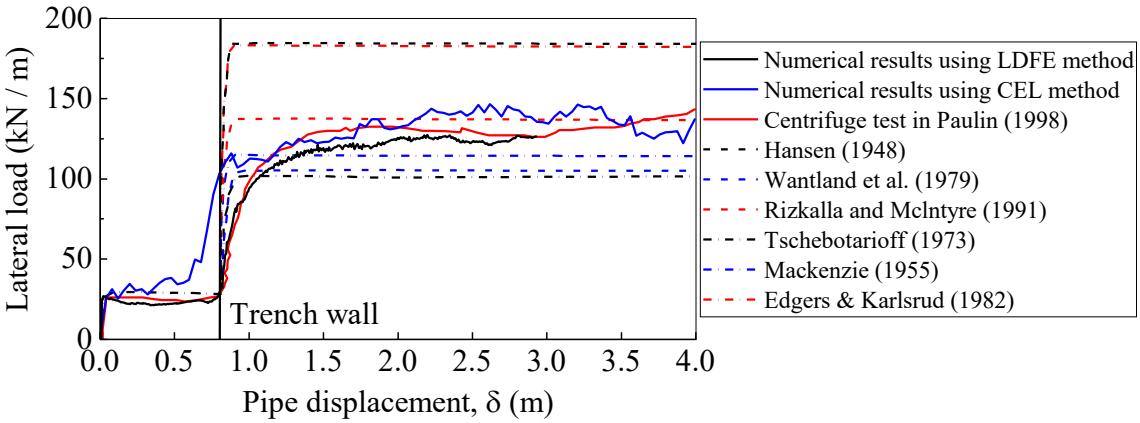

Figure 4-7. Predicted undrained ultimate loads and p-y curves based on existing methods of analysis compared with the centrifuge test data (shallow burial case in Paulin (1998)).

Table 4-7. Parameters used for model

Properties	Symbol	Unit	Shallow burial case	Deep burial case
Pipe diameter	D	m	0.95	0.95
Trench width	W	m	2.50	2.50
Cover depth	C	m	0.80	3.25
Embedment ratio	H/D	-	1.84	4.42
Average backfill soil undrained shear strength	s_{u_b}	kPa	3.30	3.50
Average seabed soil undrained shear strength	s_{u_s}	kPa	36.20	42.10
Effective unit weight of backfill soil	γ_b'	kN/m^3	8.38	8.38
Effective unit weight of seabed soil	γ_s'	kN/m^3	9.31	9.31

An example output is shown in Figure 4-7 for the load-displacement curve for trenched pipeline with large lateral displacement. Six theoretical p-y curves (Mackenzie 1955; Tschebotarioff 1973; Rizkalla and Mclntyre 1991; Hansen 1948; Wantland et al. 1979) are given in Figure 4-7 and Figure 4-8 for comparison in addition to the results from the CEL modelling and centrifuge test (Paulin 1998).

It is shown that for the shallowly buried pipe (see Figure 4-7), all theoretical estimations of resistance for pipe moving in backfilling materials are adequate. But when the pipe penetrates towards the trench wall, the results from the numerical modellings show significant advantages in predicting the smooth increase of lateral resistance observed in centrifuge test other than step changes in theoretical curves. Comapred to the results from the RITSS simulations, CEL model shows a slower increase in lateral resistance while the pipe penetrates into the native ground and gives an overpredicted ultimate response. Besides, for the shallowly buried pipe, Rizkalla and Mclntyre (1991); and the ASCE (1984) / Hansen (1948) and Edgers and Karlsrud (1982) overpredict the ultimate responses of the pipe, while the Tschebotarioff (1973), Wantland et al. (1979), Mackenzie (1955) underpredict the ultimate response. Numerical prediction well matches the ultimate response of centrifuge tests. The theoretical prediction closest to the centrifuge data is Rizkalla and Mclntyre (1991).

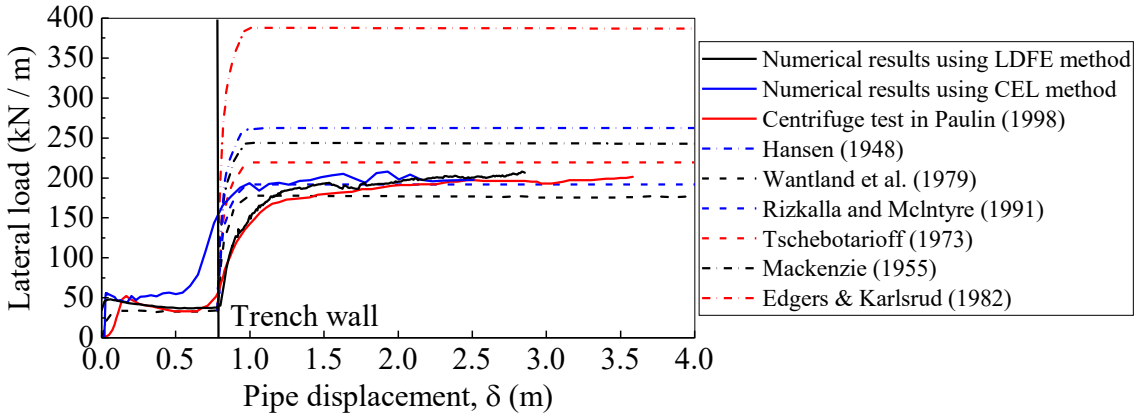

Figure 4-8. Predicted undrained ultimate loads and p-y curves based on existing methods of analysis compared with the centrifuge test data (deep burial case in Paulin (1998)).

As for the deeply buried pipe (see Figure 4-8), all theoretical estimations of resistance of pipe moving in backfilling material were a bit insufficient. And when the pipe penetrates towards the trench wall, the smooth increase trend of lateral load on pipe observed in centrifuge test were failed to be captured by the theoretical curves. Rizkalla and Mclntyre (1991) and Wantland et al. (1979) underestimate the ultimate responses of the pipe while the ASCE (1984) / Hansen (1948), Tschebotarioff (1973), Mackenzie (1955), and Edgers and Karlsrud (1982) overpredict the ultimate response. The theoretical prediction on the safe side which is closest to the centrifuge data is Tschebotarioff (1973). Numerical prediction using RITSS method provides better match this time comparing with its performance in shallow burial case.

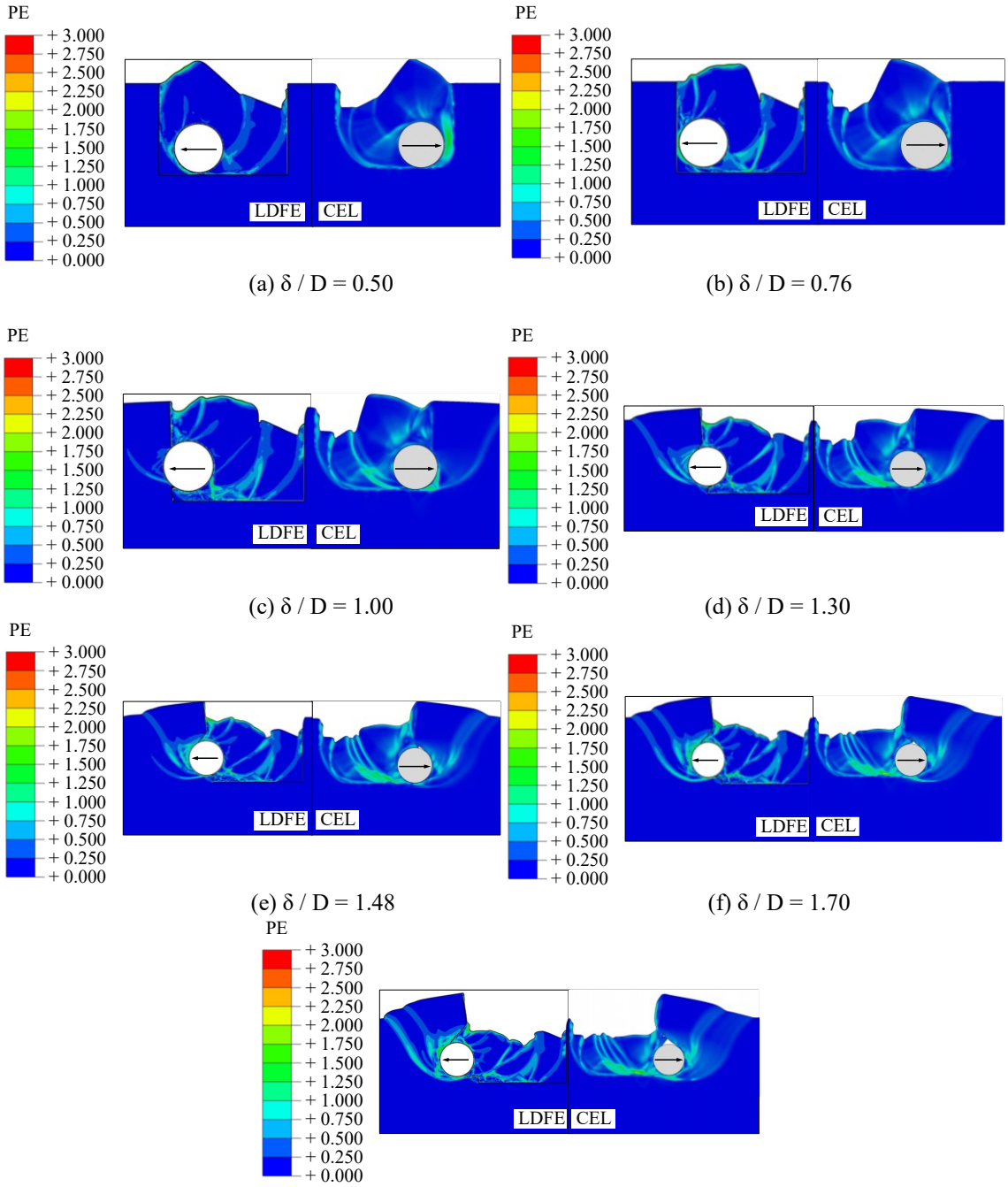

(a) δ / D = 0.50

(b) δ / D = 0.76

(c) δ / D = 1.00

(d) δ / D = 1.30

(e) δ / D = 1.48

(f) δ / D = 1.70

(g) δ / D = 1.90

Figure 4-9. Plastic strain in model while pipe penetrates to the native seabed soil from the backfilling material (shallow burial case in Paulin (1998)).

The propagation of maximum plastic strain while pipe penetrates to native seabed soil is shown in Figure 4-9. Large soil heaves could be observed on the ground surface due to the

pipe penetration. Deformations of soil are well shown in Figure 4-9 and failure mechanisms can be observed along with the propagated shear bands. In T1P1, the pipe is shallowly buried and the global shear band under the pipe is observed to develop towards the ground surface and arrives at the ground surface. The active wedge in Figure 4-9 is clearly shown as a spiral shear band. Comparing the shear bands obtained using LDFE model with RITSS and CEL model, the general trends are quite similar but results from RITSS model give a clearer view on the shape and location of shear bands and show significant advantages in demonstrating details of failure mechanism. For example, the CEL model also captures the shape and location of shear bands left behind the pipe as we could see in Figure 4-9 d, and f.

From Figure 4-9 c, the formation of the first shear band in front of the pipe starting from the pipe bottom is observed. With further penetration of pipe into the seabed soil, the propagation and formation of the second shear band in front of the pipe starting from the pipe bottom is observed (see Figure 4-9 e and f). Those shear bands gradually reach the seabed and dents on the seabed could be observed in Figure 4-9 g.

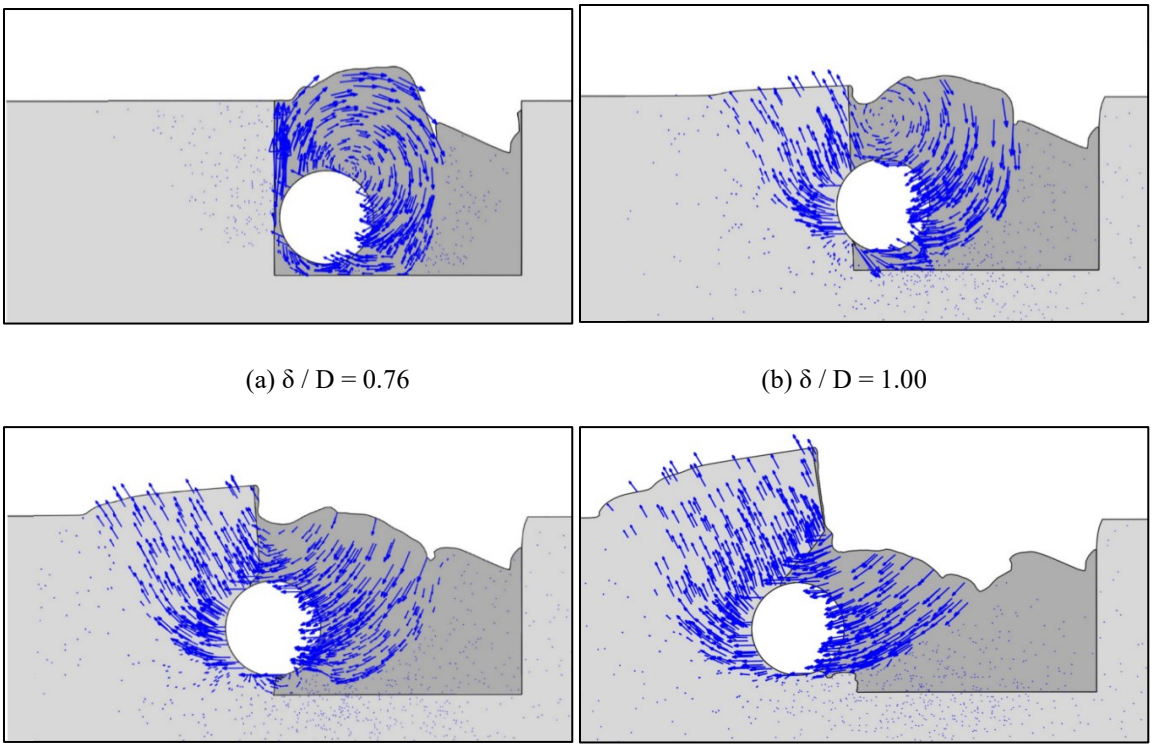

(a) δ / D = 0.76 (b) δ / D = 1.00

(c) δ / D = 1.30 (d) δ / D = 1.90

Figure 4-10. Displacement vectors in LDFE model while pipe penetrates into the native seabed soil from the backfilling material (shallow burial case in Paulin (1998)).

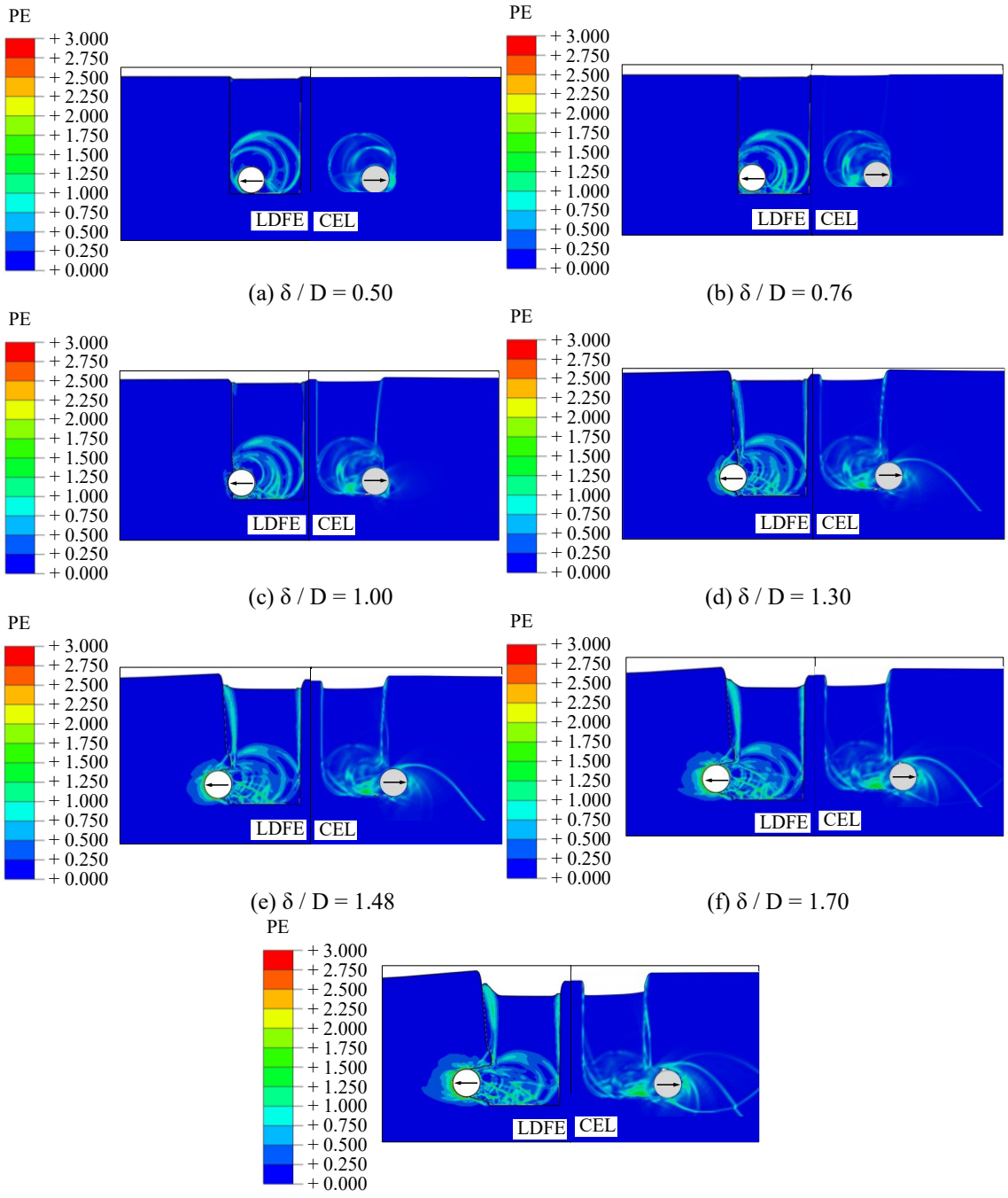

(a) δ / D = 0.50

(b) δ / D = 0.76

(c) δ / D = 1.00

(d) δ / D = 1.30

(e) δ / D = 1.48

(f) δ / D = 1.70

(g) δ / D = 1.90

Figure 4-11. Plastic strain in model while pipe penetrates to the native seabed soil from the backfilling material (deep burial case in Paulin (1998)).

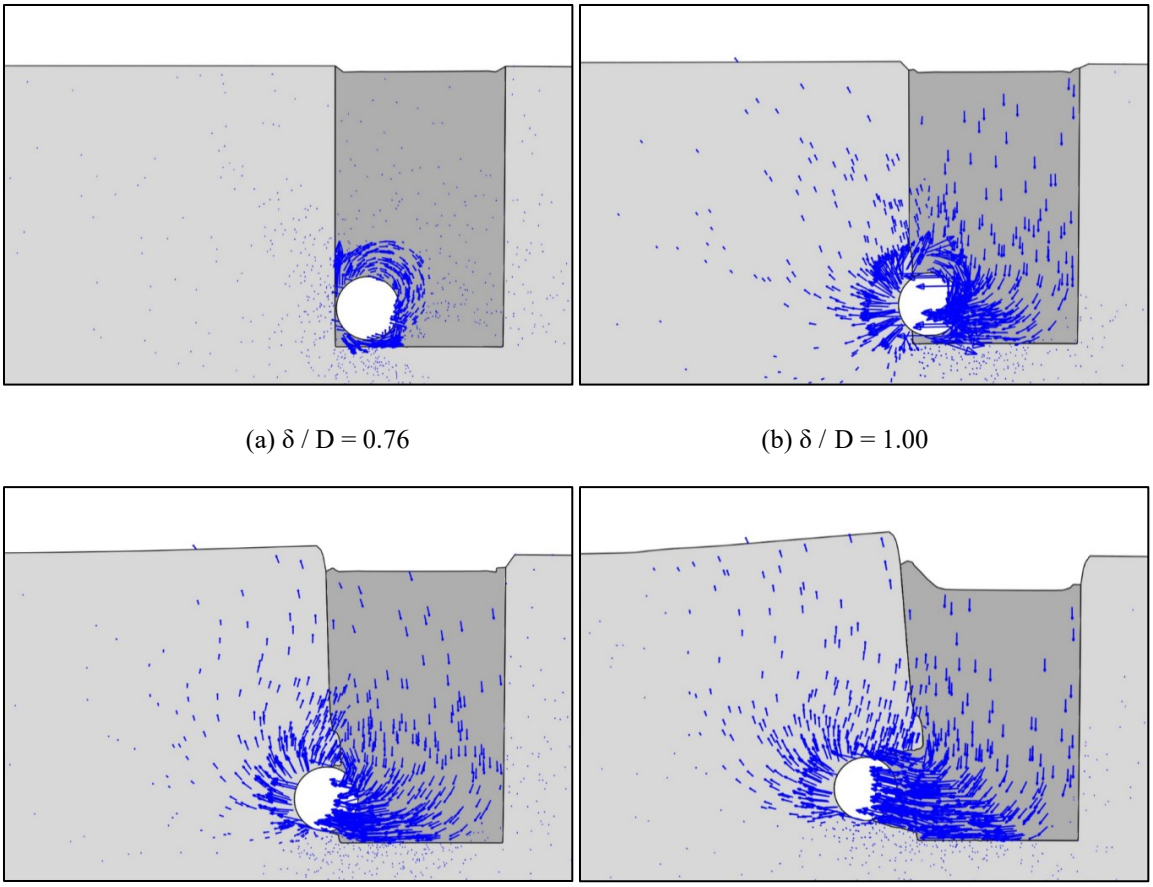

(a) δ / D = 0.76 (b) δ / D = 1.00

(c) δ / D = 1.30 (d) δ / D = 1.90

Figure 4-12. Displacement vectors in LDFE model while pipe penetrates into the native seabed soil from the backfilling material (deep burial case in Paulin (1998)).

For the depply buried case, comparisons between numerical results obtained from RITSS model and CEL model are made in Figure 4-11. A clearer view on the locations and shapes of shear bands is available in the results using RITSS method. The shape of shear bands forming before the pipe reaches the trench wall seems to have been affected by the burial depth ratio (comparing Figure 4-9 b and Figure 4-11 b), which could be explained by the displacement fields obtained in shallowly buried case (Figure 4-10 a) and in deeply buried case (Figure 4-12 a). The rotating circle of soil formed with the displaced pipe reaches

beyond the surface of backfilling soil in shallowly buried case (Figure 4-10 a) and significantly involves the soil surface of backfilling materail into rotation as well, while in deeply buried case (Figure 4-12 a) has not been that much significantly involved into the soil rotation circle but it is still somewhat moving downwards to fill in the space left behind the displaced pipe. When the pipe splits the trench wall and further penetrates into the seabed soil, the native ground in front of and above the pipe tend to be lifted upwards while the backfilling soil near trench wall tends to moving downwards. Due to this phenomenon, shear bands with almost vertical formation could be clearly observed near the trench walls in the backfilling soil (see Figure 4-11 d-g) after the pipe splits the trenchwall and further enters into the native seabed soil (see Figure 4-12 b-d). Actually this vertically-formed shear bands could also been observed in the shallowly buried case (see Figure 4-9 d-g) above the pipe in the backfilling soil near the left trench wall but is not as significant as it could be in the deeply buried case (see Figure 4-11 d) because the upper region of backfilling soil are more involved in the rotation circle (see Figure 4-10 b-d) and the shape of the formed shear bands adjacent to the trench wall is closer to a spiral line (see Figure 4-9 e-g) instead of the initial vertical line (see Figure 4-9 d). This indicates the stiffness of backfilling soil tends to have different influence on the shallowly buried pipe and deeply buried pipe when the moves from trench to native ground.

Although dents on seabed surface were not clearly formed in deeply buried case comparing (see Figure 4-11 g) with the shallowly buried case (Figure 4-9 g), but the shear band in front of pipe propagating from the pipe bottom tends to form (see Figure 4-11 g) which is similar to the one shows in shallowly buried case (see Figure 4-9 c), and lifting trend of native soil to forming the moving spiral wedge in front of pipe staring from the pipe bottom

to the seabed surface is observed in deeply buried case (see Figure 4-12 d) which is similar to the one shows in shallowly buried case (see Figure 4-10 d).

4.4. Conclusions

A two-dimensional RITSS (re-meshing and interpolation technique using small strain) model was developed for large deformation analysis of pipeline-backfill-trench interaction. The total stress framework was developed using ABAQUS/standard with a modified Tresca model (Zhang et al. 2015, 2018) facilitated by subroutine USDFLD. Python scripts were coded to automate the large deformation finite element (LDFE) analysis without any user intervention. The powerful mesh generation and solution mappings were combined and verified through comparing bearing capacity curves in design code with numerical results with pipeline embedded in homogenous seabed and comparing centrifuge tests results with numerical results with trenched pipelines. CEL model was developed with the modified Tresca model adjusted to VUSDFLD subroutine in the explicit analysis to provide comparisons with the performance of the 2D RITSS framework. Failure mechanisms were clearly showed by plotting the shear bands propagated during the large displacement of pipe. Following key observations were made:

- The developed RITSS model was proven a strong tool for pipeline-backfill-trench interaction. The developed model can be applied to clearly show the failure mechanism propagation in soil during the large lateral displacement of pipe.

- It was observed that the developed 2D RITSS frameworks had significant advantages in modeling large lateral displacement of embedded pipe. The predicted load-displacement curves match well with recommended curves provided in

guidelines and managed to pull the pipe by several times pipe diameter than conventional numerical model with Lagranigian meshes.

- The differences in stiffness between backfilling soil and seabed soil significantly affect the pipe responses during lateral displacement.

- While the pipe moves from backfill soil zone into the seabed soil zone, the predicted curves obtained using numerical model developed in this chapter give predictions closer to the test results other than the prediction curves obtained from design codes.

- Initial embedment depth of pipe into the trench bed will significantly affect the magnitude of the soil resistance. Which shows the response curve should not be considered as purely determined by the different soil stiffness of backfill soil and seabed soil, instead it should be a complex results from the pipeline-backfill-trench interaction which depends on the configuration of the whole system.

- The 2D RITSS model developed in this chapter shows significant advantages in tracking the details failure mechanisms and is able to provide more accurate load-displacement curves than the CEL model. While CEL model overcomes the difficulties showing in large deformation problem using conventional Lagrangian mesh analysis (e.g. overdistortion of Lagrangian meshes, lack of accuracy after mesh over distorted, etc.), even with relatively fine meshes, the CEL model failure to capture some details which can be very important for the failure mechanism analysis.

- While CEL is a convenient tool for numerically modelling the large deformation problems, the developed 2D RITSS framework has a unique advantage that it could be incorporated into coupled pore fluid pressure analysis for partially drained tests to well represent the rate effects, which is currently being done by the authors.

- A modified Tresca model was adopted to incorporate the strain softening. This could well represent the soil in the undrained condition test. Studies on extending the developed RITSS framework with pipeline-backfill-trench interaction to different drainage condition tests is currently being done by the authors, and effective stress constitutive model will be used to introduce the pore fluid pressure into the analysis.

It is worth mentioning that consolidation effects are usually significantly affect the response of pipeline during lateral displacement. However, the CEL (Coupled Eulerian Lagrangian) technique, which is the convenient and popular tool in LDFE analysis, is not able to be used together with the ABAQUS built-in coupled pore fluid pressure method. By now, most published studies were restricted to two limits conditions, drained or undrained. Partially drained conditions are most common conditions as the transition between these two limits and had not got enough attention. Studies on pipeline embedded in homogenous seabed displaced with different interaction rates (resulting in different drainage conditions) are currently being done by authors using the coupled pore fluid pressure analysis and it would be great if the pore fluid pressure could be successfully introduced into the trenched pipeline model developed here using RITSS method. This challenging area needs further investigations that are currently going on by the authors

through the incorporation of the coupled pore fluid pressure analysis into the developed RITSS framework for large deformation analysis of lateral pipeline-backfill-trench interaction.

4.5. Acknowledgments

The authors sincerely acknowledge the financial support of “Wood Group,” that established a Research Chair program in Arctic and Harsh Environment Engineering at Memorial University of Newfoundland, the “Natural Science and Engineering Research Council of Canada (NSERC)”, and the “Newfoundland Research and Development Corporation (RDC) (now InnovateNL)” through “Collaborative Research and Developments Grants (CRD)”. Also, the Authors acknowledge the visiting research funding provided by Mitacs through Globalink program and also the Center of Offshore Foundation Systems and the University of Western Australia for providing the visiting opportunity and collaboration. Special thanks are also extended to Memorial University for providing excellent resources to conduct this research.

References

ABAQUS analysis User's Manual. 2017. Dassault Systemes Simulia Corp.

ALA. Guidelines for the design of buried steel pipe. In ASCE, 2005.

ASCE. 1984. Guidelines For The Seismic Design Of Oil And Gas Pipeline Systems.

Bhushan, K., Haley, S.C., and Fong, P.T. 1979. Lateral Load Tests on Drilled Piers in Stiff Clays ASCE. Journal of the Geotechnical Engineering Division, ASCE, 105(GT8), pp. 969–985.

Chaloulos, Y., Bouckovalas, G., Zervos, S., and Zampos, A. 2015. Lateral soil-pipeline interaction in sand backfill: effect of trench dimension, Computers and Geotechnics, vol. 69, pp. 442-451.

Das, B.M., Moreno, R., and Dallo, K. 1985. Ultimate pullout capacity of shallow vertical anchors in clay. Soils and Foundations, vol. 25(2), pp. 148–152.

Das, B.M., Tarquin, A.J., and Marino, R. 1987. Model Tests for Pullout Resistance of Vertical Anchors in Clay. Soils and Foundations, vol. 17(2), pp. 52–56, 1987.

Edgers, L. and Karlsrud, K. 1982. Soil flows generated by submarine slides - case studies and con-sequences. In Third International Conference on the Behaviour of OffShore Structures. pp. 425–437.

Hansen, J.B. 1948. The Stabilizing Effect of Piles in Clay. In CN Post No. 3, Christiani and Nielson, Copenhagen, Denmark, November. pp. 14–15.

Hansen, J.B. and Christensen, N.H. 1961. The ultimate resistance of rigid piles against transversal forces. Geoteknisk Institut, Copenhagen.

Hsu, T., 1993. Rate effect on lateral soil restraint of pipelines. Soils and Foundations vol. 33(4), pp.159-169.

Hu, Y. and Randolph, M.F. 1998. A practical numerical approach for large deformation problems in soil. Int. J. Numer. Analyt. Meth. Geomech., vol. 22, pp. 327-350.

Kianian, M., Esmaeilzadeh, M., and Shiri, H. 2018. Lateral Response of Trenched Pipelines to Large Deformations in Clay. Offshore Technology Conference, OTC2018, Houston, TX, US, OTC-28842-MS.

Klar, A. and Randolph, M.F. 2008. Upper-bound and load–displacement solutions for laterally loaded piles in clays based on energy minimization. Géotechnique, vol. 58(10), pp. 815–820.

Kouretzis, G., Sheng, D., and Sloan, S. 2013. Sand-pipeline-trench lateral interaction effects for shallow buried pipelines, Computers and Geotechnics, vol. 54, pp. 53-59.

Luscher, U., Thomas, H.P., and Maple, J.A. 1979. Pipe-Soil Interaction. Trans-Alaska Pipeline. In Pipelines in Adverse Environments: A State of the Art. ASCE. pp. 486–502.

Mackenzie, T.R. 1955. Strength of Deadman Anchors in Clay. M.Sc. Thesis, Princeton University, Princeton, USA.

Merifield, R.S., Sloan, S.W., and Yu, H.S. 2001. Stability of plate anchors in undrained clay. Géotechnique, vol. 51(2), pp. 141–153.

Oliveira, J.R.M.S., Almeida, M.S.S., Almeida, M.C.F., and Borges, R.G. 2010. Physical Modeling of Lateral Clay-Pipe Interaction. Journal of Geotechnical and Geoenvironmental Engineering, vol. 136, pp. 950–956.

Paulin, M. 1998. An investigation into pipelines subjected to lateral soil loading. Memorial University of Newfoundland, St. John's, Canada.

Phillips, R., Nobahar, A., and Zhou, J. 2004, Trench effects on pipe-soil interaction, Proceeding of International Pipeline Conference, Calgary, Alberta, Canada, IPC2004-141.

Pike, K. 2016. Physical and numerical modeling of pipe/soil interaction events for large deformation geohazards. Memorial University of Newfoundland, St. John's, Canada.

Poorooshasb, F., Paulin, M., Rizkalla, M., and Clark, J. 1994. Centrifuge modeling of laterally loaded pipelines. Transportation research record, pp. 33–40.

Poulos, H.G. 1995. Design of Reinforcing Piles to Increase Slope Stability. Canadian Geotech-nical Journal, 32(5): 808–818.

PRCI. 2009. Guidelines for constructing natural gas and liquid hydrocarbon pipelines through areas prone to landslide and subsidence hazards. In Pipeline Research Council International.

Ragni, R., Wang, D., Mašín, D., Bienen, B., Cassidy, M.J., and Stanier, S.A. 2016. Numerical modelling of the effects of consolidation on jack-up spudcan penetration. Computers and Geotechnics, vol. 78, pp. 25-37.

Rajah, S., Shumaker, S., Bardakjian, H., Botteicher, B., Bushdiecker, K., Conner, R., Cox, A., Fisher, C., LeBlanc, J., McCabe, M.W., Walker, R., and Whidden, W. 2014. Soil parameters for assessing axial and transverse behavior of restrained pipelines—Part 2: Transverse behavior. In Pipelines 2014: From Underground to the Forefront of Innovation and Sustainability. ASCE, Portland. pp. 1849–1863.

Ranjani, B.B., Robertson, P.K., and Morgenstern, N.R.1993. A Simplified Method for Pipelines Subject to Transverse Soil Movements Proceedings, vol. V, pp. 157-165. In 12th Offshore Mechanics and Arctic Engineering Symposium.

Reese, L.C. and Welch R.C. 1975. Lateral Loading of Deep Foundations in Stiff Clay. Journal of the Geotechnical Engineering Division, vol. 101(7), pp. 633–649.

Rizkalla, M. and Mclntyre, M.B.1991. A Special Pipeline Design for Unstable Slopes. Proceedings, Pipeline Engineering 1991, 14th Annual Energy-Sources Technology Conference and Exhibition, Houston, ASME, Vol. 34, pp. 69-74.

Rowe, R.K. and Davis, E.H. 1982. The Behaviour of Anchor Plates in Clay. Geotechnique, vol. 32(1), pp. 9–23.

Sumer, B.M., and Fredsøe, J. 2006. Hydrodynamics around cylindrical structures. World Scientific Pub. Co. Inc., Singapore.

Tian, Y., Cassidy, M.J., Randolph, M.F., Wang, D., and Gaudin, C. 2014. A simple implementation of RITSS and its application in large deformation analysis. Computers and Geotechnics, vol. 56, pp. 160-167.

Tschebotarioff, G.P. 1973. Foundations, Retaining and Earth Structures. McGraw-Hill Book Company, New York, 642p.

Ullah, S.N., Hou, L.F., Satchithananthan, U., Chen, Z., and Gu, H. 2018. A 3D RITSS approach for total stress and coupled-flow large deformation problems using ABAQUS. Computers and Geotechnics, vol. 99, pp. 203-215.

Wang, D., White, D.J., and Randolph, M.F. 2010. Large-deformation finite element analysis of pipe penetration and large-amplitude lateral displacement. Canadian Geotechnical Journal, vol. 47, no. 8, pp. 842-856.

Wantland, G.P., O'Neill, M.B., Reese, L.C., and Coelogyne, E.H. 1979. Lateral Stability of Pipelines in Clay. Proceedings, 11th Offshore Technology Conference, ASME, Houston, pp. 1025-1034.

Yu, L., Liu, J., Kong, X., and Hu, Y. 2008. Three-dimensional RITSS large displacement finite element method for penetration of foundations into soil. Computers and Geotechnics, vol. 35, no. 3, pp. 372-382, 2008.

Zhang, W., Wang, D., Randolph, M.F., and Puzrin, A. 2015. Catastrophic failure in planar landslides with a fully softened weak zone. Géotechnique, vol. 65, pp. 755-769.

Zhang, W., Randolph, M.F., Puzrin, A., and Wang, D. 2018. Transition from shear band propagation to global slab failure in submarine landslides. Canadian Geotechnical Journal, vol. 56.

Chapter 5

A coupled LDFE model for analysis on large lateral displacement of trenched pipeline

Xiaoyu Dong[1] and Hodjat Shiri[2]

1: Department of Civil

Engineering, Memorial University of Newfoundland

e-mail: xiaoyu.dong@mun.ca

2: Department of Civil

Engineering, Memorial University of Newfoundland

e-mail: hshiri@mun.ca

This chapter is submitted as a journal manuscript.

Abstract

Offshore pipelines delivering oil and gas are usually buried in trench for physical protection. However, the trenched pipelines may still be laterally displaced because of ground movement, landslides, ice gouging and etc. Existence of the trench and different interaction rates have been proven to significantly influence the failure mechanism in soil during the large lateral displacement of the trenched pipeline. However, the trench effect and consolidation effect have not been comprehensively expored and therefore have not been covered thoroughly in design codes. In this chapter, a coupled LDFE framework with cam-clay type constitutive model was developed in ABAQUS respectively to examine the consolidation effects and trench effects. The numerical results showed close prediction regarding the load-displacement response and tracking detailed failure mechanisms in large deformation finite element analysis.

Keywords: LDFE, Numerical modeling, Lateral pipeline-backfill-trench interaction, coupled analysis, Consolidation effect

5.1. Introduction

Subsea pipelines are usually buried in trench and backfilled with pre-excavated materials for physical protection against environmental loads etc. Relative displacement between the pipeline and the surrounding soil can be caused by the ground movements, ice gouging, etc. The force-displacement response of the displaced pipeline can be influenced by the differences between stiffness of backfill soil and native seabed soil, trench geometry, interaction rates etc (Scarpelli et al. 1999, Ng. 1994, Lever 2000). In practice, the pipeline-soil interaction response is generally idealized by defining a set of the specialized beam and spring elements expressed by bilinear or hyperbolic functions. However, large discrepancies are observed in the recommendations provided by different design codes and the empirical equations proposed in some previous studies for calculation of the ultimate lateral resistance and also the p-y response. The simplified assumptions ignoring the trench effects and consolidation effects.

The influence of different stiffness between the backfilling and native material on lateral p-y response of the pipeline is rarely considered in the proposed models and design codes, while the conducted testing programs has proven the significant influence of relative backfill-trench stiffness on lateral pipe response. Paulin (1998) conducted a series of lateral pipeline-soil interaction centrifuge tests proving the existence of trench and different interaction rates can influence the failure mechanisms. Kianian et al. conducted a series of centrifuge tests to and use advanced experimental set-up to explicitly show the progressive and interactive failure mechanisms.

Very limited number of published research works were published with physical tests modeling (Paulin 1998; C-CORE report 2003; Kianian 2018) or numerical modeling (C-

CORE report 2003) of the pipeline-backfill-trench interaction due to the high cost. And neither of these studies have been able to show the effects of induced excess pore pressure on the failure mechanisms.

To perform LDFE analysis, the current study used the remeshing and interpolation technique with small strain (RITSS) proposed by Hu and Randolph (1998). It has great advantages and is proved to work efficiently and accurately in the large deformation problems. In this study, a cam-clay type constitutive model was used together with the coupled pore fluid pressure analysis to incorporate the consolidation effects. A series of analyses were conducted to capture the pipeline-backfill-trench interaction on soil resistance using the developed coupled LDFE model. The developed coupled LDFE model has a unique advantage that it could be applied for partially drained tests to well represent the rate effects. The results of numerical analyses were validated against the published experimental, the design codes.

5.2. Methodology

The physical model in centrifuge tests (C-CORE report, 2003) was made at 1:50 scale in soil. The silty clay used in the tests was a mixture by weight of Speswhite kaolin clay (50%) and Sil-Co-Sil silt (50%). The soil was preconsolidated to 400 kPa to reach a desired undrained shear strength around 40 kPa. The model pipelines were set as 19 mm in diameter corresponding to a prototype value of 0.95 m. Cover depths investigated in the physical models were 16 mm and 65 mm corresponding to prototype value of 0.8 m and 3.25 m respectively. A model trench width was set as 50 mm which corresponds to 2.5 m in prototype scale.

5.3. Overall framework for RITSS model

The flowchart of RITSS procedure for pipeline-backfill-trench interaction is briefly shown in Figure 5-1. Overall, the large-deformation is divided into a series of incremental jobs with small strain increments. The framework is developed based on the coupled analysis model proposed by Dong et al. (2020a) and the pipeline-backfill-trench interaction model proposed by Dong et al. (2020b).

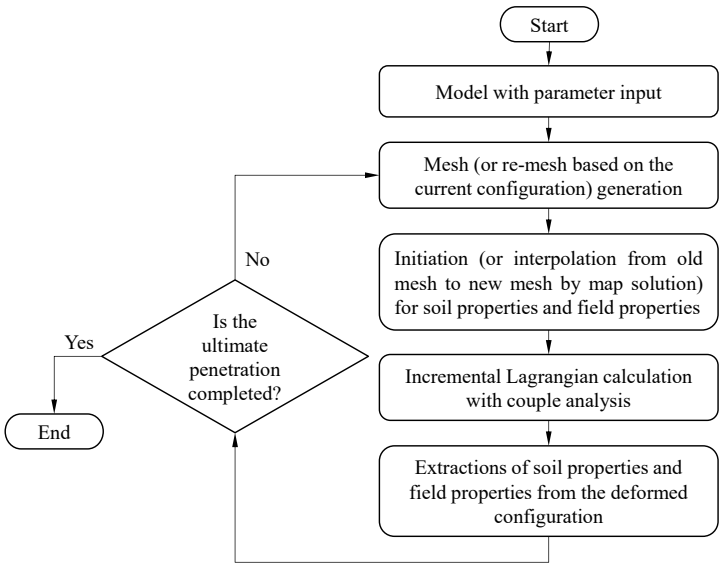

Figure 5-1. Overall scheme of calculation loop (Dong et al. 2020a)

In this way, the newly-porposed coupled LDFE model is convenient to be used with different trench geometries and different interaction rates to consider large lateral displacement of trenched pipelines with different system configurations (trench width, trench depth, angle of trench wall, etc.) or with different drainage conditions.

5.4. Details of job set-up

As shown in Figure 5-2, the initial model was set up with the undeformed configuration and geostatic step is conducted to reach the desired stress level in the soil body (same as

the configuration proposed in Dong et al., 2020b). The deformed boundary nodes were extracted from the old job and then used to sketch the geometry parts in the new job with deformed shape.

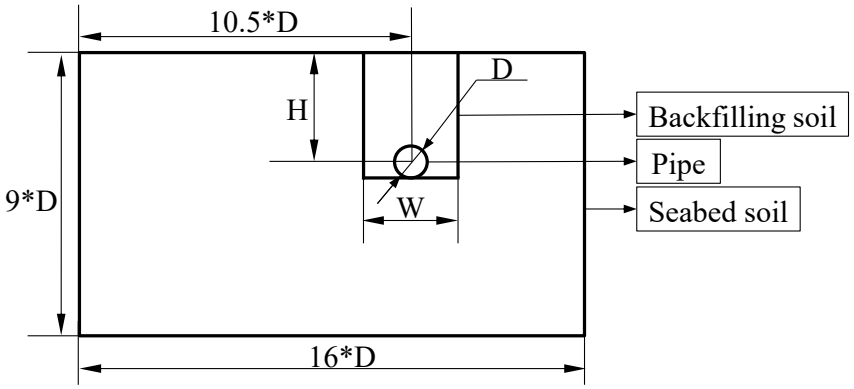

(a)

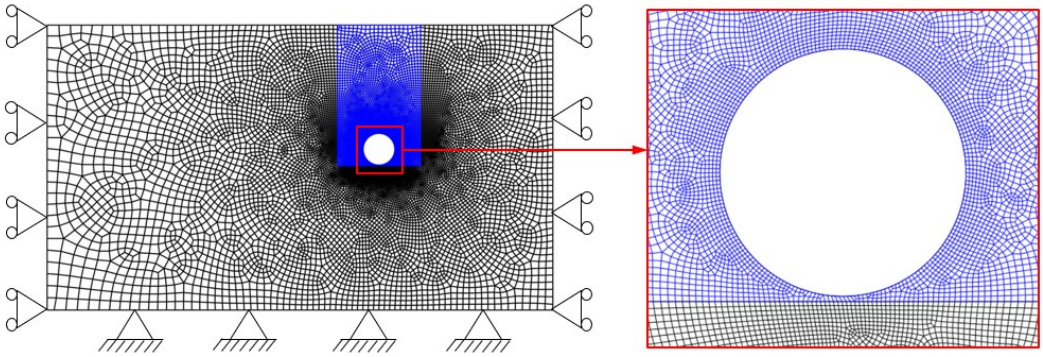

(b)

Figure 5-2. Configuration of trenched pipe (Dong et al., 2020b).

Three components have been considered in the general analysis including pipe, backfilling material, and native soil. Trench is excavated in the native soil, pipe is laid on the bottom of the trench (with one layer of backfill soil beneath the pipe) with backfilling soil placed around it inside the trench. The soil domain was modeled by using 4-node bilinear plane strain elements (CPE4P), with details shown in Figure 5-2 b. Rigid wire elements (R2D2)

were used to model the pipe. The displacements were fully restrained in the bottom boundary. The side boundaries were restrained against displacement perpendicular to the respective sides. The nodes on the contact surface of the pipe and soil were tied together.

5.5. Constitutive model

A Cam-Clay-Type constitutive model with strain hardening was used in the coupled LDFE analysis to conduct tests with different drainage conditions, which is same as the constitutive model introduced in Dong et al. (2020a). The mathematical model of soil behaviour was proposed by Lagioia and Nova (1995) originally with incorporation of the cement effect, as an improved model comparing with the one proposed by Nova in 1992. The linear elasticity was considered in alignment with the work by Lagioia and Nova (1995). Panteghini and Lagioia recently improved the numerical integration efficiency for above mentioned MCC type constitutive model with considerations of full convexity and double homothety. More details about the constitutive model can be found in Panteghini and Lagioia (2016, 2018).

5.6. Large deformation analysis of pipe-soil interaction

5.6.1. Pipe embedded in uniform seabed

Uniform seabed soil are used for benchmarking the coupled LDFE model. Responses of pipe embedded with different burial depth and displaced at different velocities wereexamined (see Figure 5-4). Burial depth ratio, interaction rates and drainage conditions are listed in Table 5-1. Soil properties in the model are given in Table 5-2. The relationship between burial depth ratio and corresponding normalized response were plotted in Figure 5-5.

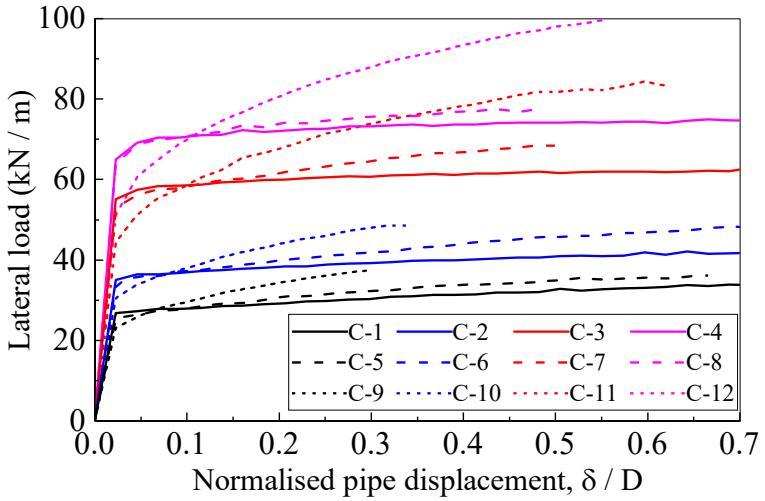

Figure 5-3. Load-displacement curves.

As shown in Figure 5-3, the different drainage conditions show significant influence on the magnitude of the lateral load on pipe. In drained test (eg. C-11), the normalized response increases quickly and becomes larger than the corresponding partially drained test (C-7) and undrained test (C-3) before the pipe is displaced by 0.15 D. For same burial depth ratio, the smaller the normalized velocity (see Table 5-1), the more obvious increase trend could be observed in the normalized response curve (see Figure 5-3).

Table 5-1. Case studies map

Burial depth ratio	H/D=1.5			H/D=2.0			H/D=3.0			H/D=3.5		
Interaction rate v	Case study	Normalized velocity V	Drainage condition	Case study	Normalized velocity V	Drainage condition	Case study	Normalized velocity V	Drainage condition	Case study	Normalized velocity V	Drainage condition
1.0×10^{-7}	C-1	71.0	U	C-2	54.3	U	C-3	37.0	U	C-4	32.0	U
1.0×10^{-9}	C-5	0.71	P	C-6	0.54	P	C-7	0.37	P	C-8	0.32	P
5.0×10^{-11}	C-9	0.036	D	C-10	0.027	D	C-11	0.018	D	C-12	0.016	D
Note: For drainage conditions, U represents for undrained conditions, P represents for partially drained conditions, and D represents for drained conditions.												

Table 5-2. Case studies map (Dong et al. 2020a)

Properties		Symbol	Value								Unit
Specific weight of pore fluid		γ_w	10								kN/m^3
Effective unit soil weight		γ	7.5								kN/m^3
Pipe diameter		D	0.95								m
Young's modulus of soil		E	5000								kPa
Poisson's ratio		υ	0.3								-
Initial void ratio		e_0	1.5								-
Coefficient of earth pressure at rest		K_0	0.65								-
Slope of CSL		M_{tc}	0.77								-
Permeability of soil		k_v	10^{-10}								m/s
Properties (*H* refers to the distance from soil surface to pipe centre, while *w* refers to the distance from soil surface to pipe bottom)		Symbol	*H/D*=1.5, *w/D*=2.0		*H/D*=2.0 *w/D*=2.5		*H/D*=3.0, *w/D*=3.5		*H/D*=3.5, *w/D*=4.0		-
			Pipe centre	Pipe bottom	Pipe centre	Pipe bottom	Pipe centre	Pipe bottom	Pipe centre	Pipe bottom	
Triaxial compression	Mean effective stress	p'	8.25	11.00		13.75	16.50	19.25		22.00	kPa
	Equivalent stress	q	3.65	4.87		6.09	7.31	8.53		9.75	kPa
	Effective vertical stress	$\sigma_{v0}^{'}$	10.69	14.25		17.81	21.38	24.94		28.50	kPa
	Stress ratio	η	0.44	0.44		0.44	0.44	0.44		0.44	-
	parameter	Λ	0.97	0.96		0.95	0.94	0.93		0.92	-
	Equivalent undrained shear strength	$s_{u,tc}$	2.14	2.87		3.60	4.34	5.08		5.82	kPa
	coefficient of volume compressibility	m_v	0.0080	0.0061		0.0049	0.0041	0.0036		0.0032	m^2/kN

	Coefficient of vertical consolidation	c_v	1.24 $\times 10^{-9}$	1.64×10^{-9}	2.03 $\times 10^{-9}$	2.41 $\times 10^{-9}$	2.79×10^{-9}	3.16 $\times 10^{-9}$	m^2/s
Compression under plane strain condition	Mean effective stress	s'	8.86	11.81	14.77	17.72	20.67	23.63	kPa
	Equivalent stress	t	1.83	2.44	3.05	3.66	4.26	4.87	kPa
	Effective vertical stress	σ'_{v0}	10.69	14.25	17.81	21.38	24.94	28.50	kPa
	Stress ratio	θ	0.21	0.21	0.21	0.21	0.21	0.21	-
	parameter	Λ	0.97	0.96	0.95	0.94	0.93	0.92	-
	Equivalent undrained shear strength	$s_{u,ps}$	2.22	2.97	3.73	4.50	5.27	6.04	kPa
	coefficient of volume compressibility	m_v	0.0075	0.0057	0.0046	0.0039	0.0034	0.0030	m^2/kN
	Coefficient of vertical consolidation	c_v	1.33 $\times 10^{-9}$	1.75×10^{-9}	2.17 $\times 10^{-9}$	2.58 $\times 10^{-9}$	2.98×10^{-9}	3.37 $\times 10^{-9}$	m^2/s

Besides, the curves in Figure 5-3 indicate the effects of burial depth ratios on normalized responses. With deeper burial, the normalized responses tend to have larger magnitude.

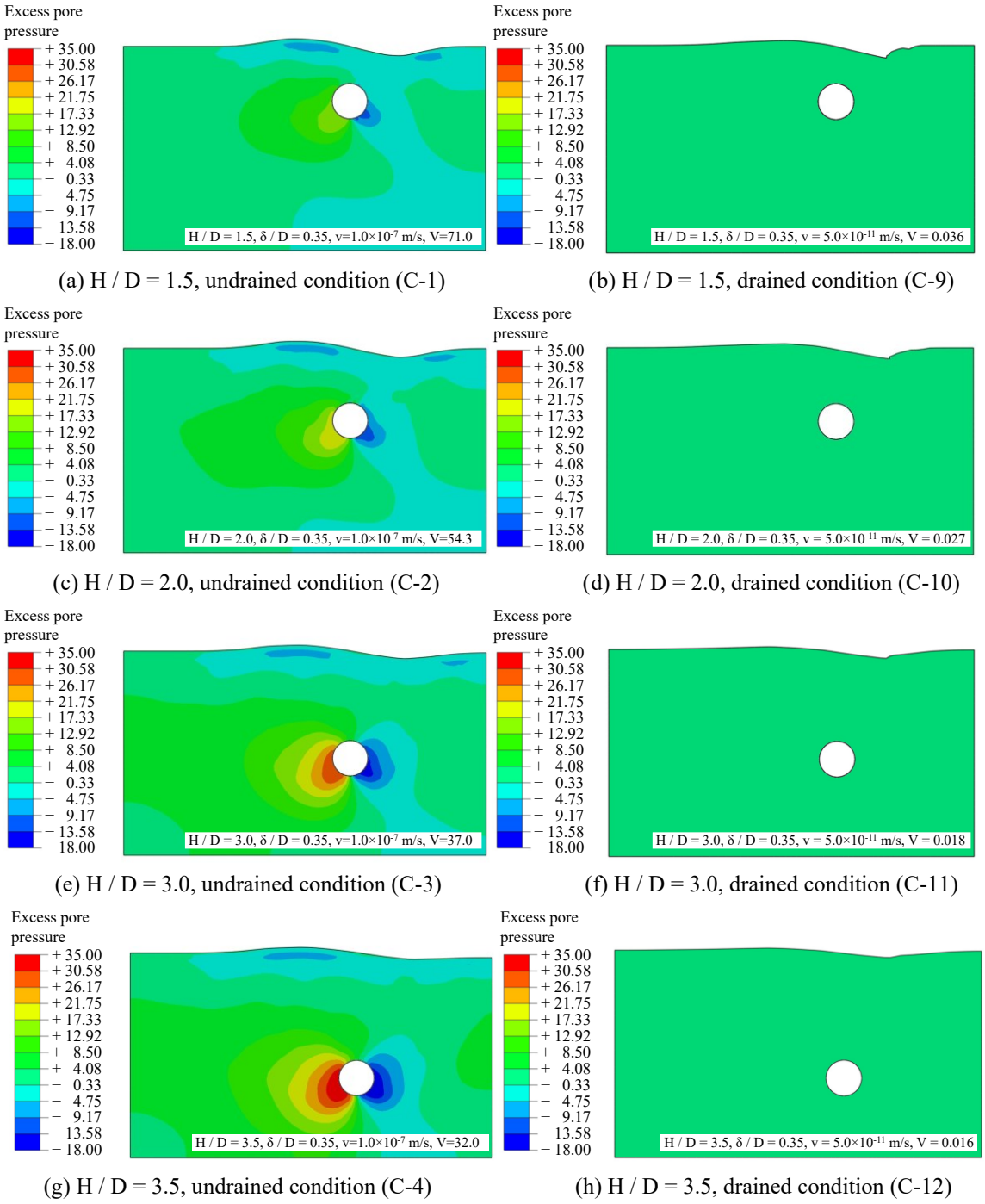

(a) H / D = 1.5, undrained condition (C-1)

(b) H / D = 1.5, drained condition (C-9)

(c) H / D = 2.0, undrained condition (C-2)

(d) H / D = 2.0, drained condition (C-10)

(e) H / D = 3.0, undrained condition (C-3)

(f) H / D = 3.0, drained condition (C-11)

(g) H / D = 3.5, undrained condition (C-4)

(h) H / D = 3.5, drained condition (C-12)

Figure 5-4. Computed induced excess pore pressure.

The induced excess pore pressure with different burial depth ratios are shown in Figure 5-4. Left column of figures are results from undrained tests, while right column of figures

are obatined from drained tests. It is indicated that the negative excess pore pressure is formed behind the laterally displaced pipe. And the magnitude of induced excess pore pressure around the pipe increases with the increase in burial depth ratio of the pipe. In drained tests, the deformation of soil surface show difference from the results obtained from undrained tests.

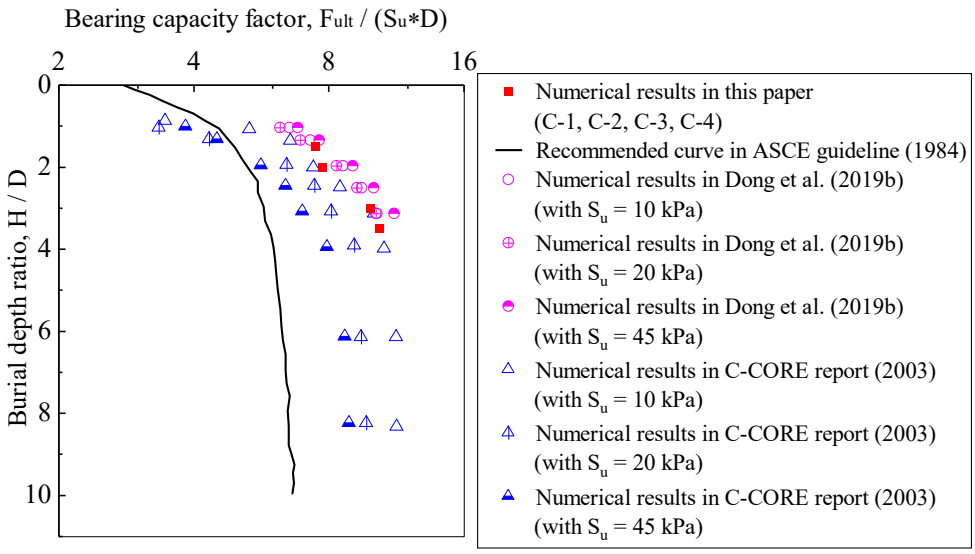

Figure 5-5. Effects of burial depth on bearing capacity factor.

Compared with the recommended curves in ASCE guidelines (1984) and published numerical work (Dong et al., 2020 b; C-CORE report, 2003), the predicted responses by developed coupled LDFE framework with MCC model are in accordance with the recommendations and showed only slight differences in some cases (see Figure 5-5).

5.6.2. Trenched pipeline

The developed LDFE model was benchmarked in Section 5.6.1, showing its advantages in predicting induced excess pore pressure and modelling tests under different drainage conditions. In this section, the developed LDFE model is applied to the trenched pipeline.

As briefly introduced at the beginning of Section 5.2, the configurations of numerical model for trenched pipelines were set based on the centrifuge tests conducted by Paulin in 1998 (Paulin 1998), including shallowly buried pipe (C-13, C-14,C-15) and the other is set for deeply buried pipe (C-16). General model parameters could be found in Table 5-3, with details of native seabed soil parameters given in Table 5-4. As for the backfill soil, Young's modulus is used as 1000 kPa and effective unit soil weight is 8 kN/m^3. Normal consolidated or slightly consolidated to achieve the desired undrained shear strength (e.g. 2~3 kPa) at specific buried depth.

Table 5-3. Parameters used for model

Properties	Symbol	Unit	C-13	C-14	C-15	C-16
Pipe diameter	D	m	0.95	0.95	0.95	0.95
Trench width	W	m	2.5	2.5	2.5	2.5
Cover depth	C	m	0.80	0.80	0.80	3.25
Embedment ratio	H/D	-	1.342	1.342	1.342	3.921
Permeability of soil	k	m/s	10^{-10}	10^{-10}	10^{-10}	10^{-10}
Backfill soil undrained shear	s_{u_b}	kPa	3.3	1.5	1.842	3.5
Seabed soil undrained shear	s_{u_s}	kPa	36.2	31.8	23.9	42.1

Table 5-4. Parameters used for native seabed soil in numerical model.

Properties		Symbol	Value				Unit
Specific weight of pore fluid		γ_w	10				kN/m^3
Effective unit soil weight		γ	9				kN/m^3
Pipe diameter		D	0.95				m
Young's modulus of soil		E	5000				kPa
Poisson's ratio		υ	0.3				-
Initial void ratio		e_0	1.5				-
Coefficient of earth pressure at rest		K_0	0.65				-
Permeability of soil		k_v	10^{-10}				m/s
Hardening parameter		B_p	0.064				-
Slope of CSL		M_{tc}	0.77				-
Triaxial compression conditions frictional angle		ϕ_{tc}	0.35				rad
Plane strain conditions frictional angle		ϕ_{ps}	0.39				rad
Properties		Symbol	H/D=1.342			H/D=3.921	-
			C-13 (T1P1)	C-14 (T4P1)	T8P1	T2P1	-
Seabed soil undrained shear strength in centrifuge tests (Paulin 1998)		s_{u_test}	36.2	31.8	23.9	42.1	kPa
Size of the initial yield surface		p_{c0}	155	130	100	190	kPa
Triaxial compression	Mean effective stress	p'	8.86	8.86	8.86	25.88	kPa
	Over Consolidated Ratio	OCR	17.50	14.68	11.29	7.34	-
	Equivalent stress	q	3.92	3.92	3.92	11.47	kPa
	Stress ratio	η	0.44	0.44	0.44	0.44	-
	parameter	Λ	0.97	0.97	0.97	0.91	-
	Equivalent undrained shear strength (NC)	$s_{u,tc,NC}$	2.30	2.30	2.30	6.88	kPa
	Equivalent undrained shear strength (OC)	$s_{u,tc,OC}$	36.77	31.01	24.05	42.41	kPa

	(using $s_{u,OC} = s_{u,NC}(OCR)^{\Lambda}$)						
	coefficient of volume compressibility	m_v	0.0075	0.0075	0.0075	0.0027	m^2/kN
	Coefficient of vertical consolidation	c_v	1.33 $\times 10^{-9}$	1.33 $\times 10^{-9}$	1.33 $\times 10^{-9}$	3.67×10^{-9}	m^2/s
Compression under plane strain condition	Mean effective stress	s'	9.51	9.51	9.51	27.79	kPa
	Over Consolidated Ratio	OCR	16.30	13.67	10.51	6.84	-
	Equivalent stress	t	1.96	1.96	1.96	5.73	kPa
	Stress ratio	θ	0.21	0.21	0.21	0.21	-
	parameter	Λ	0.97	0.97	0.97	0.91	-
	Equivalent undrained shear strength (NC)	$s_{u,ps,NC}$	2.38	2.38	2.38	7.15	kPa
	Equivalent undrained shear strength (OC) (using $s_{u,OC} = s_{u,NC}(OCR)^{\Lambda}$)	$s_{u,ps,OC}$	35.31	29.79	23.13	40.82	kPa
	coefficient of volume compressibility	m_v	0.0070	0.0070	0.0070	0.0026	m^2/kN
	Coefficient of vertical consolidation	c_v	1.43 $\times 10^{-9}$	1.43 $\times 10^{-9}$	1.43 $\times 10^{-9}$	3.91×10^{-9}	m^2/s

Two different interaction rates were adopted for the tests (C-13 and C-16) to give undrained condition and drained condition. The induced excess pore pressure is plotted in Figure 5-6 with left column of figures representing the undrained condition tests and the right column of figures representing the drained condition tests. In undrained tests, for both shallowly-buried case and deeply-buried case, negative pore pressure forms in the rear beneath the pipe and generate suction force (see Figure 5-6).

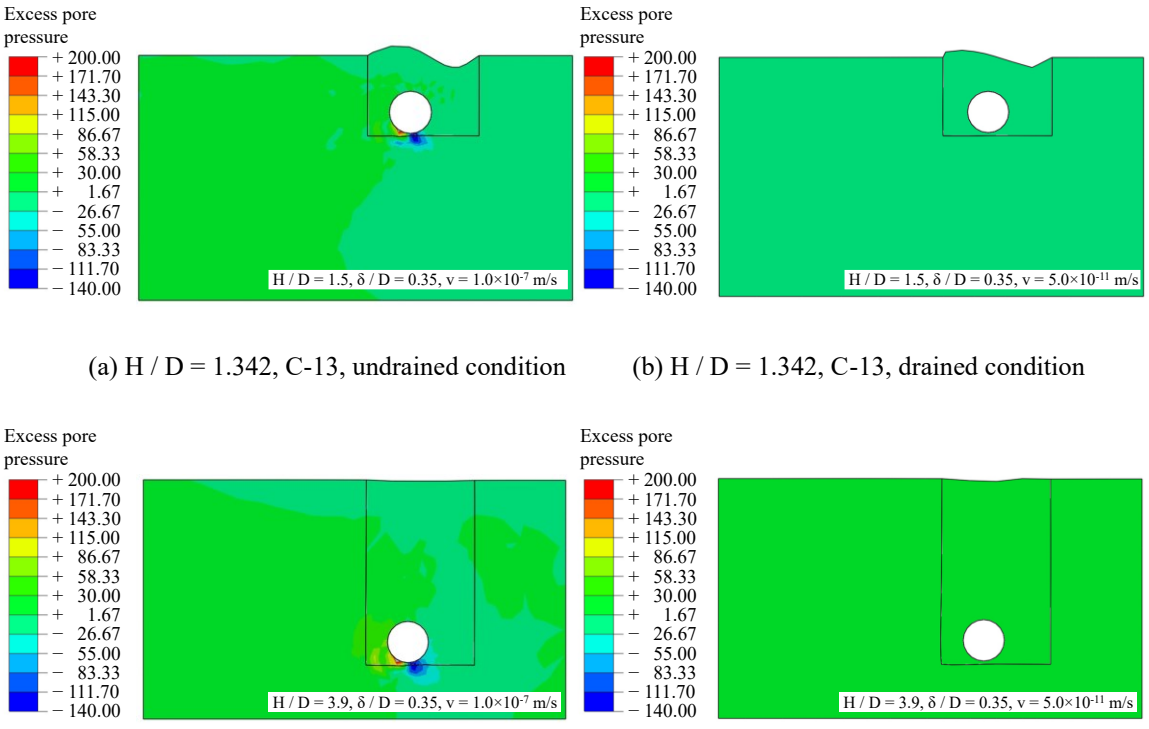

(a) H / D = 1.342, C-13, undrained condition (b) H / D = 1.342, C-13, drained condition

(c) H / D = 3.921, C-16, undrained condition (d) H / D = 3.921, C-16, drained condition

Figure 5-6. Induced excess pore pressure.

It is indicated that different soil surface shapes are formed with the lateral displacement of the trenched pipeline (see Figure 5-6). This can be further explained by the displacement vevtors plotted in Figure 5-7. Similar to different soil failure modes showed in different drainage condition tests (for pipe embeded in uniform seabed, Dong et al., 2020a), different failure modes are observed for the trenched pipeline (Figure 5-7). Local rotation of soil are observed in undrained condition, while a more global involvement of soil rotation and shear can be observed for drained condition. For example, the upper region of the backfill material is obviously involved into the displacement in the drained test for deeply-buried

pipe, while this trend is absent in the undrained test for deeply-buried pipe (comparing Figure 5-7 c and d).

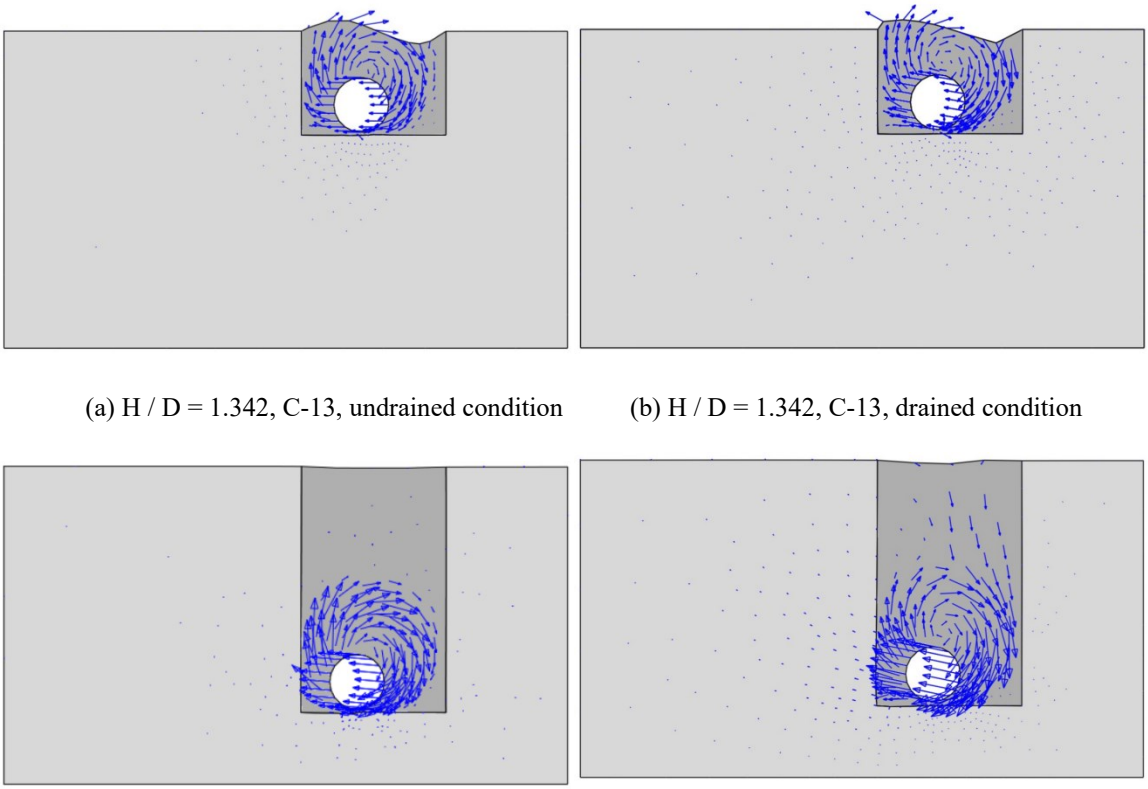

(a) H / D = 1.342, C-13, undrained condition (b) H / D = 1.342, C-13, drained condition

(c) H / D = 3.921, C-16, undrained condition (d) H / D = 3.921, C-16, drained condition

Figure 5-7. Displacement vectors generated in different cases.

The load-displacement curves are plotted in Figure 5-8. The drained tests indicate a much higher resistance of soil comparing with the results from undrained tests. The prediction of load-dispalcement curve for undrained test is in good accordance to the centrifuge tests.

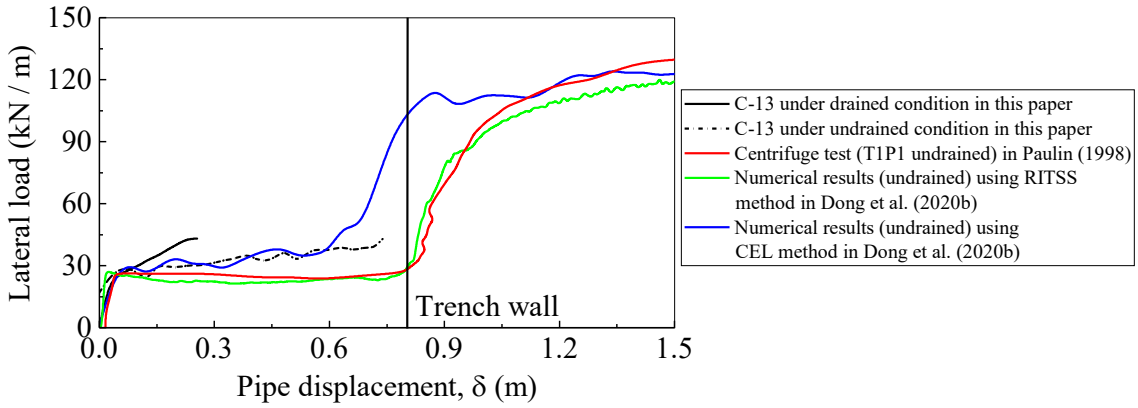

(a) H / D = 1.342, C-13

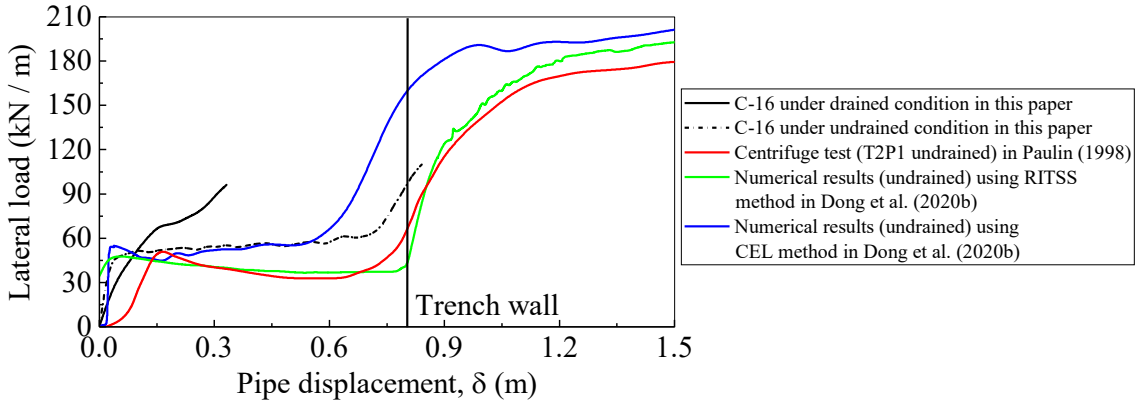

(b) H / D = 3.921, C-16

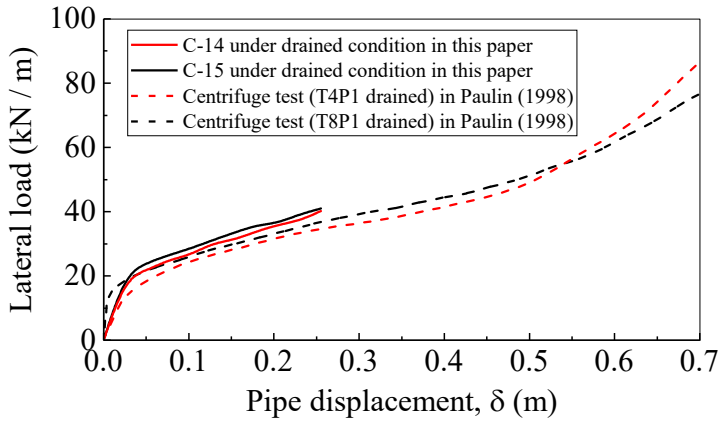

(c) H / D = 1.342, C-14 & C-15

Figure 5-8. Load-displacement curves.

As shown in Table 5-3, slight differences exist in the backfill soil strength between C-14 and C-15. Compared the numerical simulation results with the centrifuge tests (Paulin 1998), the computed resistance show good agreement with the published curves and well presents the continuing increase trend of pipe responses under drained conditions (see Figure 5-8 c).

5.7. Conclusions

A coupled LDFE model was developed for large deformation analysis of pipeline-backfill-trench interaction. The effective stress framework were developed using ABAQUS/standard with a cam-clay type constitutive model facilitated by subroutine UMAT. Python scripts were coded to automate the large deformation finite element (LDFE) analysis without any user intervention. The powerful mesh generation and solution mappings were combined and verified through comparing bearing capacity curves in design code with numerical results with pipeline embedded in homogenous seabed and comparing centrifuge tests results with numerical results with trenched pipelines. Failure mechanisms were clearly showed by plotting the displacement vectors. Following key observations were made:

- The developed RITSS model was proven a strong tool to explore the consolidation effects and trench effects in pipeline-backfill-trench interaction. The developed model can be applied to clearly show the failure mechanism in soil and induced excess pore pressure during the pipeline was laterally displaced.
- Load displacement cureves show a continuing increasing trend in drained tests at the starting stage and are in good accordance with the experimental results.

- Different interaction rates give rise to different distribution of displacement vectors, which result in different failure modes.
- A cam-clay type constitutive model was adopted to work with the coupled LDFE model. This effective stress constitutive model could well predict the soil resistance and induced excess pore pressure with pipe being displaced at different velocities (i.e., under different drainage conditions).

5.8. Acknowledgments

The authors gratefully acknowledge Dr. Rocco Lagioia and Dr. Andrea Panteghini for their valuable help on the user-coded Modified Cam-Clay model. The authors sincerely acknowledge the financial support of "Wood Group," that established a Research Chair program in Arctic and Harsh Environment Engineering at Memorial University of Newfoundland, the "Natural Science and Engineering Research Council of Canada (NSERC)", and the "Newfoundland Research and Development Corporation (RDC) (now InnovateNL)" through "Collaborative Research and Developments Grants (CRD)". Also, the Authors acknowledge the visiting research funding provided by Mitacs through Globalink program and also the Center of Offshore Foundation Systems and the University of Western Australia for providing the visiting opportunity and collaboration. Special thanks are also extended to Memorial University for providing excellent resources to conduct this research.

References

C-CORE, Honeggerm, D., D.G. Honegger Consulting, 2003. Extended Model for Pipe Soil Interaction.

Dong, X., Zhang, W., Shiri, H., and Randolph, M.F., 2020a. Large Deformation Coupled Analysis of Embedded Pipeline – Soil Lateral Interaction. Submitted as journal manuscript.

Dong, X., Shiri, H., Zhang, W., and Randolph, M.F., 2020b. A 2D RITSS model for analysis on large lateral displacement of trenched pipeline. Submitted as journal manuscript.

Lagioia, R., Nova, R., 1995. An experimental and theoretical study of the behaviour of a calcarenite in triaxial compression. Géotechnique, vol. 45(4), pp. 633-648, 1995.

Lever, J.H., 2000. Assessment of Millennium pipeline project Lake Erie crossing: Ice scour, sediment sampling, and turbidity modeling. ERDC/CRREL Technical Report 00-13.

Ng, P.C.F., 1994. Behaviour of buried pipelines subjected to external loading. PhD thesis, University of Sheffield, Sheffield, U.K.

Nova, R., 1992. Mathematical modelling of natural and engineered geomaterials. Euro. J. Mech. A: Solids. 11. 135-154

Paulin, M. 1998. An investigation into pipelines subjected to lateral soil loading. Memorial University of Newfoundland, St. John's, Canada.

Panteghini, A., Lagioia, R., 2018. An extended modified Cam-Clay yield surface for arbitrary meridional and deviatoric shapes retaining full convexity and double homothety. Géotechnique, vol. 68, no. 7, pp. 590-601.

Panteghini, A., Lagioia, R., 2018. An approach for providing quasi‐convexity to yield functions and a generalized implicit integration scheme for isotropic constitutive models based on 2 unknowns. International Journal for Numerical and Analytical Methods in Geomechanics, vol. 42, no. 6, pp. 829-855.

Scarpelli, G., Sakellariadi, E., and Furlani, G., 1999. Longitudinal pipeline-soil interaction: results from field full scale and laboratory testing. Panel Contribution in the Proc. of 12th ECSMGE, Balkema, Rotterdam, the Netherlands.

Chapter 6

Conclusions and Recommendations

6.1. Conclusions

The work outlined in this thesis was conducted to enhance the numerical analysis of pipeline and riser seabed interaction.

In the first section of the thesis (from Chapter 1 to Chapter 5), first, a coupled analysis model with cam-clay type constitutive model in terms of effective stress method is developed for comprehensively analyzing the influence of consolidation effects on soil resistance on embeded pipeline. Then, a 2D RITSS famework with a modified Tresca model considering the strain softening is developed to explore the trench effects on the soil resistance and failure mechanism. After achieving these two goals separately, the advanced coupled LDFE model considering both trench effects and consolidation effects is developed to handle the chanllenging pipeline-backfill-trench interaction problem. The developed coupled LDFE model is capable of customizing geometry of trench and modelling different drainage conditions. All these developed numerical models have been benchmarked by the published works, indluding centrifuge tests, analytical solution or numerical works. It is able to predict the soil resistance with trenched pipe displaced with different velocities (which has never been achieved before). And it can serve as a strong tool to reveal the progressing of the soil failure and give more accurate prediction of load-displacement curves.

Through the numerical analyses, it was demonstrated that:

- The ultimate resistance in test under drained condition is observed to be larger than the ultimate load obtained in tests with same configurations under undrained conditions.
- The different magnitudes in the increase of mean effective stress at front of the pipe from the same initial value under different drainage conditions were in good accordance with the induced excess pore pressure obtained.
- Different failure mechanisms were observed between tests with different drainage conditions.
- The differences in stiffness between backfilling soil and seabed soil significantly affect the pipe responses during lateral displacement.
- The developed 2D RITSS framework has its unique advantages (over CEL) to be incorporated into the ABAQUS built-in coupled pore pressure analysis for partially drained tests. This gives access to the simulation of the consoldiation effects and trench effects simultaneously, revealing the progressing of the failure mechanism in soil and induced excess pore pressure.
- Wwith the proposed equation, 2D RITSS model is able to predict the soil resistance with trenched pipe displaced with different velocities.
- Simulation of drained trenched pipe shows good agreement with the expreimental results at the starting motion stage.

6.2. Recommendations for future study

Some of the potential topics can be extended for further study. Trench-backfill-pipeline interaction is a complex phenomenon, and a lot of aspects more than the suggestions of this part can be explored.

- Consolidation effects
    - This can include considering the changes of permeability of soil, the saturation degree of soil when extended the study to onshore pipeline, and further considerations on the settings of the fluid flow.
    - Considering more accurate boundary conditions for the pore fluid transits.
    - Reducing the fluctuation of excess pore pressure caused by the solution mapping.
    - Incorporating more advanced interface models into the framework to enhance the simulation.
- Trench effects
    - Comprehensive parametric studies including trench wall angles, trench depth, trench widths, backfill materials etc.
    - Influence of existence of trench on the ultimate normalized response.
    - Prediction of soil resistance while pipe is displaced in the transition zone (form the backfilling soil to the native soil).
    - Influence of initial embedment depth of trenched pipe into trench bottom on the pipe response.
    - Influence of trenching and backfilling methods on the trench-backfill-pipeline interaction.

Bibliography

ABAQUS, Dassault Systemes Simulia Corp., 2017. ABAQUS analysis User's Manual.

ABAQUS, Dassault Systemes Simulia Corp., 2017. ABAQUS Benchmarks Manual.

ALA. In ASCE, 2005. Guidelines for the design of buried steel pipe.

ASCE, 1984. Guidelines For The Seismic Design Of Oil And Gas Pipeline Systems.

Barbosa-Cruz, E.R., Randolph, M.F., 2005. Bearing capacity and large penetration of a cylindrical object at shallow embedment. Proc. Int. Symp. on. Frontiers in Offshore Geotechnics-ISFOG, Perth, Australia.

Bemben, S., Myers, H., 1974. The influence of rate of penetration on static cone resistance in Connecticut river valley varved clay. In Proc., European Symp. on Penetration Testing, vol. 2, no. 2: National Swedish Council for Building Research Stockholm, pp. 33-43.

Bhushan, K., Haley, S.C., Fong, P.T., 1979. Lateral Load Tests on Drilled Piers in Stiff Clays ASCE. Journal of the Geotechnical Engineering Division, ASCE, 105(GT8): 969–985.

C-CORE, Honeggerm, D., D.G. Honegger Consulting, 2003. Extended Model for Pipe Soil Interaction.

Chai, J., Carter, J.P., 2011. Deformation analysis in soft ground improvement. Vol. 18. Springer Science & Business Media.

Chatterjee, S., Randolph, M.F., White, D., 2012. The effects of penetration rate and strain softening on the vertical penetration resistance of seabed pipelines. Géotechnique, vol. 62, no. 7, p. 573.

Chatterjee, S., White, D., Randolph, M.F., 2012. Numerical simulations of pipe-soil interaction during large lateral movements on clay. Géotechnique, vol. 62, no. 8, p. 693.

Chatterjee, S., Yan, Y., Randolph, M., White, D., 2012. Elastoplastic consolidation beneath shallowly embedded offshore pipelines. Géotechnique Letters, vol. 2, no. 2, pp. 73-79.

Chaloulos, Y., Bouckovalas, G., Zervos, S., Zampos, A. 2015. Lateral soil-pipeline interaction in sand backfill: effect of trench dimension, Computers and Geotechnics, 69 (2015) 442-451.

Das, B.M., Moreno, R., Dallo, K., 1985. Ultimate pullout capacity of shallow vertical anchors in clay. Soils and Foundations, 25(2): 148–152.

Das, B.M., Tarquin, A.J., Marino, R., 1987. Model Tests for Pullout Resistance of Vertical Anchors in Clay. Soils and Foundations, 17(2): 52–56.

Dong, X., Shiri, H., Zhang, W., and Randolph, M.F., 2020a. A 2D RITSS model for analysis on large lateral displacement of trenched pipeline. Prepared for submission.

Dong, X., Zhang, W., Shiri, H., and Randolph, M.F., 2020b. Large Deformation Coupled Analysis of Embedded Pipeline – Soil Lateral Interaction. Prepared for submission.

Edgers, L., Karlsrud, K., 1982. Soil flows generated by submarine slides - case studies and con-sequences. In Third International Conference on the Behaviour of OffShore Structures. pp. 425–437.

Hansen, J.B., 1948. The Stabilizing Effect of Piles in Clay. In CN Post No. 3, Christiani and Nielson, Copenhagen, Denmark, November. pp. 14–15.

Hansen, J.B., Christensen, N.H., 1961. The ultimate resistance of rigid piles against transversal forces. Geoteknisk Institut, Copenhagen.

House, A.R., Oliveira, J.R.M.S., Randolph, M.F., 2001. Evaluating the Coefficient of Consolidation using Penetration Tests. International Journal of Physical Modelling in Geotechnics, vol. 3, pp. 17-26.

Hsu, T., 1993. Rate effect on lateral soil restraint of pipelines. Soils and Foundations, vol. 33, no. 4, pp. 159-169.

Hu, Y., Randolph, M.F., 1998. A practical numerical approach for large deformation problems in soil. Int. J. Numer. Analyt. Meth. Geomech., vol. 22, pp. 327-350.

Hu, Y., Randolph, M.F., 2002. Bearing Capacity of Caisson Foundations on Normally Consolidated Clay. Soils and Foundations, Japanese Geotechnical Soiciety, vol. 42, no. 5, pp. 71-77.

Kianian, M., Esmaeilzadeh, M., Shiri, H., 2018. Lateral Response of Trenched Pipelines to Large Deformations in Clay. Offshore Technology Conference, OTC2018, Houston, TX, US, OTC-28842-MS.

Kim, K.K., Prezzi, M., Salgado, R., 2006. Interpretation of cone penetration tests in cohesive soils.

Kim, T., 2005. Dissipation of pore water pressure due to piezocone penetration in OC clay. Ph. D. dissertation, Korea Univ., Seoul, Korea.

Klar, A., Randolph, M.F., 2008. Upper-bound and load–displacement solutions for laterally loaded piles in clays based on energy minimization. Géotechnique, 58(10): 815–820.

Kouretzis, G., Sheng, D., Sloan, S., 2013. Sand-pipeline-trench lateral interaction effects for shallow buried pipelines, Computers and Geotechnics, 54 (2013) 53-59.

Lagioia, R., Nova, R., 1995. An experimental and theoretical study of the behaviour of a calcarenite in triaxial compression. Géotechnique, vol. 45(4), pp. 633-648, 1995.

Lagioia, R., Panteghini, A., 2016. On the existence of a unique class of yield and failure criteria comprising Tresca, von Mises, DruckerPrager, MohrCoulomb, GalileoRankine, MatsuokaNakai and LadeDuncan, " Proceedings of the Royal Society A: Mathematical, Physical and Engineering Sciences doi:10.1098/rspa.2015.0713.

Lehane, B.M., O'Loughlin, C.D., Gaudin, C., Randolph, M.F., 2009. Rate effects on penetrometer resistance in kaolin. Géotechnique, vol. 41(1), pp. 41-52.

Lever, J.H., 2000. Assessment of Millennium pipeline project Lake Erie crossing: Ice scour, sediment sampling, and turbidity modeling. ERDC/CRREL Technical Report 00-13.

Luscher, U., Thomas, H.P., Maple, J.A., 1979. Pipe-Soil Interaction. Trans-Alaska Pipeline. In Pipelines in Adverse Environments: A State of the Art. ASCE. pp. 486–502.

Mackenzie, T.R., 1955. Strength of Deadman Anchors in Clay. M.Sc. Thesis, Princeton University, Princeton, USA.

Merifield, R.S., Sloan, S.W., Yu, H.S., 2001. Stability of plate anchors in undrained clay. Géotechnique, 51(2): 141–153.

Ng, P.C.F., 1994. Behaviour of buried pipelines subjected to external loading. PhD thesis, University of Sheffield, Sheffield, U.K.

Nova, R., 1992. Mathematical modelling of natural and engineered geomaterials. Euro. J. Mech. A: Solids. 11. 135-154.

Oliveira, J.R.M.S., Almeida, M.S.S., Almeida, M.C.F., Borges, R.G., 2010. Physical Modeling of Lateral Clay-Pipe Interaction. Journal of Geotechnical and Geoenvironmental Engineer-ing, 136(2010): 950–956.

Paulin, M., 1998. An investigation into pipelines subjected to lateral soil loading. Memorial University of Newfoundland, St. John's, Canada.

Paulin, M.J., Phillips, R., Clark, J.I., Boivin, R., 1998. An experimental investigation into lateral pipeline/soil interaction – phase II. Centrifuge 98 – Proceedings of the International Conference Centrifuge 98.

Paulin, M.J., Phillips, R., Clark, J.I., Trigg, A., Konuk, I., 1998. A full-scale investigation into pipeline/soil interaction. Proceedings of 1998 International Pipeline Conference, ASME, Calgary, AB, vol. 2, pp. 779-787.

Panteghini, A., Lagioia, R., 2018. An extended modified Cam-Clay yield surface for arbitrary meridional and deviatoric shapes retaining full convexity and double homothety. Géotechnique, vol. 68, no. 7, pp. 590-601.

Panteghini, A., Lagioia, R., 2018. An approach for providing quasi‐convexity to yield functions and a generalized implicit integration scheme for isotropic constitutive models based on 2 unknowns. International Journal for Numerical and Analytical Methods in Geomechanics, vol. 42, no. 6, pp. 829-855.

Phillips, R., Nobahar, A., Zhou, J., 2004, Trench effects on pipe-soil interaction, Proceeding of International Pipeline Conference, Calgary, Alberta, Canada, IPC2004-141.

Pike, K., 2016. Physical and numerical modeling of pipe/soil interaction events for large deformation geohazards. Memorial University of Newfoundland, St. John's, Canada.

Poorooshasb, F., Paulin, M., Rizkalla, M., Clark, J., 1994. Centrifuge modeling of laterally loaded pipelines. Transportation research record, 33–40.

Poulos, H.G., 1995. Design of Reinforcing Piles to Increase Slope Stability. Canadian Geotech-nical Journal, 32(5): 808–818.

PRCI. 2009. Guidelines for constructing natural gas and liquid hydrocarbon pipelines through areas prone to landslide and subsidence hazards. In Pipeline Research Council International.

Ragni, R., Wang, D., Mašín, D., Bienen, B., Cassidy, M.J., Stanier, S.A., 2016. Numerical modelling of the effects of consolidation on jack-up spudcan penetration. Computers and Geotechnics, vol. 78, pp. 25-37.

Rajah, S., Shumaker, S., Bardakjian, H., Botteicher, B., Bushdiecker, K., Conner, R., Cox, A., Fisher, C., LeBlanc, J., McCabe, M.W., Walker, R., Whidden, W., 2014. Soil parameters for assessing axial and transverse behavior of restrained pipelines—Part 2: Transverse behavior. In Pipelines 2014: From Underground to the Forefront of Innovation and Sustainability. ASCE, Portland. pp. 1849–1863.

Randolph, M.F., Hope, S., 2004. Effect of cone velocity on cone resistance and excess pore pressures. Engineering Practice and Performance of Soft Deposits, Osaka, Japan, pp. 147-152.

Randolph, M.F., Wang, D., Zhou, H., Hossain, M., Hu, Y., 2008. Large deformation finite element analysis for offshore applications. In 12th International Conference

of International Association for Computer Methods and Advances in Geomechanics (IACMAG), Goa, India, pp. 1-6.

Randolph, M.F., Hope, S., 2004. Effect of cone velocity on cone resistance and excess pore pressures, pp. 147-152.

Ranjani, B.B., Robertson, P.K., Morgenstern, N.R., 1993. A Simplified Method for Pipelines Subject to Transverse Soil Movements Proceedings, vol. V, pp. 157-165. In 12th Offshore Mechanics and Arctic Engineering Symposium.

Reese, L.C., Welch, R.C., 1975. Lateral Loading of Deep Foundations in Stiff Clay. Journal of the Geotechnical Engineering Division, 101(7): 633–649.

Rizkalla, M., Mclntyre, M.B., 1991. A Special Pipeline Design for Unstable Slopes. Proceedings, Pipeline Engineering 1991, 14th Annual Energy-Sources Technology Conference and Exhibition, Houston, ASME, Vol. 34, pp. 69-74.

Rowe, R.K., Davis, E.H., 1982. The Behaviour of Anchor Plates in Clay. Geotechnique, 32(1): 9–23.

Roy, M., Tremblay, M., Tavenas, F., Rochelle, P. L., 1982. Development of pore pressures in quasi-static penetration tests in sensitive clay. Canadian Geotechnical Journal, vol. 19, no. 2, pp. 124-138.

Scarpelli, G., Sakellariadi, E., and Furlani, G., 1999. Longitudinal pipeline-soil interaction: results from field full scale and laboratory testing. Panel Contribution in the Proc. of 12th ECSMGE, Balkema, Rotterdam, the Netherlands.

Song, Z., Hu, Y., Randolph, M.F., 2008. Numerical simulation of vertical pullout of plate anchors in clay. Journal of geotechnical and geoenvironmental engineering, vol. 134, no. 6, pp. 866-875.

Terzaghi, K., Peck, R.B., Mesri, G., 1996. Soil mechanics in engineering practice. John Wiley & Sons.

Tian, Y., Cassidy, M.J., Randolph, M.F., Wang, D., Gaudin, C., 2014. A simple implementation of RITSS and its application in large deformation analysis. Computers and Geotechnics, vol. 56, pp. 160-167.

Tschebotarioff, G.P, 1973. Foundations, Retaining and Earth Structures. McGraw-Hill Book Company, New York, 642p.

Ullah, S.N., Hou, L.F., Satchithananthan, U., Chen, Z., Gu, H., 2018. A 3D RITSS approach for total stress and coupled-flow large deformation problems using ABAQUS. Computers and Geotechnics, vol. 99, pp. 203-215.

Wang, D., Bienen, B., 2014. Coupled large deformation consolidation analysis of a spudcan footing penetrating into kaolin clay. In Computer Methods and Recent

Advances in Geomechanics: Proceedings of the 14th International Conference of International Association for Computer Methods and Recent Advances in Geomechanics, 2014 (IACMAG 2014), 2015: Taylor & Francis Books Ltd, pp. 877-882.

Wang, D., Gaudin, C., Randolph, M.F., 2013. Large deformation finite element analysis investigating the performance of anchor keying flap. Ocean Engineering, vol. 59, pp. 107-116.

Wang, D., Hu, Y., Jin, X., 2006. Two-dimensional large deformation finite element analysis for the pulling-up of plate anchor. China Ocean Engineering, vol. 20, no. 2, pp. 269-278.

Wang, D., Hu, Y., Randolph, M.F., 2010. Three-dimensional large deformation finite element analysis of plate anchors in uniform clay. J. Geotech. Geoenviron. Engi ASCE 136, vol. 2, pp. 355–365.

Wang, D., Hu, Y., Randolph, M.F., 2010. Keying of rectangular plate anchors in normally consolidated clays. Journal of Geotechnical and Geoenvironmental Engineering, vol. 137, no. 12, pp. 1244-1253.

Wang, D., White, D.J., Randolph, M.F., 2010. Large-deformation finite element analysis of pipe penetration and large-amplitude lateral displacement. Canadian Geotechnical Journal, vol. 47, no. 8, pp. 842-856.

Wantland., G.P., O'Neill, M.B., Reese, L.C., Coelogyne, E.H., 1978. Lateral Stability of Pipelines in Clay. Proceedings, 11th Offshore Technology Conference, ASME, Houston, pp. 1025-1034.

Yu, L., Liu, J., Kong, X., Hu, Y., 2008. Three-dimensional RITSS large displacement finite element method for penetration of foundations into soil. Computers and Geotechnics, vol. 35, no. 3, pp. 372-382.

Zhang, W., Wang, D., Randolph, M.F., Puzrin, A., 2015. Catastrophic failure in planar landslides with a fully softened weak zone. Géotechnique, vol. 65, pp. 755-769.

Zhang, W., Randolph, M.F., Puzrin, A., Wang, D., 2018. Transition from shear band propagation to global slab failure in submarine landslides. Canadian Geotechnical Journal, vol. 56.

Zhou, H., Randolph, M.F., 2006. Large deformation analysis of suction caisson installation in clay. Canadian Geotechnical Journal, vol. 43, no. 12, pp. 1344-1357.

Zhou, H., White, D.J., Randolph, M.F., 2008. Physical and numerical simulation of shallow penetration of a cylindrical object into soft clay. in GeoCongress 2008: Characterization, Monitoring, and Modeling of GeoSystems, pp. 108-117.

Appendix A: Large deformation analysis of lateral pipeline-backfill-trench interaction by remeshing and interpolation technique with small strain model (RITSS)

Xiaoyu Dong[1], Hodjat Shiri[2], Wangcheng Zhang[3], Mark F. Randolph[4]

1: Department of Civil
Engineering, Memorial University of Newfoundland
e-mail: xiaoyu.dong@mun.ca

2: Department of Civil
Engineering, Memorial University of Newfoundland
e-mail: hshiri@mun.ca

3: Oceans Graduate School,
the University of Western Australia
e-mail: wangcheng.zhang@uwa.edu.au

4: Oceans Graduate School,
the University of Western Australia
e-mail: mark.randolph@uwa.edu.au

This chapter is submitted as a conference manuscript.

Abstract

Offshore pipelines are usually buried in a trench and covered by pre-excavated materials for physical protection. Large lateral displacement of trenched pipelines may be induced by mechanisms such as ground movement and ice gouging. The different soil properties between the backfilling material and the native ground may significantly influence the soil deformations and failure mechanisms around the pipe and affect the ultimate response of lateral displaced pipeline. Existing pipeline design codes ignore trench effects on the lateral pipe response and commonly use the undrained shear strength to assess the ultimate pipe-soil interaction force. Drained or partially drained conditions are quite common in real pipe-soil interaction events, and the soils surrounding the pipeline may benefit from consolidation during the pipe movement. In this study, first, the 2D remeshing and interpolation technique with small strain model (RITSS) was developed in ABAQUS for a LDFE framework. The pipeline-backfill-trench interaction was investigated. Then the developed model was extended to incorporate coupled consolidation analysis, accounting for excess pore pressure generation and dissipation. The study reveals a significant impact of the trench and consolidation on soil deformation, failure mechanism, and the pipe-soil lateral interaction force.

Keywords: Trench, Pipeline-soil interaction, Large deformation, Numerical modeling, Coupled analysis

A.1. Introduction

Subsea pipelines are often protected by burying inside subsea trenches to mitigate the effects of the functional and environmental loads. Using the excavated material for backfilling of the pipeline is a common practice and a cost-effective solution. Depending on trenching methodology, construction strategy, and environmental loads, the backfilling material may experience different degrees of remolding resulting in a softer material with a range of shear strengths. The difference between the stiffness of the backfill and native material affects the soil failure mechanisms under the lateral pipeline displacement (Paulin 1998). The relative displacement between the pipeline and the surrounding soil that may occur due to the ground movements, faults, slope instabilities, ice gouging, etc. exerts forces on the pipeline. The amplitude of these forces and the force-displacement response of the pipeline depend on several parameters including the submerged weight of the backfill and native soil, the horizontal component of resistance offered by interacted soil, and the suction behind the pipe (Paulin 1998). These parameters in turn depend on several parameters such as the properties of the backfill and the native soil, trench geometry, burial depth and confining pressure, pipeline roughness, pipeline size, loading rate (drained/undrained), soil stress history, extent of consolidation of the backfill, and the over-consolidation ratio of the native soil (OCR). In practice, the pipeline-soil interaction response is generally idealized by defining a set of the specialized beam and spring elements (e.g., ALA 2001), where the behavior of springs are expressed by bilinear or hyperbolic functions (PRCI 2009, ALA 2001). However, large discrepancies are observed in the recommendations provided by different design codes and the empirical equations proposed in some previous studies for calculation of the ultimate lateral resistance and the

p-y response (Paulin 1998, ALA 2001, PRCI 2009, Rajah et al. 2014, Pike 2016). The simplified assumptions, which ignore the effect of pipeline-backfill-trench interaction, and inherent differences in the frameworks of the studies conducted, are the main sources of the observed discrepancies. Also, most of the previously mentioned design codes and studies were based on onshore pipelines. The models proposed for prediction of lateral pipeline response in fine-grained material use the undrained shear strength as the key soil strength parameter, which may not be appropriate for slower loading rates where consolidation may occur (Paulin 1998). Besides, the design code for subsea pipeline-seabed interaction (DNVGL-RP-F114, 2017) also mentioned that the difficulties in assessing the effects of penetration and trench geometry brought uncertainties and challenges into the design. It becomes challenging to make assumptions and to identify the range of assumptions. In order to make more accurate prediction on the pipeline force-displacement response within large deformations, a comprehensive investigation is needed to explore the progressive failure mechanisms around the pipeline considering the penetration rates (particularly in drained and partially drained conditions) and the varying pipeline-backfill-trench interaction effects.

In this study, large deformation finite element (LDFE) analyses were conducted using the remeshing and interpolation technique with small strain (RITSS, Hu and Randolph 1998, Zhang et al. 2015) method to explore the trench effect and consolidation effect on the lateral force-displacement response of the pipeline. The interactive and progressive failure mechanisms were investigated. The models were calibrated against the results from published centrifuge tests (Paulin 1998, C-CORE et al. 2003).

A.2. Methodology

The flowchart of the LDFE model is summarized in Figure A-1. Overall, the RITSS procedure divides the large deformation into a series of incremental jobs with small strain increments. More details can be found in Zhang et al. (2015) and Dong et al. (2020a, 2020b).

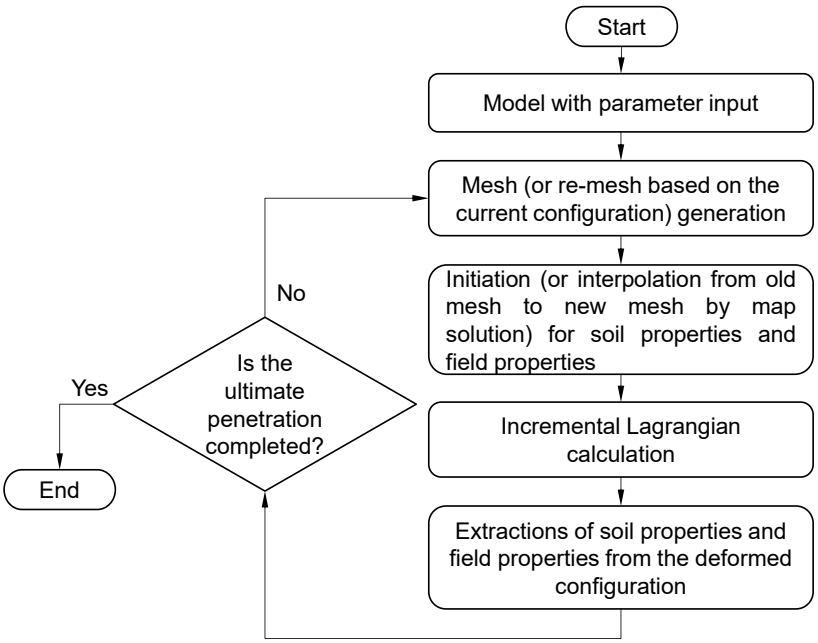

Figure A-1. Overall scheme flowchart

A.3. Trench effect

A.3.1. Numerical details

Geometry setting and soil properties of the numerical analyses were in accordance with a series of physical model tests in a centrifuge (Paulin 1998), which were conducted at 1:50 scale. The soils used in the tests was a mixture by weight of Speswhite kaolin clay (50%) and Sil-Co-Sil silt (50%). The model pipelines were 19 mm in diameter corresponding to a prototype value of 0.95 m. The trenched pipe was displaced horizontally at low speeds of 0.5 m/s, but sufficient to give undrained conditions. The pipe was free to move vertically

as it was displaced. Cover depths investigated in the physical models were 16 mm and 65 mm corresponding to prototype value of 0.8 m and 3.25 m respectively. A model trench width was set as 50 mm, which corresponds to 2.5 m at prototype scale. The LDFE framework was developed using ABAQUS/standard with a modified Tresca model (Zhang et al. 2015, 2018) considering strain softening (sensitivity of soil is used as 5). The soil domain (see Figure A-2) was modeled by using 4-node bilinear plane strain elements (CPE4), while rigid wire elements (R2D2) were used to model the pipe. The pipe-soil interface assumed 'tied' conditions (fully rough and no gap formation). Details of the model parameters can be found in Table A-1.

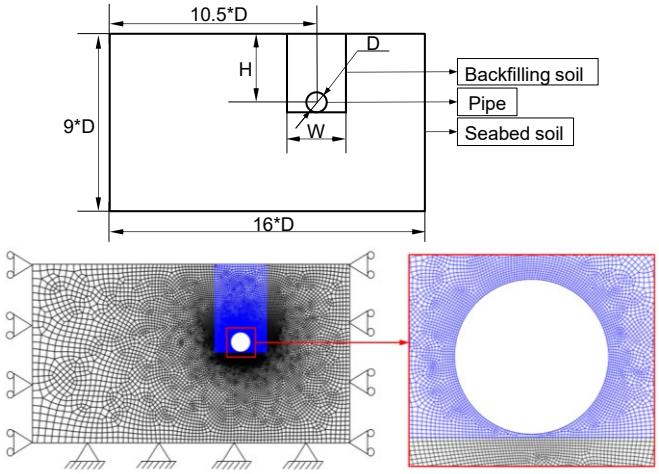

Figure A-2. LDFE model for trench effect

Table A-1. Parameters used for model

Properties	Symbol	Unit	C1	C2
Pipe diameter	D	m	0.95	0.95
Trench width	W	m	2.50	2.50
Cover depth	C	m	0.80	3.25
Embedment ratio	H/D	-	1.34	3.92
Backfill soil undrained shear strength	s_{u_b}	kPa	3.30	3.50
Seabed soil undrained shear strength	s_{u_s}	kPa	36.20	42.10
Effective unit weight of backfill soil	γ_b'	kN/m^3	8.38	8.38
Effective unit weight of seabed soil	γ_s'	kN/m^3	9.31	9.31

A.3.2. Results

Figure A-3 and Figure A-4 show the numerical and experimental p-y curves, compared with six theoretical solutions (Mackenzie 1955, Tschebotarioff 1973, Rizkalla and Mclntyre 1991, Hansen 1948, Edgers and Karlsrud 1982, Wantland et al. 1979) with burial depth ratio as 1.342 and 3.921 respectively. The position of the trench wall is shown explicitly in Figure A-3 and Figure A-4. It is shown that when the pipe penetrates towards the trench wall, the LDFE analysis can replicate the gradually increasing trend of lateral pipe resistance observed in the centrifuge tests rather than the sharp increase observed in the theoretical responses. Indeed, the overall experimental responses are matched very well both within the backfill and after entering the surrounding native ground. For the ultimate response, the theoretical solutions range either above or below the measured pipe resistance. In addition, for the shallowly buried pipe (H / D = 1.34, see Figure A-3), all theoretical estimates of resistance within the backfill were slightly lower than the measured (and numerical) values, while for the deeply buried pipe (H / D = 3.92, see Figure A-4), all theoretical estimates of resistance within the backfill were slightly above the measured resistance. The ultimate soil resistances can be normalized as F/(suD), which are calculated to be 3.59 (=123.3/(36.20*0.95), in Figure A-3) and 5.09 (=203.7/(42.10*0.95), in Figure A-4) respectively.

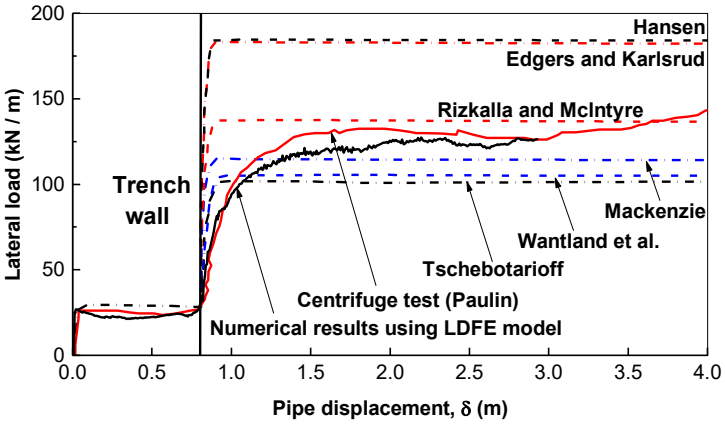

Figure A-3. Load displacement curves for H / D = 1.34

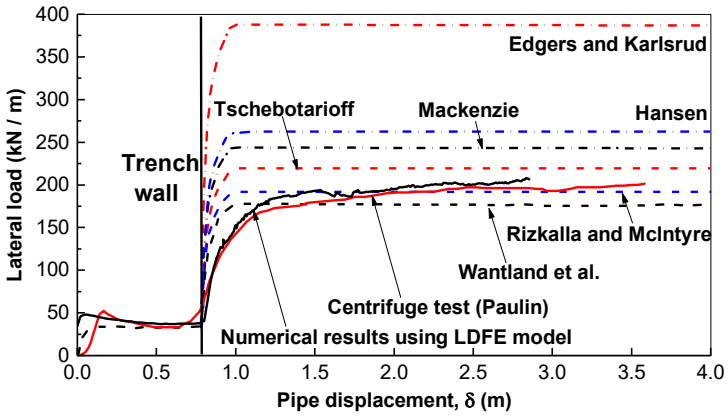

Figure A-4. Load displacement curves for H / D = 3.92

Figure A-5 and Figure A-6 show the displacement vectors and accumulated plastic shear strain, respectively, for both cover depth ratios for a pipe displacement of 1.9D. Significant soil heave is observed at the ground surface due to the pipe displacement, especially for the shallow buried case. In Figure A-6 a, for the shallow buried pipe, spiral shear bands initiating from the pipe invert are observed to extend, reaching the ground surface on the active side and changing to a block uplift mechanism nearer ground level on the passive (native ground) side. The failure mechanism is affected by the burial depth ratio (comparing Figure A-6 a and b), whereby for the deeply buried case the soil settlement

within the trench is significant (although less than for shallow embedment) while soil heave at the native ground surface is very minor.

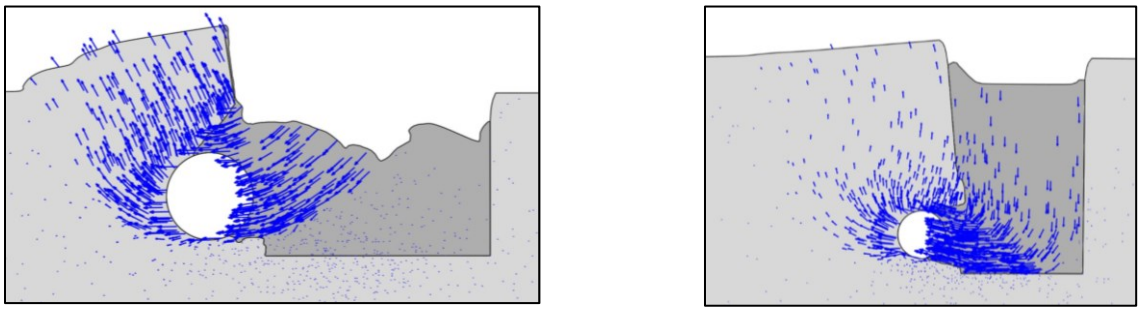

(a) H / D = 1.34, pipe moved by 1.9 D (b) H / D = 3.92, pipe moved by 1.9 D

Figure A-5. Displacement vectors in LDFE model while pipe penetrates to the native seabed soil from the backfilling material.

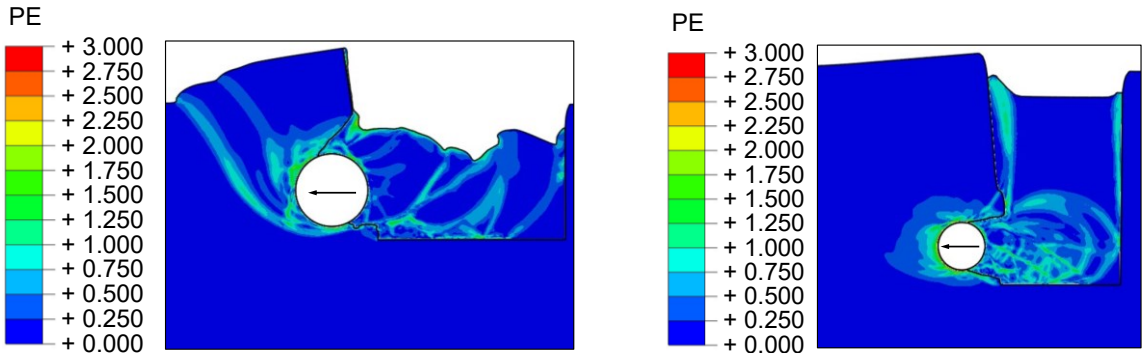

(a) H / D = 1.34, pipe moved by 1.9 D (b) H / D = 3.92, pipe moved by 1.9 D

Figure A-6. Plastic strain in model while pipe penetrates to the native seabed soil from the backfilling material.

A.4. Consolidation effect

A.4.1. Numerical details

Published results from two centrifuge tests (C-CORE et al. 2003) were selected for numerical model benchmarking. The tests were carried out identical to those discussed

previously. The pipeline was buried at a depth of 1.5 D and 3.0 D respectively. Although the analyses were fully coupled ones and could be applied for all kinds of drainage conditions, in order to make comparisons with published experimental results, the results reported here are just for undrained conditions. The two centrifuge tests were modeled numerically as well in the C-CORE report (C-CORE et al. 2003) using a small strain finite element analysis, where over-distorted meshes were observed and inaccuracies could be introduced.

Permeability of the soil was taken as 10^{-10} m/s, as in the published numerical work (C-CORE et al. 2003). The numerical model for the LDFE coupled consolidation analyses of pipe-soil interactions is shown in Figure A-7. The soil domain was modeled using 4-node bilinear displacement and pore pressure plane strain elements (CPE4P), and the pipe was modeled by rigid wire elements (R2D2). The bottom boundary was fixed and the side boundaries were restrained against displacement perpendicular to the respective sides. The contact surfaces of the pipe and soil ground were tied together. During the consolidation soil step, the excess pore pressure at the top surface of the soil ground was set as zero to allow the full drainage. The LDFE framework was developed using ABAQUS/standard with a Cam-Clay-Type constitutive model (Panteghini and Lagioia 2018a, 2018b). The hardening parameter Bp is set as 0.064 for the constitutive model. The linear elasticity was considered in alignment with the constitutive model. Here the young's modulus is used as 5000 kPa while the Poisson's ratio is set as 0.3. The seabed soil was consolidated to a vertical stress of 400 kPa to obtain the cohesion of 40 kPa. The two tests were performed by displacement control with pipe moving rates of 0.5 mm/s to fulfill undrained conditions with C_v=0.38 mm^2/s.

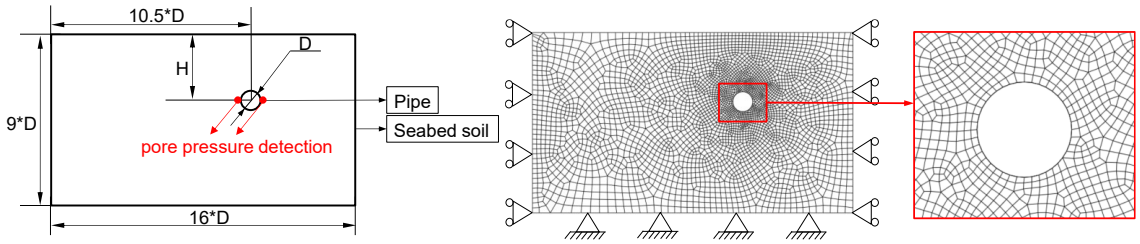

Figure A-7. Coupled LDFE model for consolidation effect

A.4.2. Results

As shown in Figure A-8, predictions of normalized soil resistance on the pipe from the LDFE coupled analysis, as a function of displacement, are compared with the results from the centrifuge tests and previous numerical modeling in C-CORE Report (C-CORE et al. 2003), recommended values by PRCI (Honegger and Nyman 2001) and ASCE (1984) guidelines (which were presented in C-CORE Report (C-CORE et al. 2003)). The slight increase over large pipe displacements, indicating hardening behaviour, for the deeper case, while staying constant for the shallow embedment. Excellent agreement was reached between centrifuge test results and previous FEA work in C-CORE report. And the LDFE showed somewhat overprediction of the soil resistance.

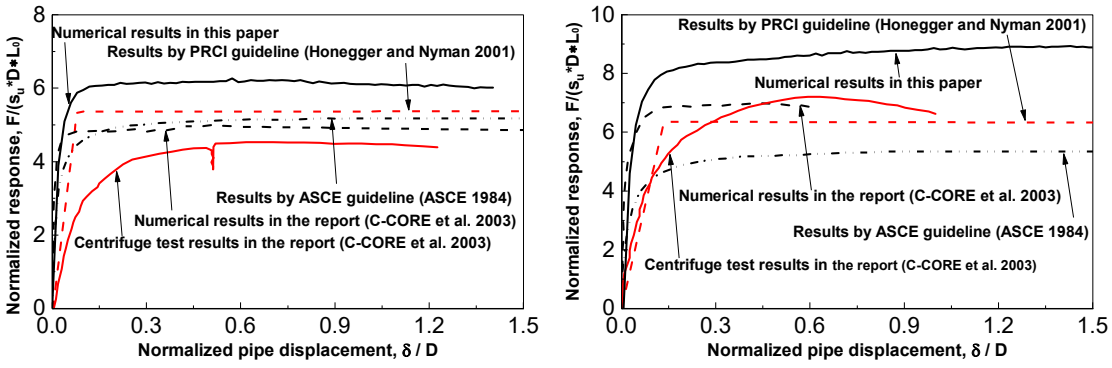

(a) H / D = 1.5, shallow buried case (b) H / D = 3.0, deep buried case

Figure A-8. Normalized force-displacement curves

As shown in Figure A-8, the ultimate normalized soil resistances are observed to be 6.01 (for H/D=1.5) and 8.89 (for H/D=3.0) respectively. Comparing with the normalized soil resistances discussed in section 3.2 (3.59 for H/D=1.34, and 5.09 for H/D=3.92), the influence of trench-backfill-pipeline interaction on the ultimate normalized soil resistance is indicated to be significant. The potential residual effect of backfill material may contribute to the decrease in ultimate normalized soil resistance.

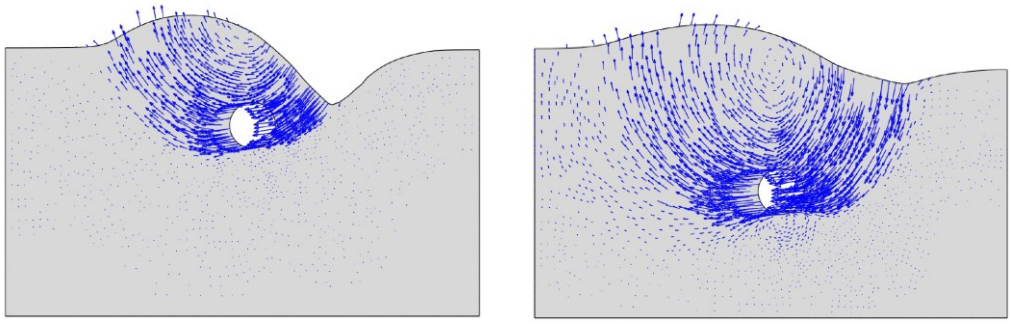

(a) H / D = 1.5, pipe moved by 1.4 D (b) H / D = 3.0, pipe moved by 1.4 D

Figure A-9. Deformed shape of soil surface in last incremental job of prediction models

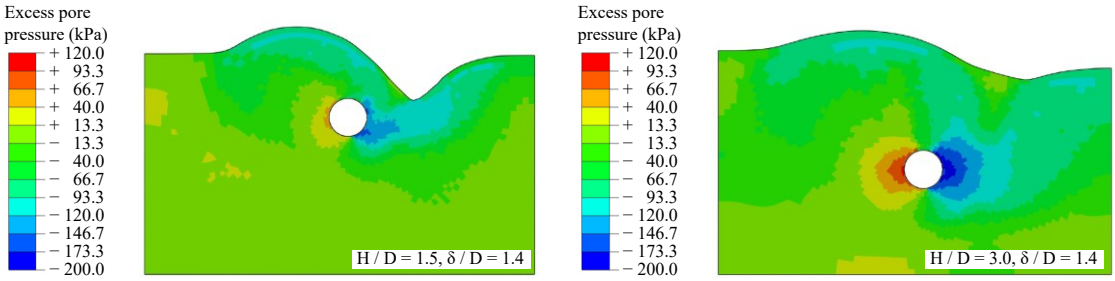

(a) H / D = 1.5, pipe moved by 1.4 D (b) H / D = 3.0, pipe moved by 1.4 D

Figure A-10. Contours of excess pore pressure for last increment of ABAQUS analyses

Figure A-10 shows contours of excess pore pressure induced when the pipe was displaced by 1.4 D for both burial depth ratios. Comparing Figure A-10 a and b, the shape of the distribution region of excess pore pressure induced at the rear of pipe is affected

significantly by the changes in soil surface in the shallow buried case, but less markedly for the deep buried case. Negative excess pore pressure induced at the rear of the pipe reflects the suction force on the pipe. And the induced negative excess pore pressure in the deep buried case is more significant.

A.5. CONCLUSION

A two-dimensional large deformation finite element (LDFE) model using RITSS (re-meshing and interpolation technique using small strain) was developed for analyzing pipeline-backfill-trench interaction. A modified Tresca model was adapted to incorporate strain softening, in order to represent the soil behavior under undrained conditions. Meanwhile, the LDFE framework was extended to explore the lateral displacement of pipeline embedded in uniform clay. Using a Cam-Clay-Type constitutive model in terms of effective stress method, the induced excess pore pressure around the pipe can be predicted to facilitate understanding the failure mechanism in soil. The models developed for the effects of a backfilled trench and consolidation were verified by comparing the numerical results with centrifuge tests results. Failure mechanisms were observed with shear band propagation and ground heave and settlement during the large displacement of the pipe. The following key observations were made:

- The LDFE model developed was effective in analyzing pipeline-backfill-trench interaction, especially for visualizing the evolving failure mechanisms as the pipe was displaced through the backfill into the surrounding native ground.
- It was observed that the RITSS based LDFE framework had significant advantages in modeling large lateral displacement of trenched pipe. The predicted load-displacement

curves have better agreement to the centrifuge test results than the prediction curves obtained from previous studies.

- The coupled LDFE framework has advantages in replicating generation and dissipation of excess pore pressure over large lateral displacement of embedded pipe, which affects the failure mechanisms and hence the mobilized lateral soil resistance. The predicted load-displacement curves match well with curves recommended in guidelines and with existing centrifuge test data.

A.6. ACKNOWLEDGEMENT

The authors gratefully acknowledge Dr. Rocco Lagioia and Dr. Andrea Panteghini for their valuable help on the user-coded Modified Cam-Clay model. And the authors sincerely acknowledge the financial support of "Wood Group," that established a Research Chair program in Arctic and Harsh Environment Engineering at Memorial University of Newfoundland, the "Natural Science and Engineering Research Council of Canada (NSERC)", and the "Newfoundland Research and Development Corporation (RDC) (now InnovateNL)" through "Collaborative Research and Developments Grants (CRD)". Also, the Authors acknowledge the visiting research funding provided by Mitacs through Globalink program and also the Center of Offshore Foundation Systems and the University of Western Australia for providing the visiting opportunity and collaboration. Special thanks are also extended to Memorial University for providing excellent resources to conduct this research.

References

ALA. Guidelines for the design of buried steel pipe. In ASCE, 2005.

ASCE. 1984. Guidelines for the seismic design of oil and gas pipeline systems. American Society of Civil Engineers, Committee on Gas and Liquid Fuel Lifelines, Technical Council on Lifeline Earthquake Engineering, ASCE, New York.

C-CORE, Honeggerm, D., and D.G. Honegger Consulting, 2003. Extended Model for Pipe Soil Interaction.

Dong, X., Shiri, H., Zhang, W., and Randolph, M.F., 2020a. A 2D RITSS model for analysis on large lateral displacement of trenched pipeline. Prepared for submission.

Dong, X., Zhang, W., Shiri, H., and Randolph, M.F., 2020b. Large Deformation Coupled Analysis of Embedded Pipeline – Soil Lateral Interaction. Submitted to Géotechnique.

DNV. 2017. Pipe-soil interaction for submarine pipelines, Recommended Practice. DNVGL-RP-F114.

Edgers, L. and Karlsrud, K., 1982. Soil flows generated by submarine slides - case studies and con-sequences. In Third International Conference on the Behaviour of OffShore Structures. pp. 425–437.

Hansen, J.B., 1948. The Stabilizing Effect of Piles in Clay. In CN Post No. 3, Christiani and Nielson, Copenhagen, Denmark, November. pp. 14–15.

Honegger, D.G. and Nyman, D.J. 2001. Manual for the seismic design and assessment of natural gas transmission pipelines. Pipeline Research Council International (PRCI), Project PR-268-9823.

Hu, Y. and Randolph, M.F., 1998. A practical numerical approach for large deformation problems in soil. Int. J. Numer. Analyt. Meth. Geomech, Vol. 22, pp. 327-350.

Mackenzie, T.R., 1955. Strength of Deadman Anchors in Clay. M.Sc. Thesis, Princeton University, Princeton, USA.

Panteghini, A. and Lagioia, R., 2018a. An extended modified Cam-Clay yield surface for arbitrary meridional and deviatoric shapes retaining full convexity and double homothety. Géotechnique, Vol. 68(7), pp. 590-601.

Panteghini, A. and Lagioia, R., 2018b. An approach for providing quasi‐convexity to yield functions and a generalized implicit integration scheme for isotropic constitutive models based on 2 unknowns. International Journal for Numerical and Analytical Methods in Geomechanics, Vol. 42(6), pp. 829-855.

Paulin, M., 1998. An investigation into pipelines subjected to lateral soil loading. Memorial University of Newfoundland, St. John’s, Canada.

PRCI. 2009. Guidelines for constructing natural gas and liquid hydrocarbon pipelines through areas prone to landslide and subsidence hazards. In Pipeline Research Council International.

Pike, K., 2016. Physical and numerical modeling of pipe/soil interaction events for large deformation geohazards. Memorial University of Newfoundland, St. John's, Canada.

Rajah, S., Shumaker, S., Bardakjian, H., Botteicher, B., Bushdiecker, K., Conner, R., Cox, A., Fisher, C., LeBlanc, J., McCabe, M.W., Walker, R., and Whidden, W., 2014. Soil parameters for assessing axial and transverse behavior of restrained pipelines—Part 2: Transverse behavior. In Pipelines 2014: From Underground to the Forefront of Innovation and Sustainability. ASCE, Portland. pp. 1849–1863.

Rizkalla, M. and Mclntyre, M.B., 1991. A Special Pipeline Design for Unstable Slopes. Proceedings, Pipeline Engineering 1991, 14th Annual Energy-Sources Technology Conference and Exhibition, Houston, ASME, Vol. 34, pp. 69-74.

Tschebotarioff, G.P., 1973. Foundations, Retaining and Earth Structures. McGraw-Hill Book Company, New York, 642p.

Wantland, G.P., O'Neill, M.B., Reese, L.C., and Coelogyne. E.H., 1979. Lateral Stability of Pipelines in Clay. Proceedings, 11th Offshore Technology Conference, ASME, Houston, pp. 1025-1034.

Zhang, W., Wang, D., Randolph, M.F., and Puzrin, A., 2015. Catastrophic failure in planar landslides with a fully softened weak zone. Géotechnique, Vol. 65, pp. 755-769.

Zhang, W., Randolph, M.F., Puzrin, A., and Wang, D., 2018. Transition from shear band propagation to global slab failure in submarine landslides. Canadian Geotechnical Journal, vol. 56.

PART II: RISER-SEABED INTERACTION

Chapter 7

Introduction

7.1. Background

Since the thesis is paper-based, each chapter has its own introduction. However, a summary of introduction in chapters from Chapter 9 to Chapter 11 was brought as Chapter 7.

Vertical interaction between steel catenary risers (SCRs) and seabed is one of the most challenging structure-soil interaction problems in offshore geotechnics. It is crucial for estimation of fatigue damage which can be influenced by the properties of fatigue loading and riser configuration. Different mechanisms contribute to the riser-seabed interaction and the trench development such as soil stiffness degradation under cyclic loads, mobilization of suction force within uplift motions of riser, trench base softening and damping, erosive mechanism by water velocity field around the SCR in TDZ and consequent variation of flow pattern of displaced water, the riser dynamics influenced by internal multi-phase flow regimes and also vessel motions (velocity and frequencies). These mechanisms cause several major uncertainties in prediction of fatigue life and the SCR design procedure. In SCR design codes, linear springs have been used to present the pipe-soil interaction. With further observations in subsea surveys and exploration projects, more sophisticated nonlinear models were proposed to better represent the mechanism of riser-seabed interaction.

7.2. Motivation

Steel catenary risers are exposed to complex environmental loads and suffered from cyclic motions and therefore fatigue damage in the SCR attachment point and the SCR in

touchdown zone (TDZ). The estimation of the fatigue damage of SCR in TDZ is extremely challanging due to non-linear riser-seabed interaction. Different mechanisms with a range of uncertainties contribute to the riser-seabed interaction and the trench development underneath the riser (see Figure 7-1). The oscillatory motions of SCR in the touchdown zone result in a complex riser interaction mechanism with surrounding media including fluid and soil.

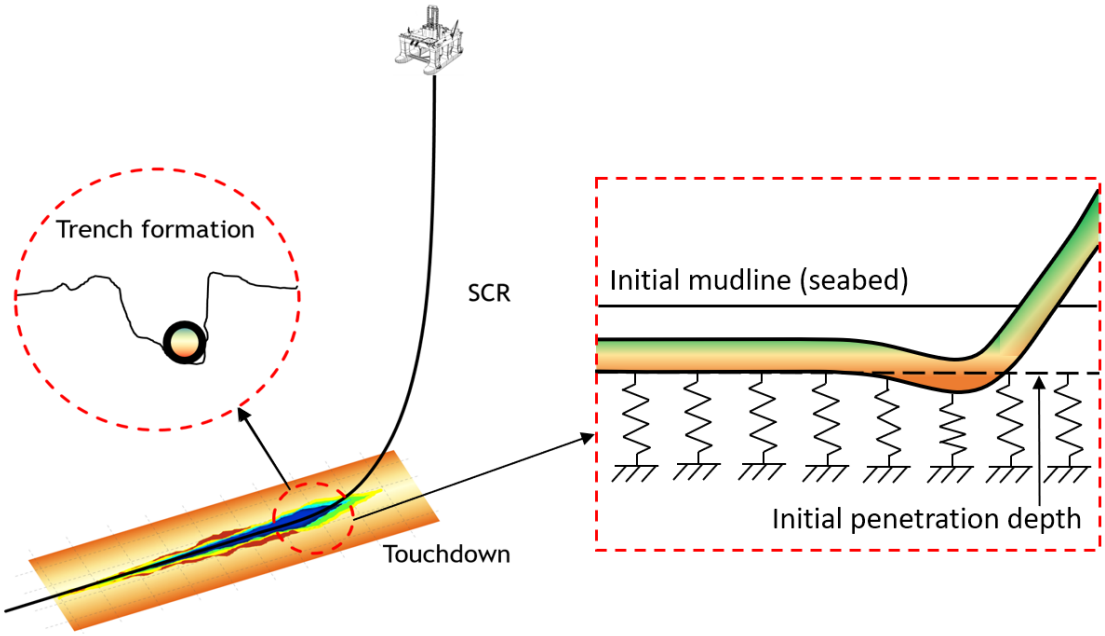

Figure 7-1. Schematic flowcharts for framework

With further observations in subsea surveys and exploration projects, more sophisticated nonlinear models were needed to better represent the mechanism of riser-seabed interaction (Phifer et al., 1994; Theti and Moros, 2001; Campbell, 1999). Based on full-scale harbor tests and some existing models, Bridge et al. (2004, 2007) developed a model capturing some of nonlinear aspects of soil behavior, except for the degradating soil stiffness and riser embedment into the seabed. Jiao (2007) proposed the degradating soil model which

could capture the cyclic softening of soil in the re-loading process but not in the unloading process. This disadvantage was overcome in new models proposed later (Aubeny and Biscontin 2009, Nakhaee and Zhang 2010). Randolph and Quiggin (2009) developed a new nonlinear seabed model for the calculation of reaction force in different penetration modes of the oscillating riser. Shiri and Randolph (2010) explored the fatigue analysis of SCR by developing a numerical model in ABAQUS with the R-Q soil model adopted in the user-defined element. Zargar et al. (2015) conducted a comparative study of two existing riser-soil interaction models (Aubeny and Biscontin 2009, Randolph and Quiggin 2009) and identified their pros and cons for future developments. SCR fatigue was further investigated and reported with newly proposed trench models (Randolph et al. 2013, Shiri 2014a, Shiri 2014b) or different case studies (e.g., different loading histories, complex riser excitations etc.) (Elliott et al. 2013, Kimiaei and Liao 2015, Clukey et al. 2017).

This part II is to examine the performance of a popular nonlinear riser-soil interaction models and their needs for further improvement of fatigue analysis of SCR in TDZ. Then the effects of the seabed evolution process on slug-induced vibrations are explored.

References

Aubeny, C.P., Biscontin, G. 2009. Seafloor–riser interaction model, Int J Geomechanics, 9: 133-141.

Bridge, C., Laver, K., Clukey, E., Evans, T. 2004. Steel catenary riser touchdown point vertical interaction models, in: Offshore Technology Conference, OTC16628, Houston, Texas.

Bridge, C., Howells, H. 2007. Observations and modeling of steel catenary riser trenches, in: 17th International Offshore and Polar Engineering Conference, ISOPE2007, Lisbon, Portugal.

Campbell, M. 1999. The complexities of fatigue analysis for deepwater risers, in: Proceedings of the 2nd International Deepwater Pipeline Technology Conference.

Clukey, E.C., Aubeny, C.P., Zakeri, A., Randolph, M.F., Sharma, P.P., White, D.J., Sancio, R., Cerkovnik, M. 2017. A Perspective on the state of knowledge regarding soil-pipe interaction for SCR fatigue assessments, in: Offshore Technology Conference, Houston, Texas, OTC27564-MS.

Elliott, B.J., Zakeri, A., Barrett, J., Hawlader, B., Li, G., Clukey, E.C. 2013. Centrifuge modeling of steel catenary risers at touchdown zone Part II: Assessment of centrifuge test results using kaolin clay, Ocean Engineering, 60: 208-218.

Jiao, Y. 2007. Non-linear load-deflection models for Seafloor Interaction with Steel Catenary Risers. Texas A&M University, College Station, USA. Master of Science, 2007.

Kimiaei, M., Liao, J. 2015. Effects of different loading time histories on fatigue design of steel catenary risers using nonlinear riser-soil interaction models, in: Frontiers in Offshore Geotechnics III, Norway, Trondheim.

Nakhaee, A., Zhang, J. 2010. Trenching effects on dynamic behavior of a steel catenary riser, Ocean Engineering, 37(2–3):277–288.

Phifer, E.H., Kopp, F., Swanson, R.C., Allen, D.W., Langner, C.G. 1994. Design and installation of Auger steel catenary risers, in: Offshore Technology Conference, OTC7620, Houston, Texas.

Randolph, M.F., Quiggin, P. 2009. Non-linear hysteretic seabed model for catenary pipeline contact, in: 28th International Conference on Ocean, Offshore and Arctic Engineering, OMAE 2009, Honolulu, Hawaii, USA.

Randolph, M., Baht, S., Jain, S., Mekha, B. 2013. Modeling the touchdown zone trench and its impact on SCR fatigue life, in: Offshore Technology Conference, Houston, OTC23975.

Shiri, H. 2014a. Influence of seabed trench formation on fatigue performance of steel catenary risers in touchdown zone, Journal of Marine Structures, 36: 1-20.

Shiri, H. 2014b. Response of a steel catenary riser on hysteretic non-linear seabed, Journal of Applied Ocean Research, 44: 20-28.

Shiri, H., Randolph, M.F. 2010. Influence of seabed response on fatigue performance of steel catenary risers in touch down area, in: 29th International Conference on Ocean, Offshore and Arctic Engineering, Shanghai, China, 5: 63-72.

Theti, R., Moros, T. 2001. Soil interaction effects on simple-catenary riser response, Pipes and Pipelines Int.; 46 (3): 15-24.

Zargar, E., Kimiaei, M., 2015. An investigation of existing nonlinear seabed models for riser-fluid-soil interaction studies in steel catenary risers. In: Proceedings of 3rd Int. Symposium on Frontiers in Offshore Geotechnics, Oslo, Norway, pp. 489–494.

Chapter 8

Literature Review

8.1. Overview

Since the thesis is paper based, each chapter has its own literature review. However, a summary of literature review in chapters from Chapter 9 to Chapter 11 was brought as Chapter 8.

Vertical interaction between steel catenary risers (SCRs) and seabed is crucial for estimation of fatigue damage which can be influenced by the properties of fatigue loading and riser configuration. Beam-spring model and constitutive soil model have been widely applied for analysis on structure-soil interactions. Together with the soil models, finite element method was used for numerically modelling the riser-seabed interaction.

8.2. Literature review

8.2.1. Riser-seabed interaction under environmental loads

Steel catenary risers (SCR) are one of the most attractive elements in the development of deep offshore oil and gas fields as their construction and installation cost is less than other riser families (Maclure and Walters, 2007; Lim and Gauld, 2003). These risers are naturally subjected to cyclic motions due to environmental loads, and consequently susceptible to fatigue damage both in SCR attachment point to the floating system and in the touchdown zone (TDZ). However, the estimation of the SCR fatigue life in TDZ is the most challenging issue in its design because of highly complex riser-seabed interaction and range of inherited uncertainties. The survey results obtained by remote operating vehicles (ROV) have proved the complex non-linear seabed response to riser fluctuations in the

TDZ, where SCR penetrates into the seabed and cyclically creates trenches often with several diameters deep (Bridge and Howells, 2007).

Various SCR design codes have traditionally proposed linear soil springs in the touchdown zone. After the first experience of SCR technology in the Auger field of the Gulf of Mexico (Phifer et al., 1994), the STRIDE and CARISIMA JIPs (1999-2001) (Giertsen et al., 2004) were the first organized attempts to investigate the need for more sophisticated riser-seabed interaction models (Theti and Moros, 2001). Bridge et al. (Bridge and Howells, 2007) examined the test data from the CARISIMA and STRIDE JIPs and also conducted a range of full-scale harbour tests, laboratory model tests and numerical simulations. A series of soil stiffness models was developed for static penetration, small and large displacements, and cyclic loading for use in finite element analysis programs. These studies included assessment of the influence of suction during uplift, and also the presence of a trench, on the performance of SCRs particularly with respect to fatigue in the TDZ. The hyperbolic model proposed by Bridge et al. (Bridge and Howells, 2007) captures various non-linear aspects of soil behaviour characteristics within the applicable displacement stages, including initial penetration, uplift, suction mobilisation, breakout and re-penetration. The hyperbolic curve of the model was developed based on the hyperbolic force-displacement interaction curve for sand developed by Audibert et al. (1984). It is similar in form to the hyperbolic pipe-soil interaction curve developed by Hardin and Drnevich (1972) that was originally proposed for clay by Kondner (1963). The soil suction during uplift was modelled based on the test data obtained from the STRIDE and CARISIMA JIPs. In order to calculate the dynamic soil stiffness, the model used the bearing load as opposed to the touchdown point reaction force. Hence, the model does not account for soil softening due

to repeated cycles, resulting in a conservative modelling at the TDZ, even though the soil behaviour in this region is highly nonlinear. Jiao (2007) proposed a non-linear discrete soil model for SCR response analysis in the TDZ. The model introduced two non-degrading and degrading schemes for different soil conditions. More recently, Aubeny & Biscontin (2009) and Randolph & Quiggin (2009) purposed two advanced nonlinear soil models for SCR analysis in TDZ. Aubeny & Biscontin (2009) proposed a simplified model consisting of four different equations that represent the soil spring characteristic in each load cycle. The first curve in this model simulates the intact soil response as a backbone curve. The second scenario is the elastic rebound curve, which simulates the soil response to SCR uplift process. The partial separation of the riser and soil within uplift episode is modelled with a third curve until complete detachment. A reloading curve then models the riser re-penetration in the disturbed soil. More intermediate equations are modelling the local load cycles. The incapability of this model in predicting comprehensive soil degradation was resolved by Nakhaee and Zhang (2008) through proposing an updated version. Randolph and Quiggin (2009) proposed a nonlinear model to predict the hysteretic soil response to SCR up and down oscillations. The model combines the hyperbolic and exponential functions within four main episodes of riser-seabed cyclic contact: initial penetration, uplift, separation and re-penetration. Shiri and Randolph (2010) implemented the model into ABAQUS through developing user-defined elements to explore the SCR fatigue performance and automated trench generation mechanism. This model was implemented into Orcaflex software in 2009 and is currently amongst the most popular non-linear models to predict the hysteretic riser-seabed interaction. Shiri (2014) used the model to study the influence of trench creation on fatigue performance of SCR in the TDZ. Zargar

and Kimiaei (2015) conducted a comparative study to investigate the advantages and disadvantages of the models proposed by Aubeny and Biscontin (2009) and Randolph and Quiggin (2009) using existing test results. Authors made an overall comparison between the equations proposed by both of the models for different episodes of riser-seabed interaction. Despite the studies conducted on the performance of these non-linear models in prediction of fatigue life and trench creation in TDZ, there is still no study in the literature to comprehensively examine the functionality and the consistency of these models over different conditions. In this chapter, the nodal performance of the model proposed by Randolph and Quiggin (2009) (R-Q model) was comprehensively studied through numerical analyses for a range of seabed soil parameters and various locations with different magnitudes of movements on the SCR.

Subsea surveys have identified the formation of a several diameter deep trench underneath the riser during the early stages of the operation life (Bridge and Howells, 2007). This process involves several mechanisms but mainly including the cyclic soil stiffness degradation and mobilization of suction force within the uplift motions of the riser. Advanced non-linear hysteretic seabed models have been developed within recent years, enabling the automatic simulation of cyclic seabed soil softening in the TDZ. Zargar and Kimiaei (2015) conducted a comparative study of the models proposed by Aubeny and Biscontin (2009), and Randolph and Quiggin (2009) (called the R-Q model from now on) that are probably the most popular models in the literature. The authors identified that the R-Q model which is a built-in interface in Orcaflex software and consists of a series of attractive features, is as an appropriate base for future developments (Zargar and Kimiaei, 2015). The model has been used in several numerical studies since its first publishing in

2009 (Zargar and Kimiaei, 2015; Shiri and Randolph, 2010; Shiri, 2014; Randolph et al., 2013; Liu et al., 2016).

8.2.2. Riser-seabed interaction under slugging loads

Slug-induced vibrations have been explored for the hanging part of the SCR but in most models the seabed end of the riser was considered as pinned and thus oscillation of SCR in the TDZ was absent from the analysis. Bordalo et al. (2008) examined the effects of two-phase flow patterns (slug, intermittent and annular) and flow rates of contents on the induced loads and riser responses by developing a laboratory-scale model. But in this research the seabed end was set as pinned and thus the responses in TDZ were absent in these tests. Pollio and Mossa (2009) compared two simple models of slug flow (with and without elastic seabed models) in a long flexible marine riser. The results showed the bending moment variation was significantly different in cases with and without the elastic seabed model. Gundersen et al. (2012) used commercially available global and local riser analysis software (e.g., RIFLEX and BFLEX) and explored the remnant fatigue life of a lazy-S flexible riser under the combined effects of wave and slug. The riser was simulated as hinged at hang off and analysis was entirely focused on the hanging part. Results showed the slug dominated the dynamic top angle response and significantly reduced the riser fatigue life during a relatively calm sea condition. Ortega et al. (2012) analyzed the dynamic responses of a lazy wave riser under slugging by coupling the slug flow tracking code (SLUGGIT) and riser structure code (RISANANL) together. The results presented the irregularities in riser structure responses to slugging and indicated the importance of considering the effects of slug flow in the fatigue analysis. However, the seabed end of riser was considered as pinned and riser responses under slugging in TDZ were not

included. Ortega et al. (2013) conducted a fully coupled analysis to examine the combined effects of slug loads and wave loads on the dynamic responses of a catenary riser. It was presented that internal slug flow generated irregular deformation time histories when the regular waves resulted in typical deformations of the riser structure. However, the riser responses in TDZ were not analyzed with the seabed end of riser considered as pinned. Chatjigeorgiou (2017) investigated the combined effects of harmonic motions of the vessel and the internal slug flow on the responses of the hanging part of the riser by incorporating the slug flow terms into the structural dynamic model formerly built by Chatjigeorgiou (2010a, 2010b). It was shown that the magnitudes of dynamic components were amplified due to the existence of internal slug flow. Bordalo et al. (2018) incorporated a slug flow load model to a 3D pipeline dynamics simulator. The simulation of slugging SCR in the case study showed that large oscillations might be induced when the slug frequency was close to any of the natural frequencies of the riser but did not focus on the pipeline-seabed interface.

The literature review shows the progress made by the published works on the riser-seabed interaction and clarifies the knowledge gap to be filled by this research. The comprehensive simulation of the complicated, nonlinear riser seabed interaction requires a deep understanding of parameters affecting nonlinear riser-seabed interaction model and behavior, vessel end motions, slugging loads on the responses of the steel catenary risers. Part II of the thesis (Chapter 9, Chapter 10, and Chapter 11) comprehensively examined the nodal and global performance of a non-linear hysteretic riser-seabed interaction model and developed an advanced model for slugging riser, providing a strong tool in capturing von Mises stress ranges of SCR in TDZ and hereby estimating the fatigue damage.

References

Aubeny, C.P., Biscontin, G., 2009. Seafloor–riser interaction model. Int. J. Geomechanics 9 (3), 133–141.

Audibert, J.M.E., Nyman, D.J., O'Rourke, T.D., 1984. Differential Ground Movement Effects on Buried Pipelines, in Guidelines for the Seismic Design of Oil and Gas Pipeline Systems. ASCE publication, New York, pp. 150–177.

Bordalo, S.N., Morooka, C.K., Cavalcante, C.C.P., 2008. Whipping phenomenon caused by the internal flow momentum on the catenary risers of offshore petroleum fields, Proceedings of the ASME 27th International Conference on Offshore Mechanics and Arctic Engineering.

Bordalo, S.N., Morooka, C.K., 2018. Slug flow-induced oscillations on subsea petroleum pipelines, J. Petrol. Sci. Eng. (2018) (In press, accepted manuscript).

Bridge, C.D., Howells, H.A., 2007. Observations and modeling of steel catenary riser trenches. In: 7th Int. Offshore and Polar Engr. Conf. (ISOPE2007), Lisbon, Portugal, pp. 803–813.

Chatjigeorgiou, I.K., 2017. Hydroelastic response of marine risers subjected to internal slug-flow, Appl. Ocean Res. 62, pp. 1–17.

Chatjigeorgiou, I.K., 2010a. Three dimensional nonlinear dynamics of submerged, extensible catenary pipes conveying fluid and subjected to end-imposed excitations, Int. J. Non-Linear Mech. 45, pp. 667–680.

Chatjigeorgiou, I.K., 2010b. On the effect of internal flow on vibrating catenary risers in three dimensions, Eng. Struct. 32, pp. 3313–3329.

Giertsen, E., Verley, R., Schroder, K., 2004. CARISIMA a catenary riser/soil interaction model for global riser analysis. In: Proceedings of the Int. Conf. On Offshore Mechanics and Arctic Engr. (OMAE2004). Vancouver, BC, Canada, pp. 633–640.

Gundersen, P., Doynov, K., Andersen, T., Haakonsen, R., 2012. Methodology for determining remnant fatigue life of flexible risers subjected to slugging and irregular waves, Proceedings of the ASME 2012 31st Int Conf on Ocean, Offshore and Arctic Engr.

Hardin, B.O., Drnevich, V.P., 1972. Shear modulus and damping in soils: measurement and parameter effects (Terzaghi Lecture). J. Soil Mech. Found Div. 98 (6), 603–624.

Jiao, Y., 2007. Non-linear Load-deflection Models for Seafloor Interaction with Steel Catenary Risers. Texas A&M University, College Station, USA. Master of Science, 121.

Kondner, R.L., 1963. Hyperbolic stress-strain response; Cohesive soils, J. Soil Mech. Found. Div. 89 (1) (1963) 115–143.

Lim, F., Gauld, S., 2003. Riser solutions for ultra-deep-water developments. In: Proceedings of 10th Annual India Oil & Gas Symposium, Mumbai, India.

Liu, J., Kimiaei, M., Randolph, M., 2016. A new user defined element for nonlinear riser-soil interaction analysis of steel catenary riser systems, ASME 2016 35th International Conference on Ocean, Offshore and Arctic Engineering.

Maclure, D., Walters, D., 2007. Freestanding Risers in the Gulf of Mexico – a Unique Solution for Challenging Field Development Configurations. 2H Offshore Engr. Ltd.Technical Paper.

Nakhaee, A., Zhang, J., 2008. Effects of the interaction with the seafloor on the fatigue life of a SCR. In: Int. Offshore and Polar Engr. Conf. Vancouver, BC, Canada, pp. 87–93.

OrcaFlex Documentation, Orcina, 2018.

Ortega, A., Rivera, A., Nydal, O.J., Larsen, C.M., 2012. On the dynamic response of flexible risers caused by internal slug flow, Proceedings of the ASME 2012 31st Int Conf on Ocean, Offshore and Arctic Engr, OMAE2012, pp. 1–10.

Ortega, A., Rivera, A., Larsen, C.M., 2013. Flexible riser response induced by combined slug flow and wave loads, Proceedings of the ASME 2013 32nd International Conference on Ocean, Offshore and Arctic Engineering, OMAE2013.

Pollio, A., Mossa, M., 2009. A Comparison between Two Simple Models of a Slug Flow in a Long Flexible Marine Riser, Thesis.

Phifer, E.H., Frans Kopp, Swanson, R.C., Allen, D.W., Langner, C.G., 1994. Design and installation of auger steel catenary risers. In: Offshore Technol. Conf. (OTC7620), Houston, Texas, USA, pp. 399–408.

Randolph, M.F., Baht, S., Jain, S., Mekha, B., 2013. Modeling the touchdown zone trench and its impact on fatigue life, Offshore Technol. Conf. (OTC23975), Houston, Texas, USA.

Randolph, M.F., Quiggin, P., 2009. Non-linear hysteretic seabed model for catenary pipeline contact. In: 28th Int. Conf. On Ocean, Offshore and Arctic Engr. (OMAE 2009), Honolulu, Hawaii, USA.

Shiri, H., 2014. Response of a steel catenary riser on hysteretic non-linear seabed. J. Of Appl. Ocean Research, Elsevier 44, 20–28.

Shiri, H., Randolph, M., 2010. Influence of seabed response on fatigue performance of steel catenary risers in touch don area. In: 29th Int. Conf. On Ocean, Offshore and Arctic Engr., Shanghai.

Theti, R., Moros, T., 2001. Soil interaction effects on simple-catenary riser response. Pipes Pipelines Int. 46 (3), 15–24.

Zargar, E., Kimiaei, M., 2015. An investigation of existing nonlinear seabed models for riser-fluid-soil interaction studies in steel catenary risers. In: Proceedings of 3rd Int. Symposium on Frontiers in Offshore Geotechnics, Oslo, Norway, pp. 489–494.

Chapter 9

Performance of non-linear seabed interaction models for steel catenary risers, part I: Nodal response

Xiaoyu Dong[1] and Hodjat Shiri[2]

1: Department of Civil

Engineering, Memorial University of Newfoundland

e-mail: xiaoyu.dong@mun.ca

2: Department of Civil

Engineering, Memorial University of Newfoundland

e-mail: hshiri@mun.ca

This chapter is a journal paper which has been published in Ocean Engineering (2018), Vol. 154, pp. 153-166, ISSN 0029-8018.

Abstract

Non-linear hysteretic riser-seabed interaction models have been developed and implemented into business software packages within recent years to simulate the riser penetration into the seabed and its influence on fatigue life in the touchdown zone. These models have shown significant impact on ultimate fatigue damage and users shall take caution while using the models paying particular attention to the selection of model parameters. The oscillation of steel catenary riser (SCR) in the touchdown zone can be quite complex, where neighbour nodes go under different episodes and magnitudes of penetration and uplift at the same time. Therefore, it is necessary to evaluate the non-linear soil models consistency in nodal performance and their extent of validity. This chapter comprehensively examined the nodal performance of a popular non-linear hysteretic riser-seabed interaction model through developing a global numerical riser model in ABAQUS and a user-defined subroutine (UEL). The model shows a dominantly strong nodal performance. However, nodal response violations and model malfunctioning were observed in the proximity of trench bottom towards the vessel, which is the most fatigue prone section of SCR in the touchdown zone. Also, it was identified that the model over-estimates the penetration and suction resistance and consequently the fatigue damage in the TDZ.

Keywords: Steel catenary risers, Non-linear seabed interaction, Numerical modeling, Nodal response, Fatigue Life

9.1. Introduction

Steel catenary risers (SCR) are one of the most attractive elements in the development of deep offshore oil and gas fields as their construction and installation cost is less than other riser families (Maclure and Walters, 2007; Lim and Gauld, 2003). These risers are naturally subjected to cyclic motions due to environmental loads, and consequently susceptible to fatigue damage both in SCR attachment point to the floating system and in the touchdown zone (TDZ). However, the estimation of the SCR fatigue life in TDZ is the most challenging issue in its design because of highly complex riser-seabed interaction and range of inherited uncertainties. The survey results obtained by remote operating vehicles (ROV) have proved the complex non-linear seabed response to riser fluctuations in the TDZ, where SCR penetrates into the seabed and cyclically creates trenches often with several diameters deep (Bridge and Howells, 2007). Different mechanisms with a range of uncertainties contribute to the riser-seabed interaction and the trench development underneath the riser. The oscillatory motions of SCR in the touchdown zone result in a complex riser interaction mechanism with surrounding media including seawater and soil. Some of the influential parameters contributing to these non-linear hysteretic interactions are:

- soil stiffness degradation under cyclic loads and riser penetration into the seabed,
- mobilization of suction force within uplift motions of riser,
- trench base softening and damping,
- the erosive mechanism by water velocity field around the SCR in TDZ and consequent variation of flow pattern of displaced water,

- the riser dynamics influenced by internal multi-phase flow regimes and also vessel motions (velocity and frequencies),
- vortex induced vibration (VIV).

These complexities cause several major uncertainties in prediction of fatigue life and the SCR design procedure (Jacob, 2005). Advanced non-linear hysteretic seabed models have been developed within the recent years, enabling automatic simulation of the different stiffness in the seabed response through the TDZ (Randolph and Quiggin, 2009; Aubeny and Biscontin, 2009). In continuation to exploring the significance of nonlinear soil response in fatigue performance of SCRs (Shiri and Hashemi, 2012; Shiri, 2014), the current chapter (Part I) comprehensively examined the nodal performance of one of the most popular nonlinear hysteretic soil models (i.e. Randolph and Quiggin (2009), called R-Q model from now on). The main objective was to explore the consistency and the extent of the model validity that has never been accomplished before. The R-Q model defines evolutionary non-linear hysteretic soil stiffness represented by springs connected to the nodes on the SCR within the TDZ. Therefore, the nodal response of the model which is the basis for longitudinal stress profiles has significant importance in fatigue response. In this chapter, a numerical model was developed in ABAQUS, and the R-Q model was coded in FORTRAN as a user defined element (UEL). A comprehensive study was conducted focusing on the nodal performance of the model within various seabed parameters and different locations on the SCR. The pros and cons of the R-Q model along with its extent of functionality was discussed. The performance of the R-Q model regarding fatigue response and longitudinal stress profiles in the TDZ will be presented in a sister chapter as Part II.

9.2. Seabed Soil Modelling Strategies

Simplified beam-spring models and also constitutive soil models combined with different numerical approaches are two main strategies in modelling the riser-seabed interaction. The latter approach results in higher accuracy and higher computational cost at the same time. Increasing the computational effort, particularly in coupled analysis makes this approach less attractive for industrial applications. However, using the constitutive soil models with proper numerical approaches such as continuum finite element models (e.g. Clucky et al. (2008)) can provide a strong tool to explore the different aspects of the riser-seabed interaction mechanisms through research projects. In beam-spring strategy, the soil response is represented by simple springs. This approach seems to be an oversimplification from the geotechnical standpoint, where some particular aspects of the soil such as dilatation and creep are lost within the soil discretization process. However, the beam-spring approach results in considerable mitigation of computational cost with no significant loss of accuracy, particularly when the soil stiffness parameters are properly adjusted. The simplicity and reasonably acceptable accuracy of this method has caused industry to apply this approach to a range of design challenges widely. The results interestingly show good agreement with experimental data and continuum models. The complexity of the riser-seabed interaction and the need for simultaneous modelling of vessel excitation, riser dynamics and non-linear seabed response within fatigue analyses have caused the industry to show more interest in SCR beam-spring modelling approach.

Various SCR design codes have traditionally proposed linear soil springs in the touchdown zone. After the first experience of SCR technology in the Auger field of the Gulf of Mexico (Phifer et al., 1994), the STRIDE and CARISIMA JIPs (1999-2001) (Giertsen et al., 2004)

were the first organised attempts to investigate the need for more sophisticated riser-seabed interaction models (Theti and Moros, 2001). Bridge et al. (Bridge and Howells, 2007) examined the test data from the CARISIMA and STRIDE JIPs and also conducted a range of full-scale harbour tests, laboratory model tests and numerical simulations. A series of soil stiffness models was developed for static penetration, small and large displacements, and cyclic loading for use in finite element analysis programs. These studies included assessment of the influence of suction during uplift, and also the presence of a trench, on the performance of SCRs particularly with respect to fatigue in the TDZ. The hyperbolic model proposed by Bridge et al. (Bridge and Howells, 2007) captures various non-linear aspects of soil behaviour characteristics within the applicable displacement stages, including initial penetration, uplift, suction mobilisation, breakout and re-penetration. The hyperbolic curve of the model was developed based on the hyperbolic force-displacement interaction curve for sand developed by Audibert et al. (1984). It is similar in form to the hyperbolic pipe-soil interaction curve developed by Hardin and Drnevich (1972) that was originally proposed for clay by Kondner (1963). The soil suction during uplift was modelled based on the test data obtained from the STRIDE and CARISIMA JIPs. In order to calculate the dynamic soil stiffness, the model used the bearing load as opposed to the touchdown point reaction force. Hence, the model does not account for soil softening due to repeated cycles, resulting in a conservative modelling at the TDZ, even though the soil behaviour in this region is highly nonlinear. Jiao (2007) proposed a non-linear discrete soil model for SCR response analysis in the TDZ. The model introduced two non-degrading and degrading schemes for different soil conditions. More recently, Aubeny & Biscontin (2009) and Randolph & Quiggin (2009) purposed two advanced nonlinear soil models for

SCR analysis in TDZ. Aubeny & Biscontin (2009) proposed a simplified model consisting of four different equations that represent the soil spring characteristic in each load cycle. The first curve in this model simulates the intact soil response as a backbone curve. The second scenario is the elastic rebound curve, which simulates the soil response to SCR uplift process. The partial separation of the riser and soil within uplift episode is modelled with a third curve until complete detachment. A reloading curve then models the riser re-penetration in the disturbed soil. More intermediate equations are modelling the local load cycles. The incapability of this model in predicting comprehensive soil degradation was resolved by Nakhaee and Zhang (2008) through proposing an updated version. Randolph and Quiggin (2009) proposed a nonlinear model to predict the hysteretic soil response to SCR up and down oscillations. The model combines the hyperbolic and exponential functions within four main episodes of riser-seabed cyclic contact: initial penetration, uplift, separation and re-penetration. Shiri and Randolph (2010) implemented the model into ABAQUS through developing user-defined elements to explore the SCR fatigue performance and automated trench generation mechanism. This model was implemented into Orcaflex software in 2009 and is currently amongst the most popular non-linear models to predict the hysteretic riser-seabed interaction. Shiri (2014) used the model to study the influence of trench creation on fatigue performance of SCR in the TDZ. Zargar and Kimiaei (2015) conducted a comparative study to investigate the advantages and disadvantages of the models proposed by Aubeny and Biscontin (2009) and Randolph and Quiggin (2009) using existing test results. Authors made an overall comparison between the equations proposed by both of the models for different episodes of riser-seabed interaction. Despite the studies conducted on the performance of these non-linear models

in prediction of fatigue life and trench creation in TDZ, there is still no study in the literature to comprehensively examine the functionality and the consistency of these models over different conditions. In this chapter, the nodal performance of the model proposed by Randolph and Quiggin (2009) (R-Q model) was comprehensively studied through numerical analyses for a range of seabed soil parameters and various locations with different magnitudes of movements on the SCR.

9.3. Construction of Numerical Model

To fully examine the nodal response of R-Q model within the up and down motions of the SCR in the TDZ, a global numerical SCR model was developed in ABAQUS. The commercial software Orcaflex does not provide access to alter all of the R-Q soil model parameters. Therefore, developing the global model in ABAQUS with the R-Q model implemented in provides full access to the model. It is worth mentioning that it might be more appropriate to say "R-Q riser-seabed interaction model" rather than use the term "R-Q soil model" because the model indeed is not a soil model, but a strong mathematical expression describing the non-linear riser-seabed interaction. However, the term "R-Q soil model" may be used here in this chapter for simplicity. The global SCR model developed in ABAQUS comprises a generic SCR connected to a Spar vessel. Seabed soil was modelled through developing user-defined elements (UEL) and implementing the R-Q model. The vessel excitation under the environmental loads was modelled using the DISP subroutine of ABAQUS.

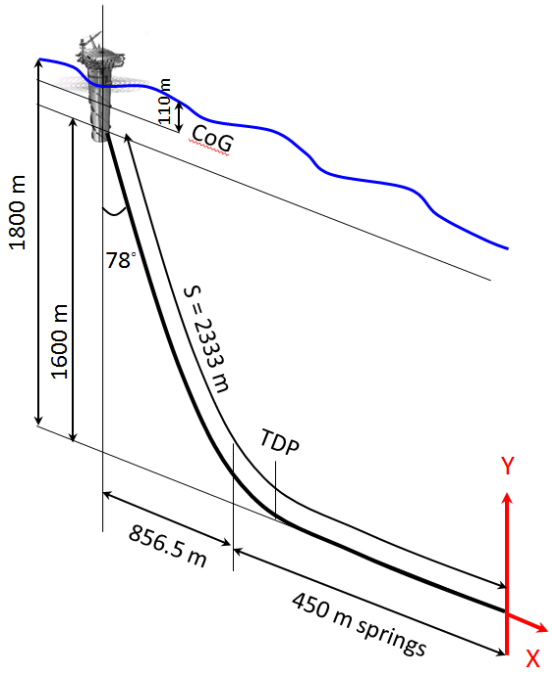

Figure 9-1. The global geometry of SCR modelled by ABAQUS

Figure 9-1 shows the SCR system configuration, where the riser is Timoshenko (shear flexible) beam using element B21 from the ABAQUS element library. The total numbers of 828 nodes were defined starting from node No. 1 at the anchor end and ending with node No. 828 at the vessel attachment point. The length of beam elements in the hanging part is 5 m (except for the last element connected to the vessel which is 3 m in length) and 1 m in the remaining part on the seabed within a length of 450 m as seen in Figure 9-1. Table 9-1 gives the mechanical properties of SCR.

Table 9-1. Riser properties

Dimension	Value
Outer diameter, D_o	0.324 m (12¾ ")
Wall thickness, t	0.0205 m
Second moment of area, I	$2.26x10^{-4}$ m^4
Steel Young's Modulus	2.07x1011 N/m^2
Steel density, ρ_s	7850 kg/m^3
In service submerged weight, m_s	100 kg/m
Fatigue S-N curve	DNV (2008), E Class weld, $a=1.05x10^{-12}$, m=3.0, SCF=1.13

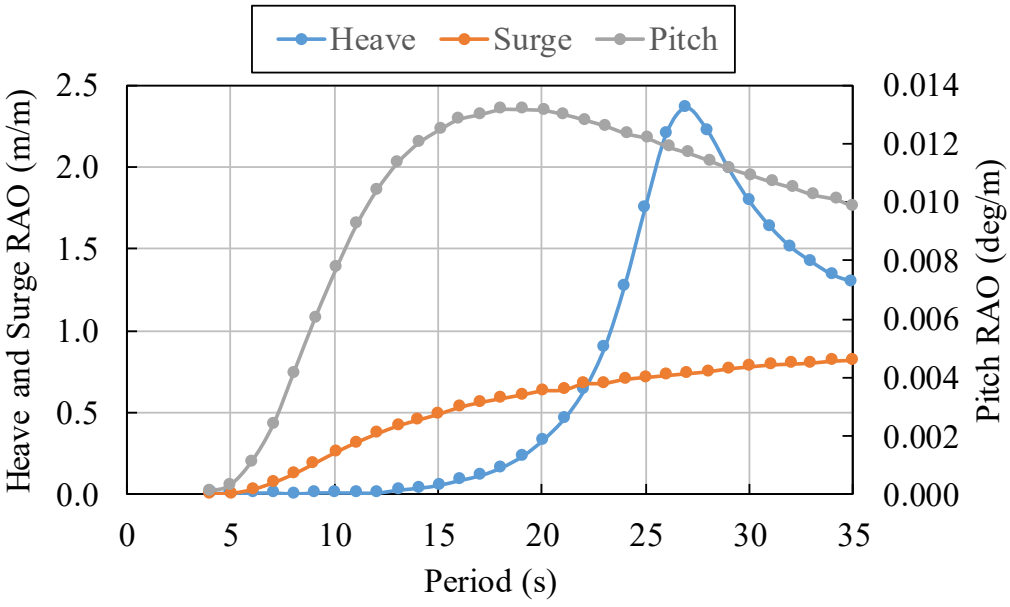

Figure 9-2. Generic Spar RAO. Head sea. Gulf of Mexico (Bridge et al., 2004).

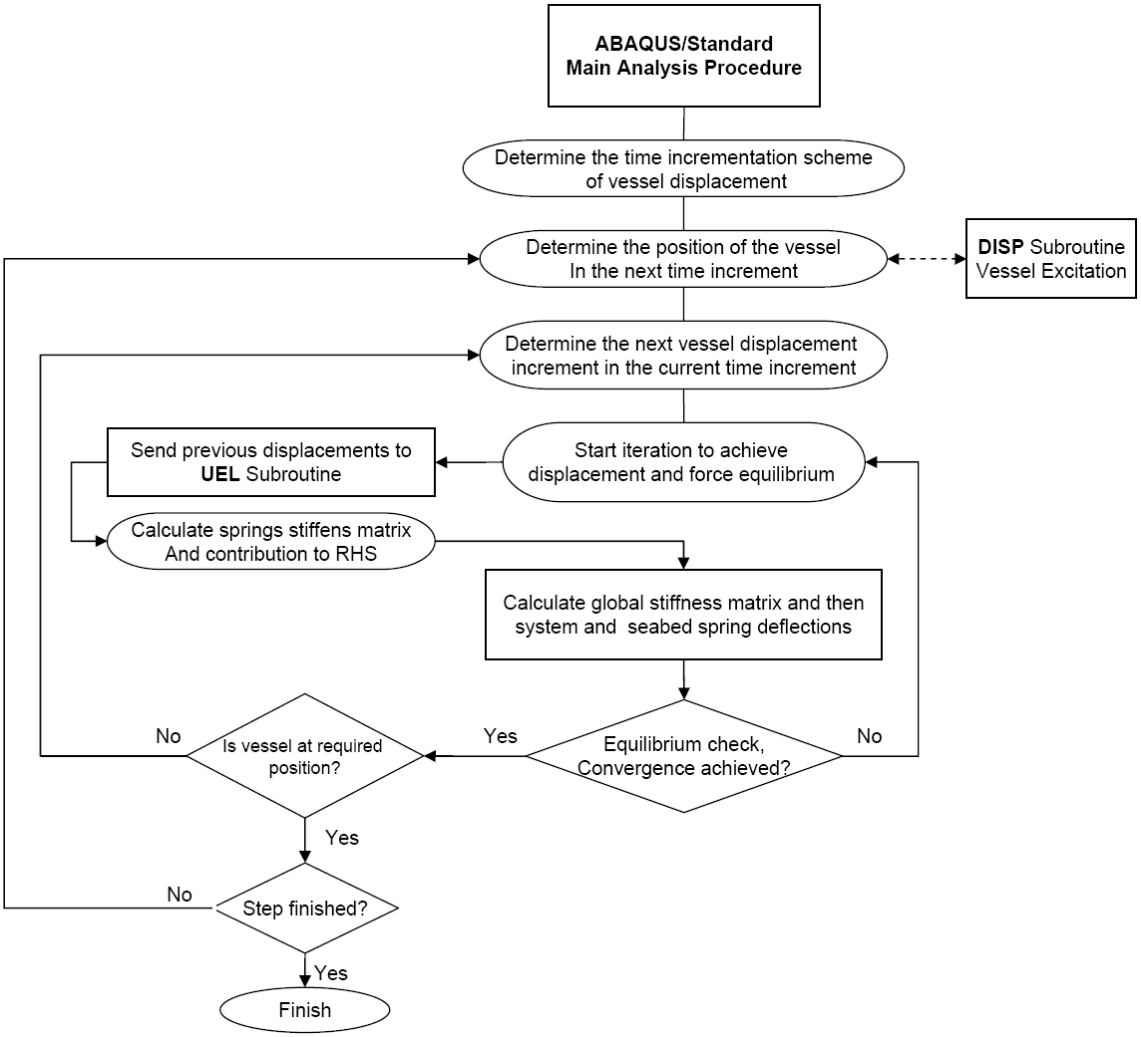

Figure 9-3. Main flowchart of riser analysis using ABAQUS.

The vessel excitation was conducted through coding the DISP subroutine and a given response amplitude operator (RAO) illustrated in Figure 9-2. A full wave scatter diagram from Gulf of Mexico was fed into the subroutine. The subroutine enabled selection of the wave bins, number of cycles to be applied and the wave train hierarchies. In this chapter, only a single wave was activated in DISP subroutine to investigate the nodal performance of the soil model, while the rest of wave bins were deactivated. To perform a full fatigue

analysis and examine the performance of the soil model, all of the wave bins could be activated in DISP subroutine. However, the full wave scatter diagram and the results of fatigue analysis have been comprehensively discussed in a sister chapter (Part II of the current chapter) that investigates the global response of the riser system using a non-linear hysteretic seabed model. To further focus on the performance of the soil model, only the wave frequency motions about the vessel mean position was modelled through quasi-static analysis, and the effect of low-frequency motions was not considered. This approach facilitated the purely monitoring of the soil model performance. In the second chapter (Part II), dynamic analysis with full vessel excitation has been performed and the results have been discussed in detail.

9.3.1. Numerical analysis steps

The model uses three steps to define the SCR connected to the floating system. The SCR was initially modelled as a straight pipe, laid on the seabed, partially supported by seabed springs, with simple support at the vessel end and fixed at the anchor end. At the first start, the submerged weight was applied to the riser, and the vessel end of the riser was lifted up simultaneously to the level equal to the height of the attachment point. Then, the vessel was shifted to the vessel's nominal position towards the anchor end to achieve the targeted lay angle (78° in this example) and start perturbing to simulate the effects of wave action. Each new position of the vessel was generated by the DISP subroutine of ABAQUS, which processes the applied regular wave data and vessel RAO at every increment of analysis. Figure 9-3 shows the flowchart of the overall analysis.

9.4. Modelling of Seabed Soil

For numerical simulation, the steel catenary riser constructed in ABAQUS was assumed to sit on user-defined springs distributed along the seabed. The behaviour of these springs was defined and coded inside the UEL subroutine based on R-Q soil model (Randolph and Quiggin, 2009). Since the current study deeply explores the R-Q model, it is worth reviewing the model characteristics before expressing the model implementation into the ABAQUS.

9.4.1. R-Q Non-linear Hysteretic Soil Model

The R-Q model uses combinations of hyperbolic and exponential functions to model the soil stiffness within four main episodes of riser-seabed cyclic contact: initial penetration, uplift, separation and re-penetration (see Figure 9-4). These different episodes were comprehensively examined in this study that will be discussed in the coming sections.

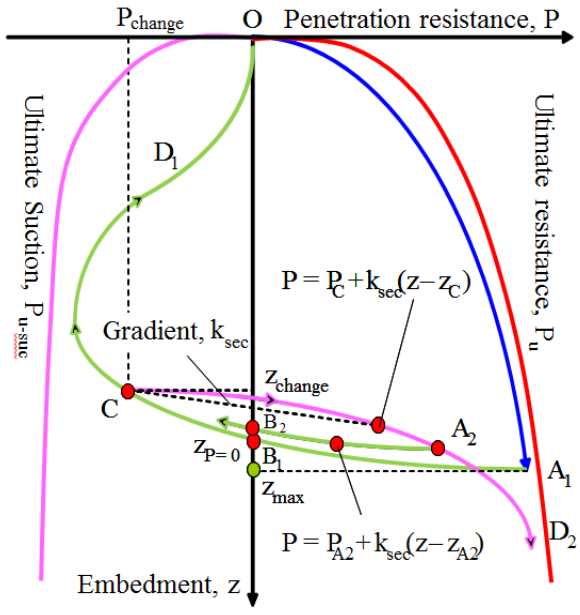

Figure 9-4. R-Q Soil model characteristics for different displacement modes.

The model starts with "Initial Penetration" mode as shown by the blue line in Figure 9-4. The resistance asymptotically approaches the ultimate penetration resistance $P_u(z)$, while the penetration depth is increased. The ultimate penetration resistance ($P_u(z)$) is calculated using few key parameters including the soil bearing factor N_c, which is defined with normalized penetration (z/D) and non-dimensional penetration resistance parameters (a and b). The soil resistance is calculated by:

$$P(z) = H_{IP}(\zeta) \cdot P_u(z) \tag{9-1}$$

Where ζ is the non-dimensional penetration in units of D/K_{max} in which K_{max} is the normalized maximum stiffness parameter of the model:

$$\zeta = z/(D/K_{max}) \tag{9-2}$$

And H_{IP} is a hyperbolic factor given by:

$$H_{IP}(\zeta) = \zeta/(1+\zeta) \tag{9-3}$$

By reversing the riser penetration direction, the model enters uplift mode, and the reaction force decreases rapidly with a high initial secant stiffness. Further uplift takes the model into the suction region with a negative reaction force. The suction resistance reaches its maximum value approaching the ultimate suction resistance, $P_{u\text{-}suc}$. The magnitude of ultimate suction resistance is a fraction of the ultimate penetration resistance controlled by parameter f_{suc}. With further uplift, the suction resistance decays to zero over a distance controlled by parameter $\lambda_{suc.}$ Re-penetration after an entire break out follows an initially convex curve reflecting the soil softening beneath the riser during uplift. The re-penetration resistance approaches the ultimate penetration resistance at a penetration depth greater than the previous maximum penetration depth, as controlled by parameter λ_{rep}. Re-penetration

may also occur when the suction resistance is partially mobilised. In such a case, the suction resistance reduces rapidly, and the model enters the positive reaction region. Further cycles of uplift and re-penetration would give further episodes of uplift and re-penetration modes and so give hysteresis loops of seabed resistance with incremental penetration at each cycle (Randolph and Quiggin, 2009). For the sake of conciseness, we only showed the equations for initial penetration above. One may review the paper published by Randolph and Quiggin (2009) for further details and R-Q model equations (Randolph and Quiggin, 2009).

9.5. Analytical Response of R-Q Model

Before examining the R-Q model through coding the UEL subroutine, an Excel spreadsheet was developed for arbitrary evaluation of a single node on SCR in the TDZ. An artificial displacement history of the node was given, and the seabed response was obtained. Figure 9-5 shows a sample response of model over a few arbitrary cycles of uplift and re-penetration. The influence of different key parameters of the model (k_{max}, f_{suc}, λ_{suc}, and λ_{rep}) was also studied (see Figure 9-6). In this example, the riser diameter is 0.324 m, the mudline shear strength is 0.65 kPa, and the shear strength gradient is 1.5 kPa/m. The power law parameters for bearing capacity factor (a, b) were taken as 6, and 0.25 respectively.

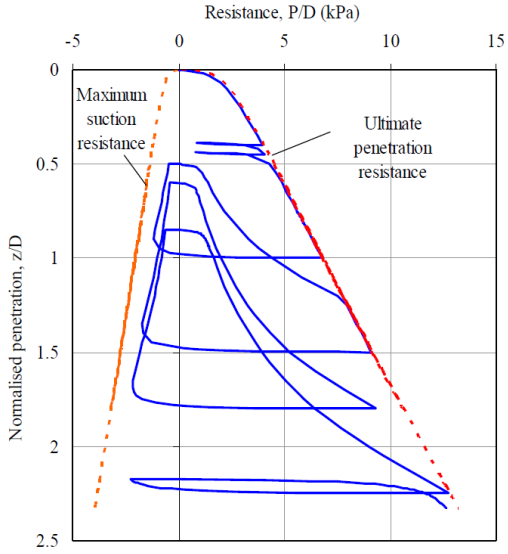

Figure 9-5. Example response of R-Q under complex arbitrary motion.

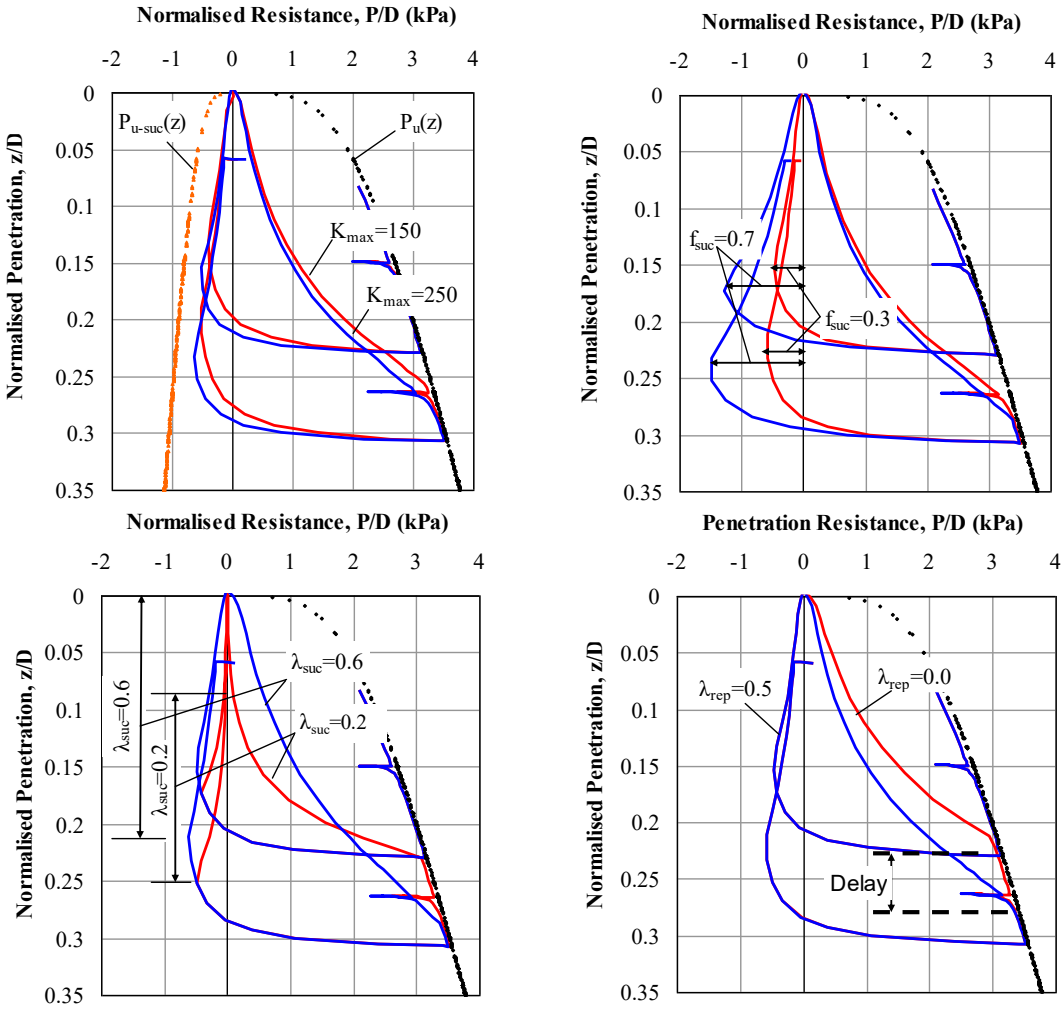

Figure 9-6. Influence of R-Q model key parameters on soil response.

Randolph and Quiggin (2009) recommend $K_{max} = 200$ in the R-Q model. Higher values of K_{max} give higher penetration resistance and lower suction force for a given penetration depth, with the maximum difference occurring in the late re-penetration and early suction stages.

As shown in Figure 9-6, the amount of suction resistance in uplift is controlled by f_{suc}. The magnitude of this parameter can lie between zero for no suction resistance to unity for maximum suction resistance equal to the ultimate penetration resistance. Randolph and Quiggin (2009) suggests a more realistic upper limit of 0.7 for f_{suc}. Since the suction force appears to reduce rapidly to a low level within a few cycles, for the single uplift of a riser, a value of 0.5 to unity is considered. For fatigue studies or other applications with many cycles, the recommended range is 0 - 0.3. In reality, various factors affect the magnitude of suction resistance, such as the uplift rate of the riser, the time over which the uplift motion is sustained and the recent history of cyclic motion (Bridge et al., 2004). However, considering the very limited published data, Randolph and Quiggin (2009) adopted a constant (but user-defined) value of f_{suc}. Figure 9-6 shows the effect of f_{suc} on the peak suction mobilised, and the following re-penetration resistance. Higher values of f_{suc} give higher suction resistance and a slower mobilisation of the re-penetration resistance. Since f_{suc} does not control the suction decay distance, larger values of f_{suc} give a higher gradient of suction decay.

The parameter λ_{suc} adjusts the suction decay distance in the R-Q model. Randolph and Quiggin (2009) considered a value range of 0.2-0.6 for λ_{suc}, which leads to small residual suction resistance after an uplift displacement of about 1 diameter. This matches experimental results showing a suction decay distance in the order of the riser diameter or

less, although the response will also be affected by the rate of motion and the previous displacement history (Aubeny and Biscontin, 2009; Bridge et al., 2004). Figure 9-6 illustrates the extension of the suction decay distance with higher values of λ_{suc} which in turn affect the peak suction mobilization and the soil softening (or reduced resistance) in the initial stages of re-penetration. Lower values of λ_{suc} give a reduced suction decay distance, lower peak suction mobilisation and a softer response in the initial stages of re-penetration (i.e. lower resistance for a given re-penetration depth).

The model parameter, λ_{rep}, simulates the progressive penetration with cumulative load-controlled cyclic movements, delaying the mobilization of ultimate re-penetration resistance. Randolph and Quiggin (2009) recommend a value in the range 0.1-0.5, which shows reasonable correlation with experimental results. Figure 9-6 shows the delay in ultimate resistance mobilization by adopting a higher value of λ_{rep}.

The results obtained from Excel spreadsheet for an arbitrary nodal displacement history show a smooth and consistent response. However, the real nodal displacement history on SCR can be much more complex and need a sophisticated model to investigate. In the coming sections the performance of the model will be discussed over complex SCR motions using the constructed numerical model in ABAQUS.

9.6. Developing User-defined Subroutine (UEL)

The R-Q model was coded into a user-defined element (UEL) to model the seabed soil response to cyclic loads. At every time increment, the UEL subroutine is called by ABAQUS for the elements identified as a user-defined element. ABAQUS then passes key variables to the UEL, including updated displacements of the nodes. The UEL subroutine uses the historical displacements of the nodes and calculates the stiffness matrix of each

element and its contribution to external forces through the right-hand side vector (RHS). This information is returned to ABAQUS to calculate the global stiffness matrix and update the variables to be passed to the UEL again. Figure 9-7 illustrates the local flowchart of UEL calculation process.

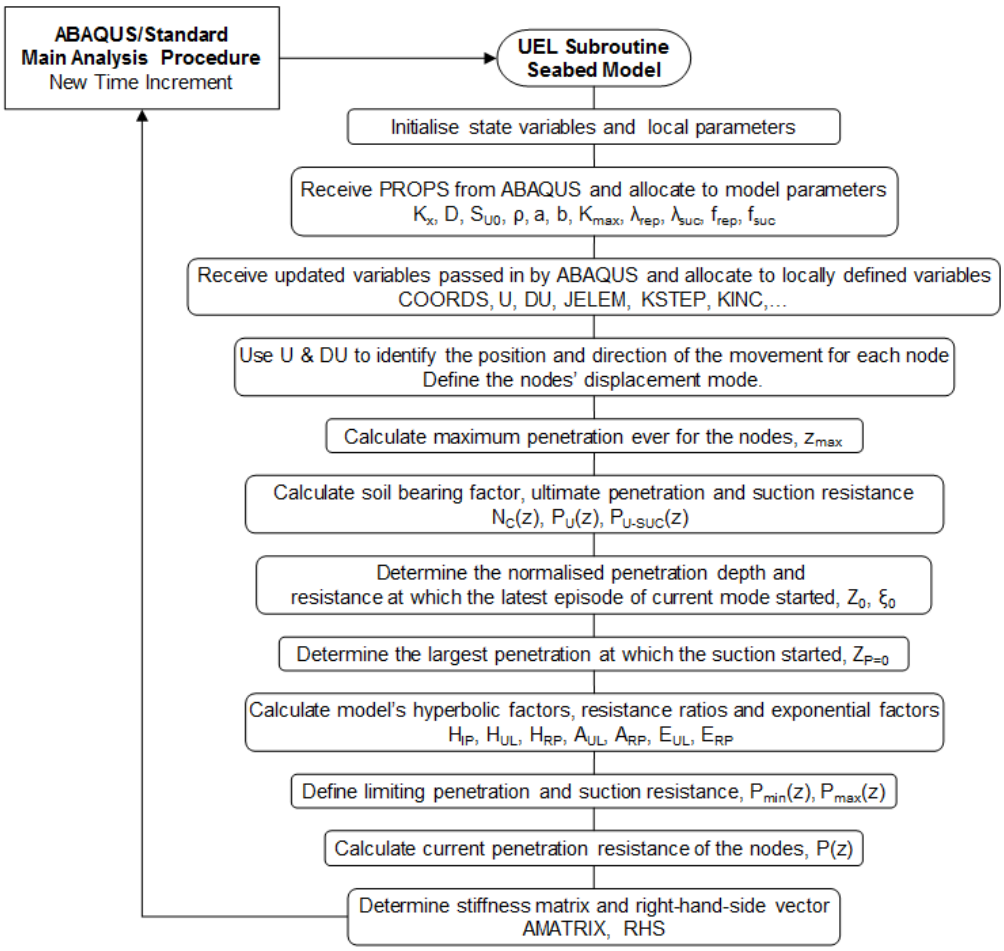

Figure 9-7. UEL subroutine internal flowchart.

9.7. Nodal Response of R-Q Soil Model

A regular wave with a height of 16.5 m and a period of 11 s was applied on Spar vessel by ten cycles, and the response of SCR to R-Q soil model in the TDZ was obtained in various

nodes. The number of cycles is arbitrary only to illustrate the model performance. Increasing the load cycles stabilizes the von Mises stress variation range that will be further investigated in part II of this chapter. A comprehensive parametric study was conducted through series of simulations varying the R-Q soil model parameters, one at a time including mudline shear strength, shear strength gradient, suction ratio, suction decay parameter, and re-penetration offset parameter. Table 9-1 shows the default R-Q model parameters used in the current study. Table 9-2 presents the overall parametric study map comprising 21 different case studies to cover different nodal events fully.

Table 9-1. Default values of R-Q model parameters

Parameter	Symbol	Value
Mudline shear strength	s_{u0}	0.65 kPa
Shear strength gradient	ρ	1.5 kPa/m
Power law parameter	a	6
Power law parameter	b	0.25
Normalized maximum stiffness	K_{max}	200
Suction ratio	f_{suc}	0.3
Suction decay parameter	λ_{suc}	0.5
Repenetration parameter	λ_{rep}	0.5

Table 9-2. Parametric study map

Case study	Input soil model parameters					Case study	Input soil model parameters				
	s_{um}	ρ	f_{suc}	λ_{suc}	λ_{rep}		s_{um}	ρ	f_{suc}	λ_{suc}	λ_{rep}
CS-1	0.0	D	D	D	D	CS-13	D	D	D	0.0	D
CS-2	0.35	D	D	D	D	CS-14	D	D	D	0.2	D
CS-3	0.65	D	D	D	D	CS-15	D	D	D	0.5	D
CS-4	1.5	D	D	D	D	CS-16	D	D	D	1.0	D
CS-5	D	0.0	D	D	D	CS-17	D	D	D	D	0.0
CS-6	D	0.2	D	D	D	CS-18	D	D	D	D	0.2
CS-7	D	0.5	D	D	D	CS-19	D	D	D	D	0.5
CS-8	D	1.0	D	D	D	CS-20	D	D	D	D	0.8
CS-9	D	D	0.0	D	D	CS-21	D	D	D	D	1.0
CS-10	D	D	0.3	D	D						
CS-11	D	D	0.5	D	D	Note: D refers to "Default" values in Table 9-1.					
CS-12	D	D	1.0	D	D						

Different groups of seabed nodes on the displaced SCR may move in different direction and experience different episodes. Figure 9-8 shows the movement directions of various node families corresponding to displacement of the vessel away from the SCR. The initial and displaced profiles are numbered as 1 and 2 respectively. Certain nodes towards the vessel end of the TDZ undergo upward movements, while nodes further towards the anchor end of the SCR undergo further penetration. In the hysteretic non-linear model (Randolph and Quiggin, 2009), the suction starts when the mobilized penetration resistance in the last stage is quickly decayed, and the riser proceeds with further lift up. Then the breakout is started when the mobilized suction force is entirely decayed. Various sample nodes shown in Figure 9-9 are selected to illustrate the nodal response of the R-Q model to different movement scenarios.

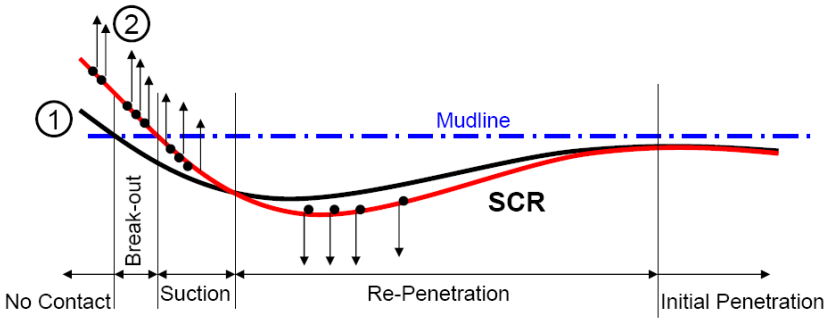

Figure 9-8. Nodes at the seabed with various displacement stages at the same time for vessel far offset.

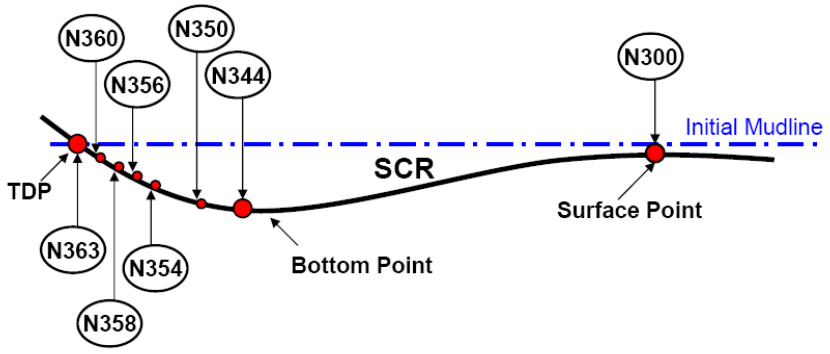

Figure 9-9. Schematically location of the sample nodes on final profile of SCR.

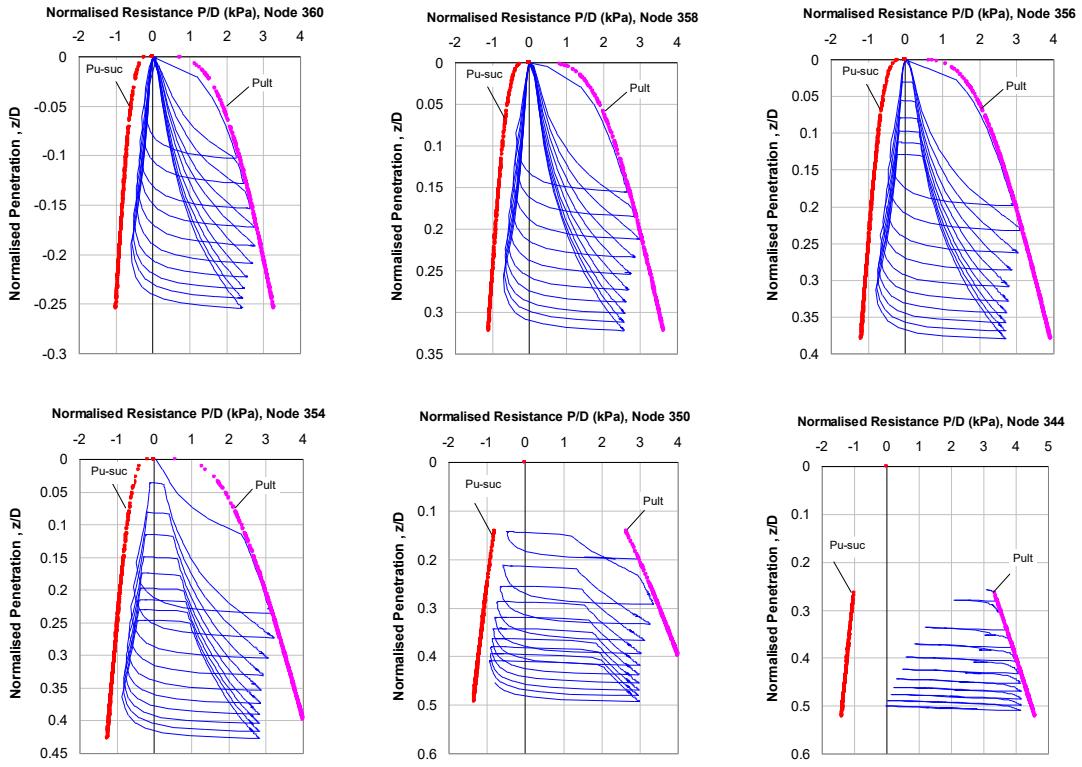

Figure 9-10. Nodal response of numerical model at various locations (default model parameters).

As a result of numerical simulations, the hysteretic load-displacement response of nodes 360, 358, 356, 354, 350, and 344 is illustrated in Figure 9-10, spanning positions from the TDP towards the anchor end of the touchdown zone. For instance, the node 358 experiences penetration, full suction and full breakout over ten load cycles where the Spar end of the riser and the TDP moved respectively by ±5.13 m and ±3.8 m. The penetration depth increases from the initial monotonic penetration of z/D = 0.15 to a final normalised depth of 0.32 at the end of the 10th cycle. This limited change implies that a slight trench is formed beneath the riser under cyclic loading. As shown, incremental penetration under cyclic loading has been appropriately captured through the gradual soil softening by the R-

Q hysteretic non-linear soil model. The results presented for nodes 356 and 354 seem similar but are different; in contrast with node 354, node 356 experiences breakout. Since the spring spacing is 1 m throughout the region on the seabed, the node ID reflects the node distance from the anchor end. For this analysis, the initial TDP is about node 356 and transfers to about node 363 after ten cycles of excitation. In these plots, the penetration has been considered positive ignoring the signs of local coordinate system in analysis.

9.7.1. Nodal Response Violation in Minor Motion Reversal

A comprehensive examination of the R-Q model over a wide range of various parameters and different nodes shows a reasonable nodal response. However, there are some occasions that the model malfunctions, which will be discussed here. The model defines a high stiffness value when the nodal movement episode is getting reverse, i.e. turning from penetration to uplift or vice versa. This is a key requirement and well correlated with conducted centrifuge test results when the penetration or uplift episode is reasonably sustained for a while. However, on some occasions, the model is cheated by minor changes in movement direction of a node within a large penetration or uplift episode. This violates the nodal contact pressure causing an immediate increase in penetration or suction resistance, which is not supposed to happen in real soil. This short reversal may be a real event or numerical fluctuation, but the soil model is supposed to respond to all motion episodes properly. Figure 9-11 shows two samples of violation in nodal responses, one in penetration and another in uplift phase.

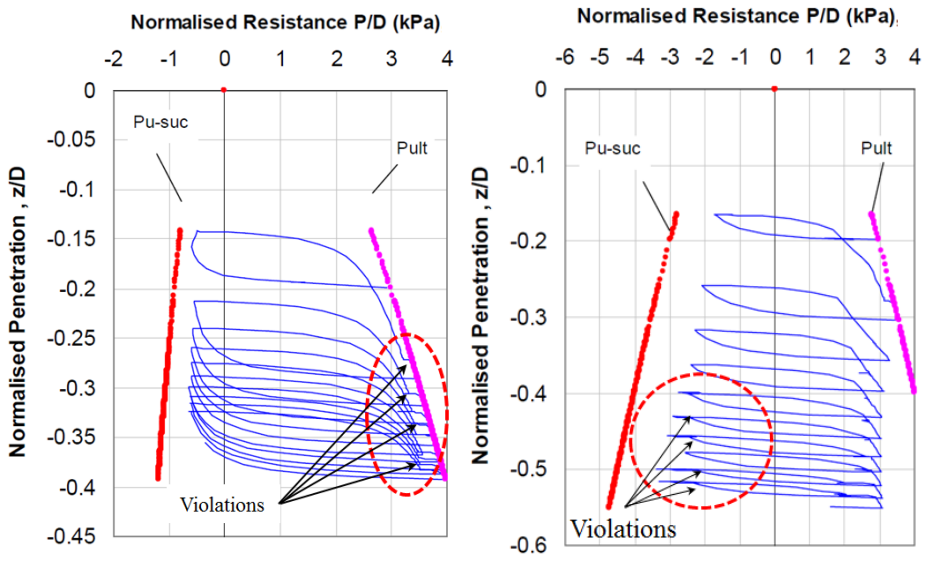

Figure 9-11. Nodal violated response in motion reversal.

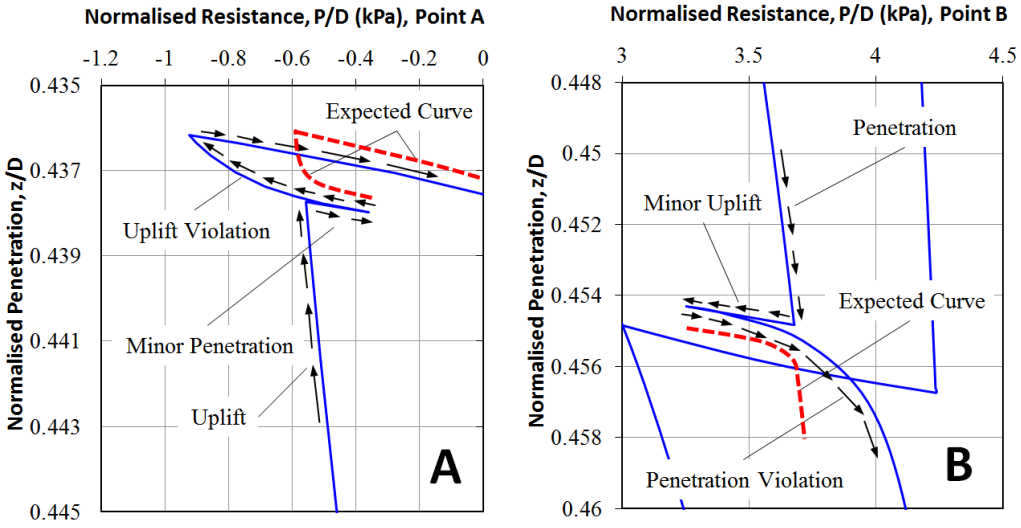

Figure 9-12. Simultaneous uplift and penetration violation in minor motion reversal.

A larger view of sample nodes with violations in suction and resistance (A and B) is shown in Figure 9-12, where a minor motion reversal within the penetration or uplift phase may cause an artificial jump. The sudden variation of penetration resistance or suction force can

widely vary (2% -100%) depending on the model input parameters, node location, and displacement range.

Further investigation shows that nodal violation is more likely to happen in higher magnitudes of penetration or suction, fairly close to the backbone curves. A comparative example is shown in Figure 9-13, where minor motion reversal has only violated the penetration curves closer to the ultimate penetration resistance.

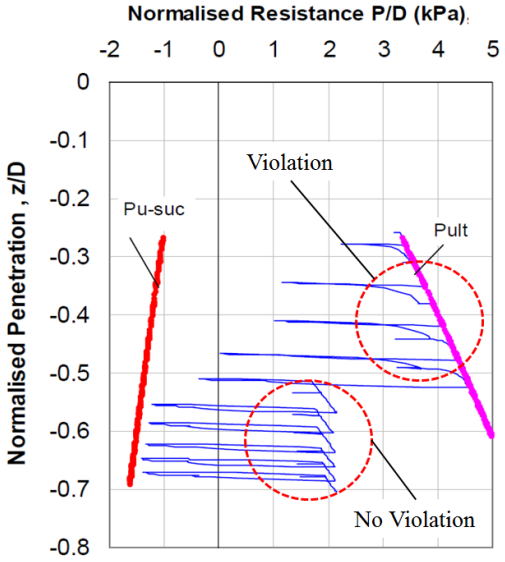

Figure 9-13. Nodal violation in responses closer to ultimate resistance/uplift.

The area of normal and violated response is separated in another sample node in Figure 9-14. This may affect the total force mobilization both in suction and resistance and consequently contact pressure, which in turn affects the shear and bending stress distribution and fatigue life of SCR. In this sample, the suction force has been violated by 35% and the resistance by about 12% within ten cycles. The trend shows that increasing the number of cycles results in higher values of residual violation.

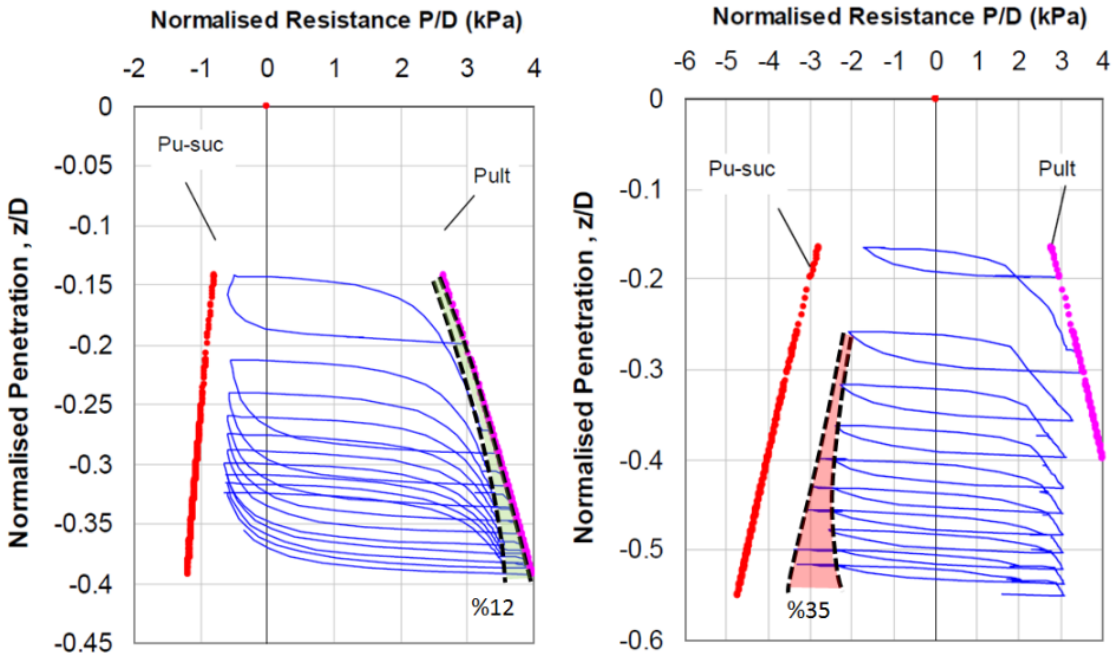

Figure 9-14. Sample range of nodal violation both in suction and penetration resistance.

A comprehensive examination of the results of the parametric study shows that the probability of nodal violation occurrence is relatively independent of model input parameters. However, the nodes located in the proximity of the trench bottom point toward the vessel are more likely to show response violation (Nodes 344 to 350 from Figure 9-9).

9.7.2. Nodal Response Violation in Low Embedment

A detailed evaluation of the nodal response within various analyses with different input parameters shows that for higher values of undrained shear strength at mudline (S_{u0}), the nodal responses at trench mouth are also violated. In this region with low penetrations, the resistance is quickly increased because of the high value of undrained shear strength. However, the R-Q soil model cannot properly simulate the suction decay within a full uplift

episode in the low range of embedment depth. This causes the suction decay curve to re-enter into the penetration resistance region without any reversal motion, which is unexpected in a real soil response. Figure 9-15 shows sample responses of nodes 360, 358 and 356 close to trench mouth (please see Figure 9-9), for three different values of undrained shear strength in mudline i.e. 0.0, 0.35 and 1.0 kPa. The nodal responses of these nodes are violated using 1.0 kPa undrained shear strength. Dashed red circles show the violation area.

Figure 9-16 shows a larger view of sample load cycle in node 360.

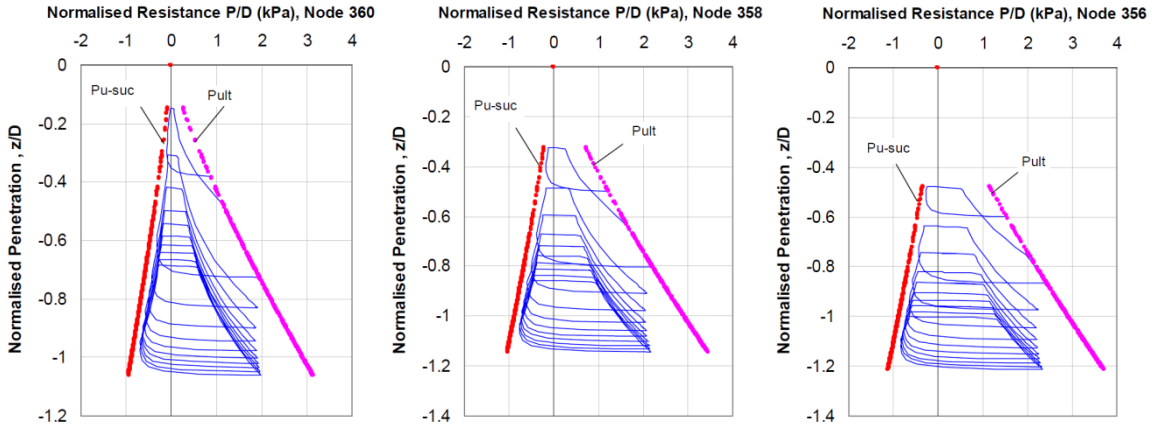

S_{u0} = 0.0 kPa

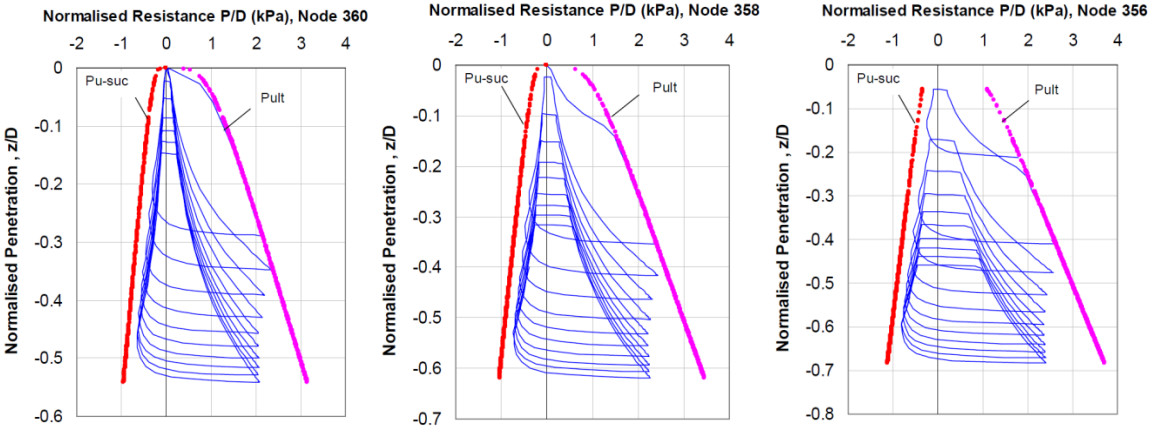

S_{u0} = 0.35 kPa

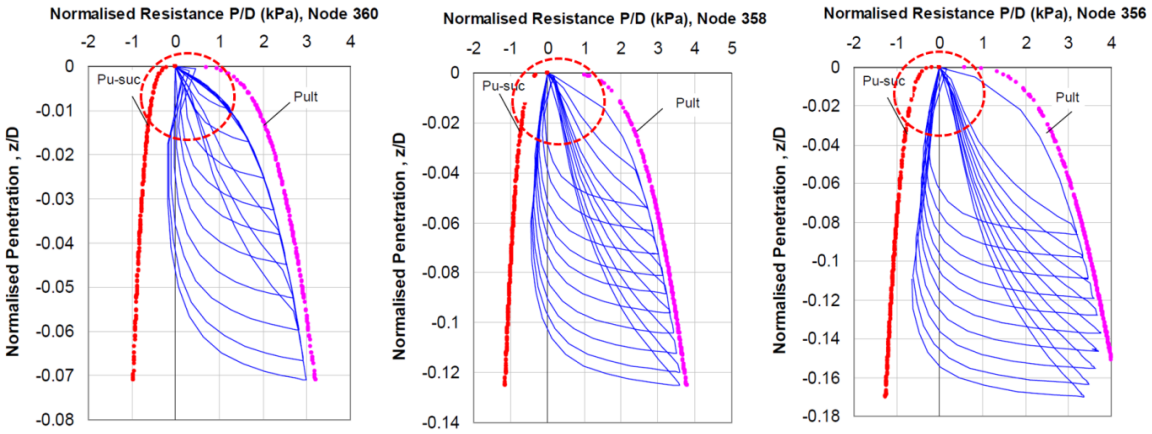

S_{u0} = 1.0 kPa

Figure 9-15. Violation of nodal response in trench mouth for higher undrained shear strength.

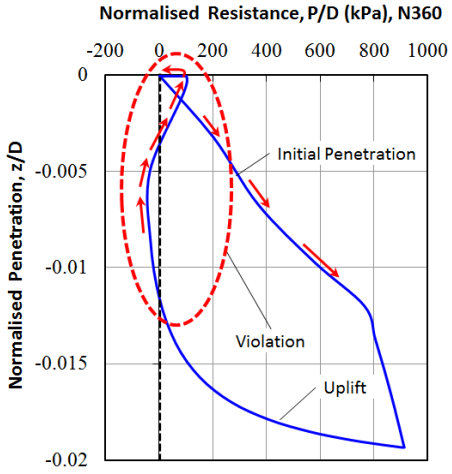

Figure 9-16. Close-up view of nodal response violation for node 360.

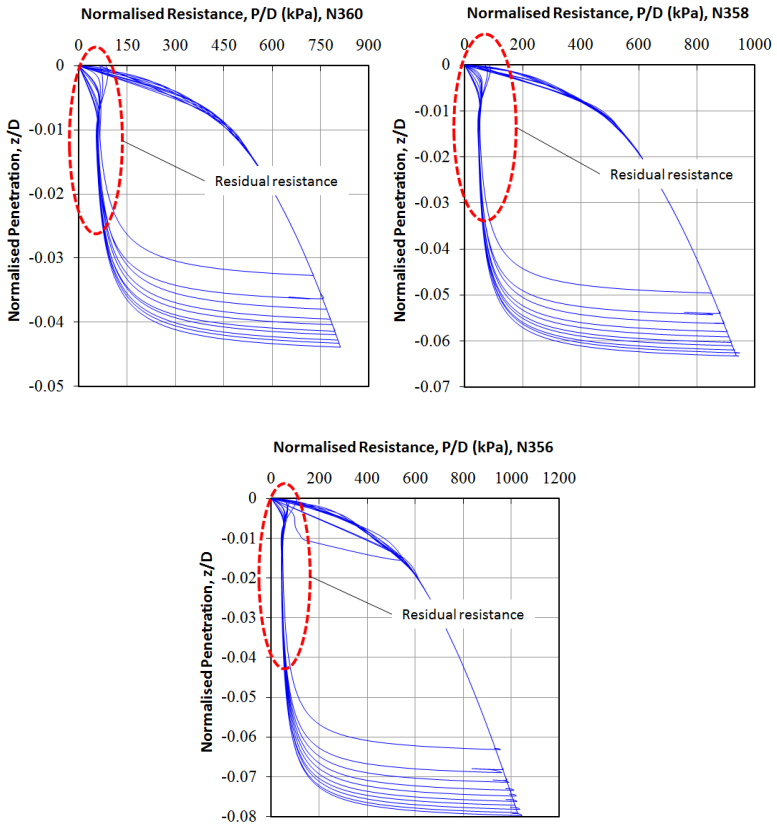

Figure 9-17. Model misconduct in low suction over limited uplifts.

The same scenario happens in nodal responses with limited embedment for the normal values of undrained shear strength but the extremely low values (near zero) of suction force mobilization parameter f_{suc}. Figure 9-17 shows examples of nodal responses in such conditions, where an unexpected residual penetration resistance is remained over the entire uplift and forced to be zero in breakout. The field surveys show that the remoulded soil inside the trench is washed out under current action and water entraps into the trench by riser motions. Therefore, the suction force mobilization is significantly reduced over the time and the soil model needs to be able to capture the soil response for low suction values over limited uplifts. These show that R-Q soil model has a better performance when relatively large episodes of nodal motions are applied.

9.7.3. Pre-mature Stabilization of Nodal Response

The filed surveys conducted by remote operating vehicles (ROV) have shown that a trench is created underneath the SCR in touchdown area within few years after installation (Bridge and Howells, 2007). Various trench depths have been reported from 3 to 10 times the pipeline diameter. To examine the model capability in simulating the trench creation, an individual regular wave (H_s = 7 m, T_z = 8.7 s) has been applied on SCR by a large number of cycles (1539 cycles). The results show that an ultimate penetration depth of less the 0.5D to 1.0D is achieved in TDZ within few load cycles at the beginning of analysis (see Figure 9-18). The model is then rapidly stabilized, and further cycles make no further embedment. In another word, using the usual range of the R-Q model input parameters, the model is not able to simulate the trench creation because of pre-mature stabilization. Figure 9-19 shows the pre-mature stabilization of SCR embedment into the seabed.

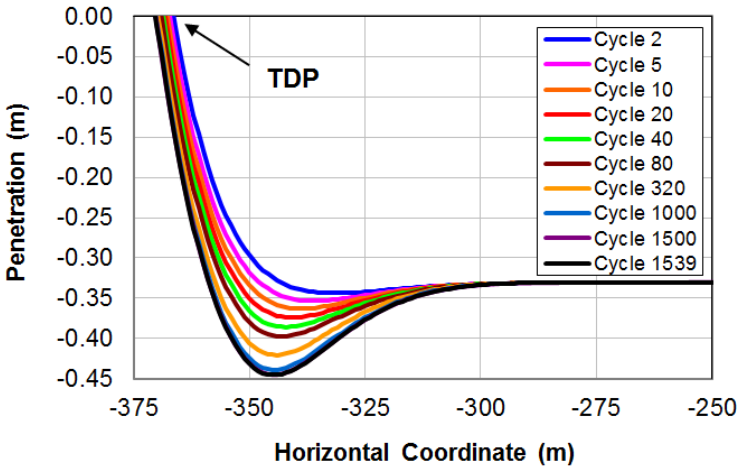

Figure 9-18. Pre-mature stabilization of SCR embedment profile.

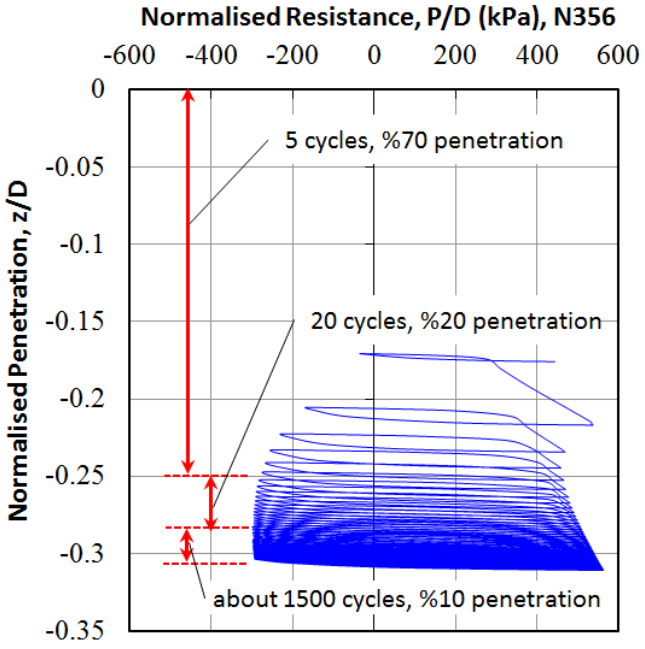

Figure 9-19. Nodal pre-mature stabilization of R-Q model.

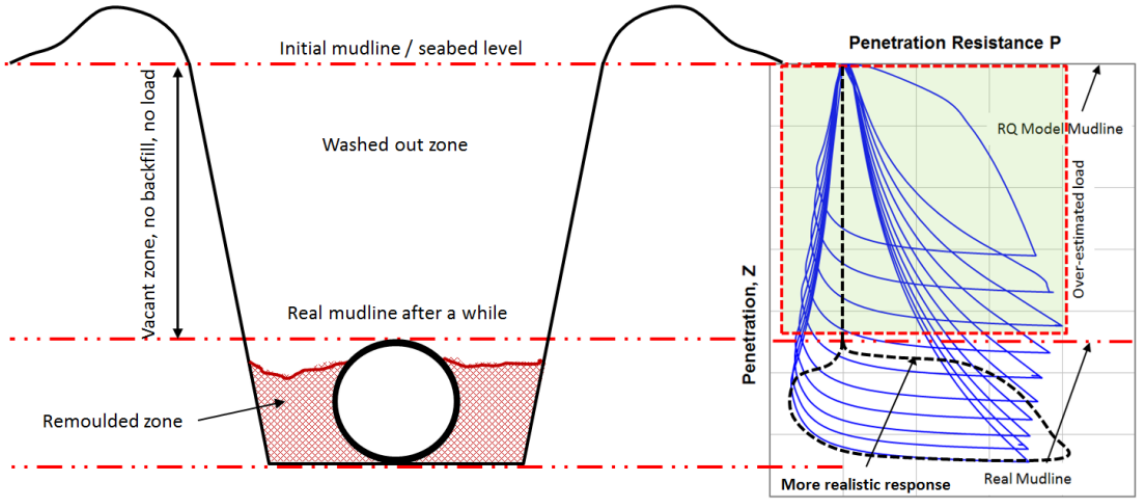

Figure 9-20. Over-estimation of resistance after developing the trench beneath the SCR.

Figure 9-20 shows the nodal response around node 356 in the TDZ, where about 70% of the total embedment is achieved only by five load cycles, and the 97% of the cycles has only contributed to 10% of total embedment. One may ask why 1539 cycles has been applied. Indeed, the analysis was terminated when no further embedment was achieved. The capabilities of R-Q riser-seabed interaction model have been used before to study the influence of trench on fatigue performance (Shiri and Randolph, 2010; Randolph et al., 2013). The pre-mature stabilization of the nodal response has caused the authors to feed unrealistic extreme input values to model key parameters to obtain a large embedment. This, in turn, results in a relatively unrealistic trench profile leading to a fatigue response affected by a trench, which needs a reliability check. Authors currently study this separate issue in another research project.

9.7.4. Over-estimation of Nodal Resistance

Our conducted analyses show that R-Q riser-soil interaction model simulates the gradual shallow embedment of riser into the seabed under the cyclic loads. The model simulates the trench formation, neither regarding the penetration depth nor penetration resistance. The main parameter heavily governing the penetration resistance is the evolutionary undrained shear strength continuously degraded under SCR cycle motions. The R-Q model assumes that the remoulded soil underneath the riser is degraded but never disappeared (e.g., because of erosion). In reality, several mechanisms wash out the soil inside the trench as the riser is gradually penetrating into the seabed. These mechanisms comprise the scour under seabed currents action, scour because of the water pushed inside the trench by riser motion, and the active pressure of riser on the seabed. Therefore, going deeper than initial shallow embedment, the real mudline travels down the trench and after a while, SCR can fluctuate inside the trench with no contact with the seabed soil. The R-Q model does not lower the mudline elevation around the riser in TDZ by gradual embedment. Therefore, the model generates nodal resistance that does not existed in reality, and this leads to over-estimation of nodal resistance and consequently fatigue response (see Figure 9-20). Using the lower values of the suction decay parameter (λ_{suc}) in R-Q model can mitigate the conservative estimation of resistance but cannot delete the unrealistic residual resistance remaining in the SCR after developing the trench.

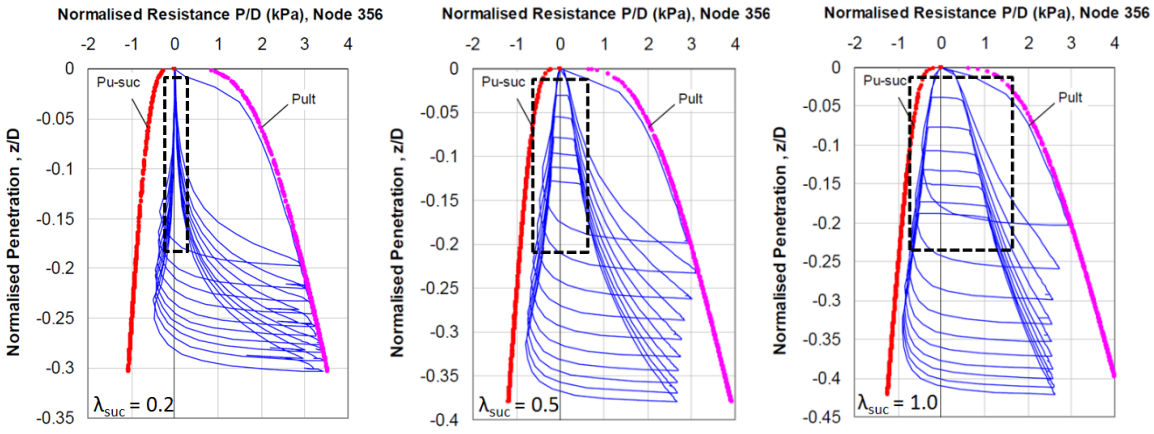

Figure 9-21. Influence of different suction decay parameters on a sample nodal response.

Figure 9-21 shows an example node response, where a lower suction decay parameter (i.e. 0.2), a common magnitude (i.e. 0.5), and an extreme magnitude (i.e. 1.0) were considered.

9.8. Impact of Nodal Response Violation on Fatigue

The cyclic variation of resultant stress in SCR cross-section area leads to cumulative fatigue damage in the TDZ. Barltrop & Adams (Barltrop and Adams, 1991) described a standard form of S-N curves for marine structures which is used in fatigue damage calculation of SCR as well:

$$N = a\Delta\sigma_f{}^{-m} \tag{9-4}$$

where

N is the number of cycles until failure

a is an empirical coefficient (equivalent to the fatigue life for $\Delta\sigma_f = 1$ MPa)

$\Delta\sigma_f$ is the factored stress variation range in MPa

m is the inverse slope of the S-N curve (typically around 3).

For operating life of SCR, many millions of cycles of various stress ranges contribute, and the accumulated fatigue damage can be calculated using a linear cumulative damage (Palmgren, 1924), according to the method commonly known as Miner's rule:

$$D = \sum_{i=1}^{k} \frac{n_i}{N_i} \tag{9-5}$$

where

D is the total accumulated fatigue damage

k is the number of stress blocks

i is the number of a particular constant stress range block in the stress histogram

n_i is the number of stress cycles in stress block i over the design life

N_i is the number of stress cycles to failure for the constant stress range i

From Equation (9-4), taking m = 3, the relative fatigue damage for two different stress ranges σ_{f2} and σ_{f1} is:

$$\frac{D_2}{D_1} = \left(\frac{\sigma_{f2}}{\sigma_{f1}}\right)^{3.0} \tag{9-6}$$

The stress range in SCR cross-section area is directly related to the shear force distribution along the riser (Shiri and Hashemi, 2012), which in turn is governed by riser-seabed contact pressure and soil stiffness. Using the boundary layer method proposed by Pesce et al. (1998), the shear force may be expressed as a function of the normalised seabed stiffness, so that

$$\frac{D_2}{D_1} = \left(\frac{K_2^{0.25}}{\sqrt{2}+K_2^{0.25}} \frac{\sqrt{2}+K_1^{0.25}}{K_1^{0.25}}\right)^{3.0} \quad \text{where} \quad K = k\frac{EI}{H^2} \approx 0.274k \tag{9-7}$$

where

K is the non-dimensional soil rigidity parameter

k is the soil rigidity per unit area

E is the SCR Young's modulus

I is the SCR second moment of inertia

H is the horizontal tension force at the TDP

Substituting the actual stiffness with k_1 and k_2 gives:

$$\frac{D_2}{D_1} = \left(\frac{k_2}{k_1}\right)^{3/4} \left(\frac{\sqrt{2} + (0.274 k_1)^{0.25}}{\sqrt{2} + (0.274 k_2)^{0.25}}\right)^3 \tag{9-8}$$

As shown in previous sections, the range of nodal violations in R-Q model can be quite high on some occasions. However, even a low rate of change (e.g. 20%) in the soil stiffness, gives about 10% increase in fatigue damage:

$$\frac{D_2}{D_1} = \left(\frac{1.2k_1}{k_1}\right)^{3/4} \left(\frac{\sqrt{2} + (0.274 k_1)^{0.25}}{\sqrt{2} + (0.274 \times 1.2 k_1)^{0.25}}\right)^3 \approx 1.10 \tag{9-9}$$

The obtained value highlights the importance of potential violations in seabed soil stiffness on the prediction of cumulative fatigue damage and consequently fatigue life. Comprehensive fatigue analysis has been presented in another chapter (Part II) investigating the effects of non-linear soil model on global response of the SCR. However, an accurate assessment of the impact of R-Q model nodal violation on fatigue response needs improvements in existing model. Therefore, further works need to be conducted to improve the accuracy and consistency of R-Q model for fatigue assessment in non-linear hysteretic seabed soil conditions.

9.9. Conclusions

Degradation of seabed soil stiffness and trench formation under the cyclic motions of steel catenary risers in the touchdown zone is proven by ROV survey (Bridge and Howells, 2007). These alter the contact pressure, the stress range variation, and consequently the cumulative fatigue damage throughout the SCR in the touchdown zone. Non-linear

hysteretic riser-seabed interaction models have been developed and implemented into business software packages within recent years to simulate the riser penetration into the seabed within fatigue analysis. A popular model referred to as R-Q model purposed by Randolph and Quiggin (2009) was selected, and its nodal performance was comprehensively studied through developing a numerical model in ABAQUS with R-Q model coded through a user-defined subroutine (UEL). The study showed there are some over-conservative assumptions and nodal response violations in R-Q model resulting in over-estimation of penetration and suction resistance and consequently the fatigue damage in TDZ. The nodal response violation was frequently observed within the nodes in the proximity of trench bottom towards the vessel. This area is the most fatigue prone section of SCR in the touchdown zone. The results obtained from this study suggest that modifications are needed to improve the nodal performance of R-Q model, though comfort may be taken from the fact that the R-Q model overestimates the fatigue damage. Particular attention shall be paid to the updating of the mudline elevation throughout the load cycles enabling the trench development underneath the SCR. Also, any new model to be developed in this field in the future need to be widely examined in different nodes on the SCR through realistic cyclic motions and range of model parameters representing the seabed soil conditions.

It is worth mentioning that in reality there are several complex riser-soil-fluid interactions and a wide range of loading scenarios that affect the ultimate trench profile and consequently the accumulated fatigue damage. It is quite difficult to make any robust reference about the real effect of the trench on the SCR fatigue without modelling more realistic conditions. Extensive research work should be conducted to simultaneously

consider the proper effects of all contributing events that will be hopefully achieved in future studies.

9.10. Acknowledgements

The authors gratefully acknowledge the financial support of this research by Memorial University of Newfoundland through VP start-up fund (#210751). This work is in continuation to the research project conducted in Centre for Offshore Foundation Systems, University of Western Australia.

References

Aubeny, C.P., Biscontin, G., 2009. Seafloor–riser interaction model. Int. J. Geomechanics 9 (3), 133–141.

Audibert, J.M.E., Nyman, D.J., O'Rourke, T.D., 1984. Differential Ground Movement Effects on Buried Pipelines, in Guidelines for the Seismic Design of Oil and Gas Pipeline Systems. ASCE publication, New York, pp. 150–177.

Barltrop, N.D.P., Adams, A.J., 1991. Dynamics of Fixed Marine Structures. Atkins Oil & Gas Engr. Ltd., Epsom, UK.

Bridge, C.D., Howells, H.A., 2007. Observations and modeling of steel catenary riser trenches. In: 7th Int. Offshore and Polar Engr. Conf. (ISOPE2007), Lisbon, Portugal, pp. 803–813.

Bridge, C.D., Laver, K., Clukey, E., Evans, T., 2004. Steel catenary riser touchdown point vertical interaction models. In: Offshore Technol. Conf. (OTC16628), Houston, Texas, USA.

Clukey, E., Jacobs, P., Sharma, P.P., 2008. Investigation of riser seafloor interaction using explicit finite element methods. In: Offshore Technol. Conf. (OTC-19432-MS), Houston, USA.

Giertsen, E., Verley, R., Schroder, K., 2004. CARISIMA a catenary riser/soil interaction model for global riser analysis. In: Proceedings of the Int. Conf. On Offshore Mechanics and Arctic Engr. (OMAE2004). Vancouver, BC, Canada, pp. 633–640.

Hardin, B.O., Drnevich, V.P., 1972. Shear modulus and damping in soils: measurement and parameter effects (Terzaghi Lecture). J. Soil Mech. Found Div. 98 (6), 603–624.

Jacob, P., 2005. Planar Investigation of Riser Trench Formation Using Ls-dyna. MMI Engr.

Jiao, Y., 2007. Non-linear Load-deflection Models for Seafloor Interaction with Steel Catenary Risers. Texas A&M University, College Station, USA. Master of Science, 121.

Kondner, R.L., 1963. Hyperbolic stress-strain response; cohesive soils. J. Soil Mech. Found Div. 89 (1), 115–143.

Lim, F., Gauld, S., 2003. Riser solutions for ultra-deep water developments. In: Proceedings of 10th Annual India Oil & Gas Symposium, Mumbai, India.

Maclure, D., Walters, D., 2007. Freestanding Risers in the Gulf of Mexico – a Unique Solution for Challenging Field Development Configurations. 2H Offshore Engr. Ltd.Technical Paper.

Nakhaee, A., Zhang, J., 2008. Effects of the interaction with the seafloor on the fatigue life of a SCR. In: Int. Offshore and Polar Engr. Conf. Vancouver, BC, Canada, pp. 87–93.

Palmgren, A., 1924. Die Lebensdaur von Kugellagern (Life Length of Roller Bearings. In German). Z. Des. Vereines Dtsch. Ingenieure 68 (14), 339–341.

Pesce, C.P., Aranha, J.A.P., Martins, C.A., 1998. The soil rigidity effect in the touchdown boundary-layer of a catenary riser: static problem. In: Eighth Int. Offshore and Polar Engr. Conf., Montreal, Canada, pp. 207–213.

Phifer, E.H., Frans Kopp, Swanson, R.C., Allen, D.W., Langner, C.G., 1994. Design and installation of auger steel catenary risers. In: Offshore Technol. Conf. (OTC7620), Houston, Texas, USA, pp. 399–408.

Randolph, M.F., Quiggin, P., 2009. Non-linear hysteretic seabed model for catenary pipeline contact. In: 28th Int. Conf. On Ocean, Offshore and Arctic Engr. (OMAE 2009), Honolulu, Hawaii, USA.

Randolph, M.F., Baht, S., Jain, S., Mekha, B., 2013. Modeling the touchdown zone trench and its impact on fatigue life, Offshore Technol. Conf. (OTC23975), Houston, Texas, USA.

Shiri, H., 2014. Response of a steel catenary riser on hysteretic non-linear seabed. J. Of Appl. Ocean Research, Elsevier 44, 20–28.

Shiri, H., Hashemi, H., 2012. Simplified approximation of peak fatigue damage in touchdown area of steel catenary risers based on seabed soil rigidity. In: 22nd Int. Offshore Ocean and Polar Engr. Conf. Exhibition, Rhodes, Greece, pp. 287–294.

Shiri, H., Randolph, M., 2010. Influence of seabed response on fatigue performance of steel catenary risers in touch don area. In: 29th Int. Conf. On Ocean, Offshore and Arctic Engr., Shanghai.

Theti, R., Moros, T., 2001. Soil interaction effects on simple-catenary riser response. Pipes Pipelines Int. 46 (3), 15–24.

Zargar, E., Kimiaei, M., 2015. An investigation of existing nonlinear seabed models for riser-fluid-soil interaction studies in steel catenary risers. In: Proceedings of 3rd Int. Symposium on Frontiers in Offshore Geotechnics, Oslo, Norway, pp. 489–494.

Chapter 10

Performance of non-linear seabed interaction models for steel catenary risers, part II: global response

Xiaoyu Dong[1] and Hodjat Shiri[2]

1: Department of Civil

Engineering, Memorial University of Newfoundland

e-mail: xiaoyu.dong@mun.ca

2: Department of Civil

Engineering, Memorial University of Newfoundland

e-mail: hshiri@mun.ca

This chapter is a journal paper which has been published in Applied Ocean Research (2019), Vol. 82, pp. 158-174, ISSN 0141-1187.

.

Abstract

Fatigue response of steel catenary risers (SCR) in the touchdown zone (TDZ) is significantly affected by riser-seabed interaction. Non-linear hysteretic riser-seabed interaction models have been recently developed to simulate the SCR cyclic embedment into the seabed. Despite the advancements achieved in the prediction of non-linear hysteretic riser-seabed interaction, several inconsistencies have been recently identified in the performance of some of the popular models. These limitations need to be resolved by proposing new models or improving the existing models on the global performance of the riser. In this chapter, the influence of nodal inconsistencies observed in a popular riser-seabed interaction model on the global performance of the riser was comprehensively examined in the TDZ. The riser embedment profile, cyclic contact stress, contact stress envelop, mean shear force, cyclic bending moment, and consequently the cumulative fatigue damage was investigated. The study showed that the soil model overestimates the riser embedment and other global responses. Recommendations were made to overcome the identified shortcomings of the existing models in the future developments.

Keywords: Steel catenary risers, Non-linear seabed interaction, Numerical modeling, Stress profiles, Fatigue Life

10.1. Introduction

Steel catenary risers (SCRs) are popular amongst the riser families because of their low cost and technical advantages such as their applicability in a wider range of sizes and water depths (Maclure and Walters, 2007). Fatigue performance is a key issue in SCR design since they are continuously subjected to cyclic perturbations under environmental and operational loads. However, the fatigue life estimation in the touchdown zone (TDZ) is one of the most challenging issues in the SCR design, because of complicated riser-seabed interaction.

Subsea surveys have identified the formation of a several diameter deep trench underneath the riser during the early stages of the operation life (Bridge and Howells, 2007). This process involves several mechanisms but mainly including the cyclic soil stiffness degradation and mobilization of suction force within the uplift motions of the riser. Advanced non-linear hysteretic seabed models have been developed within recent years, enabling the automatic simulation of cyclic seabed soil softening in the TDZ. Zargar and Kimiaei (2015) conducted a comparative study of the models proposed by Aubeny and Biscontin (2009), and Randolph and Quiggin (2009) (called the R-Q model from now on) that are probably the most popular models in the literature. The authors identified that the R-Q model which is a built-in interface in Orcaflex software and consists of a series of attractive features, is as an appropriate base for future developments (Zargar and Kimiaei, 2015). The model has been used in several numerical studies since its first publishing in 2009 (Zargar and Kimiaei, 2015; Shiri and Randolph, 2010; Shiri, 2014; Randolph et al., 2013; Liu et al., 2016). Recently, Dong and Shiri (2018) conducted a study investigating the consistency of the nodal force-displacement performance of the R-Q model through

various seabed conditions. The authors identified the limitations and some malfunctioning in the nodal force-displacement response of the model (shortly called nodal response) that can affect the global performance of SCR and need to be resolved in future developments. In this study, the influence of nodal inconsistencies and malfunctioning reported by Dong and Shiri (2018) on the global structural response of the SCR was comprehensively investigated through an innovative numerical methodology. Several key outputs were examined as indexes of global riser performance, such as riser embedment profile, cyclic contact stress, contact stress envelope, mean shear force, cyclic bending stress, and accumulated fatigue damage.

The study shows that the R-Q riser-seabed interaction model overestimates the SCR embedment into the seabed and other global responses because of the incapability in the explicit modeling of trench formation. This over-estimation process was found to be more significant in deep trenches created by unusual extreme values of R-Q model parameters (i.e., the methodology proposed by Shiri and Randolph(2010)). The current study revealed the necessity and the areas of future developments that would have a significant influence on safety, integrity, and the cost- effectiveness of steel catenary risers as an important element of deep offshore field developments.

10.2. Modelling riser-seabed interaction in the literature

To model the riser-seabed interaction, two main approaches have been undertaken to date, (1) constitutive soil models and (2) discrete beam-spring models. The constitutive soil models implemented into continuum finite element analysis (e.g., Clukey et al., 2008) often result in higher accuracy. However, this approach usually suffers from high computational

costs and becomes less attractive for industrial applications. In a beam-spring approach, the soil response is modelled by springs. This approach considerably reduces the computational effort but sacrifices some aspects of real soil such as dilatation and creep. However, this loss of accuracy can be significantly mitigated by the proper adjustment of the soil stiffness parameters and a good agreement with experimental data and continuum models can be obtained. The simplicity and reasonably acceptable accuracy of this approach along with the complexity of the riser-seabed interaction and the need for simultaneous modeling of vessel excitation, riser dynamics and non-linear seabed response within fatigue analyses have caused the industry to show more interest in a beam-spring modeling strategy.

Various design standards have traditionally proposed linear soil springs in the TDZ for SCR design. However, after the first experience of SCR technology in the Auger field (the Gulf of Mexico, Phifer et al., 1994), the STRIDE and CARISIMA JIPs (1999–2001) revealed the complexity of the riser-seabed interaction and identified the need for more sophisticated models (Theti and Moros, 2001). Bridge et al. (2004) proposed a hyperbolic model to capture various non-linear aspects of soil behavior characteristics within the applicable displacement stages, including the initial penetration, uplift, suction mobilization, breakout and re-penetration. The model was developed based on the test data from the CARISIMA and STRIDE JIPs and also a wide range of full-scale harbor tests, laboratory model tests, and numerical simulations. The proposed hyperbolic model was based on the curve developed by Audibert et al. (1984) for sand. The general form of the model was also similar to the hyperbolic pipe-soil interaction curve developed by Hardin

and Drnevich (1972) that was originally proposed for clay soils by Kondner (1963). The model does not account for soil softening under load cycles, even though the soil behavior in this region is highly nonlinear. Jiao (2007) proposed a non-linear discrete soil model with two non-degrading and degrading schemes for different soil conditions. Aubeny and Biscontin (2009) proposed a model with four different equations to simulate soil response within load cycles. They used a backbone curve for intact soil response and an elastic rebound curve to model the uplift. The partial riser-soil separation within the uplift episode was modelled with a third curve until its complete detachment, and a reloading curve modelled the re-penetration in the disturbed soil. Subsidiary equations were proposed to model the local load cycles. The model was initially not able to predict comprehensive soil degradation, but was later resolved by Nakhaee and Zhang (2010).

Randolph and Quiggin (2009) proposed a nonlinear model to predict the hysteretic soil response to SCR up and down oscillations. The R-Q model was incorporated into OrcaFlex commercial software and currently is one of the most popular models (OrcaFlex Documentation, 2018). It was selected in this study to examine the global structural performance of the SCR. The model combines the hyperbolic and exponential functions within four main episodes of riser-seabed cyclic contact: initial penetration, uplift, separation, and re-penetration. Further details of this model will be discussed in an independent section, later in this chapter. Shiri and Randolph (2010) implemented this model into ABAQUS by developing user-defined elements to explore the SCR fatigue performance and automated trench generation mechanism. Shiri (2014) used the model to study the influence of trench creation on the fatigue performance of SCR in the TDZ. Zargar and Kimiaei (2015) conducted a comparative study to investigate the advantages

and disadvantages of the mathematical expressions proposed by Aubeny and Biscontin (2009) and Randolph and Quiggin (2009). Clucky et al. (2017) reviewed the state-of-the-art riser-seabed interaction and concluded that the performance of nonlinear hysteretic seabed models would have a significant influence on the prediction of SCR fatigue life. Dong and Shiri (2018) initiated a project to develop a new riser-seabed interaction model the limitations of the existing models. The authors investigated the nodal force-displacement response of the R-Q model and identified some shortcomings that can affect the SCR global performance. Further investigations are presented in this chapter to explore that how the global response of SCR is affected by the nodal limitations of the R-Q model. These studies listed above and the limitations of current models have prepared the ground for proposing a new model to resolve the existing drawbacks of the R-Q model.

10.2.1.R-Q soil model

The R-Q soil model proposed by Randolph and Quiggin (2009) has been coded in a UEL subroutine to model the seabed response to SCR cyclic motions in ABAQUS. The R-Q model provides a combined form of hyperbolic and exponential equations for modeling the soil stiffness within four main episodes of riser-seabed cyclic contact: initial penetration, uplift, separation and re-penetration (Figure 10-1).

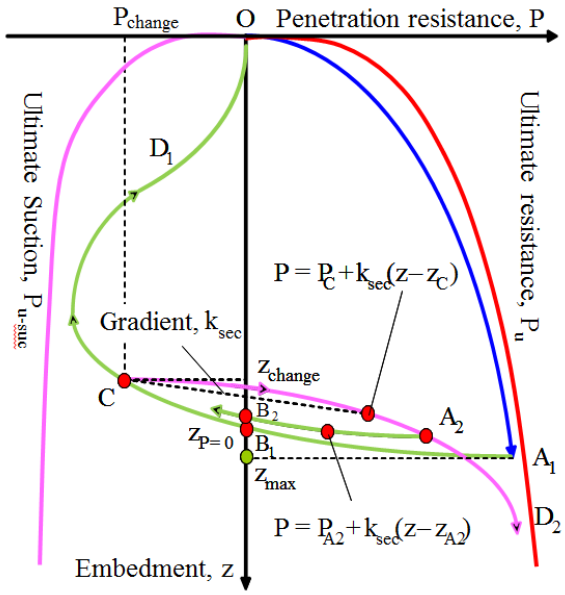

Figure 10-1. R-Q Soil model characteristics for different displacement modes.

The first episode in the model is "Initial Penetration" mode as shown by the blue line in Figure 10-1. With further penetration, the resistance asymptotically approaches the ultimate penetration resistance, P_u. By motion reversal, the model enters uplift mode and the reaction force decreases rapidly with a high initial secant stiffness. The model enters into the suction region with negative reaction force with further uplift. The suction resistance approaches the ultimate suction resistance (P_{usuc}) as a fraction of the ultimate penetration resistance controlled by parameter f_{suc}. The suction resistance is then completely decayed over a distance controlled by parameter λ_{suc}. Re-penetration after an entire break out follows an initially convex curve reflecting the soil softening beneath the riser during uplift. The re-penetration offset parameter (λ_{rep}) causes the re-penetration resistance to approach the ultimate penetration resistance at a penetration depth greater than the previous maximum penetration depth. Re-penetration may also occur when the suction resistance is

partially mobilized. In such a case, the suction resistance reduces rapidly and the model enters the positive reaction region. Further cycles of uplift and re-penetration would give further episodes of uplift and re-penetration modes and therefore give hysteresis loops of seabed resistance with incremental penetration at each cycle. The details of the R-Q model have been presented by Randolph and Quiggin (2009). However, a summary of the main equations is provided here to facilitate reading this chapter.

10.2.1.1. Ultimate resistance limits

The penetration and uplift resistances asymptotically approaching an ultimate resistance limit and corresponding ultimate suction limit are defined as below:

$$P_u(z) = N_c(z/D)s_u(z)D + f_b A_{disp}(\rho_{soil} - \rho_{sea})g \quad (10\text{-}1)$$

$$P_{u-suc}(z) = -f_{suc}P_u(z) \quad (10\text{-}2)$$

where

z is penetration depth

D is the outer diameter of the riser

F_b is the soil buoyancy factor

A_{disp} is the nominal area of the pipe below the seabed tangent plane

ρ_{soil} is the saturated density of the soil

ρ_{sea} is the seawater density at the seabed origin

g is the acceleration due to gravity

$P_u(z)$ is the ultimate penetration resistance at penetration z

f_{suc} is a model parameter giving the non-dimensional suction resistance ratio

$P_{u\text{-}suc}(z)$ is the ultimate suction resistance at penetration z

$N_c(z/D)$ is the soil bearing factor defined as (Aubeny et al., 2005; Randolph and White, 2008):

$$N_c\left(\frac{z}{D}\right) = a\left(\frac{z}{D}\right)^b \quad \text{for z / D} \geq 0.1 \tag{10-3}$$

$$N_c(z/D) = N_c(0.1)\sqrt{10z/D} \quad \text{for z / D} < 0.1 \tag{10-4}$$

Where a and b are non-dimensional penetration resistance parameters.

As for the undrained shear strength at depth z, $s_u(z)$ is idealised and calculated as:

$$s_u(z) = s_{um} + \rho z \tag{10-5}$$

where

s_{um} is the undrained shear strength at the mudline

ρ is the shear strength gradient with depth.

10.2.1.2. Initial penetration

For the initial penetration mode, the resistance is calculated by:

$$P(z) = H_{IP}(\zeta)P_u(z) \tag{10-6}$$

where

$$\zeta = z/(D/K_{max}) \tag{10-7}$$

ζ is the non-dimensional penetration in units of D/K_{max}

K_{max} is the normalised maximum stiffness parameter of the model.

10.2.1.3. Initial penetration

The penetration resistance for uplift mode is calculated as:

$$P(z) = P_0 - H_{UL}(\zeta_0 - \zeta)\big(P_0 - P_{u-suc}(z)\big) \tag{10-8}$$

where

ζ_0 is the non-dimensional penetration at which the latest episode of the current contact mode started and can be calculated as:

$$\zeta_0 = z_0/(D/K_{max}) \quad (10\text{-}9)$$

where

z_0 is the penetration z at which the latest episode of the current contact mode started.

The hyperbolic factor for uplift mode is given by:

$$H_{UL}(\zeta_0 - \zeta) = (\zeta_0 - \zeta)/[A_{UL}(z) + (\zeta_0 - \zeta)] \quad (10\text{-}10)$$

where

A_{UL} is the resistance ratio used within the hyperbolic factor to ensure correct initial stiffness on load reversal and can be calculated as:

$$A_{UL}(z) = \big(P_0 - P_{u-suc}(z)\big)/P_u(z_0) \quad (10\text{-}11)$$

The uplift resistance is limited to a negative lower bound $P_{min}(z)$ to indicate the limitation of the displacement inside which suction resistance can be sustained (Bridge et al., 2004). The adjusted uplift resistance is expressed as:

$$P_{min}(z) = E_{UL}(z)P_{u-suc}(z) \quad (10\text{-}12)$$

where

$E_{UL}(z)$ is an exponential factor limiting the uplift resistance and can be calculated as:

$$E_{UL}(z) = exp\left(Min\big(0, \big(z - z_{p=0}\big)/(\lambda_{suc}z_{max})\big)\right) \quad (10\text{-}13)$$

where

z_{max} is the maximum previous penetration depth for that point of the riser

$z_{p=0}$ is the largest penetration depth at which suction has started during any uplift

λ_{suc} is a model parameter representing a non-dimensional normalised suction decay resistance.

10.2.1.4. Re-penetration mode

The penetration resistance for re-penetration mode is calculated as:

$$P(z) = P_0 + H_{RP}(\zeta_0 - \zeta)(P_u(z) - P_0) \quad (10\text{-}14)$$

where

ζ_0 is the non-dimensional penetration at the start of this re-penetration

P_0 is the non-dimensional resistance at the start of this re-penetration

H_{RP} is the hyperbolic factor for penetration mode and can be calculated as:

$$H_{RP}(\zeta - \zeta_0) = (\zeta - \zeta_0)/[A_{RP}(z) + (\zeta - \zeta_0)] \quad (10\text{-}15)$$

where

$A_{RP}(z)$ is the resistance ratio used within the hyperbolic factor to ensure correct initial stiffness on load reversal and can be calculated as:

$$A_{RP}(z) = (P_u(z) - P_0)/P_{u^*} \quad (10\text{-}16)$$

where

$$P_{u^*} = P_u(z) \quad \text{if } P_0 \leq 0 \quad (10\text{-}17)$$

$$P_{u^*} = P_u(z^*) \quad \text{if } P_0 > 0 \quad (10\text{-}18)$$

where

$z^*$is the penetration when the preceding episode of uplift started.

The re-penetration resistance after a large uplift movement is reduced until the previous maximum penetration is approached (Bridge et al., 2004). This is achieved by restricting the re-penetration resistance below an upper bound $P_{max}(z)$ given by:

$$P_{max}(z) = E_{RP}(z)P_{IP}(z) \quad (10\text{-}19)$$

where

$E_{RP}(z)$ is an exponential factor limiting the uplift resistance and given by:

$$E_{RP}(z) = exp\left(Min\left(0, \left(z - z_{p=0}\right)/(\lambda_{suc} z_{max}) - \lambda_{rep}\right)\right) \quad (10\text{-}20)$$

where

z_{max} is the maximum previous penetration depth for that point of the riser

$z_{p=0}$ is the largest penetration depth at which suction has started during any uplift

λ_{suc} is a model parameter giving the non-dimensional normalised suction decay distance

λ_{rep} is a model parameter giving the non-dimensional re-penetration offset after uplift

10.3. Global Riser Model

The R-Q seabed model is a built-in module in the commercial software OrcaFlex. However, the software does not give access to all features of the model and this limits the possibility of an in-depth model examination. Therefore, in this chapter, a global SCR model developed by Shiri and Randolph (2010) was used in the AQUA module of ABAQUS with the R-Q model coded in a FORTRAN subroutine as a user-defined element (UEL). As schematically illustrated in Figure 10-2, the developed global model has a generic configuration connected to a Spar vessel. Series of springs are set representing the non-linear hysteretic response of the seabed using the R-Q model.

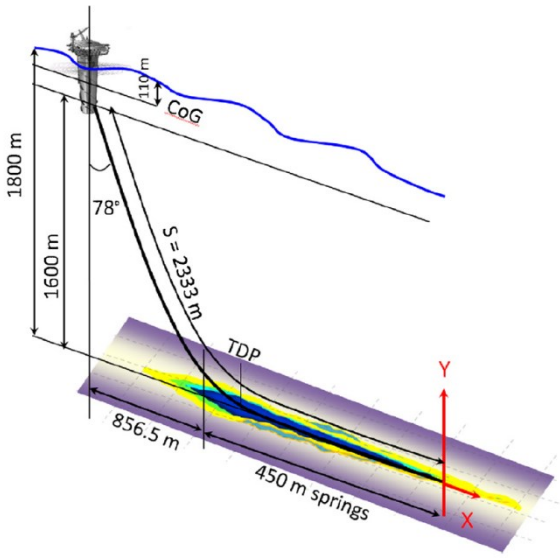

Figure 10-2. The global geometry of SCR modelled by ABAQUS.

The global riser dynamic under wave and vessel motion was obtained in time-domain, where the vessel motion was treated as a moving boundary problem, and the Morrison forces were calculated. The AQUA module of ABAQUS enabled to introduce Morison's loads for the riser immersed in seawater (ABAQUS/Standard User's Manual, 2017). Drag and inertia loads were considered as distributed loads along the length of the element (distributed drag loading was further divided into a component normal to the element's axis). Buoyancy loading was applied with a "closed-end" assumption, where the element's ends could support buoyancy loading normal to the element's cross-section. In a state-of-the-art riser analysis, the hydrodynamic coefficients need to be carefully chosen in order to achieve reasonable results. These coefficients are considered to be dependent on the Reynolds number, Keulegan-Carpenter (KC) number, and surface roughness according to experimental observations (Sumer, 2006). The hydrodynamic coefficients should be determined beforehand and are assumed to be unchanged during the entire simulation. In

this study, based on recommendations provided by DNV-RP-H103 (2011), and the other published works, the magnitudes of the drag (CD), inertia (CI), and added mass (CA) coefficients were taken as 0.7, 1.5, and 1.0 respectively.

The vessel perturbations under the wave action are modelled via coding a DISP subroutine in ABAQUS. The riser is modelled using element B21 from the ABAQUS element library (Timoshenko beam, shear flexible). These elements are commonly used for slender pipes assuming linear elastic transverse shear behavior. The length of beam elements in the catenary (1883 m) and seabed zone (450 m) is 5m and 1 m, respectively. The mechanical properties of the riser pipe are given in Table 10-1.

Table 10-1. Riser properties

Dimension	Value
Outer diameter, D_o	0.324 m (12¾ ")
Wall thickness, t	0.0205 m
Second moment of area, I	2.26×10^{-4} m^4
Steel Young's Modulus	2.07x1011 N/m^2
Steel density, ρ_s	7850 kg/m^3
In service submerged weight, m_s	100 kg/m
Fatigue S-N curve	DNV (2008), E Class weld, $a=1.05 \times 10^{-12}$, m=3.0, SCF=1.13

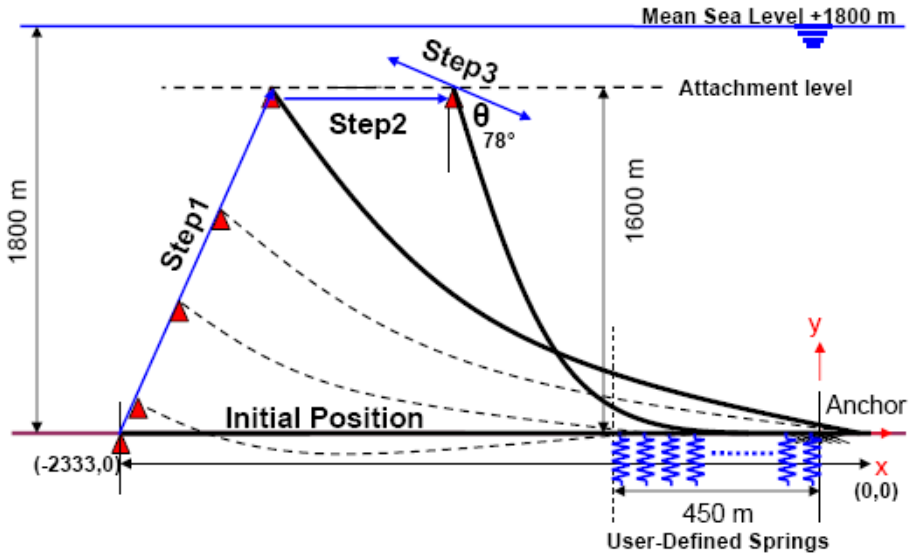

Figure 10-3. Schematic illustration of FE analysis steps.

The configuration and excitation of the SCR have been performed in three steps as schematically illustrated in Figure 10-3. The SCR was initially modelled as a straight pipe, laid on the seabed (no gravity applied yet). Partial supports were provided by seabed springs, with a simple support and a fixed support at the vessel and anchor end, respectively. Starting with Step 1, the submerged weight was applied on the riser and the vessel end was lifted up simultaneously to the height of the attachment point. The position of the vessel at this stage was selected to provide a complete SCR clear off the seabed. In Step 2, the vessel was transferred from its location at the end of Step 1 to the vessel's nominal position to achieve the targeted lay angle (78 °). While the vessel was translated to a nominal location, the SCR touched the seabed and springs were activated.

At the end of Step 2, the SCR reached its global configuration, developing full interaction with the seabed through the user-defined springs. In Step 3, the vessel was excited to simulate the wave action according to the predetermined wave sequence and RAO in a time

domain analysis. The position of the vessel was incrementally updated via DISP subroutine. A transformation matrix in the DISP subroutine was transferring the surge, heave and pitch of the vessel motions from its center of gravity (CoG) to the attachment point, causing the riser to be lifted up and lowered sequentially in the TDZ through the cycles of loading and unloading.

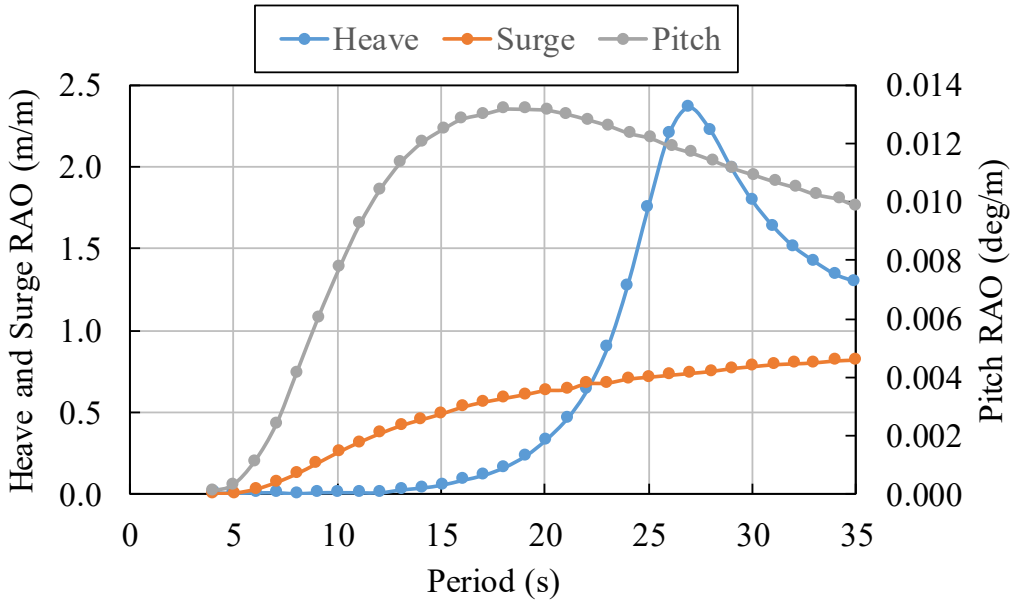

Figure 10-4. Generic Spar RAO. Head sea. Gulf of Mexico (Bridge et al., 2004).

To determine the RAOs of a particular vessel, usually, model tests or hydrodynamic analysis software are used, which was not part of the current research work. In this study, the vessel RAO was adopted from STRIDE JIP (Bridge et al., 2004) that has been used in several studies in the Gulf of Mexico (Bridge and Howells, 2007; Shiri and Randolph, 2010; Shiri, 2014; Bridge et al., 2004) (Figure 10-4). The displacement under a particular regular wave was determined by DISP subroutine using the following equation:

$$x = Ra\cos(\omega t - \varphi) \quad (10\text{-}21)$$

where

x is the vessel displacement (in length units for translations and degress for rotations)

R is the RAO amplitude

a is the wave amplitude (in length units)

ω is the frequency (in radian/second)

t is the time (in seconds)

φ is the RAO phase

The DISP subroutine was able to model the time domain motions of the vessel using a full wave scatter diagram, which was an essential capability for automative fatigue analysis. The wave scatter diagram used in this study contains a total number of 30 sea states and is a generic sample from the Gulf of Mexico. The resulting wave heights, periods and values for a 30-year design life are presented in Table 10-2. The number of applied waves was calculated based on the probabilities of occurrence, considering 30 years of service life for the SCR.

Table 10-2. Manipulated wave scatter diagram for a 30-year operational life (Gulf of Mexico).

Sea State ID	H_s (m)	T_z (s)	n applied	Sea State ID	H_s (m)	T_z(s)	n applied
1	0.5	4.2	18011291	16	8	9.1	3389
2	1	4.6	71370445	17	8.5	9.3	3011
3	1.5	5	48449608	18	9	9.5	1822
4	2	5.4	25187856	19	9.5	9.7	1395
5	2.5	5.8	13529335	20	10	9.9	1070
6	3	6.1	7473660	21	10.5	10.1	1246
7	3.5	6.5	3080495	22	11	10.2	566
8	4	6.9	1631014	23	11.5	10.4	928
9	4.5	7.3	583770	24	12	10.6	544
10	5	7.7	363725	25	12.5	10.7	813
11	5.5	8	114700	26	13	10.9	712
12	6	8.4	33676	27	13.5	11	877
13	6.5	8.5	16907	28	14	11.2	262
14	7	8.7	10864	29	14.5	11.3	343
15	7.5	8.9	5421	30	15	11.5	420

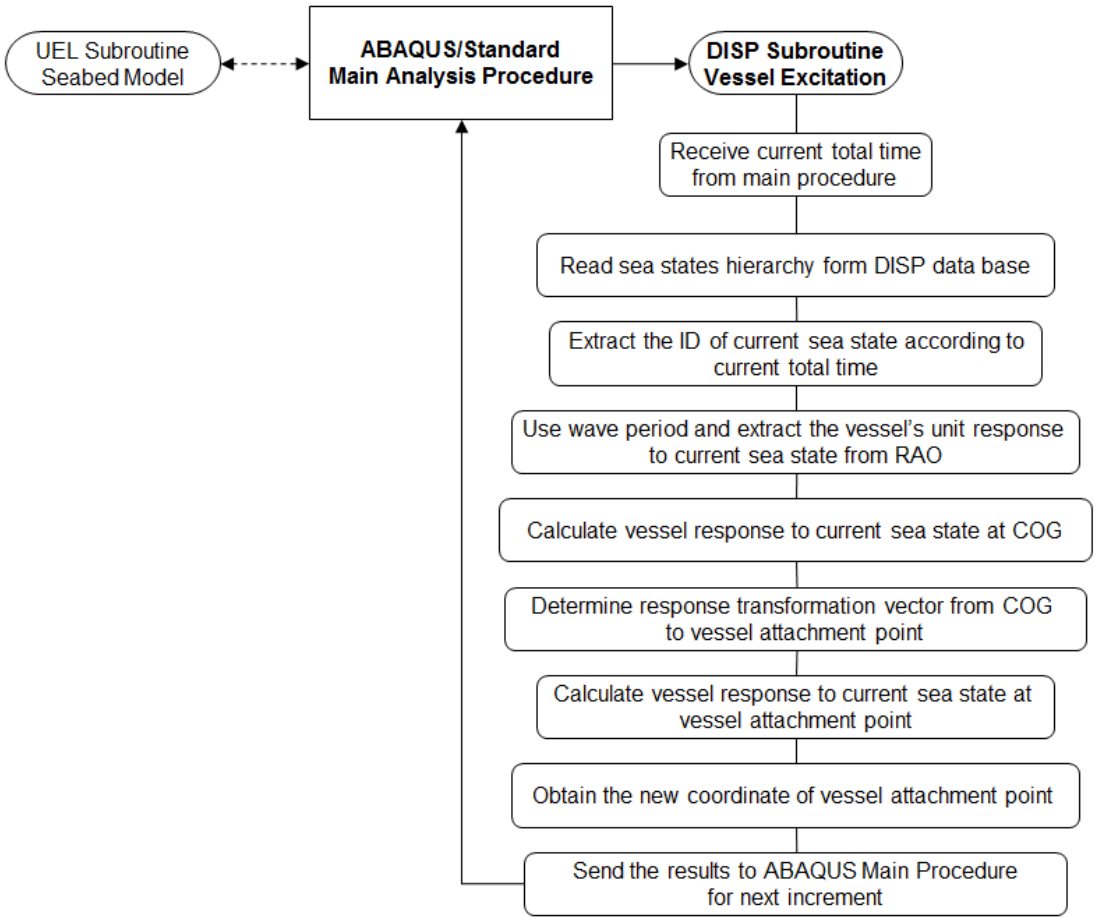

Figure 10-5. Internal flowchart of DISP subroutine for vessel excitation.

As shown in the vessel excitation flowchart (Figure 10-5), starting Step 3, ABAQUS calls the DISP subroutine and passes in the current analysis time step. The subroutine is then reading the hierarchy of sea states defined by the user. The current sea state is taken and a search is conducted inside the database to find the period, height and the number of cycles to be applied to the vessel. The period of the wave is then compared with RAO, and the unit response of the vessel to that specific sea state is extracted at the CoG. The transformation matrix obtains the corresponding response at the SCR attachment point. The response is then changed to the global coordinate system of ABAQUS and the new

coordinates of the vessel are outputted to the ABAQUS main procedure. This process continues according to the user-defined wave hierarchy until the end of Step 3.

10.4. Shortcomings in nodal performance of the R-Q soil model

The nodal performance of the R-Q soil model was comprehensively examined by Dong and Shiri (2018). The study was conducted by applying a sea state with a significant wave height of 16.5m and a period of 11 s by 10 cycles. Overall, the results showed that the R-Q soil model dominantly presented a consistent nodal performance. However, some limitations and malfunctioning were identified that are shortly summarized below:

- The model only simulated the riser profile in the TDZ, it did not update the seabed surficial profile, while the riser was cyclically penetrating into the seabed. In other words, the model did not simulate the trench creation explicitly.
- Since the trench was not modeled, the mobilized nodal suction force within the uplift motions was largely sustained until returning to the initial virgin seabed elevation. This caused a large suction force sustaining throughout a full penetration depth of the SCR, which is not realistic for fully developed trenches.
- The nodal force-displacement response was rapidly stabilized within only a few cycles (usually achieving a penetration depth of less than one diameter). This prevented the model from creating deep penetrations using the normal range of model parameters. To achieve deep embedment, as they occur in reality (several diameters deep), extreme values should be used as model parameters.
- In some occasions, minor motion reversal because of riser vibration or numerical instabilities caused a sudden jump in penetration or uplift forces, which was unexpected.

- The nodal force-displacement was violated in some nodes close to the touchdown point (TDP) when the magnitude of the surficial undrained shear strength was relatively high (about 1 kPa) and the penetration was very small. In these cases, the uplift force-displacement curve was violated in the surficial zone.

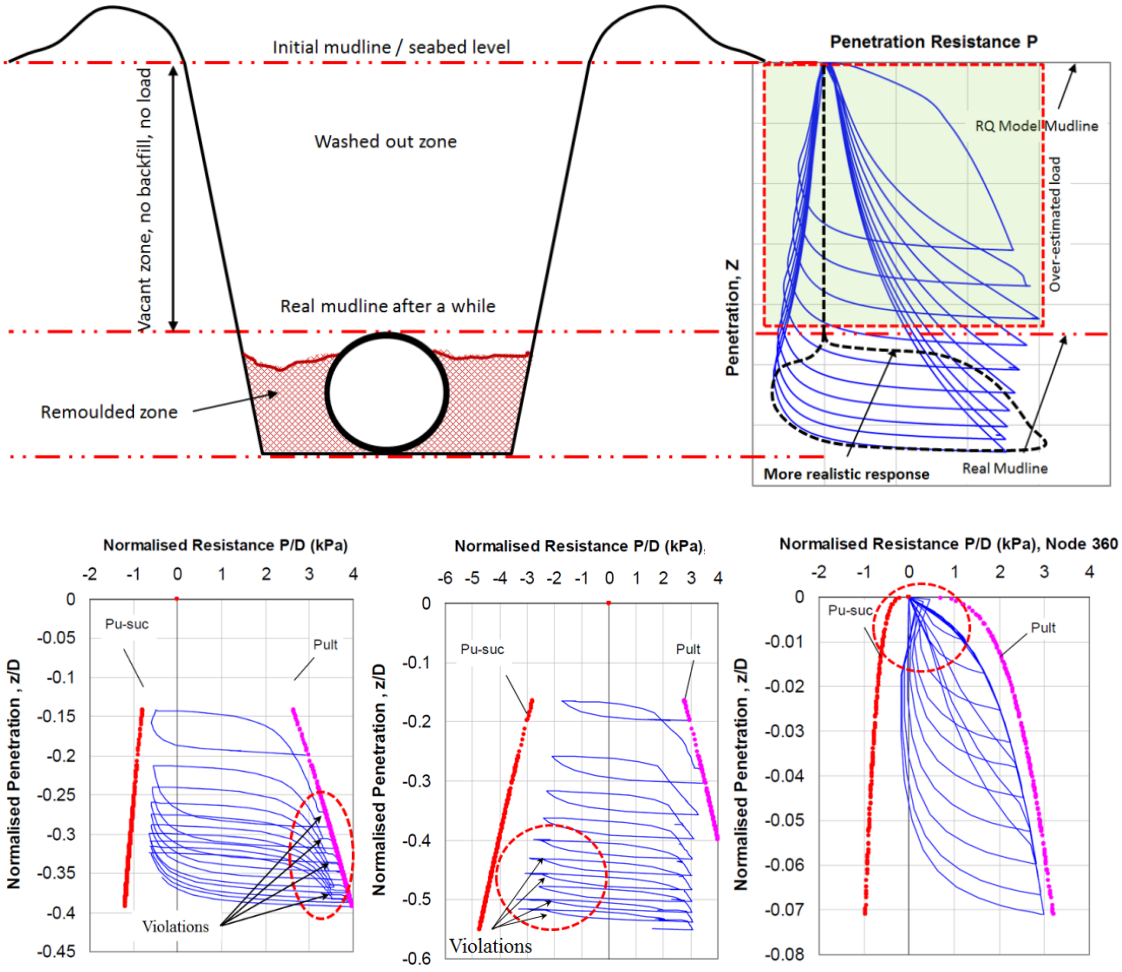

Figure 10-6. Sample of nodal malfunctioning in R-Q model (Dong and Shiri, 2018).

Figure 10-6 shows samples of nodal malfunctioning in the R-Q model. Detailed information can be found in Dong and Shiri (2018).

In addition to occasional nodal inconsistencies mentioned above, the R-Q model and other existing models do not simulate several mechanisms that exist in reality, such as rate dependency and consolidation effects, and also the seawater-soil-riser interaction effects that scours the trench by generating the water particles velocity fields These areas, particularly the contribution of fluid-soil-riser interaction to the soil stiffness degradation and trench creation, have not been well explored to date and should be considered in future developments.

10.5. Influence of nodal issues on global response of riser

As explained earlier, the R-Q model predicts the cyclic soil stiffness degradation in a single arbitrary node on the oscillating riser in the TDZ. Aside from the model parameters, the key input parameters that are used by the R-Q model to update the soil stiffness in every cycle of movement are included in the nodal displacement amplitude, the movement direction, and the movement history in a single node. These nodal responses are incrementally combined in a series of neighbour nodes throughout the SCR to result in a riser profile. A particular riser profile has its unique shear force, bending moment, contact pressure and fatigue damage distribution, which are called the global response in this chapter.

Any inconsistency in the nodal performance of the model is expected to impact the riser global performance to some extent. An accurate assessment of the impact of the aforementioned nodal inconsistencies of the R-Q model on the global performance of riser mandates having access to sufficient test results and the improved soil models that may

have resolved the existing issues, neither of which are available at the moment. The published experimental works have considered only a limited embedment of riser which is not necessarily equal to trench creation by several diameters deep. Also, there is still no new soil model in the literature that may have considerably improved the performance of the R-Q model. Therefore, in this chapter, an indirect but innovative approach has been undertaken to explore the influence of some of the nodal inconsistencies of the R-Q model on the global performance of the riser. This methodology still provides valuable insight into the global performance of SCR identifing the key areas for further developments, which is one of the main objectives of the current study.

An overview of the R-Q model limitations discussed by Dong and Shiri (2018) and summarized in the previous section suggests three distinct nodal inconsistencies (NI-1, 2 & 3) as follow:

• (NI-1) Sustaining the suction force within the full penetration depth of the riser using the common range of model parameters. This may also refer to the incapability in the explicit modeling of the trench.

• (NI-2) Premature stabilization of the cyclic embedment depth and need for virtual extreme values of the model parameters to create deep penetrations.

• (NI-3) Minor occasional malfunctioning in nodal force-displacement response.

The latter issue (NI-3) observed by Dong and Shiri (2018) may happen only in limited occasions (e.g., higher values of shear strength and very small penetrations), under specific conditions (e.g., minor motion reversal), and in a limited number of individual nodes (e.g., close to the TDP). Therefore, it can be reasonably assumed that for regular conditions, this kind of malfunctioning may have no or little impact on the global performance of the riser.

However, the influence of the first and second items was indirectly examined using different values of the key model parameters including the re-penetration offset parameter (λ_{rep}) and suction decay parameter (λ_{suc}), respectively. The rationale behind using the first parameter is well explained by Shiri and Randolph (2010), where a methodology was proposed for the creation of deep trenches using the unusual extreme values of λ_{rep} (e.g., 30 instead of 0.5). The advantage of using the second parameter for an indirect assessment can be better explained using Figure 10-7 as a comparative illustration of the influence of different values of suction decay parameter on the nodal force-displacement response.

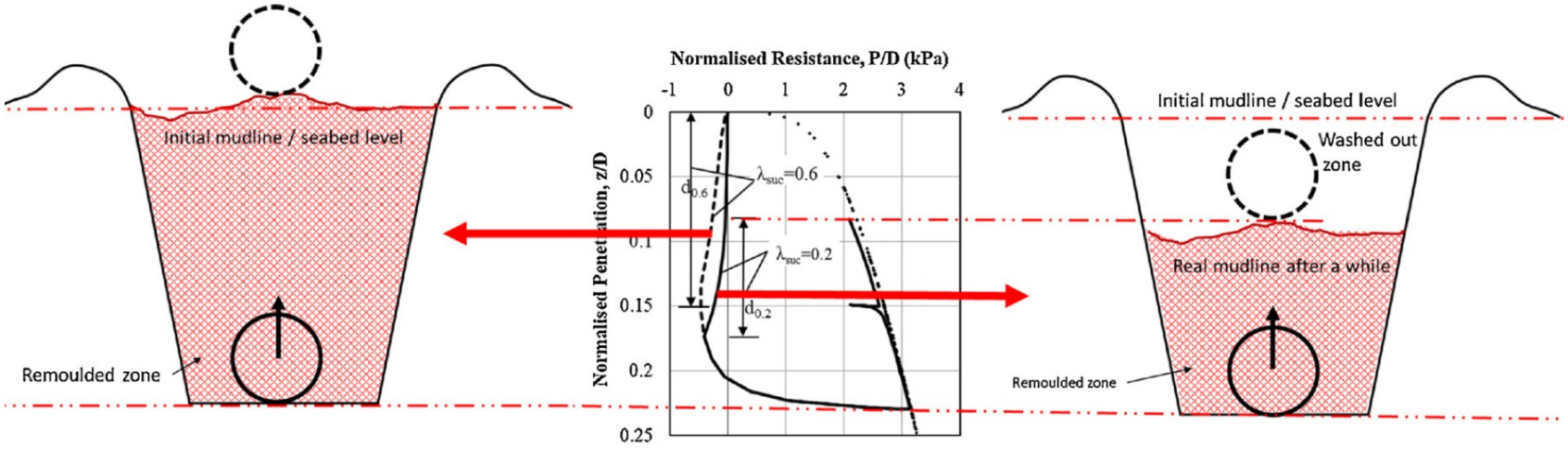

Figure 10-7. Using suction decay parameter to mimic a trench creation.

Figure 10-7 shows the force-displacement response of a given node with two different magnitudes of λ_{suc} (i.e., 0.6 and 0.2), where the suction decay has been separately shown by solid and dashed lines in the negative side of force axis. The recorded subsea surveys show that the soil inside the created trench is largely washed out within the full trench development process (Bridge and Howells, 2007). This causes the suction force underneath the riser to quickly decay within a short course of the uplift motion, while the R-Q model theoretically sustains the suction decay up to the virgin sea surface. The magnitude of suction is somehow controlled by the suction decay parameter, but the soil surface is not updated to a lower elevation inside the trench. The trends observed in Figure 10-7 shows that lower values of the suction decay parameter could be used to eliminate the washed out portion of the trench to some extent.

Therefore, taking advantage of using the model parameters in particular ranges to assess the impact of nodal inconsistencies on global performance, a comprehensive parametric study was performed through 21 different case studies summarized in Table 10-4. The series of simulations were conducted varying the R-Q soil model parameters, one at a time. The examined parameters were included in the key model parameters, i.e., suction ratio (f_{suc}), suction decay parameter (λ_{suc}), and re-penetration offset parameter (λ_{rep}). The influence of the seabed soil parameters, i.e., undrained shear strength at mudline (Sum), and shear strength gradient (ρ) was also examined to provide a wider insight into the problem. The unchanged model parameters, i.e., normalized maximum stiffness (K_{max}) and power law parameters (a, b), were set to default values given in Table 10-3. Considering the cyclic nature of the loads, the global response of the riser to the R-Q model was investigated through the production of a series of key outputs including the cyclic riser

penetration into the seabed, cyclic contact stress distribution, contact stress envelop, absolute and mean shear force, monotonic and cyclic bending moments, and consequently the accumulated fatigue damage. The overall parametric study map comprising of 21 different case studies is presented in Table 10-4.

Table 10-3. Default values of R-Q model parameters

Parameter	Symbol	Value
Mudline shear strength	s_{u0}	0.65 kPa
Shear strength gradient	ρ	1.5 kPa/m
Power law parameter	a	6
Power law parameter	b	0.25
Normalized maximum stiffness	K_{max}	200
Suction ratio	f_{suc}	0.3
Suction decay parameter	λ_{suc}	0.5
Repenetration parameter	λ_{rep}	0.5

Table 10-4. Parametric study map

Case study	Input soil model parameters					Case study	Input soil model parameters				
	s_{um}	ρ	f_{suc}	λ_{suc}	λ_{rep}		s_{um}	ρ	f_{suc}	λ_{suc}	λ_{rep}
CS-1	0.0	D	D	D	D	CS-13	D	D	D	0.0	D
CS-2	0.35	D	D	D	D	CS-14	D	D	D	0.2	D
CS-3	0.65	D	D	D	D	CS-15	D	D	D	0.5	D
CS-4	1.5	D	D	D	D	CS-16	D	D	D	1.0	D
CS-5	D	0.0	D	D	D	CS-17	D	D	D	D	0.0
CS-6	D	0.2	D	D	D	CS-18	D	D	D	D	0.2
CS-7	D	0.5	D	D	D	CS-19	D	D	D	D	0.5
CS-8	D	1.0	D	D	D	CS-20	D	D	D	D	0.8
CS-9	D	D	0.0	D	D	CS-21	D	D	D	D	1.0
CS-10	D	D	0.3	D	D						
CS-11	D	D	0.5	D	D	Note: D refers to “Default” values in Table 10-3.					
CS-12	D	D	1.0	D	D						

It is worth mentioning, for a deeper investigation, that the interaction between the model parameters should be properly incorporated. This, in turn, needs a comprehensive investigation of the dependencies between an extensive number of structural, environmental, and seabed parameters that may affect the global performance of SCR. A dimensionless group of parameters should be determined and verified against an extensive number of numerical tests (e.g., Queau et al., 2013). These kinds of studies can facilitate the interactive control of parameters and optimize the number of simulations in parametric and sensitivities studies. However, this aspect is beyond the scope of the current study and need to be carried out by independent research works. In the coming sections, the results of the conducted parametric study will be discussed in detail.

10.5.1.Riser Penetration into the Seabed

A key feature of the R-Q model is its prediction of the gradual embedment of the riser into the seabed. This is achieved by nodal simulation of the cyclic soil stiffness degradation and consequently the seabed soil softening under the oscillating riser. This nodal simulation results in varying the longitudinal riser profile in the TDZ that means altering the cyclic bending stress, and consequently the fatigue life. Therefore, the longitudinal riser profile is the theoretical connection point between the nodal performance of the R-Q model and the global response of SCR.

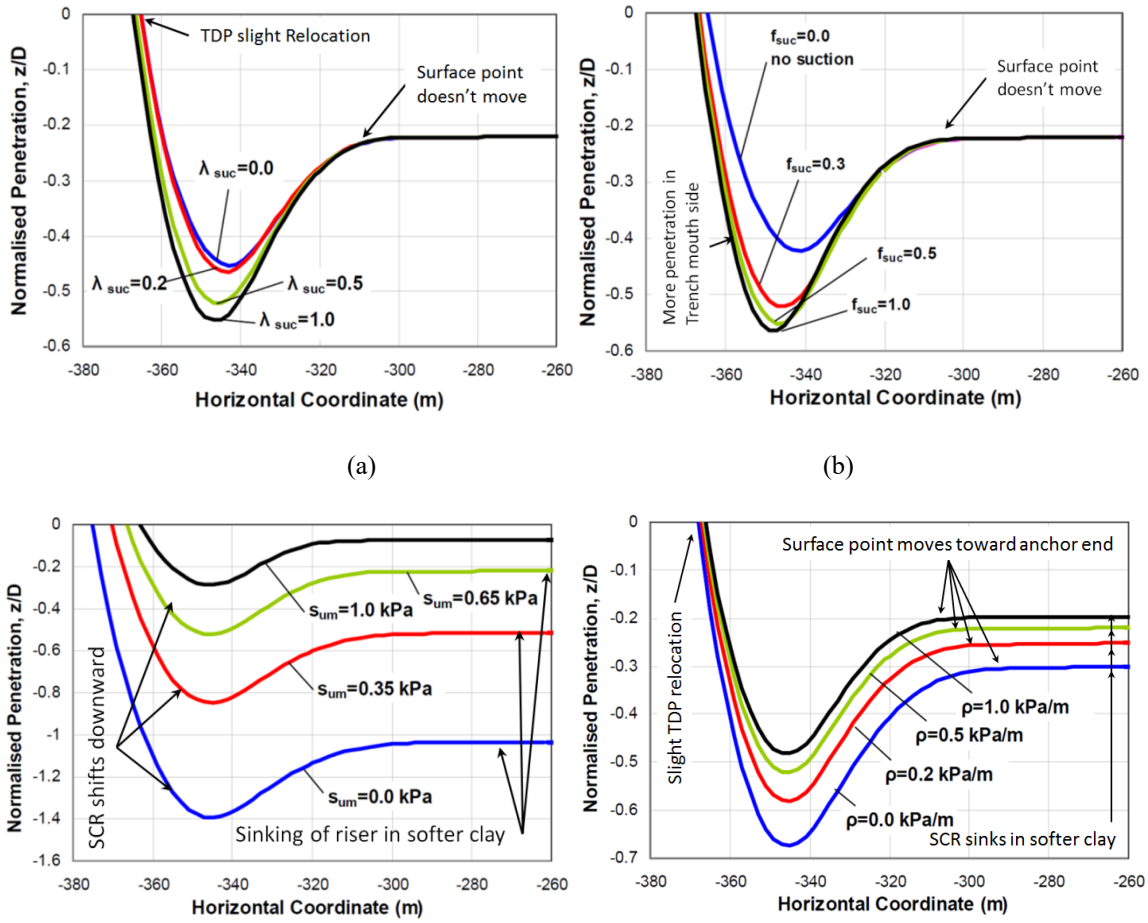

Figure 10-8. SCR embedment profile with different values of R-Q soil model parameters.

Figure 10-8 (a) shows the influence of the suction decay parameter (λ_{suc}) on SCR profile obtained by applying 10 perturbation cycles, where the vessel end of the riser and the TDP moved respectively by ± 5.13m and ± 3.8 m. It was observed that the higher values of λ_{suc} would result in a deeper embedment. Comparing Figure 10-8 (a) with the concept illustrated in Figure 10-7, it is indicated that if the R-Q model is improved to simulate the erosion of the natural in-fill inside the trench and limit the suction decay to a portion of the

embedment depth, then it will be like using a lower value of λ_{suc} and result in less embedment. This shows that the current version of the R-Q soil model overestimates the riser penetration.

The influence of suction ratio (f_{suc}) on SCR profile is shown in Figure 10-8 (b), where the higher values of f_{suc} result in a deeper embedment. A closer look at the difference between the suction decay trends illustrated in Figure 10-7 shows that lower values of λ_{suc} reduce the maximum mobilized suction force, even if the suction ratio does not change. This also confirms that the R-Q model overestimates the SCR penetration depth with a similar rationale explained above for the impact of suction decay parameter (λ_{suc}).

Although it is not directly related to the nodal response inconsistencies, assessing the influence of undrained shear strength can still provide valuable insight into the R-Q model performance. Figure 10-8 (c) and (d) show the effect of undrained shear strength intercept (Sum) and the shear strength gradient (ρ) on the SCR cyclic profile. As expected, a softer seabed causes deeper riser embedment. This shall not be considered as a significant contribution to the creation of deep trenches since this is only a downward shifting of the whole riser profile in the TDZ. In other words, if the pipeline end of the riser coincided for different values of soil strength, the maximum penetration would not be significant for lower ranges of undrained soil shear strength. However, combining the trends observed in the overestimation of embedment and the results presented in Figure 10-8 (c) and (d), it can be concluded that the essence of the R-Q model is that it makes the seabed soil softer than it is supposed to be.

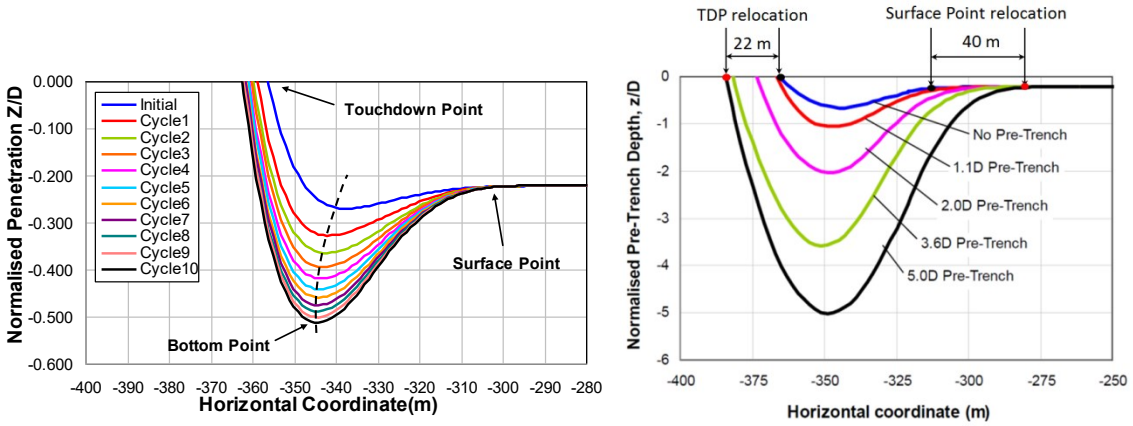

(a) (b)

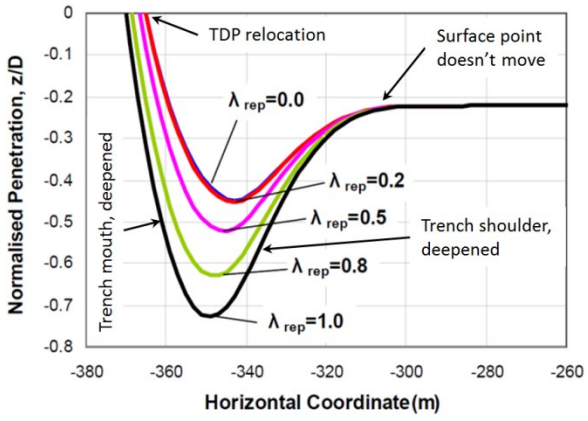

(c)

Figure 10-9. Penetration by normal and extreme values of λ_{rep} (1.5–3.0) (Randolph and Quiggin, 2009).

Figure 10-9 (c) illustrates the influence of the re-penetration offset parameter (λ_{rep}) on SCR embedment. Deeper riser embedment can be achieved by higher magnitudes of λ_{rep}. Shiri and Randolph (2010) took advantage of this parameter to suppress the premature stabilization of the R-Q model and created deep trenches using the extreme values of λ_{rep} (e.g., 3.0) (see Figure 10-9 (a) and (b)). Considering the discussed nodal inconsistencies

and having a closer look to the plots reported by the authors (Figure 10-9 (a) and (b)), it is shown that the results might not be accurate enough. First, the unrealistic suction force is significantly sustained in the created deep trench. Second, a closer look at Figure 10-9 (a) shows that the SCR profile in the TDZ comprises three key points that essentially define the trench geometry:

• TDP, where the SCR reaches the nominal level of the seabed;

• Trench bottom point (TBP), or maximum penetration point;

• Trench surface point (TSP), where the SCR reaches essentially zero gradients towards the anchored end of the riser.

As the penetration increases, the TDP and point of maximum penetration moves towards the suspended end, but the point where the SCR approaches the straight part resting on the seabed, referred to here as the 'surface point,' is less affected. However, the trenches obtained by Shiri and Randolph (2010) using extreme values of λ_{rep} (Figure 10-9 (b)) show large displacements of the surface point towards the anchor end (about 40 m) and the TDP towards the vessel end (about 22 m), which doesn't follow the same trend observed under pure wave frequency motions (Figure 10-9 (a)). It is considered as a significant artificial alteration of the SCR longitudinal profile. Therefore, the approach proposed by Shiri and Randolph (2010) overestimates the ratio of trench length to the depth and violates the overall trench profile affecting the global response of the riser, stress distribution and consequently the accumulated fatigue damage.

The study conducted by Shiri and Randolph (2010) showed that the manual insertion of a mathematical trench under the SCR could completely distort the fatigue results even through minor changes in the horizontal location of trench relative to the SCR. This was

the motivation behind proposing the methodology for the automative creation of deep trenches using extreme values for λ_{rep}. However, with the violation of trench length to depth ratio, i.e., the global longitudinal profile, the same interference may happen again in fatigue results. Therefore, the fatigue results obtained by the creation of trenches shown in Figure 10-9 (b) need to be further assessed using an improved soil model with resolved nodal inconsistencies.

In conclusion, the nodal inconsistency NI-1 causes an over-prediction of the cyclic riser penetration into the seabed as an index of the global riser response. The nodal inconsistency NI-2 necessitates using unusual extreme values of the R-Q model parameters for the creation of deep trenches. This, in turn, results in a significant violation of the riser profile, i.e., the global response in the TDZ.

It is worth mentioning that the riser profile can be translated as the riser-seabed contact pressure, which is the riser response to the seabed soil stiffness. The contact stress governs the shear force distribution throughout the pipeline end of the riser. A complex combination of the shear force gradient and the cyclic TDP oscillation amplitude produces the bending moment. Eventually, the cyclic oscillation of the bending stress accumulates the fatigue damage. Therefore, the nodal inconstancies observed in the R-Q model affects the global response of the riser through altering cyclic contact stress, mean shear force, cyclic bending moment, and consequently the fatigue damage. The influence of nodal inconsistencies on all of these aspects will be discussed in coming sections.

10.5.2.Cyclic contact stress

Contact stress is the absolute value of the difference between the maximum and minimum contact force per unit length, P, during the time history of the analysis, normalized by the

riser diameter. Therefore, the computed stresses can be regarded as the range of the cyclic contact stress variation during the contact cycles. As explained in the last section, this is a key index for assessing the global performance of the R-Q soil model affected by the identified nodal inconsistencies. Figure 10-10 shows the influence of the various R-Q model parameters on cyclic contact stress.

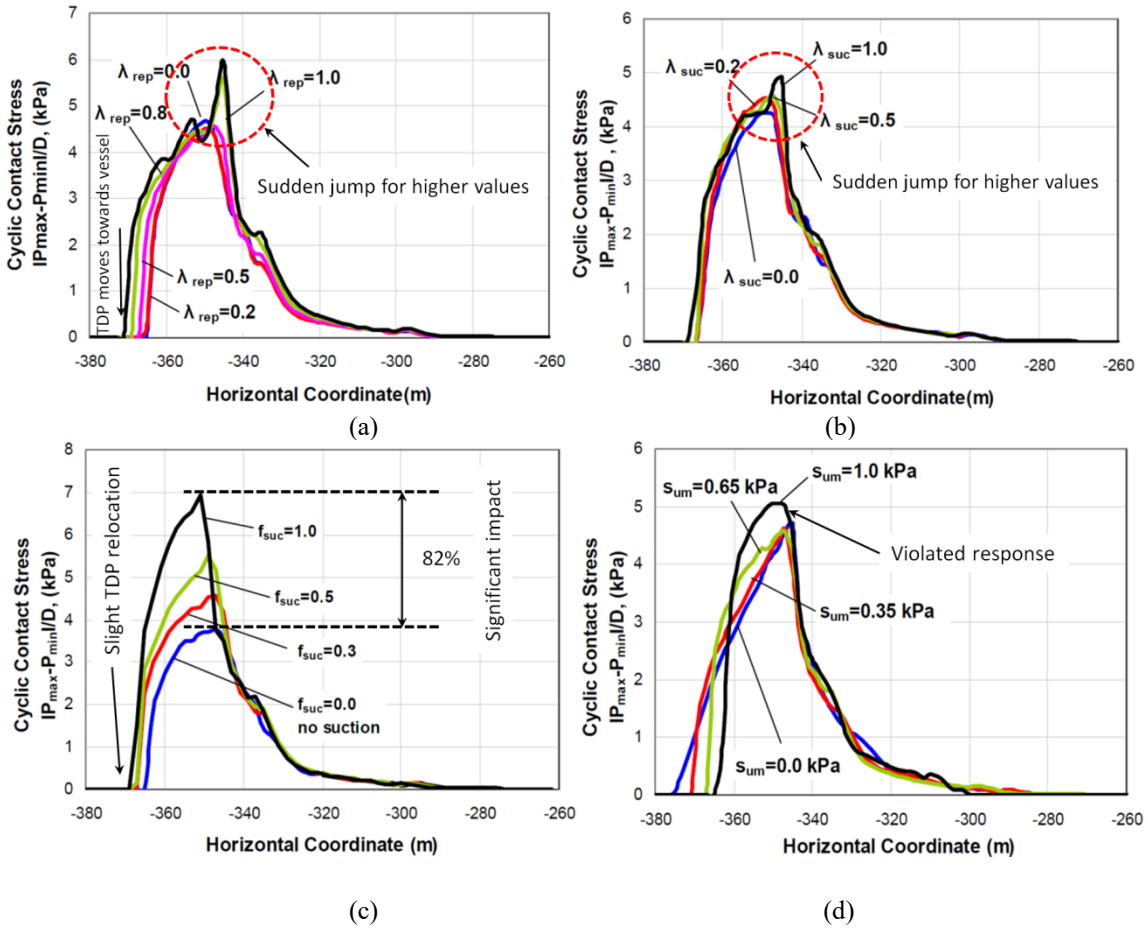

Figure 10-10. Cyclic contact stress profile with different values of R-Q soil model parameters.

The magnitude of cyclic contact stress is slightly increased using the higher values of λsuc (Figure 10-10 (a)). A sudden jump happens when the magnitude of λsuc approaches to one (λsuc = 1.0). Combining the observations about the R-Q model incapability in modeling

the washed out depth of the trench (Figure 10-7) and the results presented in Figure 10-10 (a) shows that the R-Q soil model slightly overestimates the cyclic contact stress. This overestimation can be significant if higher values of λsuc are selected as an input parameter. The suction ratio (f_{suc}) shows significant and sustaining influence on cyclic contact stress (Figure 10-10 (b)). The cyclic contact stress reaches its peak value in an area from maximum penetration depth to the TDP. This is the area with the highest cyclic load, where the SCR is repeatedly pushed into the seabed and then uplifted. The cyclic contact stress in the area between the maximum penetration depth and surface point (right side of the trench profile) is less affected by model parameters since the riser has the lowest fluctuations in this region. Recalling the effect of trench erosion on suction ratio shown in Figure 10-7, the influence of fsuc on cyclic contact stress also shows that the R-Q soil model overestimates the cyclic contact stress.

Figure 10-10 (c) and (d) shows that the soil shear strength parameters may slightly affect the peak value of cyclic contact stress, but two important points are observed in the results. First, the higher magnitude of mudline shear strength (S_{um}=1.0) violated the cyclic contact stress in Figure 10-10 (c). This can be the result of nodal malfunctioning for stiffer seabed soil addressed by Dong and Shiri (2018) and shown in Figure 10-6 (NI-3). Second, the initiation point of the cyclic contact stress in the vessel side is shifted towards the anchored end of the SCR, while the magnitude of mudline shear strength is increased. These trends show that the global response of the R-Q model affected by nodal inconsistencies may have a significant impact on the estimation of the fatigue prone zone of the SCR as well.

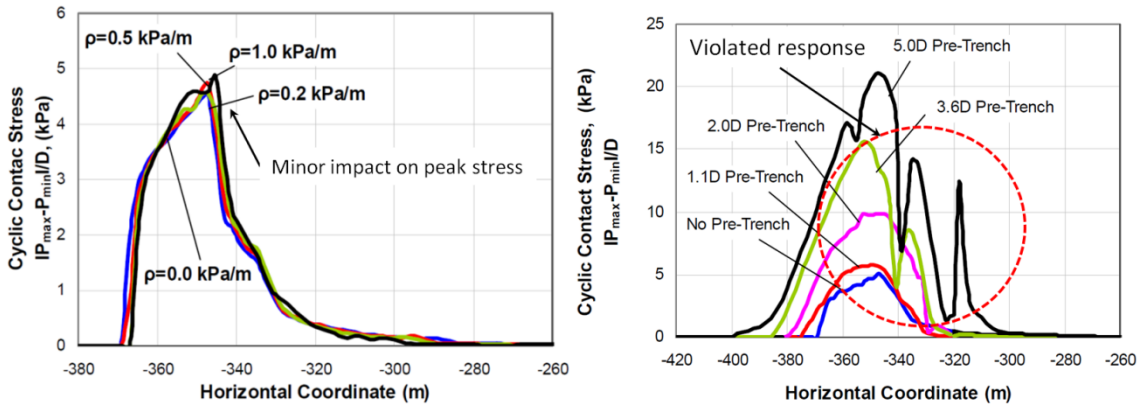

(a) (b)

Figure 10-11. Cyclic contact stress with different trench depths and extreme λ_{rep}.

The influence of re-penetration offset parameter (λ_{rep}) on cyclic contact stress is shown in Figure 10-11 (a). The higher values of λrep (> 0.5) result in a sudden jump by about 25% in cyclic contact stress, while nothing abnormal happens in penetration profile in Figure 10-8 (a). This can be more significant (105% in this case) if extreme values of λ_{rep} are used to create deep trenches as done by Shiri and Randolph (2010). Figure 10-11 (b) illustrates the cyclic shear stress obtained by Shiri and Randolph (2010) through the creation of deep trenches using extreme values for the R-Q model parameters. The peak magnitude of the contact stress has been dramatically increased, and the overall shape of the stress distribution has been significantly violated. Two more peaks are also observed between the trench bottom and surface point for the extreme value of re-penetration offset (λ_{rep} = 3.0), which is unusual. These results are in close agreement with the trends observed in the SCR embedment profile and show that using extreme values for automative creation of deep trenches may violate the cyclic contact stress as well and be less reliable (NI-2).

It is also worth referring to another interesting trend that was observed in these series of results. Despite λ_{rep}, the suction ratio parameter (f_{suc}) relocates the peak cyclic contact stress towards the vessel, while the TDP is relocated in the same direction for both parameters. It is well correlated with the results of the maximum penetration depth in Figure 10-8. This shows that the suction ratio has a more significant influence on the penetration profile and cyclic contact stress in the area of the trench mouth.

Overall, the nodal inconsistency NI-1 causes an over-prediction of the cyclic contact stress. The nodal inconsistency NI-2 and using unusual extreme values of the R-Q model parameters for creation of deep trenches may violate the cyclic contact stress. Also, the nodal inconsistency NI-3 may violate the contact stress distribution and consequently the global performance of the SCR.

10.5.3.Contact stress envelope

It would be beneficial to illustrate the contact stress in the form of the contact stress envelope to have another view from a different angle. The contact stress envelope represents the upper and lower bounds of contact stress over a series of load cycles. Figure 10-12 shows the influence of key model parameters on contact stress envelops.

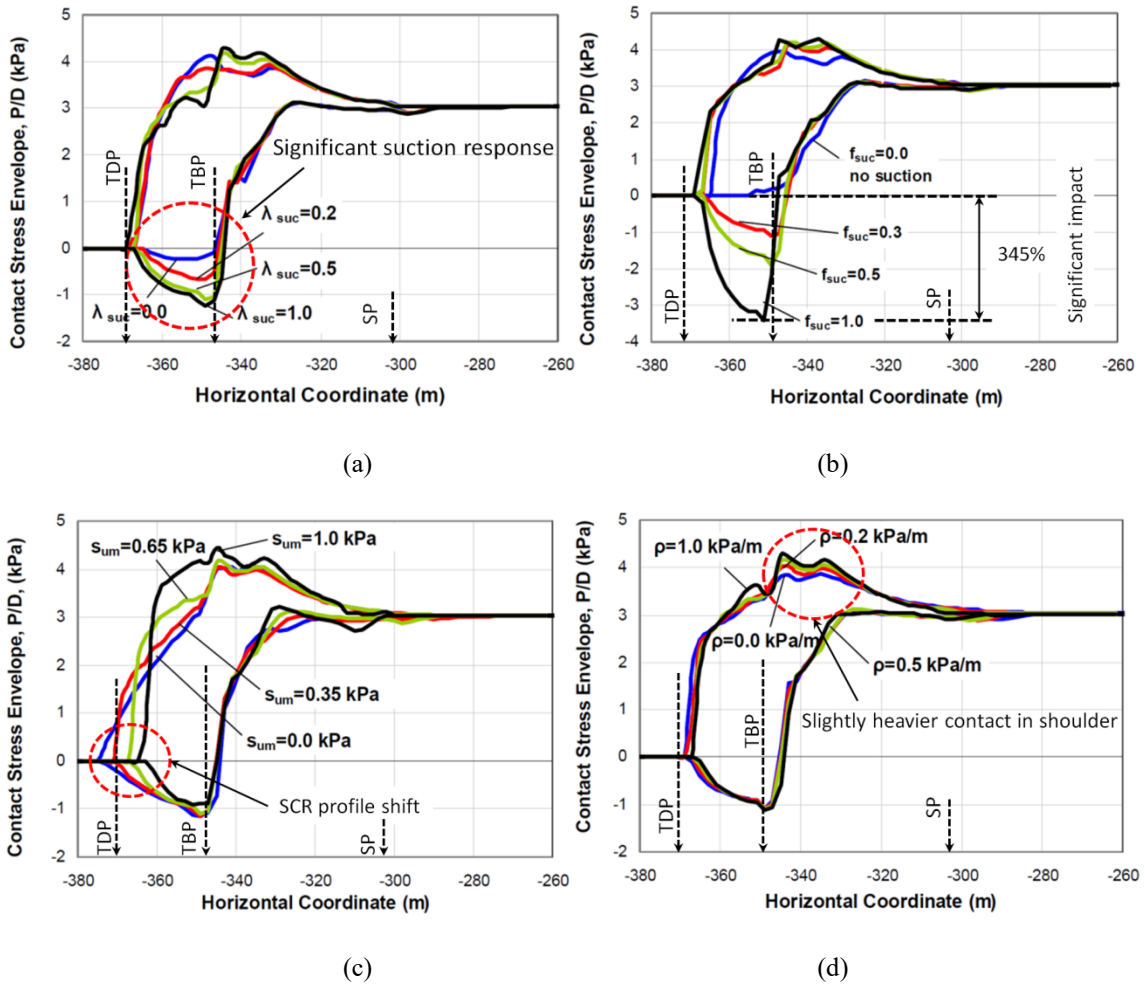

Figure 10-12. Contact stress envelop with different values of R-Q soil model parameters.

The trends agree exactly with the results presented for cyclic contact stress. The parameters jointly defining the suction force, i.e., λsuc and fsuc, have a significant impact on uplift contact stress (Figure 10-12 (a), (b)). It is more significant in suction ratio, where about a 60% increase in negative contact stress is achieved for the parameter value changing from 0.5 to 1.0 (Figure 10-12 (b)). There is only an increase 9% for the suction decay parameter (λ_{suc}) (Figure 10-12 (a)). The suction decay parameter was used in this chapter only for a qualitative assessment of the impact of nodal inconsistencies on global performance riser,

so it doesn't necessarily mean that an improved soil model would have the same level of influence on model performance as λ_{suc}. An overestimation by the R-Q soil model was also observed in the prediction of the contact stress envelope. The soil shear strength parameters also showed a similar impact on contact stress envelope (Figure 10-12 (c) and (d)). However, the variation of the contact stress in Figure 10-12 (c) is mainly caused by a large penetration of the pipeline end of the SCR into the seabed in lower values of Sum.

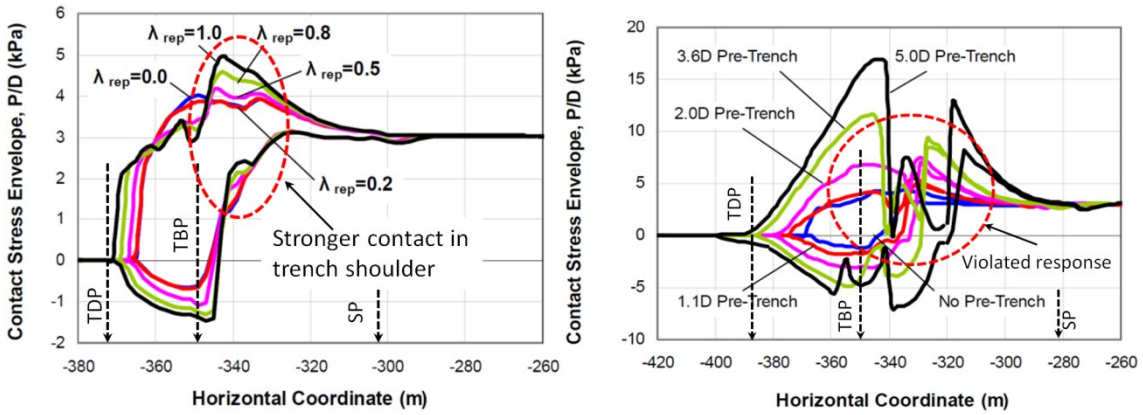

(a) (b)

Figure 10-13. Contact stress envelope with different trench depths and extreme λ_{rep}. ((b), Randolph and Quiggin (2009)).

Regarding re-penetration offset, the results presented in Figure 10-13 show that λrep has the same order of influence on penetration and uplift contact stresses, in the proximity of TDP. However, the trend is a complete reversal on different sides of the trench bottom point. The upper bound of penetration contact stress is increased towards the anchor end of the SCR, while it is decreased towards the vessel end. The lower bound penetration contact stress is also slightly increased on the anchor side of the trench bottom point. The

contact stress envelopes for different depth of trenches have been plotted in Figure 10-13 (Shiri and Randolph (2010)). The earlier distorted results caused by the extreme value of λ_{rep} are observed in the contact stress envelope as well. The upper bound contact stress for a trench with 3.6D and 5.0D depth (λ_{rep}=0.5) is zero in trench bottom point (x = -340 m), which is not seemed to be realistic. This shows that the unusual values of the R-Q model parameters (NI-2) may violate the stress profile. It was also observed that the lower bounds of the contact stresses in deep trenches have been dramatically increased compared to the cases with shallow embedment. This is too far from reality, where the remoulded soil inside the trench is washed out under different mechanisms, and the magnitude of the suction force is decreased over time. The results observed in the contact stress envelope are all in agreement with cyclic contact stress and shows the earlier observations of this study from a different angle.

10.5.4.Mean shear force

The influence of different model parameters on the distribution of mean shear force throughout the riser is shown in Figure 10-14.

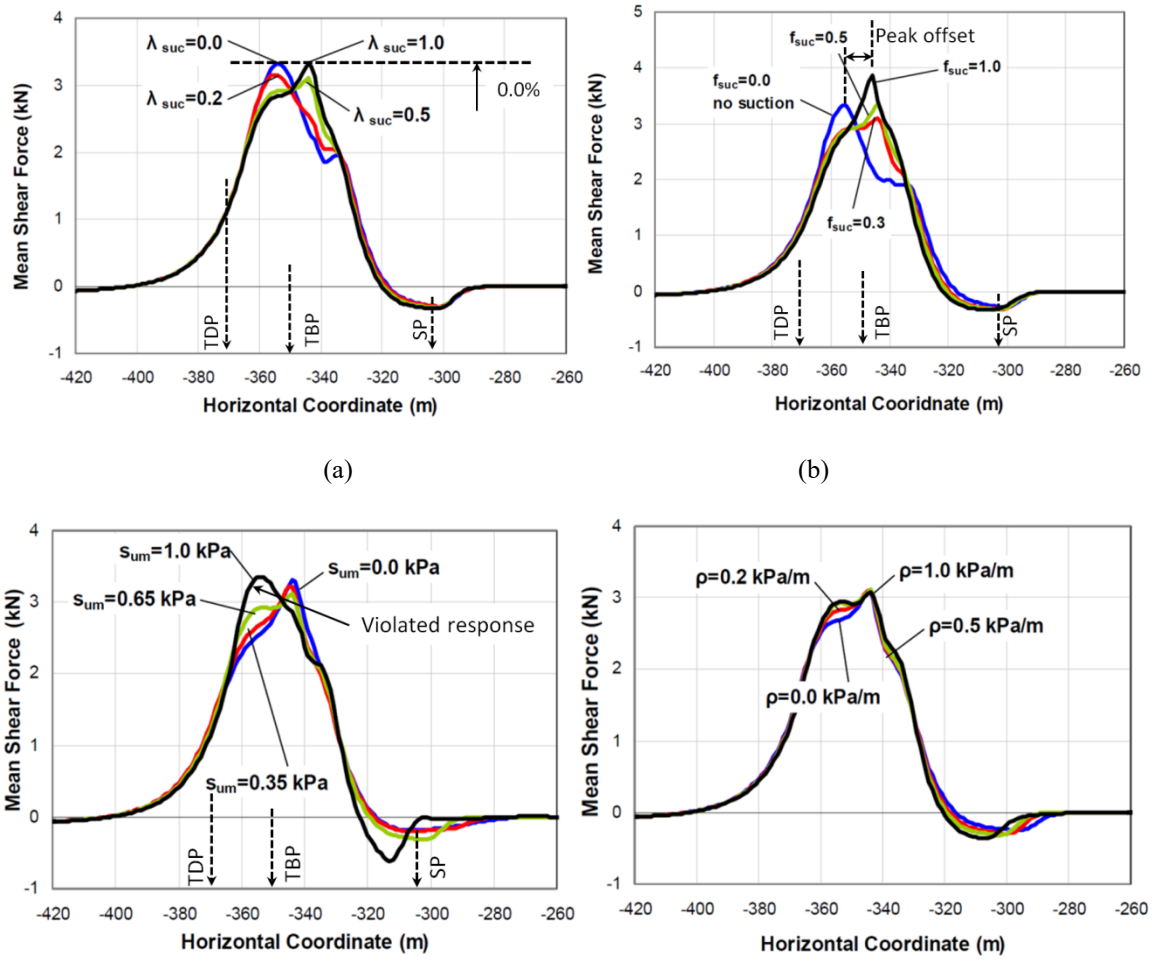

Figure 10-14. Mean shear force for different values of the R-Q soil model parameters.

Overall, the gradual embedment of SCR into the seabed causes the peak value of mean shear force to disappear in the vicinity of the TDP and a new peak to be created around the trench bottom point towards the anchor end of SCR. As shown in Figure 10-14 (a), higher values of suction decay parameter (λ_{suc}) result in the migration of the peak mean shear force towards the anchored end. Integrating this trend with the observations showed in Figure 10-7 shows that the R-Q soil model virtually shifts the peak shear force away from the vessel, which is an important aspect. Variation of λ_{suc} shows no impact on the peak

magnitude of the mean shear force (Figure 10-14 (a)). Higher values of the suction ratio (f_{suc}) increase the peak shear by about 15% (Figure 10-14 (b)).

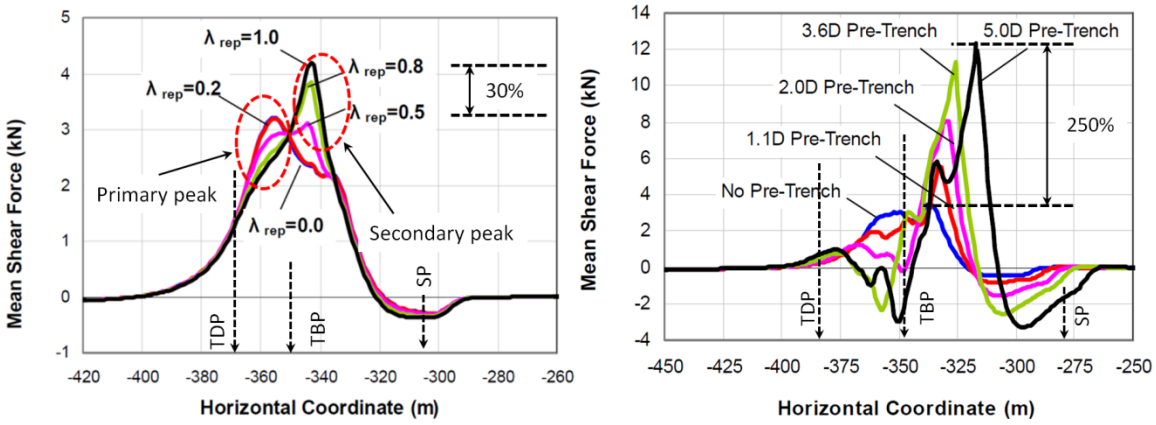

(a) (b, Randolph and Quiggin (2009))

Figure 10-15. Mean shear force for different trench depths and extreme λ_{rep}.

This increasing value is about 30% for the re-penetration offset parameter (λ_{rep}), which is quite significant (Figure 10-15 (a)). Increasing the magnitude of λ_{rep} has translated the peak point of mean shear force by about 13m towards the anchor end of the SCR. These relocations are about 11m for λ_{suc} and 10m for f_{suc}, which remain a considerable amount. A similar trend is observed for the impact of the soil strength parameters (S_{um}, and ρ). The results show that the R-Q model parameters can have a significant impact on the location of mean shear force. Figure 10-15 (b) shows how the extreme values of the re-penetration offset parameter used for the creation of deep trenches affect the distribution of mean shear force (Shiri and Randolph (2010)). Changing the parameter λ_{rep} from its default value (0.5) to 3.0 has caused the peak point of mean shear force to be increased by 357% and relocated by 50m towards the anchor end. The significant shifting of the peak shear towards the

anchored end caused by increased values of λ_{rep} shows that the results presented in Figure 10-15 (b) are less reliable and need to be re-investigated by improved soil models.

These series of results show that the nodal inconsistency NI-1 and NI-2 may virtually shift the peak stress points in the global response due to incapability in the explicit modeling of the trench. Shifting the peak stress point is currently one of the practical solutions for preventing fatigue accumulation in a single spot. In this method, the vessel mean position is changed from time to time to ensure the distribution of fatigue damage in a wider region of the TDZ instead of in a single spot. This shows that the nodal inconsistencies in the R-Q model may affect the global assessment of the peak fatigue point.

10.5.5.Cyclic bending moment

The cyclic bending moment is defined as the difference between the maximum and minimum bending moment in any given point on SCR within cycles of vessel excitation under wave action. This global response is perhaps the most important item directly contributing to cumulative fatigue damage. Figure 10-16 illustrates the results of the cyclic bending moment affected by various ranges of the R-Q model parameters. Increasing the suction decay parameter (λ_{suc}) from 0.2 to 1.0 has caused about a 13% rising of the peak cyclic bending moment with no shift in the location of peak point (Figure 10-16 (a)). Combining these results with the trends shown earlier in Figure 10-7 shows that the R-Q model may slightly overestimate the peak cyclic bending moment.

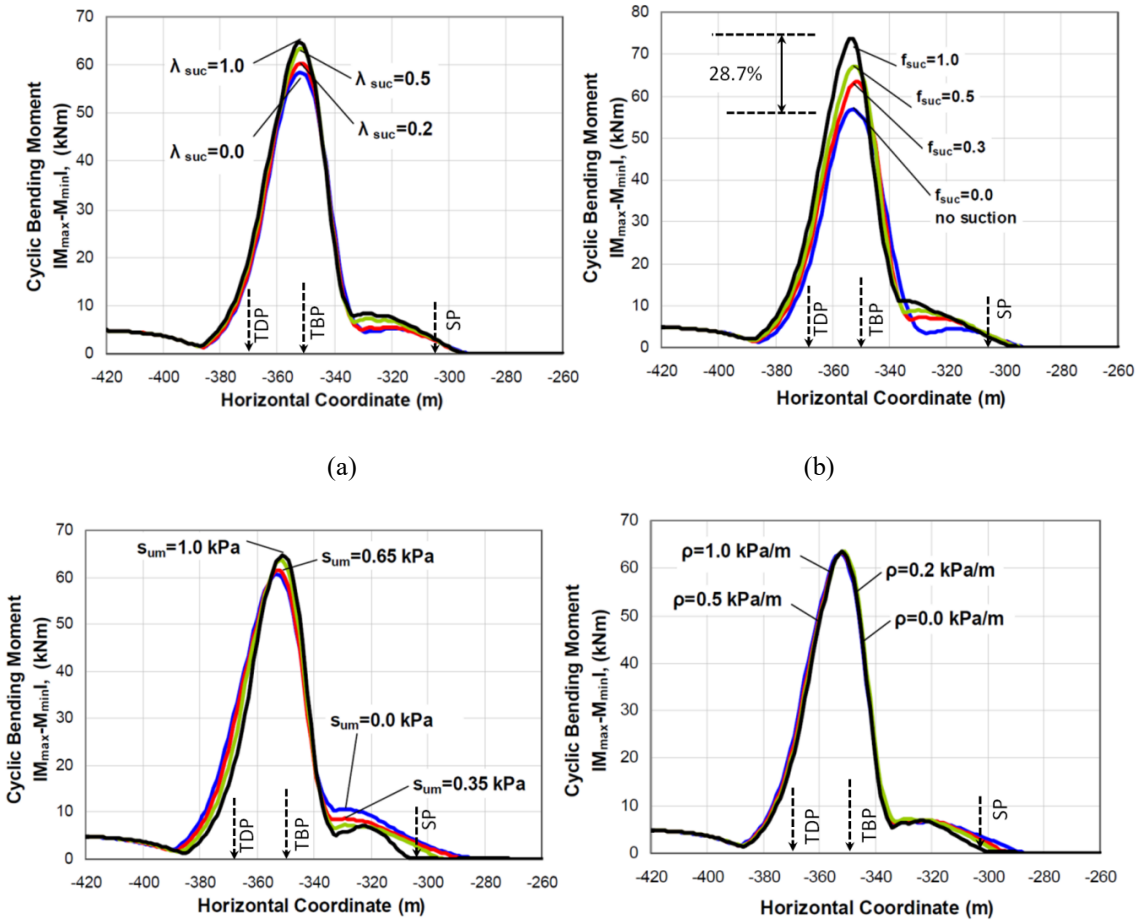

Figure 10-16. Cyclic bending moment for different values of R-Q soil model parameters.

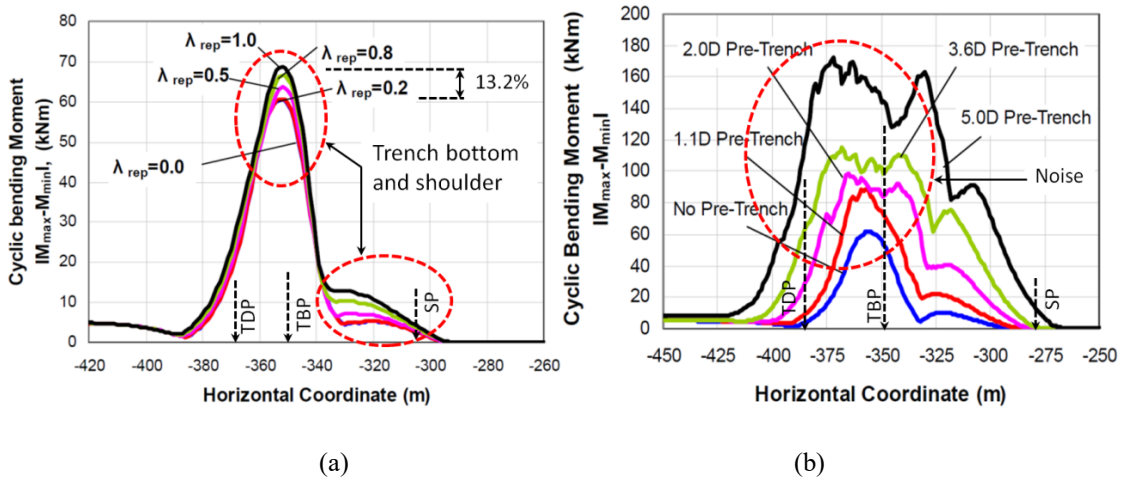

Figure 10-17. Cyclic bending moment for different trench depths and extreme λ_{rep}.

The suction ratio (f_{suc}) (Figure 10-16 (b)) and re-penetration offset parameter (λ_{rep}) (Figure 10-17 (a)) were found to have the most significant influence on the cyclic bending moment, where its peak value has been increased by 28.7% and 13.2% respectively for the highest values of these parameters (1.0). For default values of these parameters (f_{suc}=0.3, and λ_{rep} = 0.5), the peak value of cyclic bending moment has been increased by 9.6% and 5.0% respectively compared with the condition in which these parameters are zero. All of the parameters have a very slight influence on the relocation of the peak point. The slight relocation of the peak point in Figure 10-16 (c) caused by mudline undrained shear strength parameter is the result of the large penetration of the pipeline end into the seabed for low values of this parameter, which is considered to be a geometrical translation rather than the impact of the parameter itself. Figure 10-16 (d) shows that the gradient of undrained shear strength has no impact on a cyclic bending moment. The distribution of the cyclic bending moment for different trench depths that was created by using extreme values of re-penetration offset parameter (λ_{rep}) is plotted in Figure 10-17 (b) (Shiri and Randolph (2010)). Increasing the trench depth, fluctuations appear around the TDP, and the peak point almost disappeared. The maximum value of the cyclic bending moment in the 5.0D trench has been dramatically increased by 183% compared with no pre-trench condition. These fluctuations are getting back to the methodology used in the creation of the trench and seem to have no theoretical rationale (NI-2). Since the peak value of the cyclic bending moment is highly influential in the calculation of peak fatigue damage, the noisy results shown in Figure 10-17 (b) need accurate reassessment using improved soil models.

As a result, the nodal inconsistencies (NI-1&2) and the incapability of the R-Q soil model in the explicit modeling the trench creation and updating the elevation of mudline inside

the trench may cause the total stresses mobilized by penetration and suction forces to be overestimated.

10.5.6.Fatigue damage

The direct influence of the R-Q model parameters and the identified inconsistencies in fatigue response was examined through a methodology adopted from Shiri and Randolph (2010). Figure 10-18 shows the influence of different R-Q model parameters on cumulative fatigue damage in the TDZ. To simply concentrate only on the trend of the impact of the model parameters on fatigue damage, a single sea state (No. 30 from Table 10-2) has been applied to excite the vessel over 10 cycles. The resulting fatigue damage has been calculated by increasing the number of applicable waves over the SCR life to 10,000. Although this is unrealistically high (compared with the realistic 420 in Table 10-2), it brings the level of fatigue damage to a similar level as applying the full 30 sea states.

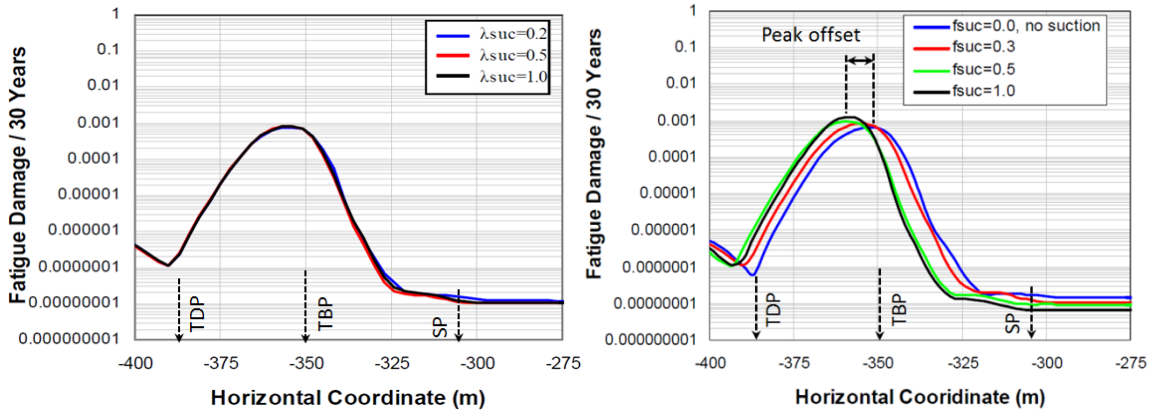

(a) (b)

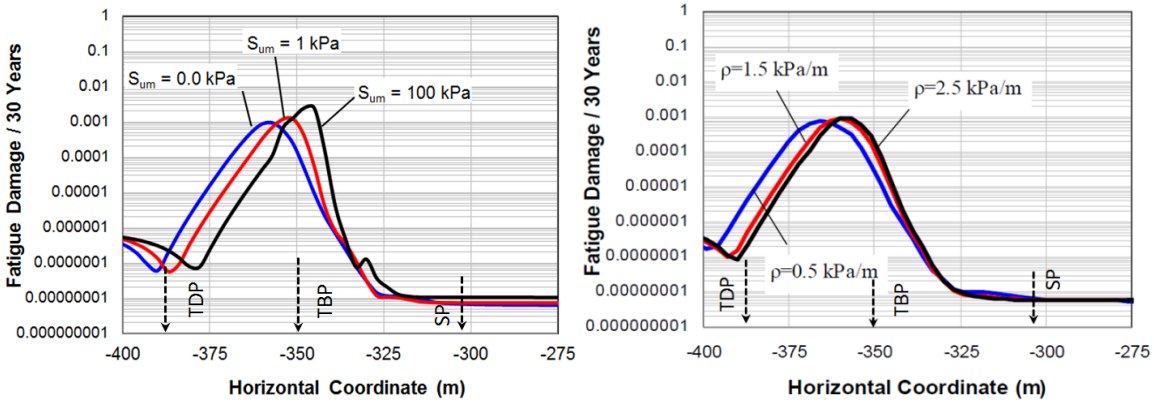

(c) (d)

Figure 10-18. Fatigue damage for different values of R-Q soil model parameters.

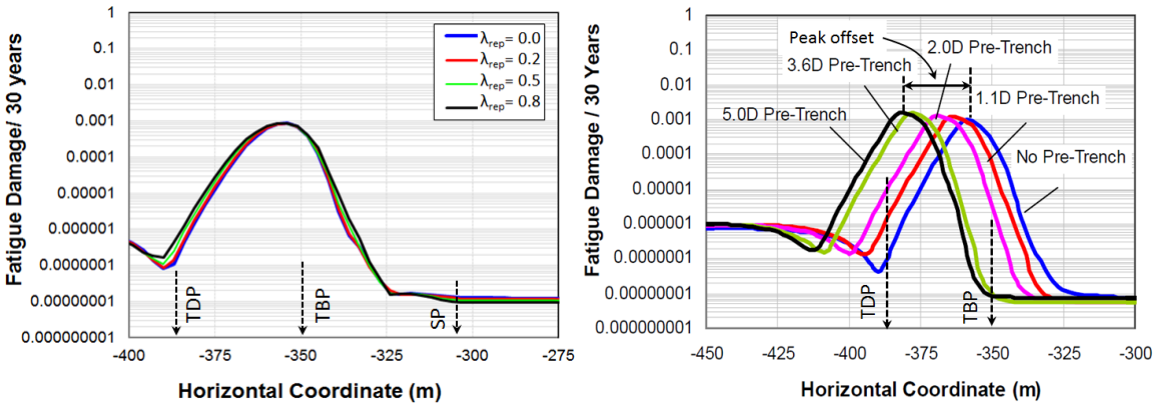

(a) (b)

Figure 10-19. Fatigue damage for different trench depths and extreme λ_{rep}.

The re-penetration offset and suction decay parameters (λ_{rep} and λ_{suc}) show almost no impact on fatigue damage in logarithmic scale (Figure 10-18 (a) and Figure 10-19 (a)). These two parameters both affect the magnitude of the dissipated energy in each load cycle, but do not affect the ultimate magnitude of the mobilized force. Since the fatigue is sensitive to the variation amplitude of the stress, but not the stress itself, these parameters show no impact on accumulated fatigue damage.

The suction ratio (f_{suc}) shows an increasing effect on fatigue damage migrating the peak fatigue damage towards the vessel for higher values of the parameter (Figure 10-18 (b)). Overall, the integrated suction force mobilization defined by its parameters in the R-Q model has a significant contribution to fatigue and the relocation of its peak point. In reality, the soil particles inside the trench are scoured and the suction force is gradually decreased over the SCR life. Therefore, the nodal inconsistency NI-1 causes the R-Q model to overestimate the global fatigue damage. It is recommended to use lower values of suction parameters in the current version of the R-Q model to reduce this effect and to better simulate the seabed condition.

The undrained shear strength at mudline (S_{um}) and its gradient (ρ) both are causing the peak fatigue damage to increase and shift towards the anchor end (Figure 10-18 (c) and (d)). Figure 10-19 (b) shows the influence of trench creation on fatigue damage using the methodology proposed by Shiri and Randolph (2010), where extreme values of re-penetration offset parameter (λ_{rep} is 1.5–3.0) are used to push the SCR down the seabed artificially. The peak value of fatigue damage shows a slight increase in the logarithmic scale, but the peak point is dramatically shifted towards the vessel. Recalling the discussion

on the influence of the extreme model parameters on the riser profile in Fig. 9(b), the migration of a peak fatigue point shown in Figure 10-19 (b) would not be reliable and would need deeper investigation using improved soil models. This shows that the nodal inconsistency NI-2 may violate the global response of the riser in terms of the ultimate fatigue damage and its peak point location.

10.6. Conclusions

It is generally accepted that the non-linear hysteretic seabed models can have a significant impact on the prediction of SCR fatigue life in the TDZ (e.g., Clukey et al., 2017). There are a few riser-seabed interaction models in the literature, but the model proposed by Randolph and Quiggin (2009) (the R-Q model) is one of the most popularly used models, as evidenced by its incorporation into commercial software such as OrcaFlex (Randolph and Quiggin, 2009; OrcaFlex Documentation, 2018). The nodal force-displacement performance of this model has been recently investigated by Dong and Shiri (2018), and several nodal inconsistencies were identified. These nodal inconsistencies would affect the global performance of the riser such as SCR profile, shear force, and bending moment distribution and consequently the fatigue damage.

Considering that there are presently no new models or test results that resolve the existing inconsistencies, an innovative methodology was used in this study to assess the influence of nodal inconsistencies in the R-Q model on the global response of SCR. The lower values of suction decay parameter (λ_{suc}), and the suction ratio (f_{suc}) were considered as indexes to mimic the resolved nodal inconsistencies in the simulation of the trench and in modeling partial suction decay. The re-penetration offset parameter was also used to interpret the deep penetrations and the corresponding global response obtained from unusual extreme

values of the model parameters. Also, the influence of mudline shear strength (Sum) and the gradient of undrained shear strength (ρ) on global responses were examined. Combining the detailed results discussed throughout the chapter, the main findings of the study can be summarized as follows:

• The identified nodal inconsistencies in the R-Q model may cause an overestimation of the SCR embedment into the seabed, cyclic contact stress, and other global responses.

• The incapability of the R-Q model in the explicit modeling of the trench formation mandates the use of unusual extreme values for model parameters to create deep trenches. This inconsistency may result in a violation of the global response and the unrealistic relocation of the peak fatigue point.

• Despite the identified inconsistencies, the R-Q soil model still has several attractive features that render it useful for further developments. However, a reliable assessment of global riser performance, particularly the fatigue life, needs to resolve the current nodal inconsistencies.

• The interaction between the model parameters may affect the obtained results. This is one of the limitations of the methodology proposed in this study that considers the changing of individual parameters at a time. Further investigation is needed in defining and evaluating a dimensionless group of parameters to investigate the potential effect of interaction between the global model parameters.

It is worth mentioning that there are still several mechanisms that contribute to the real riser-seabed interaction but are modelled neither by the R-Q model nor by other models in the literature. Some of these mechanisms are the rate dependency, consolidation effects, and the seawater-soil-riser interaction effects resulting in the scour under the SCR. These

important aspects should be addressed in the future research works to propose improved riser-seabed interaction models. The present study has demonstrated the strengths and limitations of relying on the R-Q model for understanding and predicting riser-seabed interactions. Despite the limitations it remains a valuable model for study. Nevertheless, it is necessary to be aware of how to use the model properly. Continuing to develop this model to better understand riser seabed interactions is an important area that requires further research.

10.7. Acknowledgment

The authors gratefully acknowledge the financial support of this research by Memorial University of Newfoundland through the VP start-up fund and financial support from the Research and Development Corporation (RDC) (now InnovateNL) through the ignite program. This work is in continuation to the research project conducted in the Centre for Offshore Foundation Systems, University of Western Australia.

References

ABAQUS/Standard User's Manual, SIMULIA, 2017.

Aubeny, C.P., Biscontin, G., 2009. Seafloor–riser interaction model, Int. J. Geomech. 9 (3), pp. 133–141.

Aubeny, C.P., Shi, H., Murff, J.D., 2005. Collapse loads for a cylinder embedded in a trench in cohesive soil, Int J. Geomech. 5 (4), pp. 320–325.

Audibert, J.M.E., Nyman, D.J., O'Rourke, T.D., 1984. Differential ground movement effects on buried Pipelines, Guidelines for the Seismic Design of Oil and Gas Pipeline Systems, ASCE publication, New York, pp. 150–177.

Bridge, C., Howells, H., 2007. Observations and modeling of steel catenary riser trenches, The Seventeenth International Offshore and Polar Engineering Conference, ISOPE2007, pp. 803–813.

Bridge, C., Laver, K., Clukey, E., Evans, T., 2004. Steel catenary riser touchdown Point vertical interaction models, Offshore Technology Conference.

Clukey, E.C., Aubeny, C.P., Zakeri, A., Randolph, M.F., Sharma, P.P., White, D.J., Sanico, R., Cerkovnic, M., 2017. A perspective on the state of knowledge regarding soil-pile interaction for SCR fatigue assessments, Proceedings of the Offshore Technology Conference OTC 27564-MS.

Clukey, E., Jacob, P., Sharma, P.P., 2008. Investigation of riser seafloor interaction using explicit finite element methods, Offshore Technology Conference.

Dong, X., Shiri, H., 2018. Performance of non-linear seabed interaction models for steel catenary risers, part I: nodal response, Ocean Eng. 154, pp. 153–166.

DNV-RP-H103, 2011, Recommended practice for modelling and analysis of marine operations. Oslo, Norway: Det Norske Veritas.

Hardin, B.O., Drnevich, V.P., 1972. Shear modulus and damping in soils: measurement and parameter effects (Terzaghi lecture), J. Soil Mech. Found. Div. 98 (6), pp. 603–624.

Jiao, Y., 2007. Non-Linear Load-Deflection Models for Seafloor Interaction with Steel Catenary Risers, Texas A&M University, College Station, USA, p. 121 Master of Science.

Kondner, R.L., 1963. Hyperbolic stress-strain response; Cohesive soils, J. Soil Mech. Found. Div. 89 (SM1, Part 1), pp. 115–143.

Liu, J., Kimiaei, M., Randolph, M., 2016. A new user defined element for nonlinear riser-soil interaction analysis of steel catenary riser systems, ASME 2016 35th International Conference on Ocean, Offshore and Arctic Engineering.

Maclure, D., Walters, D., 2007. Freestanding Risers in the Gulf of Mexico – A Unique Solution for Challenging Field Development Configurations, 2H Offshore Engr. Ltd. Technical Paper.

Nakhaee, A., Zhang, J., 2010. Effects of the interaction with the seafloor on the fatigue life of a SCR, Int. Offshore and Polar Engr. Conf., pp. 87–93.

OrcaFlex Documentation, Orcina, 2018.

Phifer, E.H., Frans, K., Swanson, R.C., Allen, D.W., Langner, C.G., 1994. Design and installation of auger steel catenary risers, Offshore Technology Conference.

Queau, L., Kimiaei, M., Randolph, M.F., 2013. Dimensionless groups governing response of steel catenary risers, Ocean Eng. 74, pp. 247–259.

Randolph, M.F., Baht, S., Jain, S., Mekha, B., 2013. Modeling the touchdown zone trench and its impact on SCR fatigue life, Offshore Technology Conference.

Randolph, M.F., Quiggin, P., 2009. Non-linear hysteretic seabed model for catenary pipeline contact, 28th International Conference on Ocean, Offshore and Arctic Engr. OMAE 2009 79259.

Randolph, M.F., White, D.J., 2008. Upper bound yield envelopes for pipelines at shallow embedment in clay, Géotechnique 58 (4), pp. 297–301.

Shiri, H., 2014. Response of a steel catenary riser on hysteretic non-linear seabed, J. Appl. Ocean Res. 44, pp. 20–28.

Shiri, H., Randolph, M.F., 2010. Influence of seabed response on fatigue performance of steel catenary risers in touch don area, 29th Int. Conf. on Ocean, Offshore and Arctic Engr.

Sumer, B.M., 2006. Hydrodynamics around Cylindrical Structures, World Scientific Publishing., Singapore.

Theti, R., Moros, T., 2001. Soil interaction effects on simple-catenary riser response, Pipes Pipelines Int. 46 (3), pp. 15–24.

Zargar, E., Kimiaei, M., 2015. An investigation on existing nonlinear seabed models for riser-fluid-soil interaction studies in steel catenary risers, Proceedings of 3rd Int. Symposium on Frontiers in Offshore Geotechnics, pp. 489–494.

Chapter 11

The influence of nonlinear hysteretic seabed interaction on slug-induced stress oscillations in steel catenary risers

Xiaoyu Dong[1] and Hodjat Shiri[2]

1: Department of Civil

Engineering, Memorial University of Newfoundland

e-mail: xiaoyu.dong@mun.ca

2: Department of Civil

Engineering, Memorial University of Newfoundland

e-mail: hshiri@mun.ca

This chapter is a journal paper which has been published in Applied Ocean Research (2019), Vol. 82, pp. 175-190, ISSN 0141-1187.

.

Abstract

Steel catenary risers (SCRs) are usually cost-effective solutions in development of offshore fields and the transferring of the hydrocarbons from seabed to the floating facilities. These elements are subjected to the fatigue loads particularly in the touchdown zone (TDZ), where the oscillating SCR is exposed to cyclic contact with the seabed. The slug-induced oscillation is a significant contributor to the fatigue loads in the TDZ. The cyclic seabed soil softening under the wave-induced riser oscillations and the gradual penetration of the SCR into the seabed are widely accepted to have a significant influence on SCR fatigue performance. However, this has never been investigated for slug-induced oscillations due to the lack of integrated access to comprehensive numerical models enabling the simulation of the riser slugging and nonlinear hysteretic riser-seabed interaction at the same time. In this chapter, an advanced interface was developed and verified using the multi-point moving tie constraint in order to examine the influence of cyclic seabed soil softening on slug-induced oscillations of SCR. The interface was integrated with a pre-developed user subroutine for modelling of the nonlinear hysteretic riser-seabed interaction and incorporated into a global SCR model in ABAQUS. A comprehensive parametric study was conducted to investigate the influence of slug characteristics and nonlinear seabed soil model on slug-induced, wave-induced, and combined wave/slug induced oscillations of SCR in the TDZ. It was observed that the nonlinear seabed model could significantly affect the embedment of the SCR into the seabed under the slug-induced oscillations and consequently improve the fatigue life. The developed user interface was found to be a strong framework for modelling riser slugging.

Keywords: Steel catenary risers, Slug loading, Non-linear hysteretic riser-seabed interaction, Fatigue analysis, Numerical modeling

11.1. Introduction

Steel Catenary Risers (SCRs) are a series of welded steel pipes hanging freely from a floater in a catenary shape to move hydrocarbons between the sea floor and floating facilities. The SCRs are subjected to oscillations and consequently the fatigue damage in the touchdown zone (TDZ), where the catenary part arrives at the seabed. These oscillations in the TDZ are caused by external and internal loads applied to the SCR. The external loads are generated by vessel motions under the action of environmental loads and also the vortex-induced vibra- tions of the riser due to the sea current. The internal loads are generated by irregular multi-phase flow regimes inside the riser mainly due to slugging, where the fluid accumulates into slugs filling the diameter of the pipe and blocking the gas passage. Subsea surveys have observed that the oscillations in TDZ cause the riser to penetrate into the seabed by several diameter depths creating a trench (Bridge and Howells, 2007). The penetration is mainly happening due to the cyclic soil stiffness degradation caused by SCR oscillations in the TDZ. The seabed soil softening and trench creation alters the SCR contact pressure and the riser profile in the seabed, respectively. This, in turn, affects the cross-sectional stress os- cillation range in the SCR and consequently the fatigue life in the TDZ (see Figure 11-1). Several studies have been conducted to investigate the influence of soil stiffness degradation on the external load-induced fatigue damage of SCR (Shiri, 2010; Shiri and Randolph, 2010; Clukey et al., 2017; Dong and Shiri, 2018).

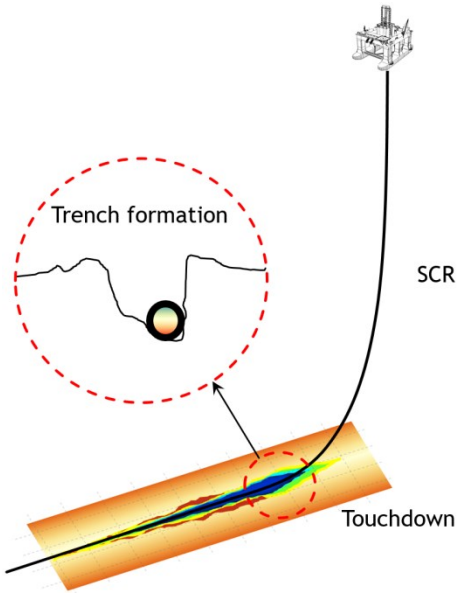

Figure 11-1. Trench underneath SCR in the TDZ.

However, the effect of cyclic soil stiffness degradation on the internal load-induced or slug-induced fatigue damage has never been explored in the literature. Instead, pinned end, rigid or simple linear elastic springs have been commonly used to model the seabed in the slug-induced fatigue analyses (e.g., Kansao et al., 2008; Ortega et al., 2012). Simplifying the seabed soil with rigid or elastic springs results in ignoring many of the influential characteristics of the riser-seabed interaction such as cyclic soil stiffness degradation, suction force mobilization during the riser uplift, variation of the riser profile in the seabed, variation of the stress oscillation amplitude and consequently the variation of ultimate fatigue life. Slugging is an important aspect in riser engineering and can cause serious flow

assurance and structural integrity problems in operation. The current study has focused on the latter item, i.e., the structural integrity or fatigue performance of the slugging riser in the TDZ.

In this study, an advanced numerical model was developed in ABAQUS to simulate slug-induced and vessel-induced oscillations of the SCR simultaneously, incorporating the nonlinear hysteretic riser-seabed interaction. An innovative methodology was developed using the multi- point constraint (MPC) to model and fully control a range of complex slug patterns. Also, to investigate the influence of the model's complexity on ultimate system response, a simplified model using the au- tomated distributed load concept (DLOAD) was initially developed to compare with the performance of the advanced model. A popular nonlinear hysteretic riser-seabed interaction model proposed by Randolph and Quiggin (R-Q model) was coded to a user-defined element (UEL) in FORTRAN to simulate the cyclic soil stiffness degradation, cyclic suction force mobilization, and gradual trench formation. The wave frequency and low-frequency vessel motions were modeled by incrementally updating boundary conditions coded to a user-defined subroutine (DISP) using the methodology proposed by Shiri and Randolph. The developed model was verified against the published works, and a comprehensive parametric study was conducted to investigate the influence of nonlinear hysteretic riser-seabed interaction on slug-induced stress oscillations (or accumulated fatigue damage) in the TDZ.

The study made significant contributions to filling the existing knowledge gaps in the field of riser-seabed interaction and provided insight into the slug-induced riser-seabed interaction. Also, the developed numerical model was found to be a strong tool for advanced slug-induced fatigue analysis of SCR with customized plastic seabed soil

condition, vessel excitation, and complex slugging regimes. The results showed that the riser oscillation due to slugging could be a key contributor to cyclic seabed soil stiffness degradation and consequently the trench formation in the TDZ. It was observed that the slug-induced stress oscillation amplitude in a nonlinear hysteretic seabed could be less severe than the linear elastic seabed and is cyclically decreased leading to further relaxation. However, this can be complicated when the slug-induced oscillations are combined with vessel motions, where the oscillations may be combined in opposite ways. In most of the cases, more severe responses were obtained by the combined impact of the cause serious flow assurance and structural integrity problems in operation. The current study has focused on the latter item, i.e., the structural integrity or fatigue performance of the slugging riser in the TDZ.

In this study, an advanced numerical model was developed in ABAQUS to simulate slug-induced and vessel-induced oscillations of the SCR simultaneously, incorporating the nonlinear hysteretic riser-seabed interaction. An innovative methodology was developed using the multi- point constraint (MPC) to model and fully control a range of complex slug patterns. Also, to investigate the influence of the model's complexity on ultimate system response, a simplified model using the automated distributed load concept (DLOAD) was initially developed to compare with the performance of the advanced model. A popular nonlinear hysteretic riser-seabed interaction model proposed by Randolph and Quiggin (R-Q model) was coded to a user-defined element (UEL) in FORTRAN to simulate the cyclic soil stiffness degradation, cyclic suction force mobilization, and gradual trench formation. The wave frequency and low-frequency vessel motions were modeled by incrementally updating boundary conditions coded to a user-defined subroutine (DISP)

using the methodology proposed by Shiri and Randolph. The developed model was verified against the published works, and a comprehensive parametric study was conducted to in- vestigate the influence of nonlinear hysteretic riser-seabed interaction on slug-induced stress oscillations (or accumulated fatigue damage) in the TDZ.

The study made significant contributions to filling the existing knowledge gaps in the field of riser-seabed interaction and provided insight into the slug-induced riser-seabed interaction. Also, the developed numerical model was found to be a strong tool for advanced slug-induced fatigue analysis of SCR with customized plastic seabed soil condition, vessel excitation, and complex slugging regimes. The results showed that the riser oscillation due to slugging could be a key contributor to cyclic seabed soil stiffness degradation and consequently the trench formation in the TDZ. It was observed that the slug-induced stress oscillation amplitude in a nonlinear hysteretic seabed could be less severe than the linear elastic seabed and is cyclically decreased leading to further relaxation. However, this can be complicated when the slug-induced oscillations are combined with vessel motions, where the oscillations may be combined in opposite ways. In most of the cases, more severe responses were obtained by the combined impact of the wave and slug. Therefore, from a design perspective, it would be more conservative to add up the contribution of the slugging and wave frequency motions. This will be further discussed in later sections.

11.2. Review of the literature for modeling the seabed in slug-induced vibrations

The seabed end of the riser is commonly modeled as a simple pin when the slug-induced vibrations of the hanging part of risers are investigated (Bordalo et al., 2008; Ortega et al.,

2012, 2013; Chatjigeorgiou, 2010a, 2010b, 2017) . There are only a few published works incorporating the elastic or rigid seabed models (Pollio and Mossa, 2009) and no published works incorporating the plastic or nonlinear hysteretic seabed response in riser slugging analysis in the TDZ. However, it is still worth reviewing some of these published works from the viewpoint of the seabed condition and the combined effects of slug and wave-induced oscillations, which are amongst the key investigations in the current study.

Pollio and Mossa compared two simple models of slug flow in a long flexible marine riser with the elastic seabed and without any seabed respectively. The authors considered the riser-seabed interaction with a simplified normal reaction force function of the relative displacement and a friction force in the opposite direction of the node velocity (Pollio and Mossa, 2009). The results showed that the bending moment variation was significantly different in the seabed existence case and seabed absence case. The bending moment variation was less severe in the case of seabed existence. The riser had the freedom to take its natural profile passing from the hanging part to seabed portion. Irregular inner stress responses were generated by the slug flow with variable frequency, while tension and moment variations were more regular under the slug flow with a constant frequency. Slug flow with variable frequency resulted in a greater magnitude of bending moment variation and a greater probability of higher stress in the riser in both cases. These results are in agreement with the findings of the current study. Gundersen et al. (2012) explored the remnant fatigue life of flexible risers in lazy-S configuration subjected to combined wave and slug-induced motions by coupling commercially available global and local riser analysis tools (i.e., RIFLEX and BFLEX). The case study mainly dealt with the hanging part of the riser and showed that slugging dominated the dynamic top angle response and

significantly reduced the riser fatigue life during a rela- tively calm sea condition. Ortega et al. (2012) analyzed the influence of slug loading on the dynamic responses of a flexible riser in lazy wave configuration by coupling two codes together for slug flow tracking (SLUGGIT) and riser structure (RISANANL). The seabed end of the riser was modeled by a pinned end. It presented the irregular deformation time histories of the riser structure due to the characteristic of slug flow and indicated the importance of considering the effects of slug flow in the fatigue analysis. Ortega et al. (2017) conducted a fully-coupled analysis to examine the combined effects of slug loads and wave loads on the dynamic responses of a flexible riser in catenary configuration. The seabed end of the riser was still considered as pinned. The combined effect of waves and slugs generated irregular deformation time histories. These results are partly in agreement with the findings of the current study in the TDZ. However, we observed a dominance of the combined wave and slug effects towards a shorter fatigue life in the TDZ. Chatjigeorgiou (2017) formulated the analytical equilibrium and investigated the dynamic response of catenary pipelines with combined effects of harmonic motions of the vessel and the internal slug flow. The slug model, formerly built by Chatjigeorgiou (2010a, 2010b), was incorporated with the seabed end considered as pinned. It was shown that the magnitudes of dynamic components were amplified due to the existence of internal slug flow. Bordalo and Morooka (2018) incorporated a slug flow load model to a 3D pipeline dynamics simulator assuming a rigid seabed condition. The simulation of slugging SCR in the selected case study showed that the node closer to the touchdown point presents higher average bending stress when compared to the node far above in the hanging part of SCR. The results obtained by these studies are in agreement with the findings of the current research work but are limited to

an oversimplified seabed condition. The current study focused on examining more realistic seabed conditions incorporating several influential mechanisms such as slug-induced cyclic soil stiffness degradation, mobilization of cyclic suction force during riser uplifts, and gradual trench formation underneath the riser.

11.3. Review of the literature for modeling the SCR-seabed interaction.

Today, it is widely accepted in the literature that the cyclic soil stiffness degradation leading to gradual riser penetration into the seabed has a significant influence on stress oscillation and fatigue life of the SCR in the TDZ. The seabed soil under an SCR has been traditionally modelled by linear springs in SCR design codes. Following the first use of SCR technology in the Auger field of the Gulf of Mexico (Phifer et al., 1994), the STRIDE and CARISIMA JIPs (1999–2001) were the initial studies to investigate the need for more sophisticated nonlinear riser-seabed in- teraction models (Theti and Moros, 2001; Campell, 1999). Bridge et al. (2004, 2007) captured various nonlinear aspects of soil behavior characteristics through full-scale harbor tests. They developed a model based on a hyperbolic force-displace- ment interaction curve for sand. It was similar in form to the hyperbolic pipe-soil interaction curve developed by Hardin and Drnevich (1972) that was originally proposed for clay by Kondner (1963). However, the model was unable to sequentially simulate the gradual seabed soil softening and riser embedment to the seabed. Jiao (2007) proposed two nonlinear non- degradating and degradating spring models for soils beneath the SCR. The degradating model was capable of simulating cyclic softening of the soil but only through the re-loading paths, missing the unloading episodes. Aubeny and Biscontin (2009) proposed a new model based on the work conducted by Jiao to simulate the nonlinear hysteretic soil behavior under the riser, which was further improved

by Nakhaee and Zhang (2010). The model resolved the shortcomings of Jiao's model but continued to use a non-uniform set of equations. Randolph and Quiggin (2009) proposed another nonlinear model (from now on referred to as R-Q model) with more unified sets of equations to define the hysteretic soil behavior under a vertical oscillating riser using a combination of hyperbolic and exponential functions. Shiri and Randolph (2010) and Shiri (2010) used the R-Q model for wave-induced fatigue analysis of SCR in the TDZ. Zargar and Kimiaei (2015) conducted a comparative study of two existing riser-soil interaction models (Aubeny and Biscontin, 2009; Randolph and Quiggin, 2009) and identified the R-Q model as an appropriate base for further developments. Liu et al. (2016) developed a new user-defined subroutine to implement the nonlinear seabed response to SCR fatigue analysis. Clukey et al. (2017) reported the state of knowledge of riser-soil interaction and its impact on fatigue assessment. The authors emphasized the significance of nonlinear riser-soil interaction models and the need for the further improvement of these models for fatigue analysis of SCRs in the TDZ. Dong and Shiri (2018) comprehensively investigated the performance of R-Q model. The R-Q model was found to have strong features and potentially an appropriate approach for modeling the nonlinear riser-seabed interaction. Aside from a few improvements that the R-Q model needs, the advantages of this model in the automotive simulation of cyclic soil stiffness degradation and trench creation have made it a popular model.

In the present study, the R-Q model written in a UEL subroutine was integrated with vessel motions and slug modeling subroutines (DISP and MPC). Then the integrated interface was implemented into the global SCR model in ABAQUS to investigate the effect of nonlinear hysteretic seabed response on slug-induced fatigue loads.

11.4. Development of a global SCR model

A global SCR model was developed in ABAQUS to investigate the influence of nonlinear hysteretic riser-seabed interaction on slug-induced cyclic stress variation amplitude and consequently the fatigue in the TDZ. To facilitate the global model verification, the overall configuration of the riser was adopted from a numerical and experimental case study published by STRIDE JIP (Phifer et al., 1994; Theti and Moros, 2001) that has been used in several later studies in the literature as well (Bridge and Howells, 2007; Shiri, 2010; Shiri and Randolph, 2010; Dong and Shiri, 2018).

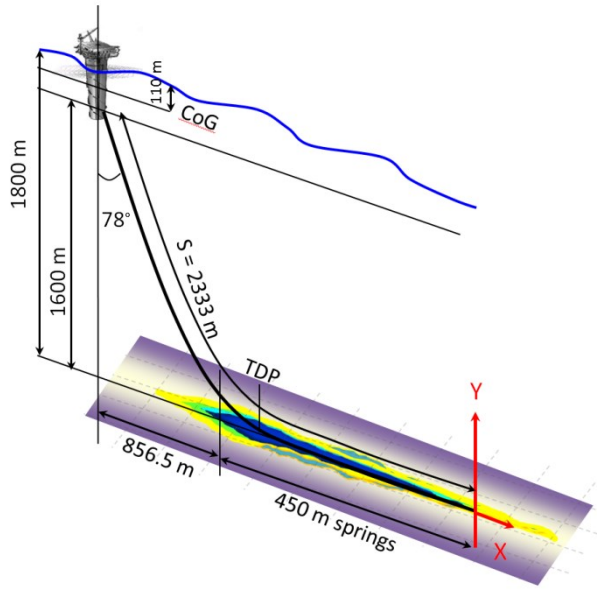

Figure 11-2. The global geometry of SCR modeled by ABAQUS.

As shown in Figure 11-2, the SCR with a total length of 2333m was constructed using beam elements B21 to capture the cross-sectional shear and bending stresses. The anchored end was set as the origin of the coordinates, and 828 nodes were defined along the riser as the axial nodes. From node 1 to node 450, 1m distance was set between the adjacent nodes

to define the zone allocated by the user-defined seabed interaction model (i.e., UEL subroutine). For the hanging section of the SCR, a 5m distance between nodes was established (except the last element, 3m in length). The mechanical properties of SCR are given in Table 11-1. The hydro- dynamic coefficients were considered as 0.7, 1, and 1.5 for drag, added mass and inertia, respectively.

Table 11-1. Generic SCR pipe properties

Dimension	Symbol	Value	Unit
Outer diameter,	D_o	0.324	m (12¾ ")
Wall thickness,	t	0.0205	m
Second moment of area,	I	2.26×10^{-4}	m^4
Steel Young's Modulus	E_{steel}	2.07×10^{11}	N/m^2
Steel density,	ρ_s	7850	kg/m^3
Fatigue S-N curve	ā	1.05×10^{-12}	-
DNV (2008)	m	3.0	-
E Class weld	SCF	1.13	-

Three user-defined modules including DLOAD/MPC, UEL, and DISP were coded in FORTRAN and integrated with ABAQUS to model slug loading, nonlinear hysteretic riser-seabed interaction, and the wave/ current-induced vessel motions, respectively. Efforts were made to efficiently balance the level of sophistication with the computational cost.

11.5. Modeling of SCR slugging

Risers may transfer multiphase contents containing oil, gas, condensate, and free water. As schematically illustrated in Figure 11-3, the slugging or separation of the flow to a film

zone, and a slug liquid zone, usually occurs in moderate flow velocities, where the fluid accumulates into slugs, filling the diameter of the pipe while the gas forms into the bubbles. The velocity, length, density, frequency, and liquid holdup are some of the key features of slugs that may widely vary depending on different field operating conditions.

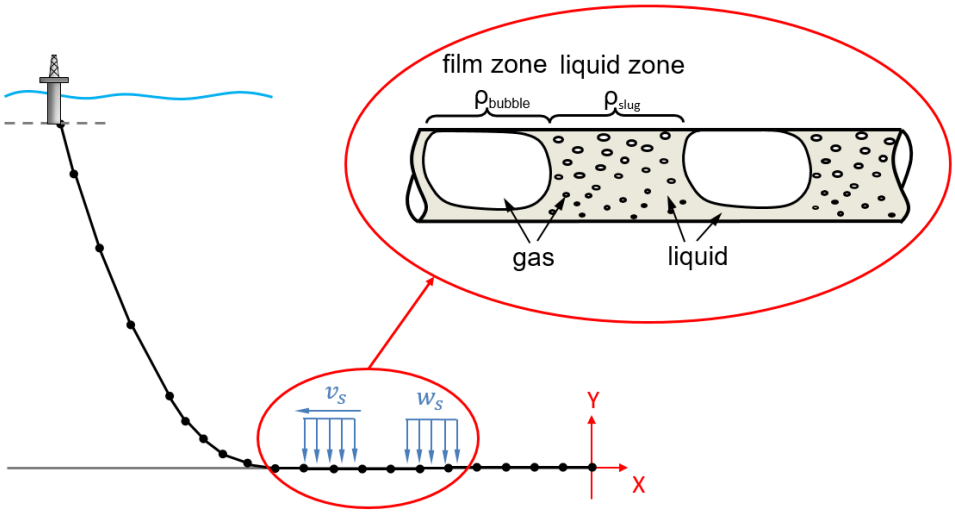

Figure 11-3. The slug flow regime.

From a structural integrity stand-point, the large difference between the density of the slug and the gas bubbles (e.g., several hundred percent), and consequently the varying weight, inertia and momentum introduce cyclic cross-sectional stress oscillation and fatigue damage in the TDZ. The magnitude of this damage is significantly affected by cyclic seabed soil softening, a topic that was comprehensively studied in this chapter. Considering the complex interactive mechanisms, the numerical modeling of slugging can be challenging depending on the target level of simulation sophistication and modeling strategies. As a result, the existing commercial software packages provide limited access

for users to customize the slug characteristics. Therefore, developing a numerical slug modeling in- terface that allows full access to defining complex slug regimes was one of the primary motivations of the current study. A secondary aspect regarding slug modeling was to examine how the level of model so- phistication affects the results both from an engineering and scientific standpoint. Therefore, two different strategies with a low and high level of sophistication were examined for developing the slug model, called the "simplified" and "advanced" strategies, respectively.

As mentioned earlier, the cyclic cross-sectional stress oscillation in the TDZ is a result of varying weight, inertia and momentum throughout the slugging riser. Therefore, an advanced slug model should capture all of these three effects simultaneously. However, a simplified strategy can be applied by changing the distributed loads to bubbles (e.g., several hundred percent), and consequently the varying weight, inertia and momentum introduce cyclic cross-sectional stress oscillation and fatigue damage in the TDZ. The magnitude of this da- mage is significantly affected by cyclic seabed soil softening, a topic that was comprehensively studied in this chapter. Considering the complex interactive mechanisms, the numerical modeling of slugging can be challenging depending on the target level of simulation sophistication and modeling strategies. As a result, the existing commercial software packages provide limited access for users to customize the slug characteristics. Therefore, developing a numerical slug modeling interface that allows full access to defining complex slug regimes was one of the primary motivations of the current study. A secondary aspect regarding slug modeling was to examine how the level of model sophistication affects the results both from an engineering and scientific standpoint. Therefore, two different strategies with a low and high level of

sophistication were examined for developing the slug model, called the “simplified” and “advanced” strategies, respectively.

As mentioned earlier, the cyclic cross-sectional stress oscillation in the TDZ is a result of varying weight, inertia and momentum throughout the slugging riser. Therefore, an advanced slug model should capture all of these three effects simultaneously. However, a simplified strategy can be applied by changing the distributed loads to incorporate only the influence of the content of varying weight. This strategy is similar to the monophase liquid with variable density model or a simple train of liquid pulses (Pollio and Mossa, 2009; Patel and Seyed, 1989) and can be implemented by developing a DLOAD subroutine in ABAQUS. However, this strategy ignores the effect of changes in the SCR inertia. An advanced strategy for modeling all of the features of slugging SCR needs to use a moving tie constraint. Using ABAQUS, this approach can be modeled through coding an advanced multi-point constraint (MPC) subroutine. The simplified and advanced strategies will be further discussed in sub- sequent sections.

11.5.1.Simplified strategy: developing a DLOAD interface

A FORTRAN code was developed using the DLOAD subroutine in ABAQUS (ABAQUS/Standard User’s Manual, 2004) to sequentially activate/deactivate the sections of pre- defined distributed load representing the weight of the slug. This ap- proach does not capture the effects of momentum and inertia, but the latter one can be modeled by adding sequentially controlled mass to the nodes. However, neither of these effects was considered to keep the strategy representing the most simplified approach for the modeling of the moving slug throughout the SCR.

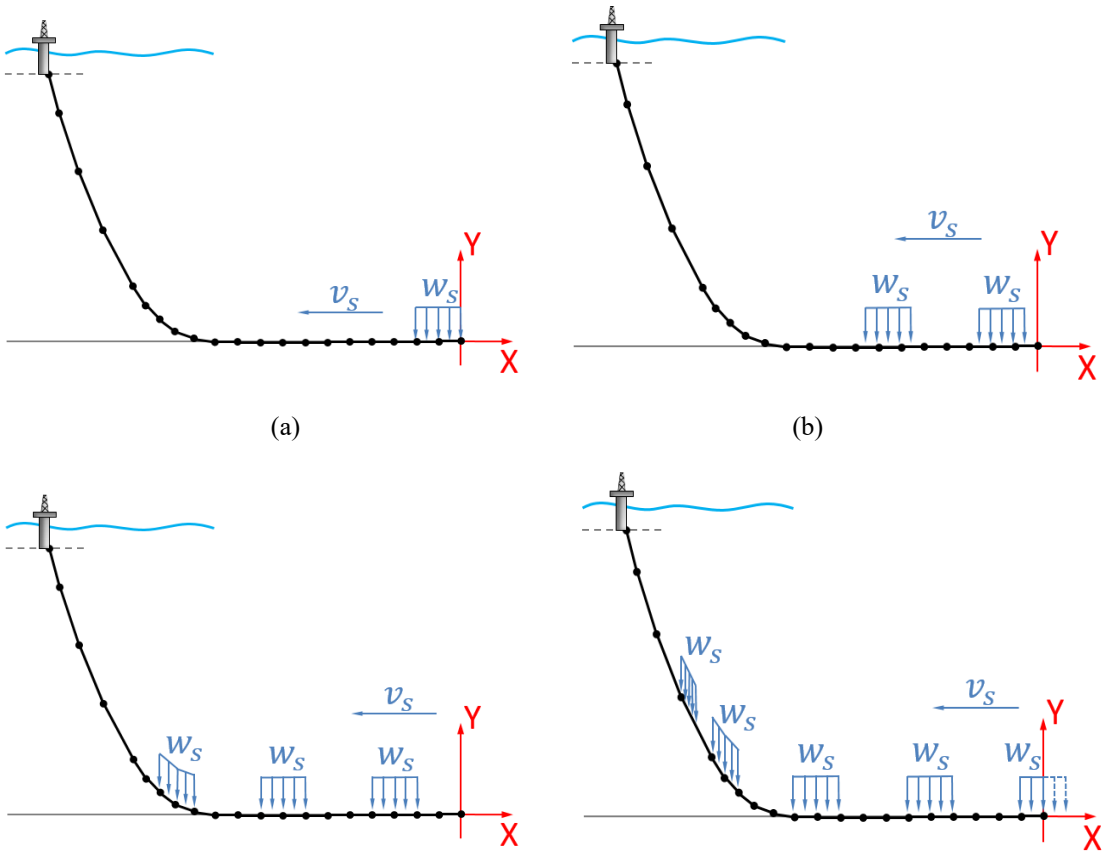

Figure 11-4. DLOAD capturing slug flow weight inside SCR.

Figure 11-4 schematically shows how the coded DLOAD subroutine switches on and off the distributed weight load over the SCR to model the moving slug with a given density, velocity, lengthy, and frequency. The incremental location of the load was defined using the velocity, length, and the total elapsed time passed in by ABAQUS.

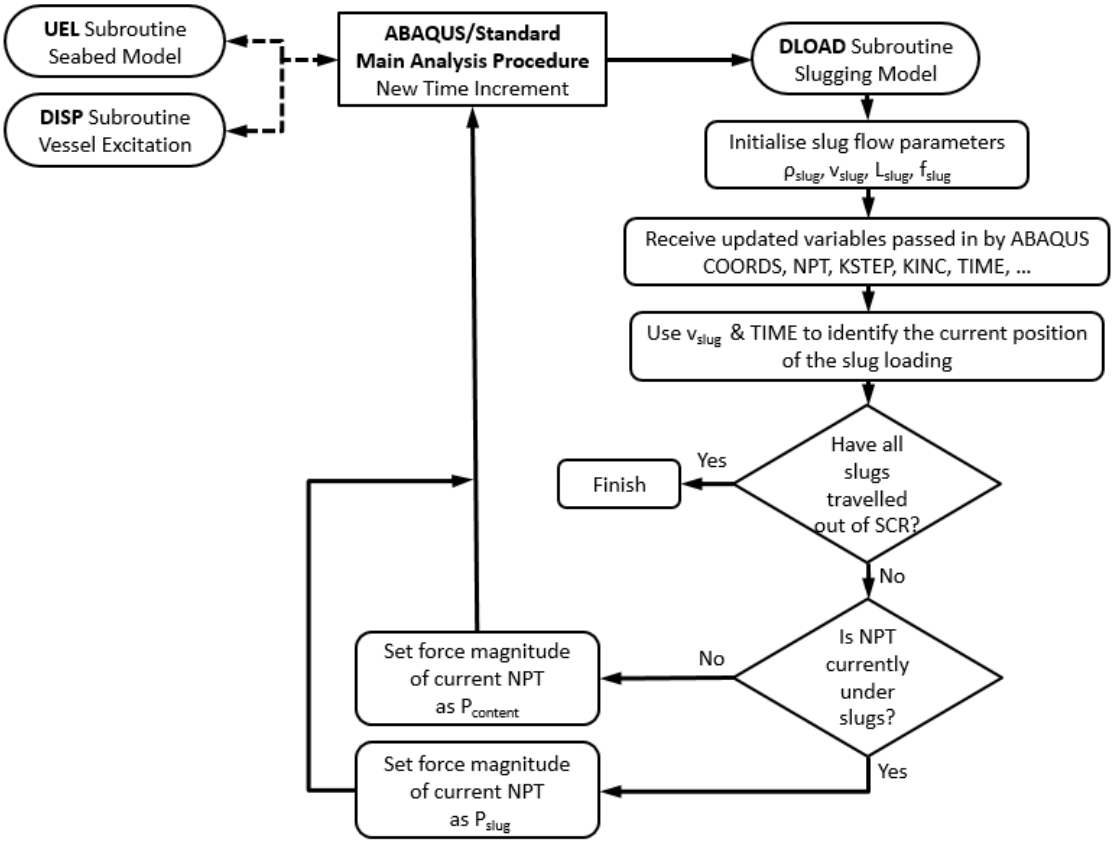

Figure 11-5. DLOAD subroutine internal flowchart.

Figure 11-5 shows the flowchart of the simplified analysis, where the subroutine determines the parts of the SCR going under the slug load at each time increment. The load blocks were sequentially switched on / off to model the traveling slug from the anchored end towards the vessel. To accomplish this process, at each time increment, ABAQUS transmitted sets of key information to the DLOAD subroutine such as global coordinates (COORDS), integration points (NPT), step numbers (KSTEP), time information (TIME), etc. Slugs were assumed to move at a constant velocity, so that the location of each slug could be determined according to its length and frequency. The passed-in COORDS were used to calculate the distance from the current NPT to the anchor end. Then, the load

magnitude at the current NPT was determined to compare its location with the calculated location of slugs, then the corresponding load was assigned. This simple process enabled the division of the SCR into a series of connected sections and integration points, where the traveling slugs were modeled by incre- mental switching on/off of the load blocks in each section.

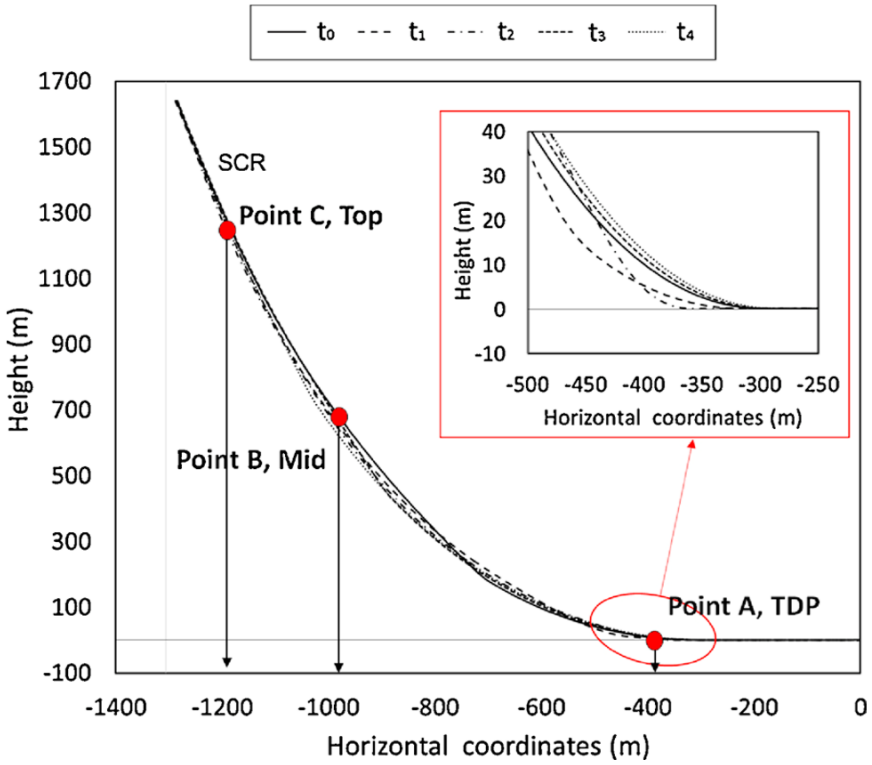

Figure 11-6. SCR oscillation under single slug travel in the rigid seabed

Table 11-2. Generic slug flow properties.

Parameter	Symbol	Value	Unit
Slug density	ρ_{slug}	600	kg/m^3
Bubble density	ρ_{bubble}	100	kg/m^3
Flow velocity	v_{slug}	10	m/s
Slug length	L_{slug}	30	m
Slug frequency	f_{slug}	180	/hr

Figure 11-6 shows a sample DLOAD performance in modeling the SCR profile oscillation due to a single traveling slug with generic characteristics given in Table 11-2. The slug parameters given were selected based on several slug case studies published in the literature (e.g., Bordalo et al., 2008; Pollio and Mossa, 2009; Trippit et al., 2012; Ortega et al., 2012, 2013; Ortega, 2015). The points A, B, and C are the verification points that will be used later in this chapter. By increasing the slug frequency, the riser started to oscillate in the TDZ with an amplitude depending on the slugging characteristics.

11.5.2. Advanced strategy: developing an MPC interface

A multi-point constraints (MPC) user subroutine was coded in ABAQUS to create a moving tie constraint interface modeling the moving slug. This advanced approach enabled the capturing of the effects of momentum and inertia. The developed MPC subroutine tied the degrees of freedom in additional mass elements (slugs) to the functions of the degrees of freedom in the axis of SCR. Therefore, the nodes on mass elements or slugs (dependent nodes) were transported along the instantaneous axis of the catenary riser (independent nodes) with a predefined speed, while the constraint equations were incrementally updated to tie the dependent nodes only to the two independent nodes closest

to the segmental riser profile. After defining the initial velocity of the point masses, the MPC interface captured the weight of slugs, momentum, and the inertia generated by the slug traveling throughout the SCR.

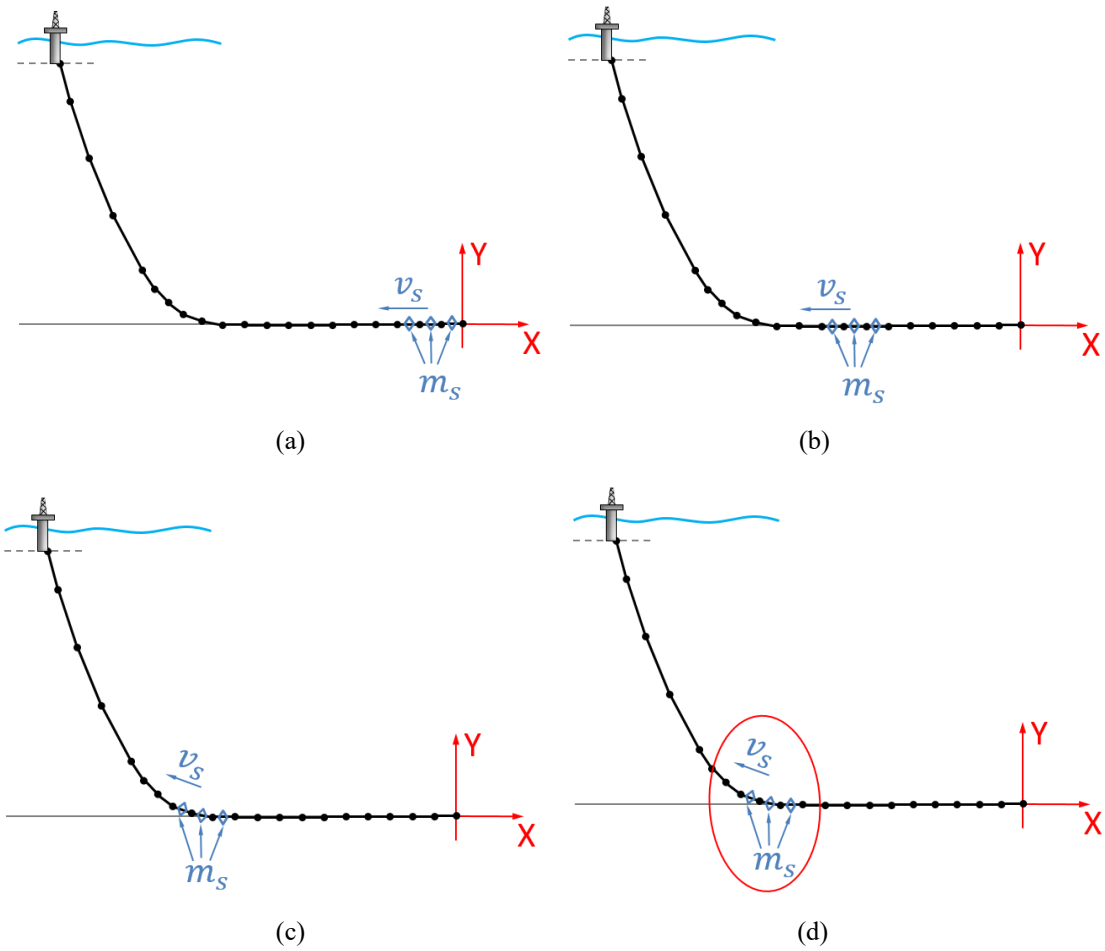

Figure 11-7. Advanced approach for modelling the slug flow using MPC interface.

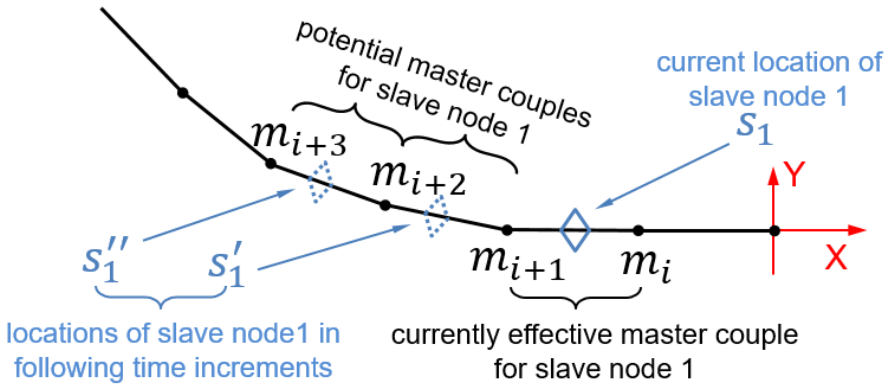

Figure 11-8. Potential and activated master couples in MPC.

Similar to any other constraint interfaces in ABAQUS, the con- straining process works based on defining sets of master and slave nodes. The nodes at additional masses were defined as slaves, and the closest pair of axial nodes were taken as the instantaneous activated masters. As shown in Figure 11-7 and Figure 11-8, the other potential masters are waiting for the arrival of the slaves to get activated. In this case, the axial nodes of SCR representing potential master nodes were listed in an external input file and called from main ABAQUS input file before executing the MPC subroutine. Also, initial velocities were defined for point masses representing the slave nodes in the ABAQUS main input file.

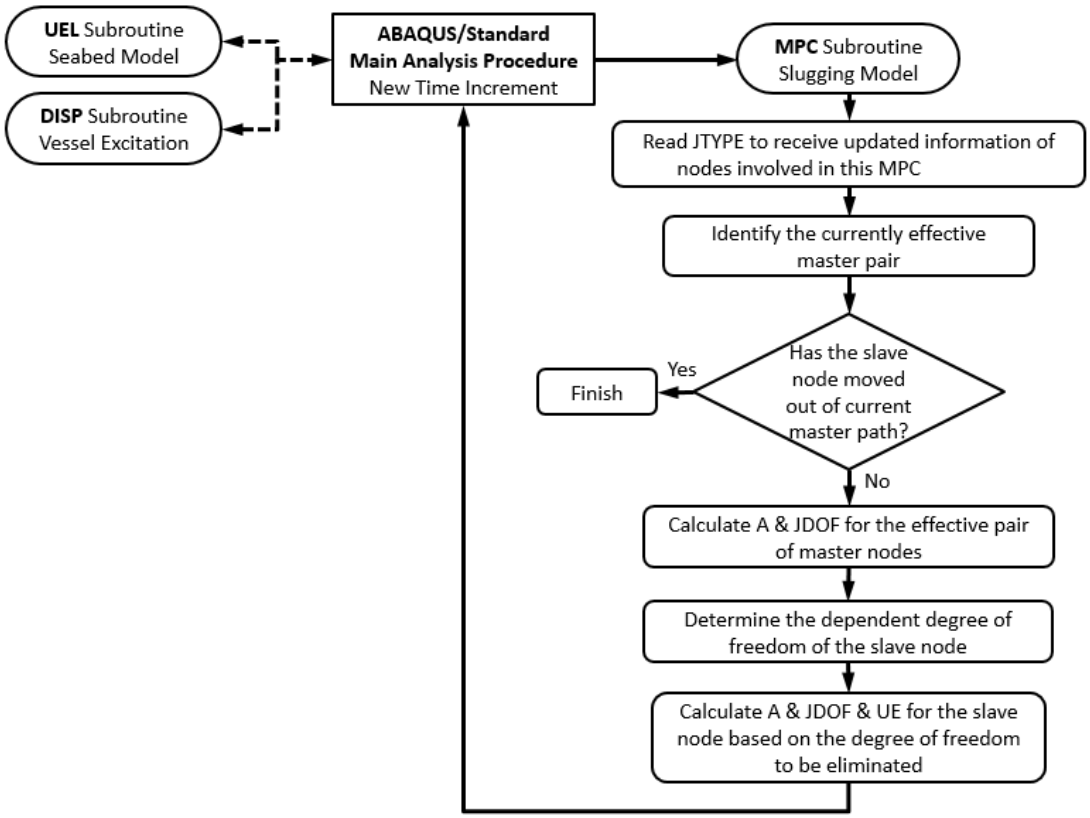

Figure 11-9. Analysis flowchart of MPC subroutine for advanced modeling of slugging.

Figure 11-9 shows the global flowchart of the advanced analysis, where the developed MPC subroutine conducts three main tasks, while the location of the moving slug is incrementally updated: (a) defining the degree of freedom (DOF) for slaves, (b) transferring loads from the slave to the currently activated masters through constraint equilibriums, and (c) eliminating the slave from the stiffness matrix. To perform this process, first, the master pairs effectively involved in the current time increment were identified using the ABAQUS information passed-in to the MPC subroutine. Then, a set of constraint equations were used to determine the dependent DOF of the slave nodes. The lateral constraint was defined so that the lateral position of the dependent nodes was

constrained to a straight line passing through the currently activated master nodes. An array of the derivatives of the constraint functions(A(N), Figure 11-9) are calculated and passed to ABAQUS to transfer the loads from the dependent DOF to other DOFs. This array is accompanied by another array, (JDOF(N), Figure 11-9), containing the DOF identifiers at the nodes involved in the constraint. The dependant DOFs were then eliminated from the stiffness matrix. The total value of the eliminated DOF (UE, Figure 11-9) of the slave node was also updated and transferred to ABAQUS at the end of the time increment.

The multi-point constraint equations are a key part of the MPC interface. Therefore, it is worth shortly reviewing the development process of these equations. The general form of the degree of freedom (DOF) can be written in the following form for the MPC constraint (ABAQUS/Standard User's Manual, 2018):

$$f(u^1, u^2, u^3, \cdots, u^N, \text{geometry}, \text{temperature}, \text{field variables}) = 0 \tag{11-1}$$

where, u^1 is the first DOF that will be eliminated to impose the constraint; $u^2, u^3, \cdots, u^N$ are any other DOFs involved in the constraint.

Assuming that the value of the dependent DOF u^1 is a function of the DOFs $u^2, u^3, \cdots, u^N$, the linearized form of the constraint equation is given by:

$$u^1 = -\frac{1}{A^1}\sum_{i=2}^{N} A^i \cdot u^i \tag{11-2}$$

where A^i is an array of the derivatives given below:

$$A^1 = \frac{\partial f}{\partial u^1}, A^2 = \frac{\partial f}{\partial u^2}, A^3 = \frac{\partial f}{\partial u^3}, \cdots \tag{11-3}$$

By using a simple triangle similarity rule, the axial constraint equations for linear 2D slider can be established as below for the slave node(s) according to its currently activated master pair (m_1 and m_2).

$$f(u^s, v^s, u^{m_1}, v^{m_1}, u^{m_2}, v^{m_2}) = (x^s - x^{m_1})(y^{m_2} - y^{m_1}) - (y^{m_2} - y^{m_1})(x^{m_2} - x^{m_1}) = 0 \quad (11\text{-}4)$$

Where, x and y are the nodal coordinates. The array of derivatives in X and Y directions can then be calculated as:

$$A^1 = \frac{\partial f}{\partial u^s} = \frac{\partial[(x^s - x^{m_1})\cdot(y^{m_2} - y^{m_1}) - (y^s - y^{m_1})\cdot(x^{m_2} - x^{m_1})]}{\partial x^s} = y^{m_2} - y^{m_1} \quad (11\text{-}5)$$

$$A^2 = \frac{\partial f}{\partial v^s} = \frac{\partial[(x^s - x^{m_1})\cdot(y^{m_2} - y^{m_1}) - (y^s - y^{m_1})\cdot(x^{m_2} - x^{m_1})]}{\partial y^s} = x^{m_1} - x^{m_2} \quad (11\text{-}6)$$

$$A^3 = \frac{\partial f}{\partial u^{m_1}} = \frac{\partial[(x^s - x^{m_1})\cdot(y^{m_2} - y^{m_1}) - (y^s - y^{m_1})\cdot(x^{m_2} - x^{m_1})]}{\partial x^{m_1}} = y^s - y^{m_2} \quad (11\text{-}7)$$

$$A^4 = \frac{\partial f}{\partial v^{m_1}} = \frac{\partial[(x^s - x^{m_1})\cdot(y^{m_2} - y^{m_1}) - (y^s - y^{m_1})\cdot(x^{m_2} - x^{m_1})]}{\partial y^{m_1}} = x^{m_2} - x^s \quad (11\text{-}8)$$

$$A^5 = \frac{\partial f}{\partial u^{m_2}} = \frac{\partial[(x^s - x^{m_1})\cdot(y^{m_2} - y^{m_1}) - (y^s - y^{m_1})\cdot(x^{m_2} - x^{m_1})]}{\partial x^{m_2}} = y^{m_1} - y^s \quad (11\text{-}9)$$

$$A^6 = \frac{\partial f}{\partial v^{m_2}} = \frac{\partial[(x^s - x^{m_1})\cdot(y^{m_2} - y^{m_1}) - (y^s - y^{m_1})\cdot(x^{m_2} - x^{m_1})]}{\partial y^{m_2}} = x^s - x^{m_1} \quad (11\text{-}10)$$

By assuming the 2D condition of the model and the sliding of the slave between the currently activated pair of master nodes, only one DOF was eliminated at a time. The direction of the motion was set as a dependent DOF and then the DOF to be eliminated was determined by the inclination of the master pair through the following simple criterion:

The direction of DOF to be eliminated

$$= \begin{cases} X, & |x^{m_2} - x^{m_1}| \geq |y^{m_2} - y^{m_1}| \\ Y, & |x^{m_2} - x^{m_1}| < |y^{m_2} - y^{m_1}| \end{cases} \quad (11\text{-}11)$$

This process is conducted for each slave node in every time increment to simulate a continuous flow of slug throughout the SCR. The analysis is stopped when the MPC subroutine confirms that the slave node has completed travelling along the master path. The innovative strategy presented above enabled the advanced modelling of the moving slug with capturing the effects of weight, inertia and momentum.

11.5.3.Verification of DLOAD and MPC interfaces

Before adding the riser-seabed interaction effects and its complex- ities to the global model, the performance of the DLOAD and the MPC interfaces were validated in three steps against the commercial software FLEXCOM and the research work conducted by Ortega. Ortega has validated their work against two verified codes called SLUGIT and RISANANL.

First, adapting the riser configuration from Ortega, a 770 m riser (400 mm diameter and 20 mm thickness) with an effective weight of 0.58 kN/m was modeled in a water depth of 300 m. The bending rigidity was assumed as 206 GPa, and a horizontal tension force of 400 kN was applied at the vessel end. One hundred beam elements discretized the riser, and the boundary conditions at each end of the riser were simplified as pins. Figure 11-10 shows a perfect agreement between the FLEXCOM, ABAQUS, and Ortega in the prediction of the static catenary profile.

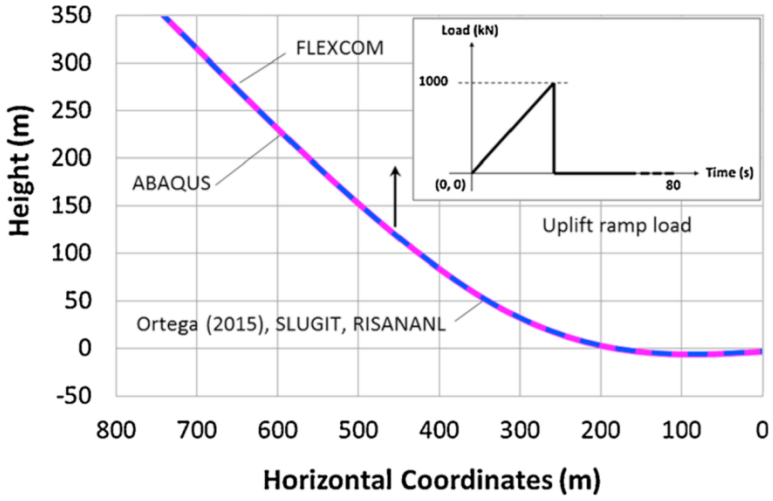

Figure 11-10. Catenary profile predicted by FLEXCOM, ABAQUS, and Ortega.

Second, the verification process was conducted with a simple analysis, where an arbitrary uplift ramp load was applied in the middle part of the SCR, and the resultant displacements in the direction perpendi- cular to the load was captured to examine the riser dynamics and the nonlinear geometrical configuration. The load was not moved but was linearly increased from zero to 1000 kN and then disappeared (see Figure 11-10). This load was defined as a shortly distributed load using DLOAD and as an attached mass point using the MPC interface, both of which are varying over time. The hydrodynamic coefficients were considered as 1, 1, and 2 for drag, added mass and inertia, respectively. Figure 11-11 shows the time history of the horizontal displacement of the load point extracted from FLEXCOM, DLOAD, MPC, and Ortega. Ne- gative signs denote the displacement towards the anchored end. A high level of agreement was observed between the FLEXCOM, DLOAD, MPC, and Ortega.

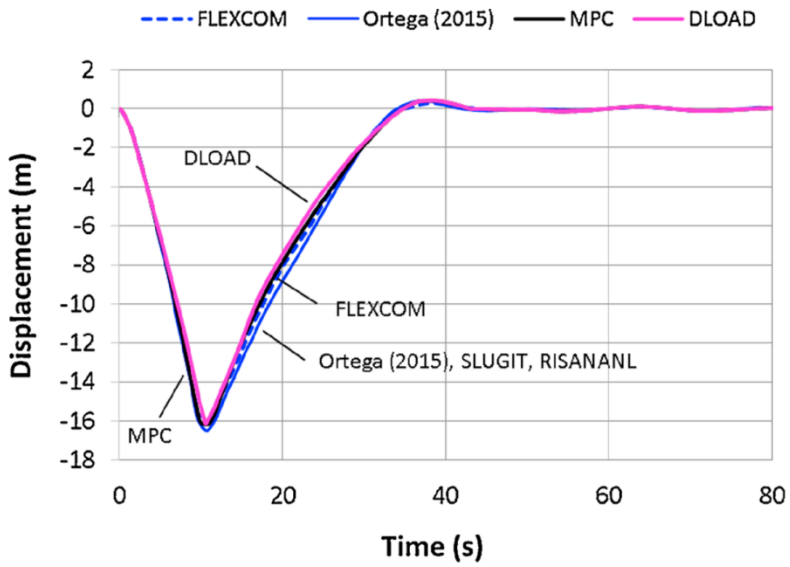

Figure 11-11. Horizontal oscillation of the point lifted by ramp load.

In the third step, the performance of DLOAD and MPC interfaces were verified against FLEXCOM using a single moving slug with the same characteristics given in Table 11-2. However, the slug frequency has been adjusted to allow only one slug travel over the full length of the SCR. This single slug enters from the anchored end of the riser and exits from the vessel end. This verification process was conducted using the global SCR configuration given in Figure 11-12, which was used for riser-seabed interaction as well. For simplicity, the seabed was modeled as a rigid flat surface, and the horizontal oscillation of points (A, B, and C) corresponding to the TDZ, catenary mid part, and the hang-off area of the SCR were extracted as time histories. Figure 11-12 (a, b, and c) shows the comparison of the FLEXCOM, DLOAD, and MPC interfaces. A great agreement was observed between FLEXCOM and MPC having a remarkable offset with DLOAD. This accuracy offset is properly showing the inability of the DLOAD interface in capturing the momentum and inertia effects of the moving slug. The three steps verification process well proved the reliable performance of the MPC model and demon- strated the accuracy offset of the simplified approach using the DLOAD interface.

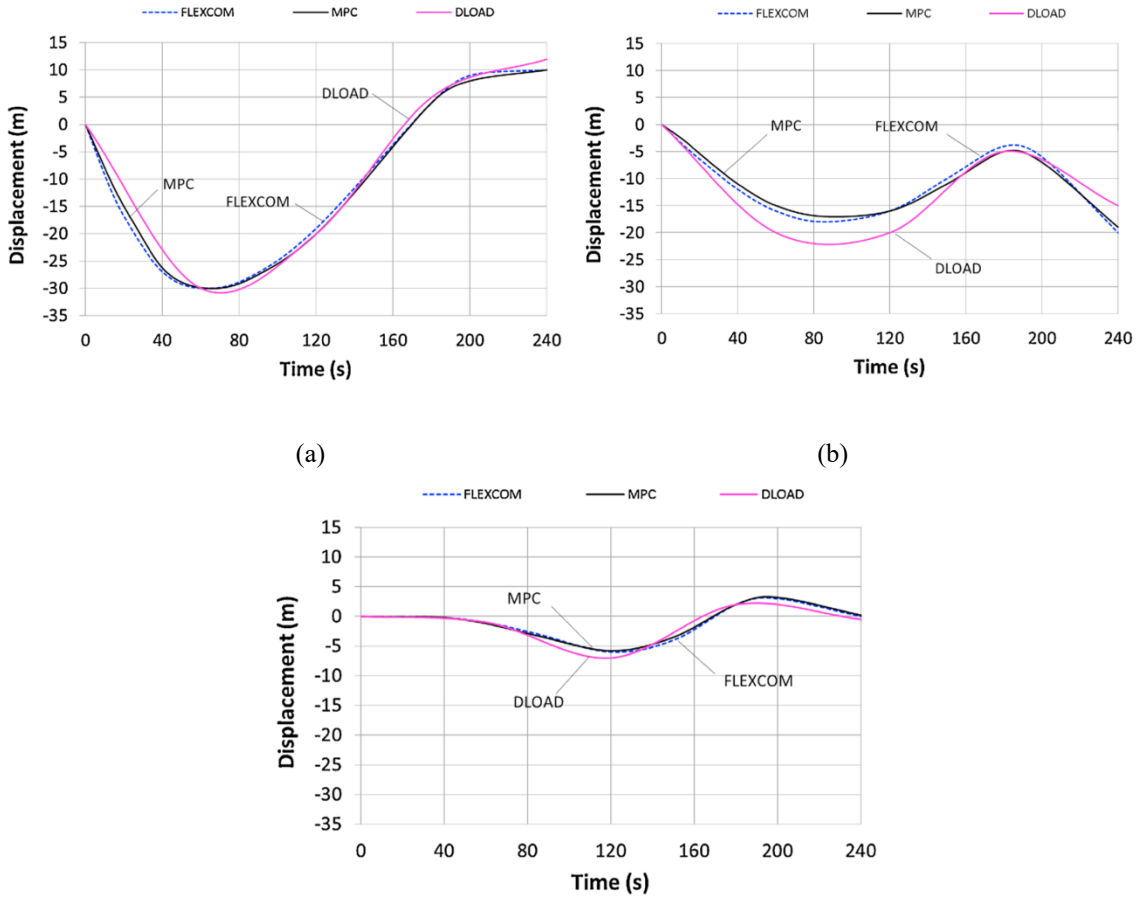

Figure 11-12. SCR oscillation by MPC, DLOAD, and FLEXCOM under a single moving slug.

It is worth mentioning that besides the advantages of MPC interface in capturing all of the effects of the slugging, the interface was found to have some level of mesh sensitivity. The element size or the spacing of the nodes in the linear B21 beam element was needed to be sufficiently fine for enhanced continuity. The variation of the momentum where the beam direction is changed at nodes may result in unexpected vibrations. This was overcome by the proper definition of the time increments. However, further works are needed on the element type and integration schemes to limit the mesh dependency of MPC approach.

11.6. Modelling of Seabed Soil

The nonlinear hysteretic riser-seabed interaction model was adopted from Randolph and Quiggin (2009) (R-Q model) which is a popular model in the literature. The model can automatically capture the cyclic soil stiffness degradation, soil suction, and gradual riser pe- netration into the seabed, while the SCR is oscillating in the TDZ. The R-Q model uses a combination of hyperbolic and exponential functions within four main episodes of riser motions: (a) initial penetration, (b) uplift, (c) break out, and (d) re-penetration (see Figure 11-13, Randolph and Quiggin, 2009). Further details of the model including the governing equations and selection of the model parameters can be found in the original paper (i.e., Randolph and Quiggin, 2009).

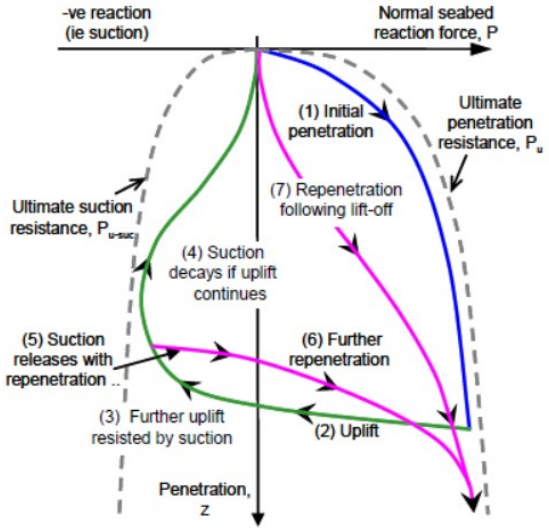

Figure 11-13. R-Q riser-soil interaction model showing different motion episodes (Randolph and Quiggin, 2009).

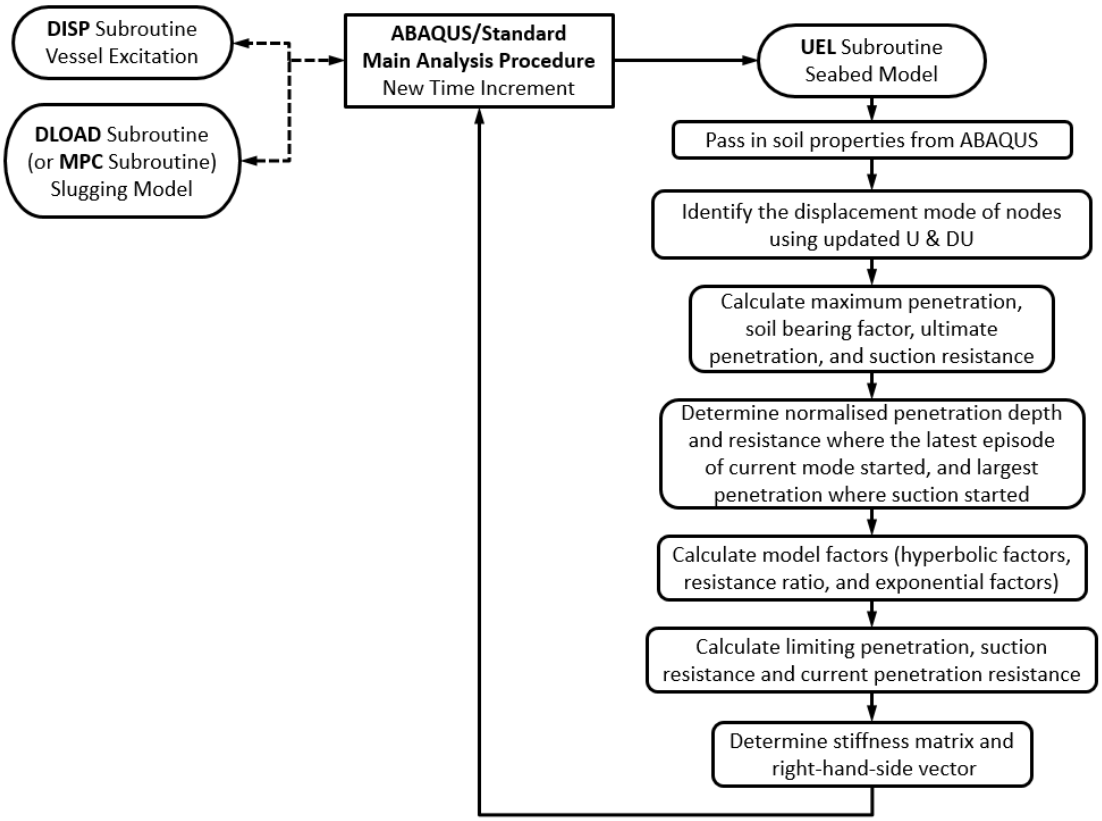

Figure 11-14. UEL subroutine internal flowchart.

In this study, the R-Q model was incorporated using a verified user-defined element (UEL) developed by Shiri and Randolph and integrated with MPC and DLOAD interfaces in ABAQUS. Figure 11-14 illustrates the analysis flowchart of UEL subroutine implementing the nonlinear riser- seabed interaction to the global riser model.

Table 11-3. Default parameters of R-Q soil models (Randolph and Quiggin, 2009).

Parameter	Symbol	Value	Unit
Mudline shear strength	s_{u0}	0.65	kPa
Shear strength gradient	ρ	1.5	kPa/m
Power law parameter	a	6	-
Power law parameter	b	0.25	-
Normalized maximum stiffness	K_{max}	200	-
Suction ratio	f_{suc}	0.3	-
Suction decay parameter	λ_{suc}	0.5	-
Re-penetration parameter	λ_{rep}	0.5	-

Table 11-3 gives the key model parameters that have been recommended by Randolph and Quiggin and were used in the current study.

11.7. Modeling of wave-induced vessel motions

To simulate the wave and current-induced vessel motions a verified user-defined subroutine (DISP) was adopted to test a series of regular waves characterized by wave height, wave period, and the probability of occur- rence. The subroutine was originally developed by Shiri and Randolph to simulate the wave frequency motions and further developed by Shiri to model the current-induced low-frequency vessel motions.

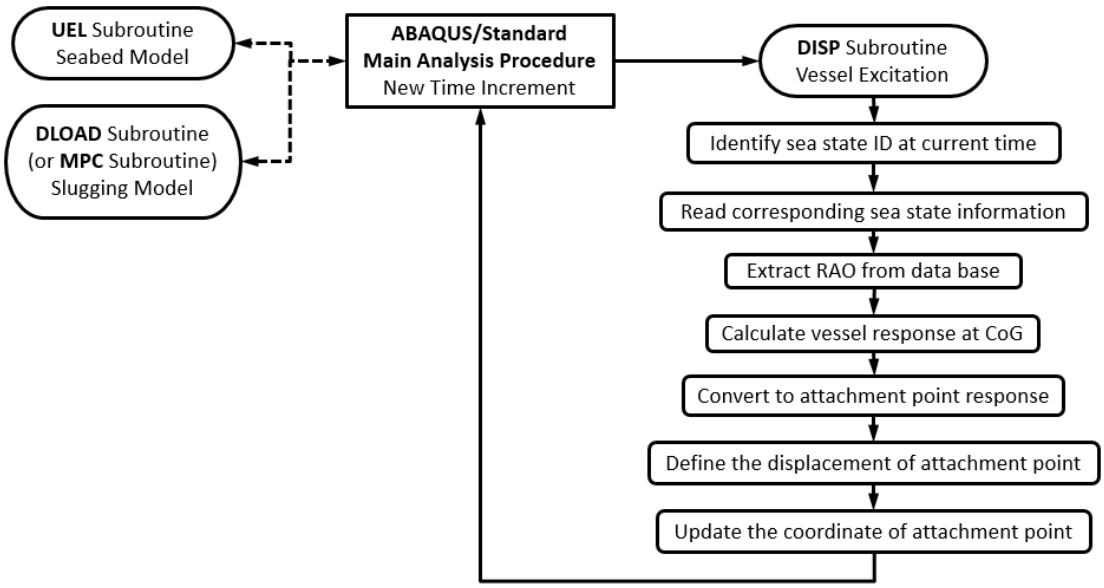

Figure 11-15. DISP subroutine flowchart.

Figure 11-15 shows the procedure followed by the subroutine to update the vessel position under the defined environmental loads in every time increment.

11.8. Nodal seabed response to slug and wave-induced oscillations

Figure 11-16 shows the cyclic penetration-resistance response of node 380 in proximity of the touchdown point. The plots (a) and (b) illustrate the slug-induced oscillation by DLOAD and MPC interfaces, respectively, that have been provided by trails of slugs characterized in Table 11-2. The plot (c) shows the nodal response to a wave-induced oscillation that has been created by applying a single cyclic surge motion with an arbitrary amplitude of 15m and period of 11.5 s using the DISP subroutine. The characteristics of the soil model were provided earlier in Table 11-3. The overall performance of the current model is in strong agreement with the published experimental and numerical works (Randolph and Quiggin, 2009; Shiri and Randolph, 2010) (see Figure 11-17). The cyclic soil stiffness degradation, suction force mobilization during the riser uplift, and the gradual

penetration of the riser into the seabed due to the slug-induced oscillations have been well simulated.

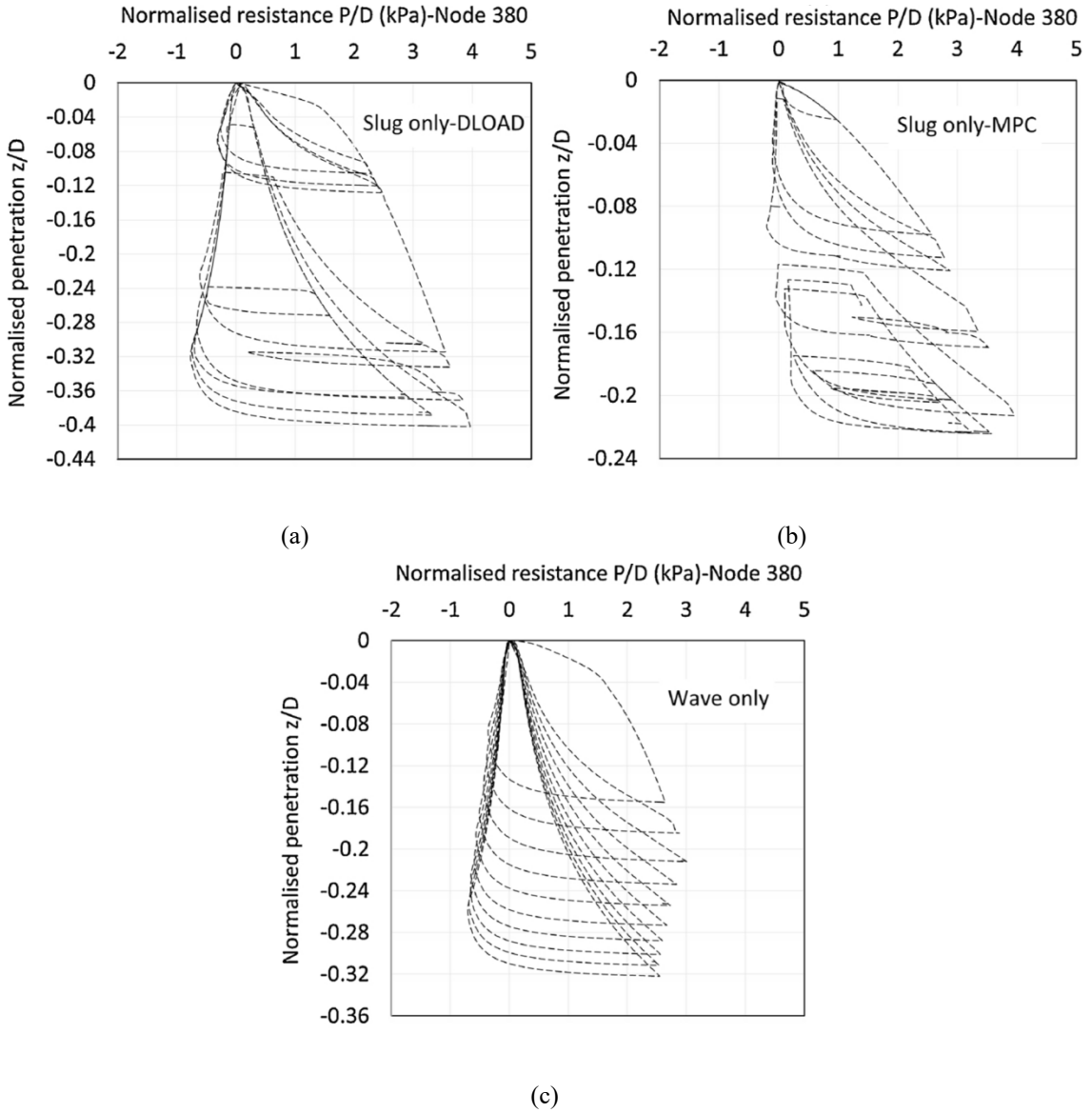

Figure 11-16. A sample of nodal load-penetration responses under slug-induced oscillations using simplified DLOAD interface.

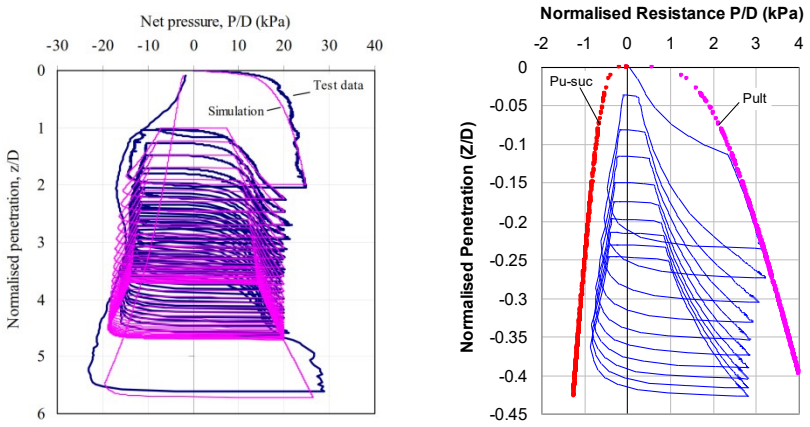

Figure 11-17. Simulation of cyclic soil response using R-Q model, (left, Randolph and Quiggin, 2009;, right, Shiri and Randolph, 2010).

These sample results contribute significantly to fulfilling of the key objectives of the current research work. First, the plots (a) and (b) show the high influence of slug-induced oscillations on seabed response that causes gradual embedment of the SCR into the seabed. The magnitude of penetration is significant in comparison with the wave-induced oscillations shown is a plot (c). This penetration further contributes to the understanding of the variation of the catenary profile, the resultant cross-sectional stress distribution, and consequently the fatigue life. Second, the different magnitude of SCR penetration predicted by MPC and DLOAD interfaces in plots (a) and (b) shows the importance of the momentum and inertial effects of the riser slugging that may have a significant impact on ultimate penetration depth. For the analyses ex- pecting high accuracy results, the DLOAD interface is not recommended for modeling the riser slugging. Therefore, the DLOAD interface was no longer used in this chapter.

11.9. Global riser response to the slug and wave-induced oscillations

Proving the significant contribution of the slug-induced vibrations to modelling the SCR penetration into the real seabed, it was essential to examine the extent of this important aspect regarding riser structural response and its interaction with the wave-induced oscillations. A comprehensive parametric study was conducted to investigate the pure slugging oscillations and also the combined wave/slug oscillations. In two rounds, the key slug characteristics and the seabed model para- meters were examined one at a time. Then the results were compared in linear elastic and the nonlinear hysteretic seabed. It is challenging to determine the magnitude of elastic soil stiffness that is equal to the nonlinear hysteretic model. However, as per the explanations provided by Randolph et al., a soil stiffness of 300 kPa was used to represent the elastic seabed equal to the nonlinear seabed defined in Table 11-3.

Table 11-4 and Table 11-5 show the summaries of conducted parametric studies containing 22 case studies (CS-1 to CS-22). The first twelve cases (CS-1 to CS-12) examine the variation of slug characteristics, and the remaining ten case studies (CS-13 to CS-22) investigate the various soil model parameters.

Table 11-4. The first round of parametric study to investigate the effect of slug parameters.

Case study	Input slug model parameter					
	ρ_{slug} (kg/m^3)	ρ_{gas} (kg/m^3)	v_{slug} (m/s)	L_{slug} (m)	f_{slug} (/hr)	Seabed (E/N)
CS-1	D	D	D	D	D	E
CS-2	D	D	D	D	D	N
CS-3	700	D	D	D	D	E
CS-4	700	D	D	D	D	N
CS-5	D	150	D	D	D	E
CS-6	D	150	D	D	D	N
CS-7	D	D	25	D	D	E
CS-8	D	D	25	D	D	N
CS-9	D	D	D	50	D	E
CS-10	D	D	D	50	D	N
CS-11	D	D	D	D	100	E
CS-12	D	D	D	D	100	N
Note	D refers to "Default" values for slug model as described in Table 11-2. From CS-1 to CS-12, soil parameters were adopted from Table 11-3.					

Table 11-5. The second round of parametric study to investigate the effect R-Q seabed interaction model parameters.

Case study	Input soil model parameters				
	s_u	ρ	f_{suc}	λ_{suc}	λ_{rep}
CS-13	0.35	D	D	D	D
CS-14	0.95	D	D	D	D
CS-15	D	0.5	D	D	D
CS-16	D	1.0	D	D	D
CS-17	D	D	0.5	D	D
CS-18	D	D	1	D	D
CS-19	D	D	D	0.2	D
CS-20	D	D	D	1.0	D
CS-21	D	D	D	D	0.2
CS-22	D	D	D	D	0.8
Note	D refers to "Default" values for non-linear soil model as described in Table 11-3. From CS-13 to CS-22, slug parameters in Table 11-2 were adopted for slug model.				

It is noteworthy that the cross-sectional von Mises stress variation is a key parameter in the calculation of SCR fatigue. The von Mises is also mainly governed by variation of the bending moment, which, in turn, is the accumulation of the area under the shear force distribution. The shear force is governed by the riser-seabed contact stress, which directly depends on the seabed soil stiffness. Therefore, the riser profile in the seabed, shear force, bending moment distribution, and von Mises stress variation were selected as the key outputs from the conducted analyses. Also, to further focus on the influence of seabed nonlinearity on fatigue instead of an accurate estimation of fatigue life, only a single regular wave with a wave a height of 11.0m and a period of 11.5 s was applied by ten cycles in all case studies. For a full fatigue analysis, the DISP subroutine is capable of defining and applying a full range of wave scatter diagram with the desired wave hierarchy. This capability was not used in the current study. Due to a large amount of the output results extracted from the conducted parametric study, only samples of results were presented in this chapter to report the main findings of the study effectively.

11.9.1.Slug-induced oscillation profiles

The catenary profile of the SCR plays a vital rule in its structural response to external and internal loads. A close investigation of the riser profile provides valuable insight into its structural response to the slug- induce oscillations. The current study showed that the slug-induced riser oscillations results in a progressive penetration into the nonlinear hysteretic seabed, ending up with an irregular ultimate riser profile (see Figure 11-18, CS-2). The ultimate profile will be completely different from the elastic seabed, where the displacements are returned while the slug is moving on and the riser profile does not change

over the time (reference line-1: z / D ≈ 0.028, in Figure 11-18 (a)). The individual points P1 to P5 in the proximity of the touchdown point (Region A) and the anchored end (Region B) are referring to the key geometrical points in the riser profile. Also, Figure 11-18 (b) shows that the slug-induced cyclic oscillation amplitude is reduced, while the SCR is penetrating into the seabed. The magnitude of reduction depends on the slug characteristics and the soil parameters. This shows that the seabed model and the riser catenary profile are cyclically stabilized over time.

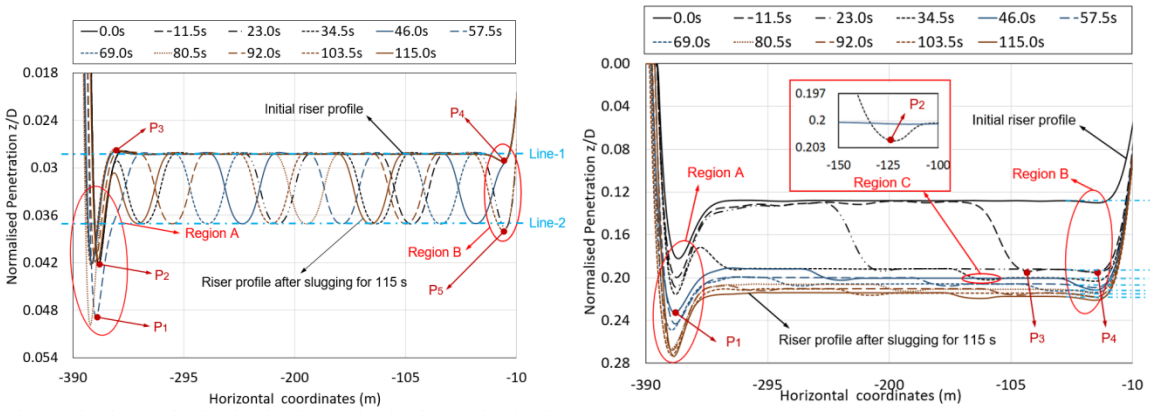

(a) CS-1 (b) CS-2

Figure 11-18. Slug-induced oscillation profiles in elastic and nonlinear hysteretic seabeds.

A similar trend has been reported in the literature for the cases of wave-induced oscillations (Shiri and Randolph, 2010; Clukey et al., 2017; Dong and Shiri, 2018). The touchdown point was also found to move slightly towards the vessel during the slugging cycles. The variation of the ultimate profile and migration of the touchdown point under the slug cycles

are expected to affect the structural response and the ultimate fatigue life that will be discussed later in this chapter.

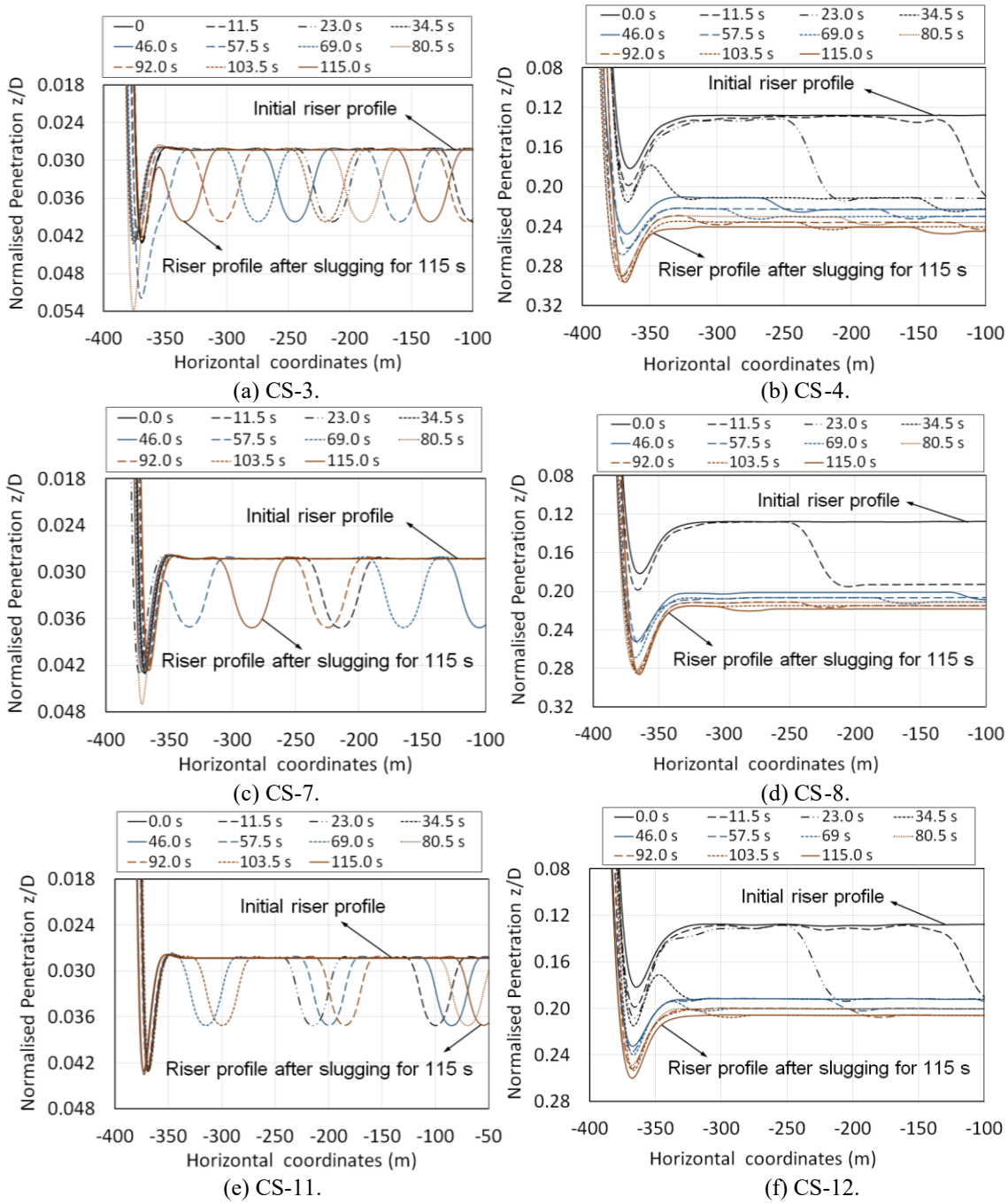

Figure 11-19. Influence of slug parameters on riser profile in elastic and nonlinear hysteretic seabeds.

Further comparative examples from the first round of the para- metric study are shown in Figure 11-19, where the oscillation profile in linear elastic and nonlinear hysteretic seabed were studied that adjusted slug characteristics one at a time (i.e., slug density, velocity, and frequency).

As shown in Figure 11-19 (a) and (b), increasing the slug density (from 600 kg/m^3 in CS-1 to 750 kg/m^3 in CS-3) may result in larger oscillation amplitude and a deeper embedment both in linear elastic and nonlinear seabed (e.g., the bottom point in elastic seabed, increased from 0.050 to 0.054 at 103.5s; the same point in R-Q seabed increased from 0.192 to 0.212). Increasing the slug velocity (from 10 m/s in CS-1 to 25 m/s in CS-7) showed almost no impact on oscillation amplitude in the elastic seabed. Only a slight decrease was observed in oscillation amplitude after cycle No. 10 (time 103.5 s in Figure 11-19 (c)). In the case of the R-Q seabed, increasing the velocity caused a longer portion of the riser on the seabed to penetrate further (i.e., the normalized penetration at the bottom point increased from 0.231 (Figure 11-19 (a)) to 0.249 (Figure 11-19 (d)) at 46.0 s). The slug frequency showed a significant influence on oscillation patterns but no impact on penetration depth. The slug frequency in CS-11 was set to 100 /hr, resulting in a new slug being entered into the SCR from the anchored end every 36 s. Compared with the frequency of 180 /hr in CS-1, larger oscillation distances were obtained within the same range of oscillation amplitudes (Figure 11-19 (f)). In the case of the nonlinear hysteretic seabed (CS-12), fewer slugs travelled with lower slug frequency during the same period. Therefore, less normalized penetration was achieved at the final bottom point (see Figure 11-19 (f)). Overall, the slug density was found to be the most influential parameter

affecting the SCR oscillation profile, penetration depth, and consequently the variation of the stress distribution along the riser.

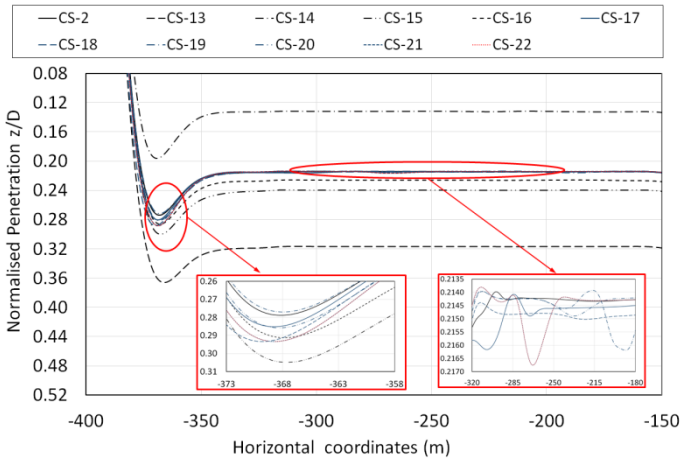

Figure 11-20. Ultimate riser profiles from CS-13 to CS-22.

Figure 11-20 shows the ultimate cyclic SCR profiles in the R-Q seabed obtained from the second round of the parametric study (CS-13 to CS-22), where the riser profile was studied by changing the R-Q model parameters one at a time. For these series of analyses, the default slug parameters were selected from Table 11-2.

Overall, it was observed that the mudline undrained shear strength (s_{u0}) is the most influential parameter in achieving the maximum slug- induced penetration. Increasing the mudline shear from 0.35 kPa in CS-13 to 0.95 kPa in CS-14, the final normalized penetration at the bottom point was decreased by 46% (dropped from 0.366 to 0.196 in Figure 11-20). This is more significant in the initial normalized penetration in the middle region, where it was dropped by about 65% from 0.220 to 0.079. The same trend with less intensity was observed by changing the undrained shear strength gradient (ρ), where

increasing its magnitude from 0.5 kPa/m in CS-15 to 1.0 kPa/m in CS-16 resulted in 4.7% re- ductions in the ultimate penetration amplitude. The suction ratio (f_{suc}) and suction decay parameter (λ_{suc}) control the magnitude of the suction force mobilization and decay during the uplift and re-penetration episodes. It was observed that both of these parameters did affect the slug- induced penetration and oscillation pattern in different orders. When the suction ratio was increased from the default magnitude to 0.5 in CS- 17, a larger ultimate embedment was achieved at the bottom point of the riser ($z / D \approx 0.288$ in CS-18, see Figure 11-20). Increasing the suction decay parameter from 0.2 in CS-19 to 1.0 in CS-20, the normalised ultimate penetration at the bottom point was increased by 3.6% ($z / D \approx 0.27$ in CS-19 and ≈ 0.28 in CS-20). Also, increasing the value of the re-penetration offset parameter (λ_{rep}) was found to deepen the ultimate slug-induced embedment. Changing this parameter from 0.2 in CS-21 to 0.8 in CS-22 caused a 7% increase in normalised ultimate penetration at bottom point ($z / D \approx 0.27$ in CS-21 and ≈ 0.29 in CS-22, see Figure 11-20). Overall, these results emphasize the significant impact of the seabed model parameters on the structural response of slugging riser. The default values of the model parameters have been recommended by Randolph and Quiggin. However, care should be taken when the site- specific parameters are defined. Further developments seem necessary to improve the accuracy of the surficial site investigation in deep waters for proper selection of the seabed model parameters and a reliable SCR design.

11.9.2.Slug-induced structural response

It was explained earlier in this chapter that the shear force, bending moment, and von Mises stress distribution along the slugging SCR are the key structural outputs that can be used to investigate the nonlinear hysteretic riser-seabed interaction. The shear force in the TDZ

is the riser response to the riser-seabed contact pressure, which is governed by the seabed soil stiffness. The gradient of the shear force over the touchdown point migration amplitude determines the bending moment distribution, which is the most influential contributor to the von Mises stress range and consequently the accumulated fatigue damage. Examples of these structural outputs from two rounds of the parametric study are presented and discussed here. First, the influence of key slug characteristics, and second, the effect of R-Q seabed model parameters is investigated to show how the nonlinear seabed model affects the structural response of the slugging riser.

11.9.2.1. Influence of key slug characteristics

The influence of slug-parameters on the shear force, bending moment, and von Mises stress distribution were examined through CS-1 to CS-12 both in the elastic and R-Q seabed, and the results are presented in Figure 11-21.

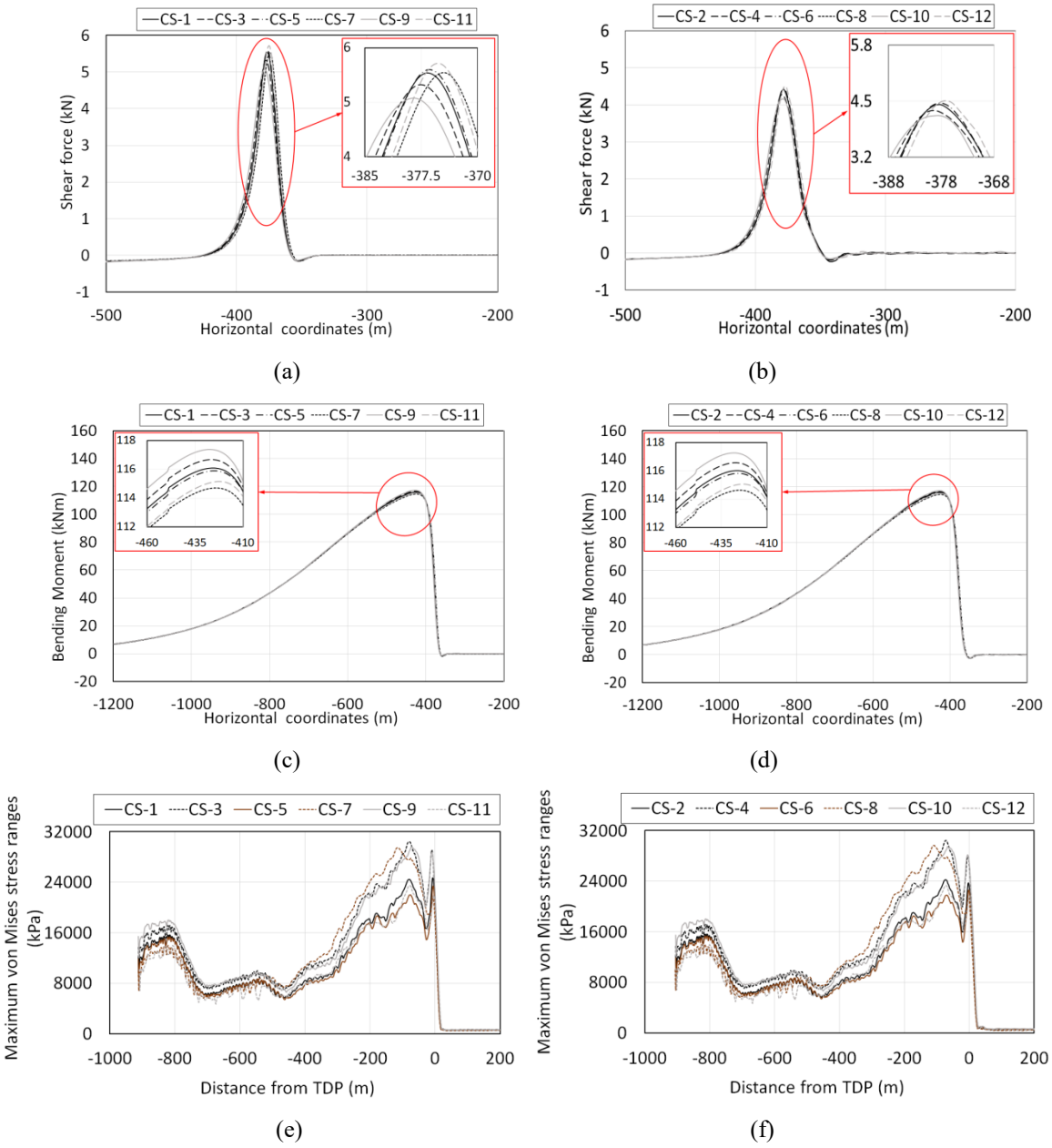

Figure 11-21. Influence of slug parameters on the stationary shear force, bending moment, and von Mises stress in the elastic and nonlinear hysteretic seabeds.

The maximum magnitude of the shear force on the elastic seabed with different slug parameters was fluctuated by about 12.17% between 5.066 kN in CS-9 and 5.713 kN in CS-11. In a nonlinear hysteretic seabed, this variation range was limited to about 8.5%,

where the shear force changed from a peak value of 4.156 kN in CS-10 to 4.508 kN in CS-12. The lower impact observed in nonlinear seabed is because of gradual SCR embedment into the seabed and the relaxation of the contact pressure and stress distribution. However, regarding the shear force, these ranges of the impacts are considered significant.

The influence of slug parameters on stationary bending moment distribution in linear elastic and nonlinear hysteretic seabed is shown in Figure 11-21 (b and c). Different slug parameters have caused the peak bending moment to change between 114.708 kNm in CS-7 to 117.368 kNm in CS-9. A similar trend was observed in the nonlinear hysteretic seabed that shows the meaningful influence of slug para- meters on riser structural response.

The variation range of the von Mises stress over the load cycles is the main parameter in the calculation of SCR fatigue life. The axial tension and the bending moment are the key contributors to the von Mises stress in SCR. However, since the variation of the axial tension over the load cycles is negligible, the oscillation of the bending stress is the most influential stress component in fatigue calculations. Figure 11-21 (e and f) shows the influence of slug parameters on the distribution of von Mises stress on linear elastic and the nonlinear hysteretic seabed (CS-1 to CS-12). The slug characteristics show a significant impact on von Mises stress distribution, particularly the slug density (30343.576 kPa in CS-3 with a distance of 85.47 m from TDP). Also, the peak stress location may be significantly affected by slug characteristics. However, similar to the bending moment, only a minor difference was observed between the elastic and R-Q seabed. As expected, the stationary von Mises stress was governed by catenary shape and not the seabed stiffness or the seabed soil model. This will be further examined in the next section.

11.9.2.2. Influence of nonlinear hysteretic seabed model parameters

The effect of R-Q model parameters on the structural response of the slugging risers was examined through CS-13 to CS-22. As illustrated in Figure 11-22 (a), the summary of the study cases from CS-13 to CS-22 shows that the nonlinear hysteretic soil model parameters have a significant influence on the peak magnitude of the shear force and almost no impact on the stationary bending moment and von Mises stress.

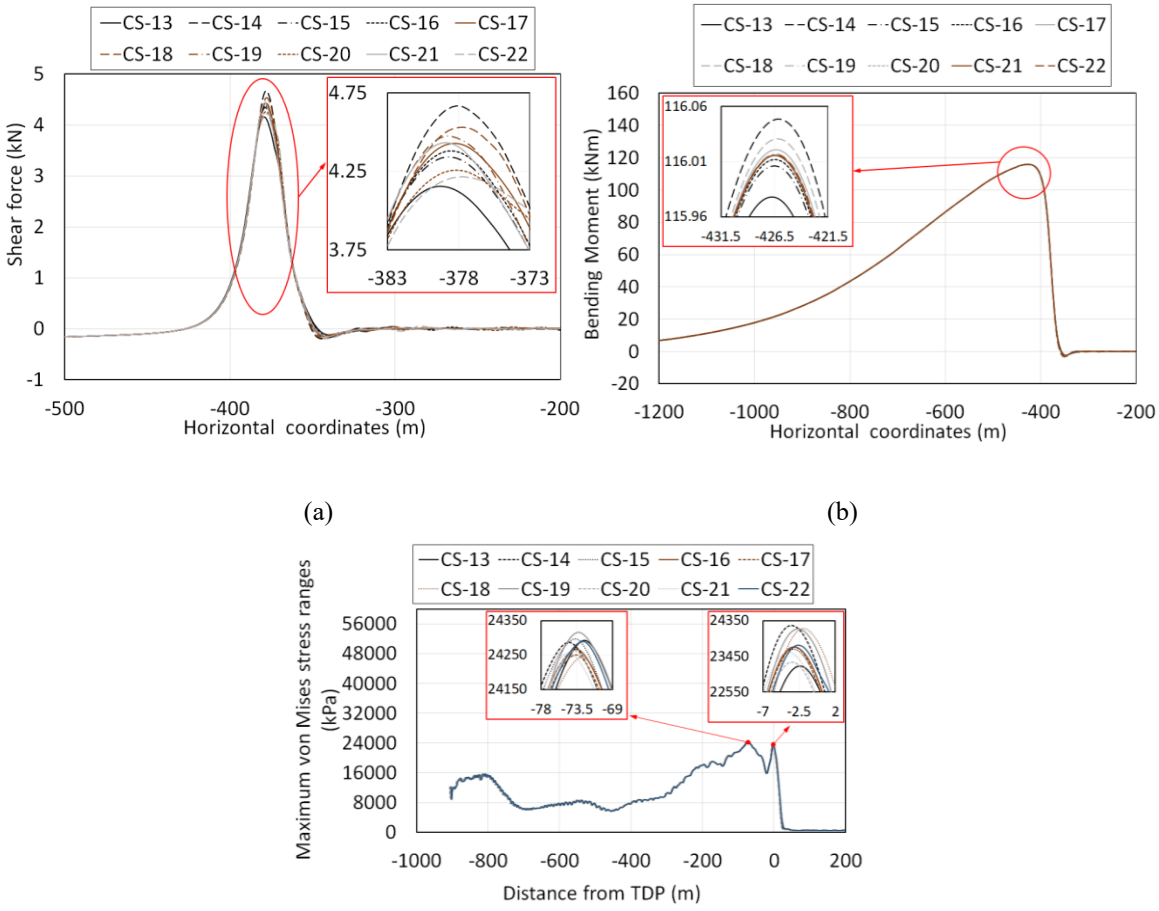

(a) (b)

(c)

Figure 11-22. Influence of R-Q model parameters on the stationary shear force, bending moment, and von Mises stress.

It should be noted that the cyclic bending moment is different from the stationary bending moment. The stationary bending moment does not influence fatigue damage (as shown in Figure 11-22), but the cyclic bending moment is the key parameter in the calculation of the von Mises stress variation range and consequently the fatigue damage. The stationary bending moment is governed by the catenary shape of the SCR, while the cyclic bending stress is a complex product of the cyclic shear force and the touchdown point migration amplitude. Therefore, the seabed model parameters have a significant influence on cyclic stresses and fatigue life of the SCR. The effect of seabed model parameters on the nodal von Mises stress variation will be further investigated within the next section, where the wave-induced oscillations will be shown to also contribute to the riser response.

11.9.3.The combined influence of wave and slug-induced oscillations

It is important to further verify the obtained results through the simulation of more realistic load conditions, where the effect of slugging and wave induced motions are co-existing. The default high-frequency vessel motions and slug-induced oscillations were combined in order to investigate their integrated nodal effects. The touchdown point oscillations have a direct relationship with the gradual SCR embedment into the seabed. Therefore, using the predefined parameters in CS-2, the horizontal and vertical oscillations, shear force, bending moment, and maximum von Mises stress history were obtained and illustrated (see Figure 11-23).

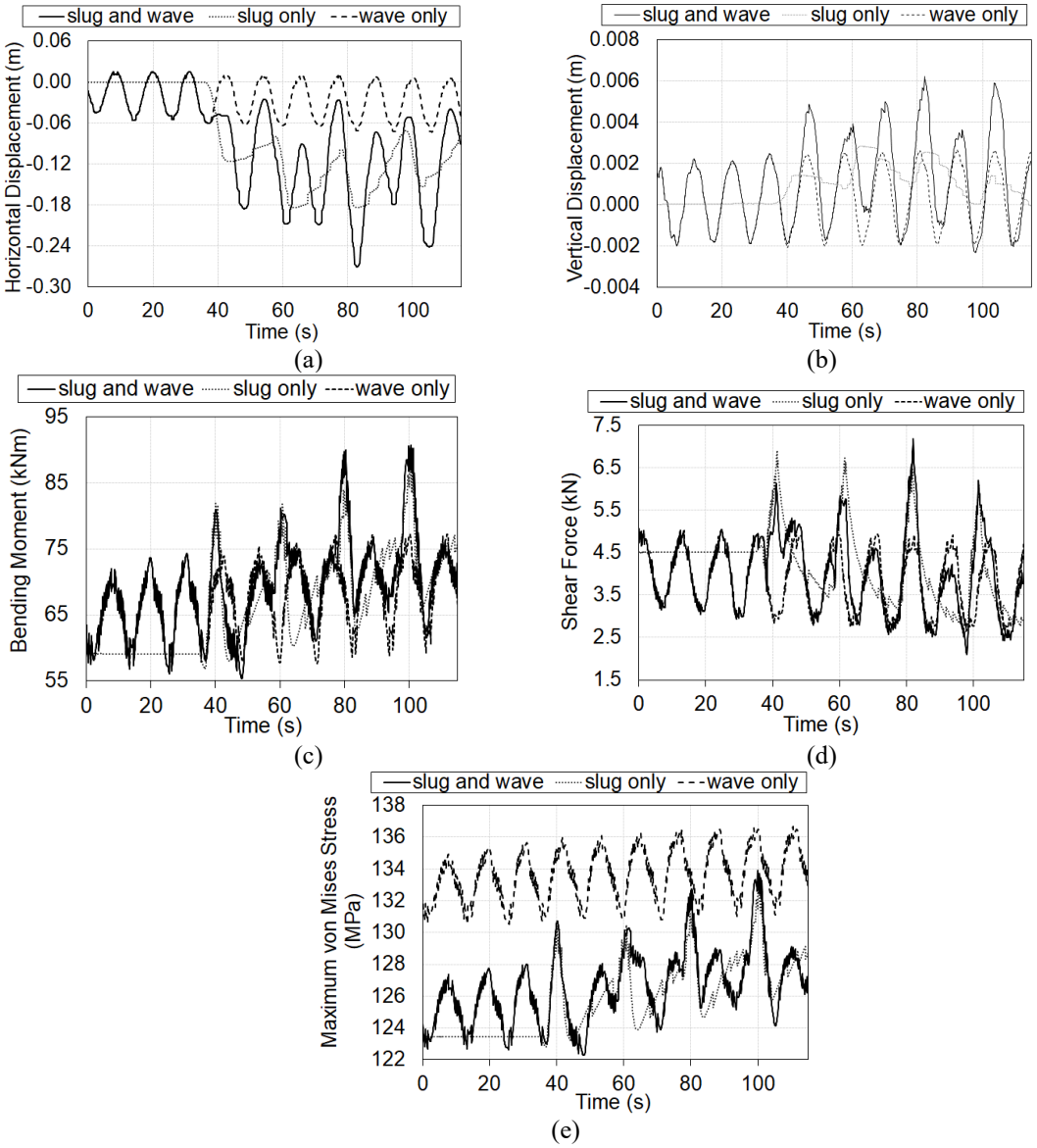

Figure 11-23. Time history of touchdown point oscillation, shear force, bending moment, and von Mises stress variation.

Several important trends were observed showing the significance of the combined wave and slug-induced oscillations. As shown in Figure 11-23 (a and b) the wave and slug-induced oscillation amplitudes in a nonlinear hysteretic seabed may be summed up or subtracted irregularly, depending on the oscillation phase angles. Figure 11-23 (c) shows

that the time history of the shear force at the touchdown point may reach a high value of 7.18 kN when the effects of the slugging and high-frequency motions were combined at particular time frames (e.g., at 85 s). The peak shear forces over the 5.5 kN occur whenever the slug is reaching the node and drops under the 3.5 kN after passing through the node. Figure 11-23 (d) illustrates the bending moment oscillation under the slugging, wave action and combined wave/slug loading in the R-Q seabed. A sharp increase in bending moment was observed when the wave-induced oscillation met the slug-induced oscillation in a same oscillation phase angle. The resultant bending moment at the touch- down point may be mitigated depending on the varying phase angle difference. This shows that the occurrence of the maximum magnitude of the bending moment depends on wave and slug characteristics, such as the wave period, wave height, slug velocity, slug frequency, etc. The time history of the von Mises stress variation at the touchdown point in the nonlinear seabed (Figure 11-23) shows the high impact of slugging when it is combined with wave action. A peak von Mises stress of 133.72 MPa was observed when the wave and slug were in-phase at about 100s. Overall, the comparisons showed that the contribution of the slug-induced stresses and its combination with wave action could be significantly important in cross-sectional stress evaluation of the SCR in a nonlinear hysteretic seabed.

11.10. Conclusion

The influence of complex nonlinear hysteretic riser-seabed interac- tion on slug-induced oscillations of SCRs and the resultant structural response was comprehensively investigated in this study. An advanced user interface was developed, verified, and incorporated into ABAQUS in order to model SCR slugging. Pre-developed user subroutines were used to model the nonlinear hysteretic riser-seabed interaction and the

vessel motions. For the first time, the global model enabled simulta- neous modeling of the wave and slug-induced oscillations in nonlinear hysteretic seabed conditions. The comprehensive parametric study was conducted in two rounds. First, to examine the influence of various slug characteristics, and second, the effect of different nonlinear hysteretic seabed model parameters on slug-induced, wave-induced, and com- bined wave/slug induced oscillations of the SCR.

Several significant conclusions were determined:

• The cyclic soil stiffness degradation and the gradual embedment of the SCR into the seabed have a significant impact on slug-induced stress oscillations and the resultant stresses in the TDZ.

• The slug-induced oscillations contribute to the gradual trench creation underneath the riser. The contribution may further be significant if combined with wave-induced oscillations.

• Stress oscillation amplitude in the nonlinear hysteretic seabed is less severe than the linear elastic seabed and is cyclically decreased leading to further relaxation.

• The slug-induced oscillations may be combined with high-frequency vessel motions in opposite ways. In most of the cases, more severe responses were obtained by the combined impact of the wave and slug. Therefore, from a design perspective, it would be more conservative to add up the contribution of the slugging and wave frequency motions.

• The slug-induced fatigue damage, in reality, is most likely to be less than the conventional elastic seabed with the observations made in the nonlinear hysteric seabed. Therefore, representing the seabed with linear elastic springs is a conservative approach in SCR design.

• The MPC approach was found to be a strong framework for advanced research purposes, where advanced users wish to have full access to the slug and seabed soil models; the possibility that is not commonly provided by commercial software. However, the following limitations were observed in this study that may cause the MCP approach to be computationally expensive and ineffective for day-to-day engineering practice:

• MPC can be cumbersome and redundant when a large number of master nodes are needed to be incrementally defined for each slave or mass node. This will be much more challenging when the moving path is highly nonlinear and is continuously oscillating. An extensive amount of advanced programming work is needed to address all of these challenges.

• The MPC interface is mesh dependent. The size and spacing of mass elements and also the size of the pipe section should be fine enough to satisfy the continuum. The generation of momentum forces due to the sudden direction change in each segment of the linear path may cause spurious vibrations. The time step may need repetitive adjustments to eliminate the effect of these dependencies.

• ABAQUS assumes the same array of derivatives for transferring the loads from slaves to master nodes and for the elimination of slaves from the stiffness matrix. This approach is appropriate for many of the constraints but may cause non-quadratic convergence that would necessitate reducing the time steps.

It is worth mentioning, in this study, the wave-induced vessel motions were simply created with a single regular wave to further focus on riser-seabed interaction instead of comprehensive fatigue analysis. For future works, it is recommended that the obtained results be examined through a full range of fatigue analysis using stochastic wave spectra.

Also, the interaction of the slugging SCR with the seawater surrounding the riser in the TDZ and its influence on seabed soil softening and trench formation are the areas that need new explorations during the future studies.

11.11. Acknowledgment

The authors gratefully acknowledge the financial support of this research by Research and Development Corporation (RDC) (now Innovate NL) through Ignite funding program and the Memorial University of Newfoundland through VP start-up funding support.

References

ABAQUS/Standard User's Manual, 2018.

Aubeny, C.P., Biscontin, G., 2009. Seafloor–riser interaction model, Int. J. Geomech. 9, pp. 133–141.

Bordalo, S.N., Morooka, C.K., Cavalcante, C.C.P., 2008. Whipping phenomenon caused by the internal flow momentum on the catenary risers of offshore petroleum fields, Proceedings of the ASME 27th International Conference on Offshore Mechanics and Arctic Engineering.

Bordalo, S.N., Morooka, C.K., 2018. Slug flow-induced oscillations on subsea petroleum pipelines, J. Petrol. Sci. Eng. (2018) (In press, accepted manuscript).

Bridge, C., Laver, K., Clukey, E., Evans, T., 2004. Steel catenary riser touchdown point vertical interaction models, Offshore Technology Conference, OTC16628.

Bridge, C., Howells, H., 2007. Observations and modeling of steel catenary riser trenches, 17th International Offshore and Polar Engineering Conference.

Campbell, M., 1999. The complexities of fatigue analysis for deepwater risers, Proceedings of the 2nd International Deepwater Pipeline Technology Conference.

Chatjigeorgiou, I.K., 2017. Hydroelastic response of marine risers subjected to internal slug-flow, Appl. Ocean Res. 62, pp. 1–17.

Chatjigeorgiou, I.K., 2010a. Three dimensional nonlinear dynamics of submerged, extensible catenary pipes conveying fluid and subjected to end-imposed excitations, Int. J. Non-Linear Mech. 45, pp. 667–680.

Chatjigeorgiou, I.K., 2010b. On the effect of internal flow on vibrating catenary risers in three dimensions, Eng. Struct. 32, pp. 3313–3329.

Clukey, E.C., Aubeny, C.P., Zakeri, A., Randolph, M.F., Sharma, P.P., White, D.J., Sancio, R., Cerkovnik, M., 2017. A perspective on the state of knowledge regarding soil-pipe interaction for SCR fatigue assessments, Offshore Technology Conference.

Dong, X., Shiri, H., 2018. Performance of nonlinear seabed interaction models for steel catenary risers, part I: nodal response, J. Ocean Eng. 154, pp.153–166.

Gundersen, P., Doynov, K., Andersen, T., Haakonsen, R., 2012. Methodology for determining remnant fatigue life of flexible risers subjected to slugging and irregular waves, Proceedings of the ASME 2012 31st Int Conf on Ocean, Offshore and Arctic Engr.

Hardin, B.O., Drnevich, V.P., 1972. Shear modulus and damping in soils: measurement and parameter effects (Terzaghi lecture), J. Soil Mech. Found. Div. 98 (6), pp. 603–624.

Jiao, Y., 2007. Non-Linear Load-Deflection Models for Seafloor Interaction with Steel Catenary Risers, Texas A&M University, College Station, USA, 2007 Master of Science.

Kansao, R., Casanova, E., Blanco, A., Kenyery, F., Rivero, M., 2008. Fatigue life prediction due to slug flow in extra-long submarine gas pipelines, Proceedings of the ASME 2008 27th Int Conf on Offshore Mechanics and Arctic Engr, OMAE2008, pp. 1–8.

Kondner, R.L., 1963. Hyperbolic stress-strain response; Cohesive soils, J. Soil Mech. Found. Div. 89 (1) (1963) 115–143.

Liu, J., Kimiaei, M., Randolph, M., 2016. A new user defined element for nonlinear riser-soil interaction analysis of steel catenary riser systems, ASME 2016 35th International Conference on Ocean, Offshore and Arctic Engineering.

Nakhaee, A., Zhang, J., 2010. Trenching effects on dynamic behavior of a steel catenary riser, Ocean Eng. 37 (2–3), pp. 277–288.

Ortega, A., Rivera, A., Nydal, O.J., Larsen, C.M., 2012. On the dynamic response of flexible risers caused by internal slug flow, Proceedings of the ASME 2012 31st Int Conf on Ocean, Offshore and Arctic Engr, OMAE2012, pp. 1–10.

Ortega, A., Rivera, A., Larsen, C.M., 2013. Flexible riser response induced by combined slug flow and wave loads, Proceedings of the ASME 2013 32nd International Conference on Ocean, Offshore and Arctic Engineering, OMAE2013.

Ortega, A., 2015. Dynamic Response of Flexible Risers Due to Unsteady Slug Flow, Doctoral thesis at NTNU.

Ortega, A., Rivera, A., Larsen, C.M., 2017. Slug flow and waves induced motions in flexible riser, J. Offshore Mech. Arctic Eng. 140 (1) 011703.

Patel, M.H., Seyed, F.B., 1989. Internal flow-induced behavior of flexible risers Eng. Struct. 11 (4), pp. 266–280.

Pollio, A., Mossa, M., 2009. A Comparison between Two Simple Models of a Slug Flow in a Long Flexible Marine Riser, Thesis.

Phifer, E.H., Kopp, F., Swanson, R.C., Allen, D.W., Langner, C.G., 1994. Design and installation of auger steel catenary risers, Offshore Technology Conference, OTC7620.

Randolph, M.F., Quiggin, P., 2009. Non-linear hysteretic seabed model for catenary pipeline contact, 28th International Conference on Ocean, Offshore and Arctic Engineer.

Shiri, H., 2010. Influence of Seabed Response on Fatigue Performance of Steel Catenary Risers in Touchdown Zone, [dissertation] University of Western Australia, 2010.

Shiri, H., Randolph, M.F., 2010. Influence of seabed response on fatigue performance of steel catenary risers in touch don area, 29th International Conference on Ocean, Offshore and Arctic Engineering.

Theti, R., Moros, T., 2001. Soil interaction effects on simple-catenary riser response, Pipes Pipelines Int. 46 (3), pp. 15–24.

Trippit, B., Chee, K.Y., Aizad, S., 2012. Pipeline dynamics with flowing contents in ABAQUS/Standard, 2012 SIMULIA Community Conference.

Zargar, E., Kimiaei, M., 2015. An investigation on existing nonlinear seabed models for riser-fluid-soil interaction studies in steel catenary risers, Proceedings of 3rd Int. Symposium on Frontiers in Offshore Geotechnics, pp. 489–494.

Chapter 12

Conclusions and Recommendations

12.1. Conclusions

The work outlined in this thesis was conducted to enhance the numerical analysis of riser seabed-interaction.

The second section of the thesis (from Chapter 7 to Chapter 11), first, a popular non-linear riser-seabed interaction model is comprehensively examined regarding its nodal and global performance. This work has significant importance in evaluating consistency and the extent of the model and its performance on estimation of SCR fatigue life. And it is crucial in terms of the applicability of the model and has never been accomplished before. In addition, the research work is extended to examine the influence of internal multi-phase flow regimes and vessel motions (velocity and frequencies) on riser dynamics and riser seabed interaction in touchdown zone to fill the knowledge gap in literature.

Through the numerical analyses, it was demonstrated that:

- Some over-conservative assumptions and nodal response violations were found in R-Q model resulting in over-estimation of penetration and suction resistance and consequently the fatigue damage in TDZ. The incapability of the R-Q model in the explicit modeling of the trench formation mandates the use of unusual extreme values for model parameters to create deep trenches.
- The cyclic soil stiffness degradation and the gradual embedment of the SCR into the seabed have a significant impact on slug-induced stress oscillations and the resultant stresses in the TDZ. The R-Q model was found to be an appropriate option for

modelling slug-induced seabed soil degradation in the absence of any slug-specific riser-seabed interaction model.

- The slug-induced oscillations may be combined with high-frequency vessel motions in opposite ways. In most of the cases, more severe responses were obtained by the combined impact of the wave and slug. Therefore, from a design perspective, it would be more conservative to add up the contribution of the slugging and wave frequency motions.
- The slug-induced fatigue damage, in reality, is most likely to be less than the conventional elastic seabed with the observations made in the nonlinear hysteretic seabed. Therefore, representing the seabed with linear elastic springs is a conservative approach in SCR design.

12.2. Recommendations for future study

Some of the potential topics can be extended for further study. Riser-seabed interaction is a complex phenomenon, and a lot of aspects more than the suggestions of this part can be explored.

- Sediments wash-out

  With frequent vibrations of SCR upwards and downwards, together with the wave and currents (or sometimes with vortex), the softened sediments may be flushed out and the geometry of trench can be influenced.

- Non-linear riser-seabed interaction model considering trench geometry

  Considering the evolution of trench formed beneath the riser to better calculate the stress on the riser.

- Fatigue calculation.

- Considering the changes in gas slug (block length, velocity) and liquid slug (density) instead of constant weight/velocity slugs.

Bibliography

ABAQUS/Standard User's Manual, SIMULIA, 2017.

Aubeny, C.P., Biscontin, G., 2009. Seafloor–riser interaction model. Int. J. Geomechanics 9 (3), 133–141.

Aubeny, C.P., Shi, H., Murff, J.D., 2005. Collapse loads for a cylinder embedded in a trench in cohesive soil, Int J. Geomech. 5 (4), pp. 320–325.

Audibert, J.M.E., Nyman, D.J., O'Rourke, T.D., 1984. Differential Ground Movement Effects on Buried Pipelines, in Guidelines for the Seismic Design of Oil and Gas Pipeline Systems. ASCE publication, New York, pp. 150–177.

Barltrop, N.D.P., Adams, A.J., 1991. Dynamics of Fixed Marine Structures. Atkins Oil & Gas Engr. Ltd., Epsom, UK.

Bordalo, S.N., Morooka, C.K., Cavalcante, C.C.P., 2008. Whipping phenomenon caused by the internal flow momentum on the catenary risers of offshore petroleum fields, Proceedings of the ASME 27th International Conference on Offshore Mechanics and Arctic Engineering.

Bordalo, S.N., Morooka, C.K., 2018. Slug flow-induced oscillations on subsea petroleum pipelines, J. Petrol. Sci. Eng. (2018) (In press, accepted manuscript).

Bridge, C.D., Howells, H.A., 2007. Observations and modeling of steel catenary riser trenches. In: 7th Int. Offshore and Polar Engr. Conf. (ISOPE2007), Lisbon, Portugal, pp. 803–813.

Bridge, C.D., Laver, K., Clukey, E., Evans, T., 2004. Steel catenary riser touchdown point vertical interaction models. In: Offshore Technol. Conf. (OTC16628), Houston, Texas, USA.

Campbell, M., 1999. The complexities of fatigue analysis for deepwater risers, Proceedings of the 2nd International Deepwater Pipeline Technology Conference.

Chatjigeorgiou, I.K., 2017. Hydroelastic response of marine risers subjected to internal slug-flow, Appl. Ocean Res. 62, pp. 1–17.

Chatjigeorgiou, I.K., 2010a. Three dimensional nonlinear dynamics of submerged, extensible catenary pipes conveying fluid and subjected to end-imposed excitations, Int. J. Non-Linear Mech. 45, pp. 667–680.

Chatjigeorgiou, I.K., 2010b. On the effect of internal flow on vibrating catenary risers in three dimensions, Eng. Struct. 32, pp. 3313–3329.

Clukey, E.C., Aubeny, C.P., Zakeri, A., Randolph, M.F., Sharma, P.P., White, D.J., Sanico, R., Cerkovnic, M., 2017. A perspective on the state of knowledge regarding soil-pile interaction for SCR fatigue assessments, Proceedings of the Offshore Technology Conference OTC 27564-MS.

Clukey, E., Jacobs, P., Sharma, P.P., 2008. Investigation of riser seafloor interaction using explicit finite element methods. In: Offshore Technol. Conf. (OTC-19432-MS), Houston, USA.

Dong, X., Shiri, H., 2018. Performance of non-linear seabed interaction models for steel catenary risers, part I: nodal response, Ocean Eng. 154, pp. 153–166.

DNV-RP-H103, 2011, Recommended practice for modelling and analysis of marine operations. Oslo, Norway: Det Norske Veritas.

Giertsen, E., Verley, R., Schroder, K., 2004. CARISIMA a catenary riser/soil interaction model for global riser analysis. In: Proceedings of the Int. Conf. On Offshore Mechanics and Arctic Engr. (OMAE2004). Vancouver, BC, Canada, pp. 633–640.

Gundersen, P., Doynov, K., Andersen, T., Haakonsen, R., 2012. Methodology for determining remnant fatigue life of flexible risers subjected to slugging and irregular waves, Proceedings of the ASME 2012 31st Int Conf on Ocean, Offshore and Arctic Engr.

Hardin, B.O., Drnevich, V.P., 1972. Shear modulus and damping in soils: measurement and parameter effects (Terzaghi Lecture). J. Soil Mech. Found Div. 98 (6), 603–624.

Jacob, P., 2005. Planar Investigation of Riser Trench Formation Using Ls-dyna. MMI Engr.

Jiao, Y., 2007. Non-linear Load-deflection Models for Seafloor Interaction with Steel Catenary Risers. Texas A&M University, College Station, USA. Master of Science, 121.

Kansao, R., Casanova, E., Blanco, A., Kenyery, F., Rivero, M., 2008. Fatigue life prediction due to slug flow in extra-long submarine gas pipelines, Proceedings of

the ASME 2008 27th Int Conf on Offshore Mechanics and Arctic Engr, OMAE2008, pp. 1–8.

Kondner, R.L., 1963. Hyperbolic stress-strain response; Cohesive soils, J. Soil Mech. Found. Div. 89 (1) (1963) 115–143.

Lim, F., Gauld, S., 2003. Riser solutions for ultra-deep-water developments. In: Proceedings of 10th Annual India Oil & Gas Symposium, Mumbai, India.

Liu, J., Kimiaei, M., Randolph, M., 2016. A new user defined element for nonlinear riser-soil interaction analysis of steel catenary riser systems, ASME 2016 35th International Conference on Ocean, Offshore and Arctic Engineering.

Maclure, D., Walters, D., 2007. Freestanding Risers in the Gulf of Mexico – a Unique Solution for Challenging Field Development Configurations. 2H Offshore Engr. Ltd.Technical Paper.

Nakhaee, A., Zhang, J., 2008. Effects of the interaction with the seafloor on the fatigue life of a SCR. In: Int. Offshore and Polar Engr. Conf. Vancouver, BC, Canada, pp. 87–93.

Nakhaee, A., Zhang, J., 2010. Trenching effects on dynamic behavior of a steel catenary riser, Ocean Eng. 37 (2–3), pp. 277–288.

OrcaFlex Documentation, Orcina, 2018.

Ortega, A., Rivera, A., Nydal, O.J., Larsen, C.M., 2012. On the dynamic response of flexible risers caused by internal slug flow, Proceedings of the ASME 2012 31st Int Conf on Ocean, Offshore and Arctic Engr, OMAE2012, pp. 1–10.

Ortega, A., Rivera, A., Larsen, C.M., 2013. Flexible riser response induced by combined slug flow and wave loads, Proceedings of the ASME 2013 32nd International Conference on Ocean, Offshore and Arctic Engineering, OMAE2013.

Ortega, A., 2015. Dynamic Response of Flexible Risers Due to Unsteady Slug Flow, Doctoral thesis at NTNU.

Ortega, A., Rivera, A., Larsen, C.M., 2017. Slug flow and waves induced motions in flexible riser, J. Offshore Mech. Arctic Eng. 140 (1) 011703.

Palmgren, A., 1924. Die Lebensdaur von Kugellagern (Life Length of Roller Bearings. In German). Z. Des. Vereines Dtsch. Ingenieure 68 (14), 339–341.

Patel, M.H., Seyed, F.B., 1989. Internal flow-induced behavior of flexible risers Eng. Struct. 11 (4), pp. 266–280.

Pollio, A., Mossa, M., 2009. A Comparison between Two Simple Models of a Slug Flow in a Long Flexible Marine Riser, Thesis.

Pesce, C.P., Aranha, J.A.P., Martins, C.A., 1998. The soil rigidity effect in the touchdown boundary-layer of a catenary riser: static problem. In: Eighth Int. Offshore and Polar Engr. Conf., Montreal, Canada, pp. 207–213.

Phifer, E.H., Frans Kopp, Swanson, R.C., Allen, D.W., Langner, C.G., 1994. Design and installation of auger steel catenary risers. In: Offshore Technol. Conf. (OTC7620), Houston, Texas, USA, pp. 399–408.

Queau, L., Kimiaei, M., Randolph, M.F., 2013. Dimensionless groups governing response of steel catenary risers, Ocean Eng. 74, pp. 247–259.

Randolph, M.F., Baht, S., Jain, S., Mekha, B., 2013. Modeling the touchdown zone trench and its impact on fatigue life, Offshore Technol. Conf. (OTC23975), Houston, Texas, USA.

Randolph, M.F., Quiggin, P., 2009. Non-linear hysteretic seabed model for catenary pipeline contact. In: 28th Int. Conf. On Ocean, Offshore and Arctic Engr. (OMAE 2009), Honolulu, Hawaii, USA.

Randolph, M.F., White, D.J., 2008. Upper bound yield envelopes for pipelines at shallow embedment in clay, Géotechnique 58 (4), pp. 297–301.

Shiri, H., 2010. Influence of Seabed Response on Fatigue Performance of Steel Catenary Risers in Touchdown Zone, [dissertation] University of Western Australia, 2010.

Shiri, H., 2014. Response of a steel catenary riser on hysteretic non-linear seabed. J. Of Appl. Ocean Research, Elsevier 44, 20–28.

Shiri, H., Hashemi, H., 2012. Simplified approximation of peak fatigue damage in touchdown area of steel catenary risers based on seabed soil rigidity. In: 22nd Int. Offshore Ocean and Polar Engr. Conf. Exhibition, Rhodes, Greece, pp. 287–294.

Shiri, H., Randolph, M., 2010. Influence of seabed response on fatigue performance of steel catenary risers in touch don area. In: 29th Int. Conf. On Ocean, Offshore and Arctic Engr., Shanghai.

Sumer, B.M., 2006. Hydrodynamics around Cylindrical Structures, World Scientific Publishing., Singapore.

Theti, R., Moros, T., 2001. Soil interaction effects on simple-catenary riser response. Pipes Pipelines Int. 46 (3), 15–24.

Trippit, B., Chee, K.Y., Aizad, S., 2012. Pipeline dynamics with flowing contents in ABAQUS/Standard, 2012 SIMULIA Community Conference.

Zargar, E., Kimiaei, M., 2015. An investigation of existing nonlinear seabed models for riser-fluid-soil interaction studies in steel catenary risers. In: Proceedings of 3rd Int. Symposium on Frontiers in Offshore Geotechnics, Oslo, Norway, pp. 489–494.

APPENDICES

Appendix B: Nonlinear hysteretic seabed response to vibrations of slugging steel catenary risers

Xiaoyu Dong[1] and Hodjat Shiri[2]

1: Department of Civil

Engineering, Memorial University of Newfoundland
e-mail: xiaoyu.dong@mun.ca

2: Department of Civil
Engineering, Memorial University of Newfoundland
e-mail: hshiri@mun.ca

This chapter was published in GeoEdmonton 2018 and it is a summary of chapter 11.

Abstract

Fatigue analysis of steel catenary risers (SCR) in the touchdown zone (TDZ) is extremely challenging because of complex mechanisms between the riser, seabed soil, seawater, and internal fluid. In this chapter, an advanced numerical model was developed with complex modules including a) a DISP subroutine to simulate the vessel motions under realistic environmental loads, b) a user defined element (UEL) subroutine to model the nonlinear hysteretic riser-seabed interaction in the TDZ, c) a structural model of SCR and riser hydrodynamics, and d) MPC/DLOAD subroutines to simulate the slug regime and transportation inside the SCR. Two groups of comprehensive parametric studies were conducted to explore the impacts of seabed soil and slug models on the responses of slugging SCR. The results showed that the nonlinear seabed model might significantly affect the slug-induced stress variation distribution and consequently the fatigue of SCR.

RÉSUMÉ

L'analyse de la fatigue des risers caténaires en acier (SCR) dans la zone de toucher des roues (TDZ) est extrêmement difficile en raison des mécanismes complexes entre la colonne montante, le sol du fond marin, l'eau de mer et le fluide interne. Dans cet article, un modèle numérique avancé a été développé avec des modules complexes comprenant a) un sous-programme DISP pour simuler les mouvements du vaisseau sous des charges environnementales réalistes, b) un sous-programme UEL pour modéliser l'interaction hystérétique non montante TDZ, c) un modèle structurel de l'hydrodynamique SCR et de la colonne montante, et d) des sous-programmes MPC / DLOAD pour simuler le régime

des limaces et le transport à l'intérieur du SCR. Deux groupes d'études paramétriques exhaustives ont été menés pour explorer les impacts des modèles de sols et de limaces du fond marin sur les réponses de SCR. Les résultats ont montré que le modèle de fond marin non linéaire pourrait affecter de manière significative la distribution de la variation de contrainte induite par les limaces et, par conséquent, la fatigue du SCR.

B.1. Introduction

Steel Catenary Risers (SCR) are widely used in offshore industry for transportation of oil and gas. Due to the slim and hanging nature of the structure, SCR suffers from the vibrations and oscillations induced by dynamic, cyclic loads. Fatigue damage of SCR has been a concern and efforts have been made to evaluate the fatigue especially for the critical area, the touchdown zone (TDZ) of SCR, where the SCR touches the seabed. However, the evaluation is quite challenging since complex mechanisms contribute to the loads, inducing riser oscillations in the TDZ including wave and low-frequency vessel motions, vortex induced vibrations, and slugging. In this chapter, slugging was investigated as a key factor to the accumulated fatigue damage (Kansao et al. 2008, Ortega et al. 2012). In addition to this, observations in subsea surveys and exploration projects indicate the complexities of the mechanisms in riser-seabed-seawater interactions. These complexities result in cyclic soil stiffness degradation, suction force mobilization during the riser uplift, and eventually a trench formation underneath the SCR in the touchdown zone. Nonlinear seabed models are required to be developed to model the seabed soil response to the complex coupled mechanisms. The advanced nonlinear hysteretic riser-seabed interaction models have been developed and evaluation of wave and current-induced fatigue loads of the SCR has been widely studied in the literature (Nakhaee and Zhang 2008, Shiri 2010, Shiri and Randolph

2010, Shiri and Esmaeilzadeh 2011, Hashemi 2011, Shiri and Hashemi 2012, Rezazadeh 2012, Shiri 2014, Kimiaei and Liao 2015, Clukey et al. 2017). However, the effect of these significant mechanisms and the nonlinear seabed soil response on slug-induced fatigue loads of SCR have never been investigated until now.

In this study, the impact of the nonlinear hysteretic seabed response and its consequences on slug-induced loads of the SCR was comprehensively investigated as an important knowledge gap. An advanced numerical model was developed using ABAQUS with several subroutines (e.g., user-defined element (UEL), multi-point constraints (MPC), and user-defined boundary conditions (DISP)) developed in FORTRAN and linked to the main analysis model to simulate slugging regimes, nonlinear hysteretic riser-seabed interaction, and various vessel excitation modes (including wave and low-frequency motions) under the act of environmental loads.

B.2. Literature review

The influence of seabed soil evolution on wave and current-induced fatigue damage of SCR have been well investigated in the literature (Shiri 2010, Shiri and Randolph 2010, Clukey et al. 2017, Dong and Shiri 2017, Dong and Shiri 2018), but it has never been studied in slug-induced fatigue. Slug-induced vibrations have been explored for the hanging part of the SCR but in most models the seabed end of the riser was considered as pinned and thus oscillation of SCR in the TDZ was absent from the analysis. Bordalo et al. (2008) examined the effects of two-phase flow patterns (slug, intermittent and annular) and flow rates of contents on the induced loads and riser responses by developing a laboratory-scale model. But in this research the seabed end was set as pinned and thus the responses in TDZ were absent in these tests. Pollio and Mossa (2009) compared two simple models

of slug flow (with and without elastic seabed models) in a long flexible marine riser. The results showed the bending moment variation was significantly different in cases with and without the elastic seabed model. Gundersen et al. (2012) used commercially available global and local riser analysis software (e.g., RIFLEX and BFLEX) and explored the remnant fatigue life of a lazy-S flexible riser under the combined effects of wave and slug. The riser was simulated as hinged at hang off and analysis was entirely focused on the hanging part. Results showed the slug dominated the dynamic top angle response and significantly reduced the riser fatigue life during a relatively calm sea condition. Ortega et al. (2012) analyzed the dynamic responses of a lazy wave riser under slugging by coupling the slug flow tracking code (SLUGGIT) and riser structure code (RISANANL) together. The results presented the irregularities in riser structure responses to slugging and indicated the importance of considering the effects of slug flow in the fatigue analysis. However, the seabed end of riser was considered as pinned and riser responses under slugging in TDZ were not included. Ortega et al. (2013) conducted a fully coupled analysis to examine the combined effects of slug loads and wave loads on the dynamic responses of a catenary riser. It was presented that internal slug flow generated irregular deformation time histories when the regular waves resulted in typical deformations of the riser structure. However, the riser responses in TDZ were not analyzed with the seabed end of riser considered as pinned. Chatjigeorgiou (2017) investigated the combined effects of harmonic motions of the vessel and the internal slug flow on the responses of the hanging part of the riser by incorporating the slug flow terms into the structural dynamic model formerly built by Chatjigeorgiou (2010a, 2010b). It was shown that the magnitudes of dynamic components were amplified due to the existence of internal slug flow. Bordalo et al. (2018) incorporated

a slug flow load model to a 3D pipeline dynamics simulator. The simulation of slugging SCR in the case study showed that large oscillations might be induced when the slug frequency was close to any of the natural frequencies of the riser. However, the seabed interface was not the focus of the chapter.

To fill the knowledge gap, in this chapter, a nonlinear soil model was embedded into the advanced numerical model to consider the effects of the seabed evolution process on slug-induced vibrations. In SCR design codes, linear springs have been used to present the pipe-soil interaction. With further observations in subsea surveys and exploration projects, more sophisticated nonlinear models were needed to better represent the mechanism of riser-seabed interaction (Phifer et al., 1994; Theti and Moros, 2001; Campbell, 1999). Based on full-scale harbor tests and some existing models, Bridge et al. (2004, 2007) developed a model capturing some of nonlinear aspects of soil behavior, except for the degradating soil stiffness and riser embedment into the seabed. Jiao (2007) proposed the degradating soil model which could capture the cyclic softening of soil in the re-loading process but not in the unloading process. This disadvantage was overcome in new models proposed later (Aubeny and Biscontin 2009, Nakhaee and Zhang 2010). Randolph and Quiggin (2009) developed a new nonlinear seabed model for the calculation of reaction force in different penetration modes of the oscillating riser. Shiri and Randolph (2010) explored the fatigue analysis of SCR by developing a numerical model in ABAQUS with the R-Q soil model adopted in the user-defined element. Zargar et al. (2015) conducted a comparative study of two existing riser-soil interaction models (Aubeny and Biscontin 2009, Randolph and Quiggin 2009) and identified their pros and cons for future developments. SCR fatigue was further investigated and reported with newly proposed trench models (Randolph et al.

2013, Shiri 2014a, Shiri 2014b) or different case studies (e.g., different loading histories, complex riser excitations etc.) (Elliott et al. 2013, Kimiaei and Liao 2015, Clukey et al. 2017). Authors emphasized the significance of nonlinear riser-soil interaction models and their needs for further improvement of fatigue analysis of SCR in TDZ. Dong and Shiri (2017) comprehensively investigated the performance of the R-Q model (Dong and Shiri 2017, Dong and Shiri 2018). The R-Q model was found to have strong features and may be an appropriate approach for modelling the nonlinear riser-seabed interaction. But some improvements may be needed since it was observed by the authors that the model was unable to explicitly simulate trench formation. In addition, the model doesn't capture the four sub-episodes of riser-soil interaction that were observed in experimental studies (Hodder and Byrne 2009). However, the advantages of this model in automotive simulation of cyclic soil stiffness degradation and trench creation has made it a popular model. In this study, the R-Q model was coded in the UEL subroutine and implemented into the global SCR model in ABAQUS to incorporate the effect of nonlinear hysteretic seabed on slug-induced fatigue loads.

B.3. Numerical model

B.3.1 Global Model

A global SCR model was developed in ABAQUS. Slug loading, nonlinear hysteretic riser-seabed interaction, and the wave/current-induced vessel motions were coded in MPC/DLOAD, UEL, and DISP subroutines respectively. To facilitate the comparison of results from slug-induced, wave-induced, and combined wave/slug-induced analysis, the global SCR configuration was adopted from Dong and Shiri (2018).

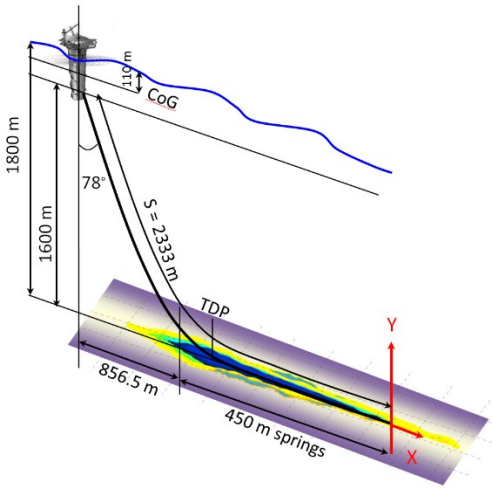

Figure B-1. The global geometry of SCR modelled by ABAQUS (Dong and Shiri).

B.3.2 Modelling of SCR Slugging

As illustrated in Figure B-1, the slugging or separation of the flow to a film zone, and a slug liquid zone usually occurs in moderate flow velocities (Kansao et al. 2008).

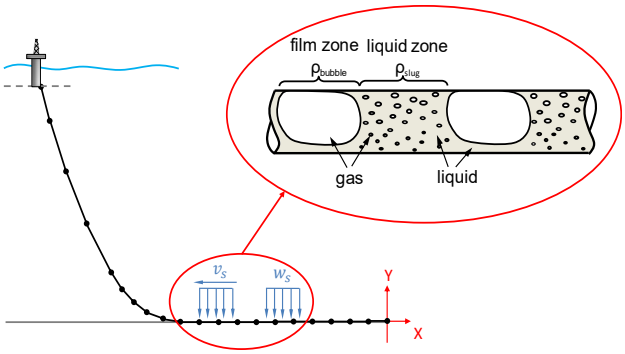

Figure B-2. The slug flow regime (Dong and Shiri).

A pre-defined distributed load representing the weight of the slug (see Figure B-2) was executed on the SCR by coding the DLOAD subroutine in FORTRAN. The key steps inside DLOAD were outlined in the flowchart as shown in Figure B-3.

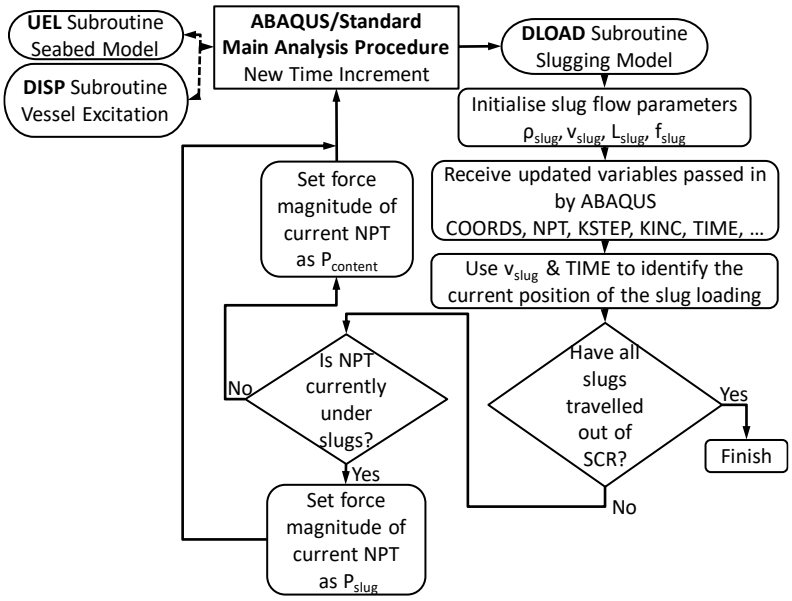

Figure B-3. DLOAD subroutine internal flowchart. (Dong and Shiri).

The ABAQUS Multi-point constraints (MPC) user subroutine was coded to create a moving tie constraint interface modelling the moving slug. The main step in MPC is to determine and eliminate the dependent DOF of the slave node and transfer the information of the derivatives of the constraint function (A, see Figure B-4) to ABAQUS for the redistribution of loads from the dependent DOF to other DOFs.

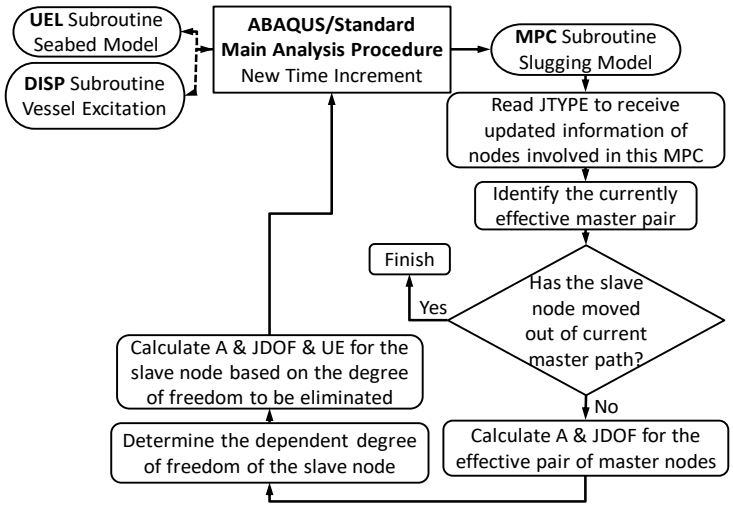

Figure B-4. MPC subroutine internal flowchart. (Dong and Shiri).

B.3.3 Modelling of Seabed Soil

In this study, one of the most popular riser-seabed interaction models (Randolph and Quiggin 2009) have been coded in a UEL subroutine in ABAQUS to capture the effect of the nonlinear seabed on slug-induced oscillation and fatigue. The R-Q model was first coded by Shiri and Randolph (2010) in a user-defined element (UEL) to investigate the influence of seabed soil stiffness degradation and trench creation on wave-induced fatigue response of SCR. Figure B-5 illustrates the analysis flowchart of the UEL subroutine incorporated in ABAQUS.

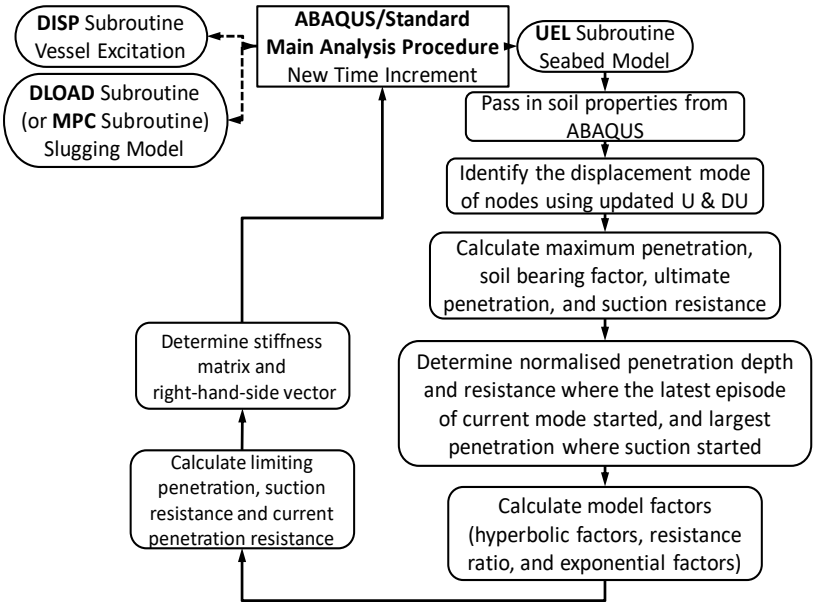

Figure B-5. UEL subroutine internal flowchart.

B.3.4 Modelling of wave-induced vessel motions

A user-defined DISP subroutine was coded in FORTRAN and linked to the global SCR model in ABAQUS to incrementally update the vessel location through modelling two translations (surge and heave) and one rotation (pitch) through 2D displacement-controlled analysis. A similar methodology was originally proposed by Shiri and Randolph (2010).

Figure B-6 illustrates the schematic flow chart of DISP subroutine and its linkage with the main analysis procedure.

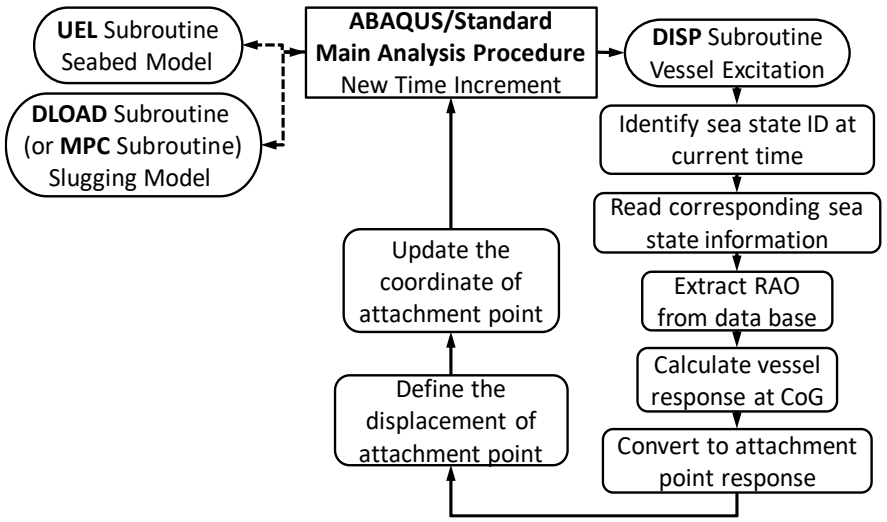

Figure B-6. UEL subroutine internal flowchart.

B.4. Parametric study

Comprehensive parametric studies were conducted to investigate the influence of cyclic seabed soil stiffness degradation and gradual SCR penetration into the seabed on slug-induced vibrations in the touchdown zone. The properties of SCR were given in Table B-1. Effects of slug-induced, wave-induced and slug/wave-induced excitations were examined at the TDP respectively. Then slug/wave induced vibrations were further examined by conducting two groups of parametric studies. Slug parameters were examined both on the linear elastic seabed and the nonlinear hysteretic seabed using Table B-4. Default slug flow parameters.. Default parameter settings for the linear elastic seabed and nonlinear hysteretic seabed were given in Table B-3 and Table B-2. An estimated equivalent soil stiffness of 300 kPa was used to represent the elastic seabed (Randolph et al. 2013). Various nonlinear soil model parameters were examined to evaluate the impact

of soil model parameters on system response to slugging, using Table B-8 with the default slug parameters given in Table B-4. Sea state information given in Table B-5 was embedded in the numerical model and sea state #30 was selected and repeated for 10 cycles in all case studies. The hydrodynamic coefficients adopted in simulation are listed in Table B-6.

Table B-1. Riser pipe properties (Dong and Shiri 2018)

Parameter	Symbol	Value	Unit
Outer diameter	D_o	0.324	M (12¾ ")
Wall thickness	t	0.0205	m
Second moment of area	I	2.26×10^{-4}	m^4
Steel Young's Modulus	E_{steel}	2.07×10^{11}	N/m^2
Steel density	ρ_s	7850	kg/m^3
Fatigue S-N curve	$\bar{a}$	1.05×10^{12}	-
DNV (2008)	m	3.0	-
E Class weld	SCF	1.13	-

Table B-2. Default parameters of R-Q soil models.

Parameter	Symbol	Value	Unit
Mudline shear strength	s_{u0}	0.65	kPa
Shear strength gradient	ρ	1.5	kPa/m
Power law parameter	a	6	-
Power law parameter	b	0.25	-
Normalized maximum stiffness	K_{max}	200	-
Suction ratio	f_{suc}	0.3	-
Suction decay parameter	λ_{suc}	0.5	-
Re-penetration parameter	λ_{rep}	0.5	-

Table B-3. Default elastic seabed parameters.

Elastic seabed	Equivalent vertical strength (kPa)	Equivalent shear strength (kPa)
Default	300	10

Table B-4. Default slug flow parameters.

Parameter	Symbol	Value	Unit
Slug density	ρ_{slug}	600	kg/m^3
Bubble density	ρ_{bubble}	100	kg/m^3
Flow velocity	v_{slug}	10	m/s
Slug length	L_{slug}	30	m
Slug frequency	f_{slug}	180	/hr

Table B-5. Wave scatter diagram for a 30-year operational life (GoM)

Sea State				
Bin #	H (m)	T (s)	Omni (1 year) p (-)	Omni (30 year) p (-)
1	0.5	4.2	600376	18011291
2	1	4.6	2379015	71370445
3	1.5	5	1614987	48449608
4	2	5.4	839595	25187856
5	2.5	5.8	450978	13529335
6	3	6.1	249122	7473660
7	3.5	6.5	102683	3080495
8	4	6.9	54367	1631014
9	4.5	7.3	19459	583770
10	5	7.7	12124	363725
11	5.5	8	3823	114700
12	6	8.4	1123	33676
13	6.5	8.5	564	16907
14	7	8.7	362	10864
15	7.5	8.9	181	5421
16	8	9.1	113	3389
17	8.5	9.3	100	3011
18	9	9.5	61	1822
19	9.5	9.7	46	1395
20	10	9.9	36	1070
21	10.5	10.1	42	1246
22	11	10.2	19	566
23	11.5	10.4	31	928
24	12	10.6	18	544
25	12.5	10.7	27	813
26	13	10.9	24	712
27	13.5	11	29	877
28	14	11.2	9	262
29	14.5	11.3	11	343
30	15	11.5	14	420

Table B-6. Hydrodynamic coefficients.

Drag (C_D)	Inertia (C_I)	Added mass (C_A)
0.7	1.5	1.0

Table B-7. Parametric study map 1-slug parameters.

Case study	Input slug model parameter					
	ρ_{slug} (kg/m^3)	ρ_{bubble} (kg/m^3)	v_{slug} (m/s)	L_{slug} (m)	f_{slug} (/hr)	Seabed (E/N)
CS-1	D	D	D	D	D	E
CS-2	D	D	D	D	D	N
CS-3	700	D	D	D	D	E
CS-4	700	D	D	D	D	N
CS-5	D	150	D	D	D	E
CS-6	D	150	D	D	D	N
CS-7	D	D	25	D	D	E
CS-8	D	D	25	D	D	N
CS-9	D	D	D	50	D	E
CS-10	D	D	D	50	D	N
CS-11	D	D	D	D	100	E
CS-12	D	D	D	D	100	N
Note	D refers to "Default" values for slug model as described in Table B-4. From CS-1 to CS-12, soil parameters in Table B-2 were adopted for nonlinear seabed models and soil parameters in Table B-3 were adopted for elastic seabed models.					

Table B-8. Parametric study map 2-nonllinear seabed parameters.

Case study	Input soil model parameters				
	s_u	ρ	f_{suc}	λ_{suc}	λ_{rep}
CS-13	0.35	D	D	D	D
CS-14	0.95	D	D	D	D
CS-15	D	0.5	D	D	D
CS-16	D	1.0	D	D	D
CS-17	D	D	0.5	D	D
CS-18	D	D	1	D	D
CS-19	D	D	D	0.2	D
CS-20	D	D	D	1.0	D
CS-21	D	D	D	D	0.2
CS-22	D	D	D	D	0.8
Note	D refers to "Default" values for soil model as described in Table B-2. From CS-13 to CS-22, slug parameters given in Table B-4 were adopted for slug model.				

B.5. Results

To give a direct view of the effects of wave and slug on SCR responses, time history outputs at TDP were investigated under vibrations induced by the slug, wave, and slug-wave respectively as predefined in CS-2 (see from Figure B-7 to Figure B-11). As shown in Figure B-7 and Figure B-8, the amplitude of resultant oscillations showed scattered results and the wave-induced oscillation amplitudes may be amplified or mitigated by the slug-induced oscillations depending on the oscillation phase angle.

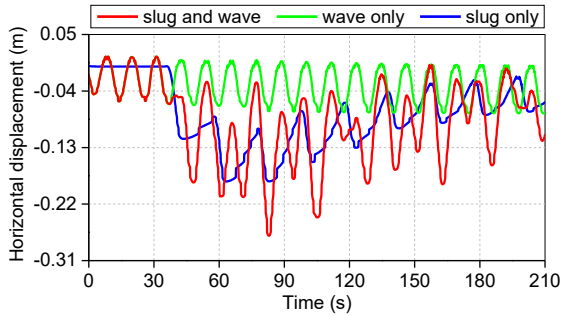

Figure B-7. Time history of horizontal displacement at TDP.

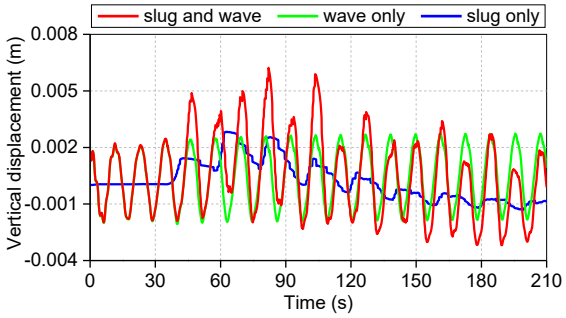

Figure B-8. Time history of vertical displacement at TDP.

As shown in Figure B-9 to Figure B-11, there was a sharp increase in the amplitudes of bending moment, shear force, and maximum von Mises stress when the liquid slugs arrived at TDP. The resultant amplitudes changed every time and the maximum amplitudes showed approximately when the wave only case and the slug only case came to extreme values at almost the same time. For instance, in Figure B-11, the peak amplitude of maximum von Mises stress at TDP occurred when the wave and slug phase angles met at about 100s.

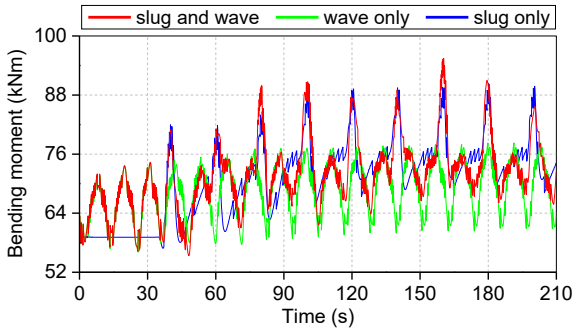

Figure B-9. Bending moment of the TDP.

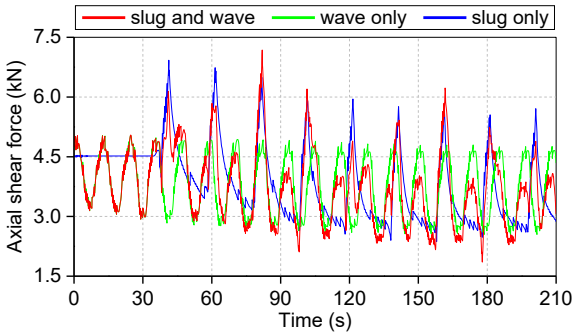

Figure B-10. Shear force at TDP.

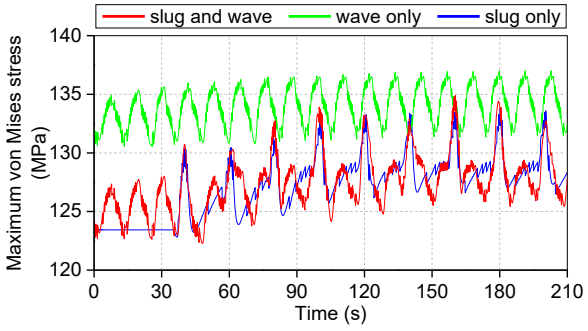

Figure B-11. Maximum von Mises stress at TDP.

Two groups of parametric studies have been conducted as described in Section 4. The influence of the slug parameters was compared on the linear seabed model and the

nonlinear seabed model in parametric study group 1 (see Table B-7). Influence of nonlinear seabed soil parameters was compared in parametric study group 2 (see Table B-8). Final riser profiles after 115 s slugging were given in Figure B-12 to Figure B-14. As shown in Figure B-12, maximum penetration location is very dependent on the slug parameters. Slug density was investigated to have the most significant impact on the depth of penetration (see CS-4 in Figure B-13). Changes in the value of soil parameters also resulted in significant differences among the final SCR profiles (e.g., CS-2, CS-13, change in mudline shear strength of soil, see Figure B-14).

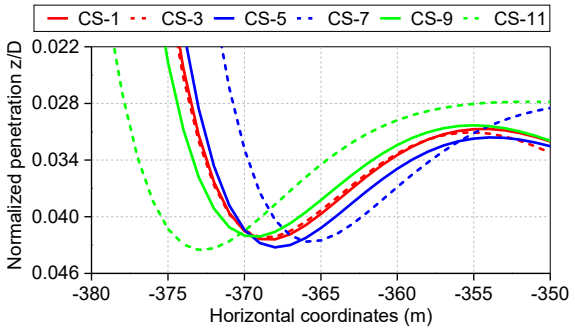

Figure B-12. Final riser profiles from CS-1 to CS-11.

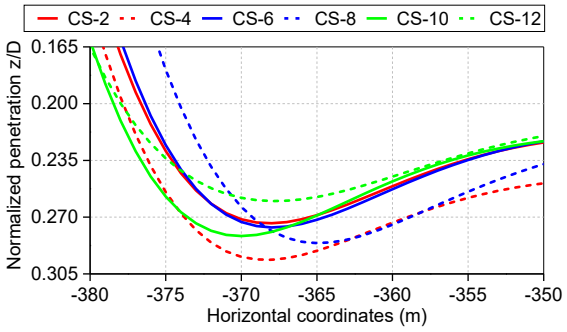

Figure B-13. Final riser profiles from CS-2 to CS-12.

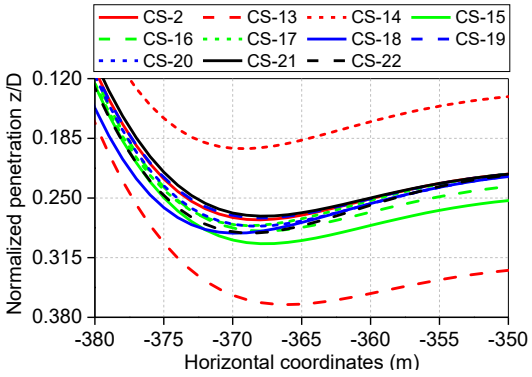

Figure B-14. Final riser profiles from CS-13 to CS-22.

Variation of the von Mises stress is the key parameter for the fatigue damage evaluation of SCR. To explore the impact of slugging and nonlinear soil parameters on the trends of fatigue, distribution of maximum von Mises stress ranges were plotted in different case studies as shown in Figure B-15 to Figure B-17. Compared with the slight differences induced by the changes in soil parameters as examined in parametric study (see Figure B-17), greater influences of slug parameters were observed, especially the slug density. However, the results on elastic seabed and plastic seabed showed minor differences (see Figure B-15 and Figure B-16). This is because the stationary von Mises stress is mainly governed by the catenary configuration and bending curvature instead of the seabed soil model.

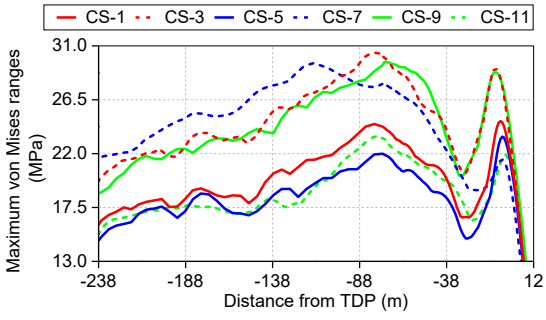

Figure B-15. Effects of slug parameters on the distribution of the maximum von Mises stress ranges along SCR on elastic seabed.

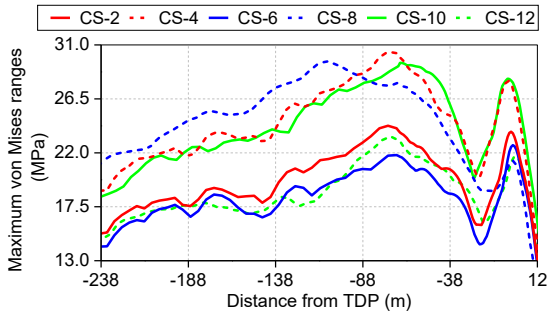

Figure B-16. Effects of slug parameters on the distribution of the maximum von Mises stress ranges along SCR on nonlinear hysteretic seabed.

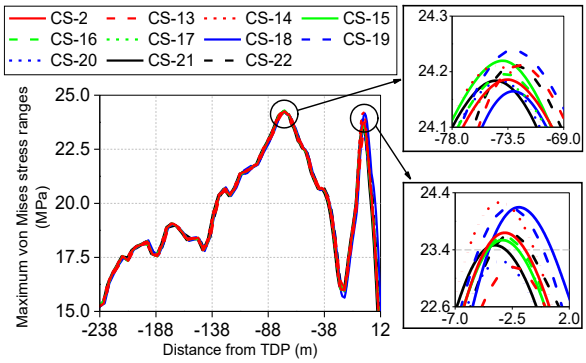

Figure B-17. Effects of nonlinear soil parameters on the distribution of the maximum von Mises stress ranges along SCR on nonlinear hysteretic seabed.

B.6. Summary and Conclusion

An advanced numerical model was developed to fill the knowledge gap in exploring the influence of complex nonlinear hysteretic riser-seabed interaction on slugging SCR. The model consists of slugging SCR, nonlinear hysteretic seabed, and the vessel excitation under the impact of environmental loads. A summary of the key conclusions can be listed as follows:

- The slug-induced oscillation and wave-induced oscillation show scattered results. Depending on the phase angles of oscillations, the slug-induced oscillation may amplify or mitigate the wave-induced oscillation at different times.
- Slug-induced oscillation significantly contributes to riser penetration into the seabed when it is coupled with wave-induced oscillation. This shall be further investigated for incorporation in any trench profile model.
- Final riser profiles on the elastic seabed and the nonlinear seabed with the same slug parameters show a difference in penetration depth. This may be caused by the capability of nonlinear seabed to consider the accumulation of penetration.
- The peak value point of the maximum von Mises stress range is located in the area close to the TDP. With a different slug model and soil model, the maximum point may fall on a different side of the TDP.
- The slug-induced fatigue damage of SCR on the nonlinear seabed is most likely to be slightly less than on the conventional elastic seabed as indicated by the distribution of the von Mises stress ranges. Therefore, it is conservative and less expensive to utilize the linear elastic seabed model in design.

B.7. Acknowledgement

The authors gratefully acknowledge the financial support of this research by the Research and Development Corporation (RDC) (now Innovate NL) through the Ignite funding program and Memorial University of Newfoundland through VP start-up funding support.

References

Aubeny, C.P., Biscontin, G. 2009. Seafloor–riser interaction model, Int J Geomechanics, 9: 133-141.

Bordalo, S.N., Morooka, C.K., Cavalcante, C.C.P. 2008. Whipping phenomenon caused by the internal flow momentum on the catenary risers of offshore petroleum fields, in: Proceedings of the ASME 27th International Conference on Offshore Mechanics and Arctic Engineering, Estoril, Portugal, OMAE 2008-57351.

Bordalo, S.N., Morooka, C.K. 2018. Slug flow induced oscillations on subsea petroleum pipelines, Journal of petroleum science and engineering (In press, accepted manuscript).

Bridge, C., Laver, K., Clukey, E., Evans, T. 2004. Steel catenary riser touchdown point vertical interaction models, in: Offshore Technology Conference, OTC16628, Houston, Texas.

Bridge, C., Howells, H. 2007. Observations and modeling of steel catenary riser trenches, in: 17th International Offshore and Polar Engineering Conference, ISOPE2007, Lisbon, Portugal.

Campbell, M. 1999. The complexities of fatigue analysis for deepwater risers, in: Proceedings of the 2nd International Deepwater Pipeline Technology Conference.

Chatjigeorgiou, I.K. 2010a. Three dimensional nonlinear dynamics of submerged, extensible catenary pipes conveying fluid and subjected to end-imposed excitations, International Journal of Non-linear Mechanics, 45: 667-680.

Chatjigeorgiou, I.K. 2010b. On the effect of internal flow on vibrating catenary risers in three dimensions, Engineering structures, 32: 3313-3329.

Chatjigeorgiou, I.K. 2017. Hydroelastic response of marine risers subjected to internal slug-flow, Applied Ocean Research, 62: 1-17.

Clukey, E.C., Aubeny, C.P., Zakeri, A., Randolph, M.F., Sharma, P.P., White, D.J., Sancio, R., Cerkovnik, M. 2017. A Perspective on the state of knowledge regarding soil-pipe interaction for SCR fatigue assessments, in: Offshore Technology Conference, Houston, Texas, OTC27564-MS.

Dong, X., Shiri, H. 2018. Performance of non-linear seabed interaction models for steel catenary risers, part I: Nodal response, Journal of Ocean Engineering, 154: 153-166.

Dong, X., Shiri, H. 2017. Performance of non-linear seabed interaction models for steel catenary Risers, part II: Global response, Journal of Ocean Engineering, Aug 2017 (submitted).

Elliott, B.J., Zakeri, A., Barrett, J., Hawlader, B., Li, G., Clukey, E.C. 2013. Centrifuge modeling of steel catenary risers at touchdown zone Part II: Assessment of centrifuge test results using kaolin clay, Ocean Engineering, 60: 208-218.

Gundersen, P., Doynov, K., Andersen, T., Haakonsen, R. 2012. Methodology for determining remnant fatigue life of flexible risers subjected to slugging and irregular waves, in: Proceedings of the ASME 2012 31st Int Conf on Ocean, Offshore and Arctic Engineering, OMAE 2012, July 1-6, Rio de Janeiro, Brazil.

Hashemi, H., Oliasani, M., Shiri, H. 2011. Simple estimation of SCR fatigue in TDZ, in: 13th Marine Industries Conference, Kish Island, IRAN.

Hodder, M.S., Byrne, B.W. 2009. 3D experiments investigating the interaction of a model SCR with the seabed, Applied Ocean Research, 32: 145-157.

Jiao, Y. 2007. Non-linear load-deflection models for Seafloor Interaction with Steel Catenary Risers. Texas A&M University, College Station, USA. Master of Science, 2007.

Kansao, R., Casanova, E., Blanco, A., Kenyery, F., Rivero, M. 2008. Fatigure life prediction due to slug flow in extra-long submarine gas pipelines, in: Proceedings of the ASME 2008 27th Int Conf on Offshore Mechanics and Arctic Engr, OMAE2008, Estoril, Portugal, 3: 685-692.

Kimiaei, M., Liao, J. 2015. Effects of different loading time histories on fatigue design of steel catenary risers using nonlinear riser-soil interaction models, in: Frontiers in Offshore Geotechnics III, Norway, Trondheim.

Nakhaee, A., Zhang, J. 2008. Effects of the interaction with the seafloor on the fatigue life of a SCR, in: Int Offshore and Polar Engr Conf, Vancouver, BC, Canada.

Nakhaee, A., Zhang, J. 2010. Trenching effects on dynamic behavior of a steel catenary riser, Ocean Engineering, 37(2–3):277–288.

Ortega, A., Rivera, A., Nydal, O.J., Larsen, C.M. 2012. On the dynamic response of flexible risers caused by internal slug flow, in: Proceedings of the ASME 2012 31st Int Conf on Ocean, Offshore and Arctic Engineering, OMAE2012, Rio de Janeiro, Brazil, 5: 647-656.

Ortega, A., Rivera, A., Larsen, C.M. 2013. Flexible riser response induced by combined slug flow and wave loads, in: Proceedings of the ASME 2013 32nd International

Conference on Ocean, Offshore and Arctic Engineering, OMAE2013, Jun 9-14, Nantes, France.

Phifer, E.H., Kopp, F., Swanson, R.C., Allen, D.W., Langner, C.G. 1994. Design and installation of Auger steel catenary risers, in: Offshore Technology Conference, OTC7620, Houston, Texas.

Pollio, A., Mossa, M. 2009. A comparison between two simple models of a slug flow in a long flexible marine riser, Thesis.

Randolph, M.F., Quiggin, P. 2009. Non-linear hysteretic seabed model for catenary pipeline contact, in: 28th International Conference on Ocean, Offshore and Arctic Engineering, OMAE 2009, Honolulu, Hawaii, USA.

Randolph, M., Baht, S., Jain, S., Mekha, B. 2013. Modeling the touchdown zone trench and its impact on SCR fatigue life, in: Offshore Technology Conference, Houston, OTC23975.

Rezazadeh, K., Shiri, H., Zhang, L., Bai, Y. 2012. Fatigue Generation Mechanism in Touchdown Area of Steel Catenary Risers in Non-Linear Hysteretic Seabed, Journal of Applied Sciences, Engineering and Technology, 4(24): 5591-5601.

Shiri, H. 2010. Influence of seabed response on fatigue performance of steel catenary risers in touchdown zone [dissertation]. University of Western Australia.

Shiri, H. 2014a. Influence of seabed trench formation on fatigue performance of steel catenary risers in touchdown zone, Journal of Marine Structures, 36: 1-20.

Shiri, H. 2014b. Response of a steel catenary riser on hysteretic non-linear seabed, Journal of Applied Ocean Research, 44: 20-28.

Shiri, H., Randolph, M.F. 2010. Influence of seabed response on fatigue performance of steel catenary risers in touch down area, in: 29th International Conference on Ocean, Offshore and Arctic Engineering, Shanghai, China, 5: 63-72.

Shiri, H., Esmaeilzadeh, M. 2011. Steel catenary risers, design challenges and fatigue performance, in: Proceeding of 13th Marine Industries Conference, Kish Island, Iran.

Shiri, H., Hashemi, H. 2012. Simplified approximation of peak fatigue damage in touchdown area of steel catenary risers based on seabed soil rigidity, in: 22nd International Offshore Ocean and Polar Engineering Conference & Exhibition, ISOPE2012, Rhodes, Greece.

Theti, R., Moros, T. 2001. Soil interaction effects on simple-catenary riser response, Pipes and Pipelines Int.; 46 (3): 15-24.

Appendix C: The influence of slug characteristics on oscillation of steel catenary risers in the non-linear hysteretic seabed

Xiaoyu Dong[1] and Hodjat Shiri[2]

1: Department of Civil

Engineering, Memorial University of Newfoundland
e-mail: xiaoyu.dong@mun.ca

2: Department of Civil
Engineering, Memorial University of Newfoundland
e-mail: hshiri@mun.ca

This chapter was published in GeoSt.John's 2019 and it is a summary of chapter 11.

Abstract

Steel catenary risers (SCR) are widely used in the development of offshore fields and are exposed to severe fatigue loads generated by environmental and operation loads. Slugging can induce SCR oscillations in the touchdown zone (TDZ) and cause the cyclic degradation of seabed soil. In this study, the influence of slug characteristics on SCR oscillation in the TDZ was comprehensively investigated by developing numerical models in ABAQUS with FORTRAN interfaces. The slugging characteristics such as density, length, velocity etc. have been examined together with the influence of non-linear hysteretic riser-seabed interaction, and complex vessel excitations. The study revealed several important trends of SCR response to slug-induced oscillations in the non-linear hysteretic seabed and consequently on accumulated fatigue damage in the TDZ.

RÉSUMÉ

Les colonnes montantes de caténaires en acier (SCR) sont largement utilisées dans le développement de champs offshore et sont exposées à des charges de fatigue sévères générées par des charges environnementales et opérationnelles. Les slugging peuvent induire des oscillations de RCS dans la zone de toucher des roues (TDZ) et provoquer la dégradation cyclique des sols des fonds marins. Dans cette étude, l'influence des caractéristiques des bouchons sur l'oscillation de la RCS dans le TDZ a été largement étudiée en développant des modèles numériques dans ABAQUS avec des interfaces FORTRAN. Les caractéristiques de slugging telles que la densité, la longueur, la vitesse, etc. ont été examinées, ainsi que l'influence de l'interaction non linéaire hystérétique entre le riser et le fond marin et les excitations complexes des navires. L'étude a révélé plusieurs

tendances importantes en matière de réponse SCR aux oscillations induites par les bouchons dans le fond marin hystérétique non linéaire et, par conséquent, aux dommages de fatigue accumulés dans le TDZ.

C.1. Introduction

Steel Catenary Risers (SCRs) are designed to deliver hydrocarbons from the sea floor and floating facilities with a catenary configuration. The subsea recordings show that the SCR penetrates into the seabed and creates a trench several diameters deep in the early stages after the installation. Several complex mechanisms contribute to the cyclic soil stiffness degradation and the gradual penetration of the SCR into the seabed. This has made the SCR fatigue assessment in the touchdown zone (TDZ) to be one of the most challenging issues in design practice. Various external loads contribute to the oscillation of SCR in the touchdown zone such as wave action (high-frequency), wind and surficial current action (low-frequency), and vortex induced vibrations. The SCR slugging is a common source of internal loads that contribute to the riser oscillations in the touchdown zone and consequently the fatigue life (Kansao et al. 2008, Ortega et al. 2012). Also, the slug-induced oscillation amplitudes may sum up to or subtract from wave-induced oscillations depending on the phase difference. Rigid or simple elastic springs are usually used as a simplified model of seabed soil in practice. However, comparing with the observations of complex riser-seabed-seawater interactions in the conducted subsea surveys, this approach is oversimplifying the riser-seabed interaction. These mechanisms result in cyclic soil stiffness degradation, suction force mobilization during the riser uplift, and eventually a trench formation underneath the SCR in the touchdown zone.

In the literature, advanced nonlinear hysteretic riser-seabed interaction models have been

proposed to explore the influence of these mechanisms on the wave and current-induced fatigue loads of the SCR (Shiri and Randolph 2010, Shiri 2014, Nakhaee and Zhang 2008, Kimiaei and Liao 2015, Clukey et al. 2017). However, the effect of the nonlinear hysteretic seabed soil response on slug-induced stress oscillations has never been investigated before. In this study, the impact of the nonlinear hysteretic seabed response and its consequences on slug-induced responses and potential fatigue of the SCR were comprehensively investigated as an important knowledge gap. Also, the model parameters and equations are not fully accessible in the commercial software with built-in slugging and soil models. Therefore, an advanced numerical model was developed using ABAQUS to address a series of severe nonlinearities in model geometry, material behavior, environmental, and functional loads. Several user-defined subroutines (e.g., UEL, MPC, and DISP) were developed in FORTRAN and linked to the ABAQUS to model slugging regimes, nonlinear hysteretic riser-seabed interaction, and various vessel excitation modes (including wave and low-frequency motions) under the act of environmental loads. Cyclic seabed soil stiffness degradation and consequently the trench formation in the touchdown zone were greatly influenced by the slug-induced oscillations of SCR. The necessity of the accurate modelling of the plastic seabed response in slug-induced fatigue analysis of SCRs was also indicated in the results of parametric studies. With full administration to customize plastic seabed soil condition, vessel excitation, and complex slugging regimes, the numerical model developed in this study was found to be a robust tool for advanced slug-induced fatigue analysis of SCR.

Considering a full examination of slug parameters, the system response to the nonlinear seabed has been entirely investigated in terms of the SCR cyclic profile changes and the

maximum von Mises stress ranges in the TDZ with different slug patterns. However, to facilitate reading the chapter, a summary of the developed numerical model was also included in this chapter. Before discussing the developed model and the analysis results, it is worth reviewing the published key research works conducted on modelling of the slugging SCRs and also the riser-soil interaction that will be presented in the next section.

C.2. Literature review

The slugging contributes to the vertical oscillation of SCR in the touchdown zone, where the riser comes to cyclic contact with the seabed soil. This cyclic contact causes the progressive soil stiffness degradation and gradual penetration of the SCR into the seabed. The slugging-induced oscillations may be combined with other kinds of motions such as wave and low-frequency vessel motions and vortex-induced vibrations. The gradual softening of the seabed soil and the trench creation affect the cross-sectional stress oscillation range and consequently the fatigue life in the touchdown zone. The influence of cyclic soil softening on the wave and current-induced fatigue damage of SCR has been well explored in the literature (Shiri and Randolph 2010, Clukey et al. 2017, Dong and Shiri 2018, Dong and Shiri 2019). However, there is no published work to investigate the effect of seabed soil stiffness degradation on slug-induced vibrations.

Bordalo et al. conducted a laboratory-scale model test to explore the dynamic response of catenary part of the riser to the internal two-phase flow. With seabed end considered as pinned, the tests were conducted with different flow patterns (slug, intermittent and annular) and flow rates (Bordalo et al. 2008). It was concluded that magnitude of whipping increased when a transition is presented between the slug and intermittent patterns or between the intermittent and annular patterns. Besides, when the air flow rates increased,

the magnitudes of whipping and variation of the sustaining force at the top increased. Pollio and Mossa compared two simple models of slug flow in a long flexible marine riser (with and without elastic seabed model) (Pollio and Mossa 2009). The riser-seabed interaction was considered with a simplified normal reaction force as a function of the relative displacement and the friction force in the opposite direction of the nodal velocity. The results showed that irregular inner stress responses might be generated by the slug flow with variable frequency, while the tension and moment variations were found to be more regular under the flow with a constant frequency. The authors observed a significant difference in variation of the bending moment in the seabed existence case and seabed absence case. The greater magnitude of bending moment variation and greater probability of higher stress in riser were induced by the slug flow with variable frequency. Gundersen et al. conducted a case study on the remnant fatigue life of flexible risers in lazy-S configuration subjected to combined wave and slug-induced motions (Gundersen et al. 2012). Commercially available global and local riser analysis tools (i.e., RIFLEX and BFLEX) were coupled to build the adopted model. They observed that the slugging dominated the dynamic top angle response and significantly reduced the riser fatigue life during a relatively calm sea condition. Ortega et al. investigated the influence of slug loading on the dynamic responses of a flexible riser in lazy wave configuration (Ortega et al. 2012). The authors coupled two distinct codes for slug flow tracking (SLUGGIT) and riser structure (RISANANL). With seabed end of SCR assumed as pinned, the results showed that depending on the characteristic of slug flow, irregular deformation time histories might be generated. This indicated the importance of considering the effects of slug flow in the fatigue analysis. A fully coupled analysis was conducted later by Ortega

et al. to examine the response of catenary flexible riser to the combined effect of slugging and wave loads (Ortega et al. 2013). It was shown that the internal slug flow might result in irregular deformation time histories. Chatjigeorgiou established an analytical approach and examined the combined effects of harmonic motions of the vessel and the internal slug flow on the dynamic response of catenary pipelines (Chatjigeorgiou 2017). The slug flow terms were incorporated into the model formerly built by Chatjigeorgiou with the seabed end considered as pinned (Chatjigeorgiou 2010). It was shown that the magnitudes of dynamic components may be amplified due to the existence of internal slug flow. Bordalo et al. incorporated a slug flow model into a 3D pipeline dynamics simulator (Bordalo et al. 2018). The case study showed that large oscillations might be induced when the slug frequency was close to any of the natural frequencies of the riser.

As mentioned earlier, the literature review shows that the effect of the cyclic seabed stiffness evolution on slug-induced stress oscillations has not been explored before. This might be due to the need for simultaneous modelling of several complex aspects related to different engineering disciplines including the nonlinear hysteretic riser-seabed interaction, slug loading, and vessel motions. However, this is an important knowledge gap and the current study has tried to explore it and fill the gap. In the next section, the previous efforts on the development of cyclic seabed soil stiffness degradation and its impact on the wave and current-induced fatigue damage will be briefly reviewed to facilitate reading the chapter.

The riser-seabed interaction in design codes is usually modelled by traditional linear springs. After first experience of SCR technology in the Auger field of the Gulf of Mexico (Phifer et al. 1994), the STRIDE and CARISIMA JIPs (1999-2001) were the first studies

to investigate the need for more sophisticated nonlinear riser-seabed interaction models (Theti and Moros 2001, Campbell 1999). A model was developed by Bridge et al. to simulate various nonlinear aspects of soil behavior through full-scale harbor tests Bridge et al. (Bridge et al. 2004, Bridge et al. 2007). It was similar in form to the hyperbolic pipe-soil interaction curve proposed by Hardin and Drnevich that was originally established for clay by Kondner (Hardin and Drnevich 1972, Kondner 1963). However, the model was unable to sequentially simulate the gradual seabed soil softening and riser embedment to the seabed. Jiao proposed two nonlinear non-degradating and degradating spring models for soils beneath the SCR (Jiao 2007). The degradating model works well in simulating cyclic softening of the soil but only through the re-loading paths. Based on the work conducted by Jiao, a new model was proposed by Aubeny and Biscontin to simulate the nonlinear hysteretic soil behavior under the riser, which was further improved by Nakhaee and Zhang (Aubeny and Biscontin 2009, Nakhaee and Zhang 2010). The model overcame the shortcomings of Jiao's model, but still adopted the non-uniform set of equations. Another nonlinear model was developed by Randolph and Quiggin (hereinafter referred to as R-Q model) with more unified sets of equations to define the hysteretic soil behavior interacting with a riser under vertical oscillations using a combination of hyperbolic and exponential functions (Randolph and Quiggin 2009). Shiri and Randolph developed a finite element model and a user-defined element in ABAQUS to conduct series of fatigue studies using the R-Q model (Shiri and Randolph 2010). A series of centrifuge tests was conducted by Elliott et al. and the soil response to complex riser excitations was examined (Elliott et al. 2013). The results of these tests will be used as a key reference in achieving the first and third short-term objectives of this program. A new trenching model was proposed by

Randolph et al. to study SCR fatigue, which was an important step in developing simplified fatigue assessment methods (Randolph et al. 2013). Different time loading histories on SCR fatigue response in a nonlinear seabed were examined by Kimiaei and Liao (Kimiaei and Liao 2015). Authors identified the most influential components of vessel motions on fatigue life. Liu et al. developed a new user-defined subroutine to implement the nonlinear seabed response to SCR fatigue analysis (Liu et al. 2016). Clukey et al. (2017) reported the state of knowledge of riser-soil interaction and its impact on fatigue assessment (Clukey et al. 2017). Authors emphasized on significance of nonlinear riser-soil interaction models and need for further improvement of these models for fatigue analysis of steel catenary risers in the touchdown zone. Dong and Shiri comprehensively investigated the performance of R-Q model (Dong and Shiri 2018, Dong and Shiri 2019). The R-Q model was found to have strong features and potentially an appropriate approach for modelling the nonlinear riser-seabed interaction. However, it was observed that the model needed further improvement to explicitly model the trench formation and resolve some nodal inconsistencies. The advantages of this model in automotive simulation of cyclic soil stiffness degradation and SCR penetration into the seabed have made it a popular model.

In this study, considering the limited access to the model parameters in commercial software, the R-Q model was coded in UEL subroutine and implemented into the global SCR model in ABAQUS to incorporate the effect of nonlinear hysteretic seabed on slug-induced fatigue loads. The emphasis is made on the influence of slug patterns on the response of the riser. Various slug parameters have been explored using the parametric study.

C.3. Numerical model

C.3.1 Global Model

A global SCR model was developed in ABAQUS. Slug loading, nonlinear hysteretic riser-seabed interaction, and the wave/current-induced vessel motions were coded in MPC/DLOAD, UEL, and DISP subroutines respectively. The global SCR configuration was adopted from Dong and Shiri (2018) (see Figure C-1).

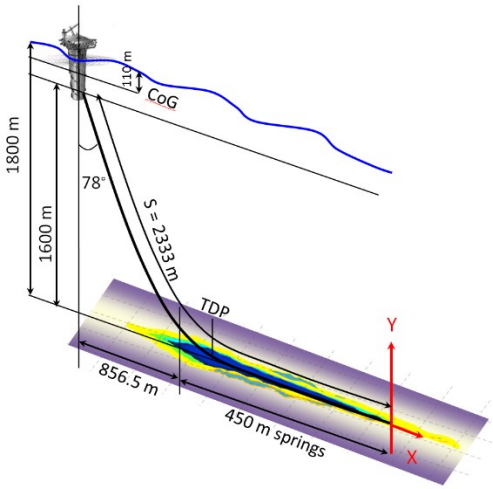

Figure C-1. The global geometry of SCR modelled by ABAQUS (Dong and Shiri).

C.3.2 Modelling of SCR Slugging

The slugging or separation of the flow to a film zone, and a slug liquid zone usually occurs in moderate flow velocities (Kansao et al. 2008). The MPC/DLOAD subroutine coded in FORTRAN is frequently called by the main code to execute the slugging by capturing the frequency, velocity, weight, and length of the slug flow (see Figure C-2).

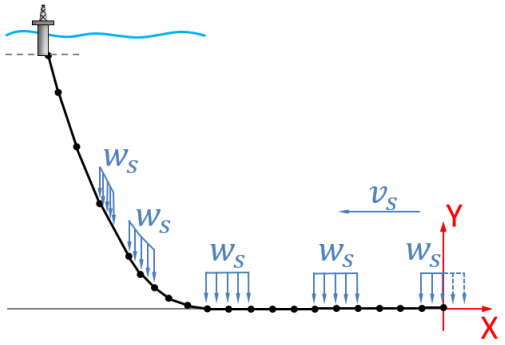

Figure C-2. Slug characteristics capture.

C.3.3 Modelling of non-linear seabed

In this study, the nonlinear riser-seabed interaction is coded in UEL subroutine according to the interaction models proposed by Randolph and Quiggin (Randolph and Quiggin 2009) capture the effect of the nonlinear seabed on slug-induced oscillation and fatigue. The R-Q model was first coded by Shiri and Randolph (2010) in a user-defined element (UEL) to investigate wave-induced fatigue response of SCR. Initial penetration, uplift, break out, and re-penetration have been considered as 4 main episodes in the subroutine (see Figure C-3).

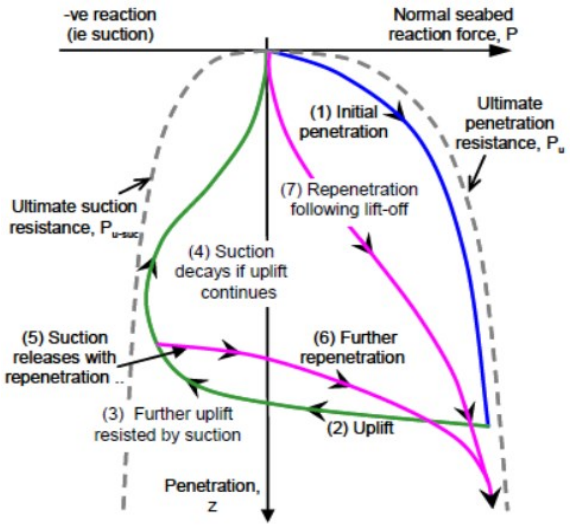

Figure C-3. R-Q soil model for different modes (Randolph and Quiggin 2009).

C.3.4 Modelling of wave-induced vessel motions

A user-defined DISP subroutine was coded in FORTRAN for the SCR vessel-end motion excited by the waves. Information of waves are transferred to the excited motions and the displacement controlled motion will then be executed to the at the vessel end of the SCR. A similar methodology was originally proposed by Shiri and Randolph (2010).

C.4. Model settings

The slug-induced vibrations of SCR in TDZ with different slug patterns were explored using parametric study. The properties of SCR were given in Table C-1. Vibrations induced by slug/wave or wave only on elastic seabed and nonlinear seabed have been examined respectively to show the different vibration modes and influence of seabed properties. Properties for the linear elastic seabed and nonlinear hysteretic seabed could be found in Table C-3 and Table C-2. The influence of slug density, flow velocity, length and slug frequency were explored respectively on the nonlinear hysteretic seabed according to Table C-4. Sea state information given in Table C-5 was embedded in the numerical model using DISP subroutine developed using FORTRAN code. Sea state #30 was selected and repeated for 10 cycles in all case studies as the excitation for vessel end motions. The hydrodynamic coefficients are listed in Table C-6.

Table C-1. Riser pipe properties (Dong and Shiri 2018)

Parameter	Symbol	Value	Unit
Outer diameter	D_o	0.324	M (12¾ ")
Wall thickness	t	0.0205	m
Second moment of area	I	2.26×10^{-4}	m^4
Steel Young's Modulus	E_{steel}	2.07×10^{11}	N/m^2
Steel density	ρ_s	7850	kg/m^3
Fatigue S-N curve	$\bar{a}$	1.05×10^{12}	-
DNV (2008)	m	3.0	-
E Class weld	SCF	1.13	-

Table C-2. Default parameters of R-Q soil models (Dong and Shiri 2018).

Parameter	Symbol	Value	Unit
Mudline shear strength	s_{u0}	0.65	kPa
Shear strength gradient	ρ	1.5	kPa/m
Power law parameter	a	6	-
Power law parameter	b	0.25	-
Normalized maximum stiffness	K_{max}	200	-
Suction ratio	f_{suc}	0.3	-
Suction decay parameter	λ_{suc}	0.5	-
Re-penetration parameter	λ_{rep}	0.5	-

Table C-3. Default elastic seabed parameters (Dong and Shiri 2018).

Elastic seabed	Equivalent vertical strength (kPa)	Equivalent shear strength (kPa)
Default	300	10

Table C-4. Default slug flow parameters (Dong and Shiri 2018).

Parameter	Symbol	Value	Unit
Slug density	ρ_{slug}	600	kg/m^3
Bubble density	ρ_{bubble}	100	kg/m^3
Flow velocity	v_{slug}	10	m/s
Slug length	L_{slug}	30	m
Slug frequency	f_{slug}	180	/hr

Table C-5. Wave scatter diagram for a 30-year operational life (GoM) (Dong and Shiri 2018).

Sea State				
Bin #	H (m)	T (s)	Omni (1 year) p (-)	Omni (30 year) p (-)
1	0.5	4.2	600376	18011291
2	1	4.6	2379015	71370445
3	1.5	5	1614987	48449608
4	2	5.4	839595	25187856
5	2.5	5.8	450978	13529335
6	3	6.1	249122	7473660
7	3.5	6.5	102683	3080495
8	4	6.9	54367	1631014
9	4.5	7.3	19459	583770
10	5	7.7	12124	363725
11	5.5	8	3823	114700
12	6	8.4	1123	33676
13	6.5	8.5	564	16907
14	7	8.7	362	10864
15	7.5	8.9	181	5421
16	8	9.1	113	3389
17	8.5	9.3	100	3011
18	9	9.5	61	1822
19	9.5	9.7	46	1395
20	10	9.9	36	1070
21	10.5	10.1	42	1246
22	11	10.2	19	566
23	11.5	10.4	31	928
24	12	10.6	18	544
25	12.5	10.7	27	813
26	13	10.9	24	712
27	13.5	11	29	877
28	14	11.2	9	262
29	14.5	11.3	11	343
30	15	11.5	14	420

Table C-6. Hydrodynamic coefficients.

Drag (C_D)	Inertia (C_I)	Added mass (C_A)
0.7	1.5	1.0

Table C-7.. Parametric study map 1-slug parameters.

Case study	Input slug model parameter					
	ρ_{slug} (kg/m^3)	ρ_{bubble} (kg/m^3)	v_{slug} (m/s)	L_{slug} (m)	f_{slug} (/hr)	Seabed (E/N)
CS-1	D	D	D	D	D	E
CS-2	D	D	D	D	D	N
CS-3	700	D	D	D	D	E
CS-4	700	D	D	D	D	N
CS-5	D	150	D	D	D	E
CS-6	D	150	D	D	D	N
CS-7	D	D	25	D	D	E
CS-8	D	D	25	D	D	N
CS-9	D	D	D	50	D	E
CS-10	D	D	D	50	D	N
CS-11	D	D	D	D	100	E
CS-12	D	D	D	D	100	N
Note	D refers to "Default" values for slug model as described in Table C-4. From CS-1 to CS-12, soil parameters in Table C-2 were adopted for nonlinear seabed models and soil parameters in Table C-3 were adopted for elastic seabed models.					

C.5. Results

Stress variations ranges from CS-2 to CS-7 are plotted in Figure C-4. During load cycles, the variation range of the von Mises stress is the main parameter for the calculation of SCR fatigue life. The slug characteristics show a significant impact on von Mises stress distribution, particularly the slug density (highest value is obtained in CS-3 with heaviest slug density). Also, the slug characteristics affect the location of the peak von Mises stress ranges. The peak point in CS-4 occurred on the right hand of the peak point in CS-2, while in CS-5 the peak point is obtained on the left hand of the peak point in CS-2.

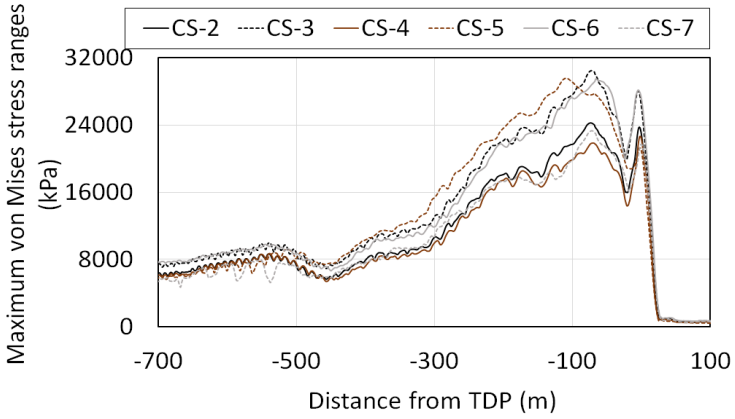

Figure C-4. Influence of slug parameters on the von Mises stress.

Compared Figure C-5 and Figure C-6, the difference in penetration depths of wave/slug combined-induced vibration and of slug induced vibration could hardly be identified. However, in Figure C-7 and Figure C-8, the difference in penetration depth can be clearly observed due to the accumulation ability of non-linear seabed. Wave-induced vibration has contributes to the deeper penetration of SCR into the non-linear seabed especially at the region around TDP.

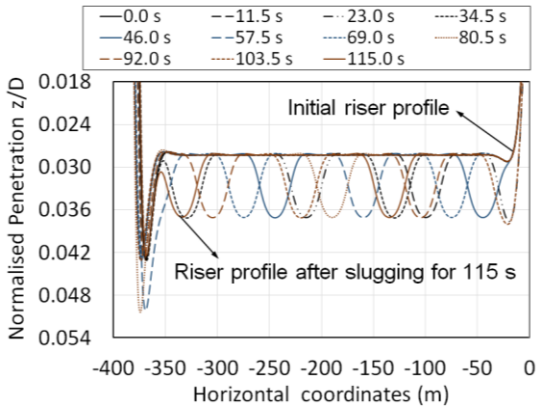

Figure C-5. CS-1-wave/slug combined.

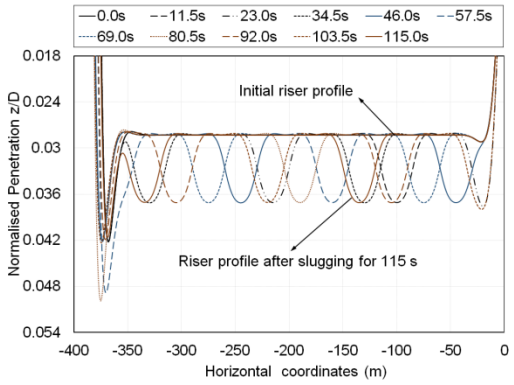

Figure C-6. CS-1-slug induced.

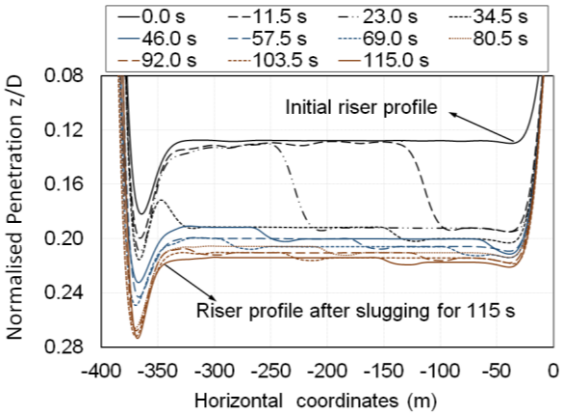

Figure C-7. CS-2-wave/slug combined.

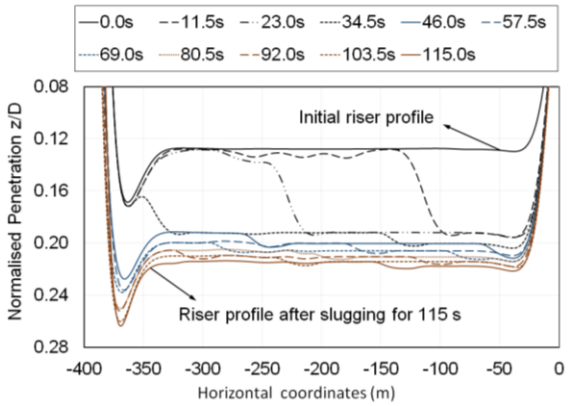

Figure C-8. CS-2-slug induced.

As shown in Figure C-9, Figure C-10, and Figure C-11, the location of the peak value of maximum shear force during the fatigue loads cycles are determined mainly by the slug induced vibrations. In the wave induced vibration, the peak value showed on the right side of the TDP (see point P_b in Figure C-9). While the peak in slug induced vibration is located on the left side of the TDP (see P_a in Figure C-10).

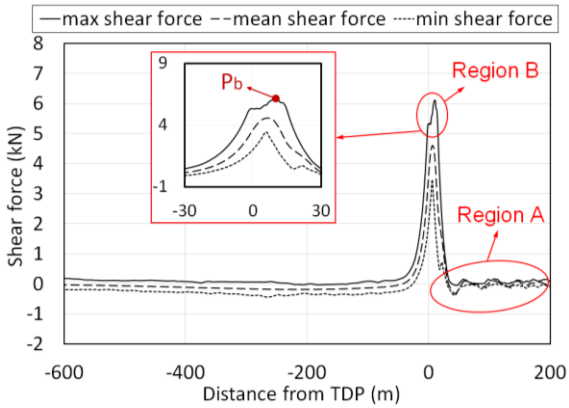

Figure C-9. CS-2-wave induced.

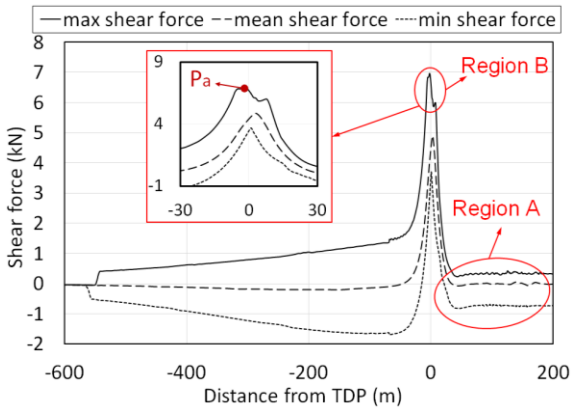

Figure C-10. CS-2-slug induced.

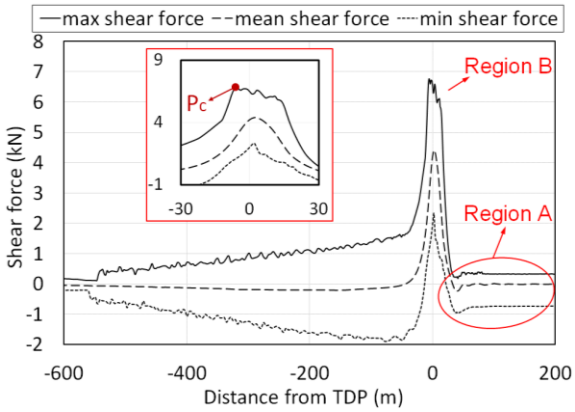

Figure C-11. CS-2-wave/slug combined.

As shown from Figure C-12 to Figure C-16, riser profiles were recorded in case studies with different slug parameters. When slug density was increased, the normalised penetration at bottom point increased from 0.274 (CS-2, see Figure C-11) to 0.296 (CS-3, see Figure C-12) at 115 s. By increasing the density of gas, slight deeper penetration could be found (CS-4, see Figure C-13) while the initial normalised penetration in the middle region (horizontal coordinates between -300 m and -100 m) can be clearly observed to increase from 0.128 (CS-2, see Figure C-11) to 0.134 (CS-4, see Figure C-13). When the

velocity of slug was increased from 10 m/s (CS-2, see Figure C-11) to 20 m/s (CS-5, see Figure C-14), longer portion at the right section of riser has deep penetration and the normalised penetration at bottom point increased from 0.231 (CS-2, see Figure C-11) to 0.249 (CS-5, see Figure C-14) at 46.0 s. But this increase may be caused by the time picked up for plotting.

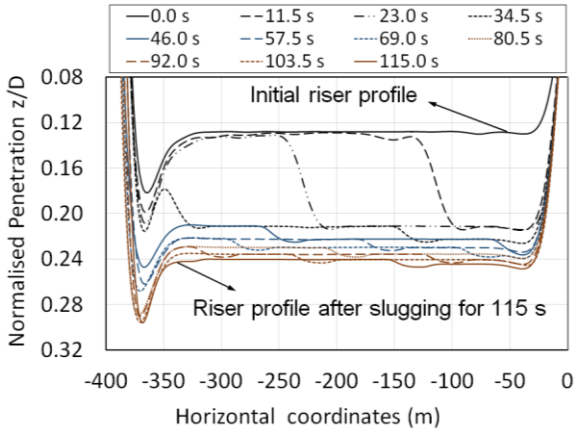

Figure C-12. CS-3.

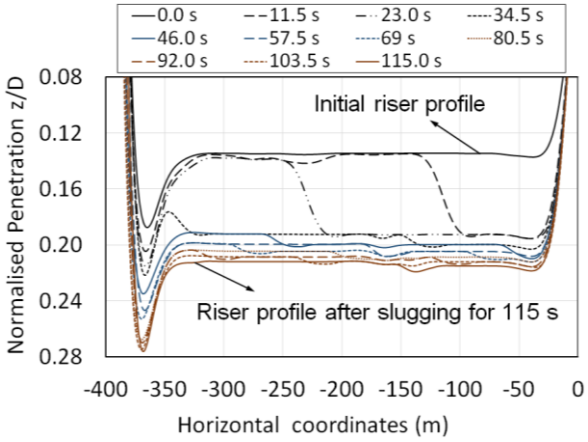

Figure C-13. CS-4.

In CS-6, slug was set with longer length and this could be observed in Figure C-15 and noting that the largest normalised penetration in CS-6 (Figure C-15) increased comparing with CS-2 (Figure C-11). Compared riser profiles in Figure C-11 and Figure C-16, higher frequency of slug flow will effect the vibration modes of the SCR in TDZ but rarely affect the penetration depth of SCR into the seabed. Within same period, longer oscillation distance is obtained when the slug frequency is higher, that is, more slugs travelled through the SCR due to the shorter interval between generation of slugs.

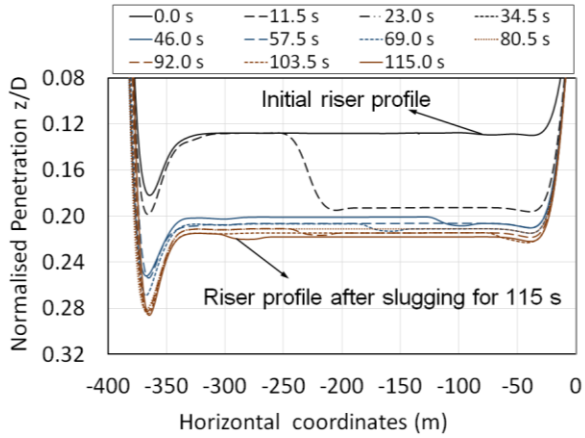

Figure C-14. CS-5.

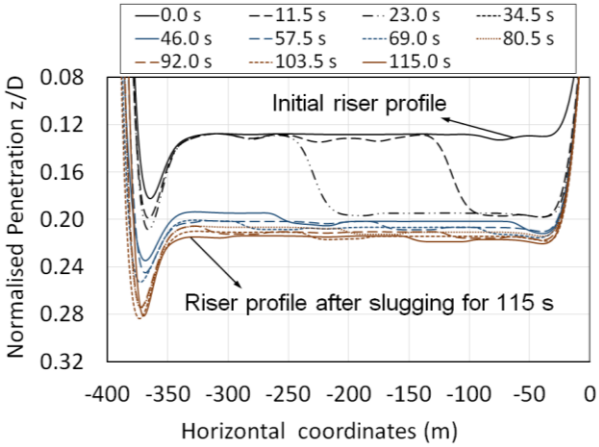

Figure C-15. CS-6.

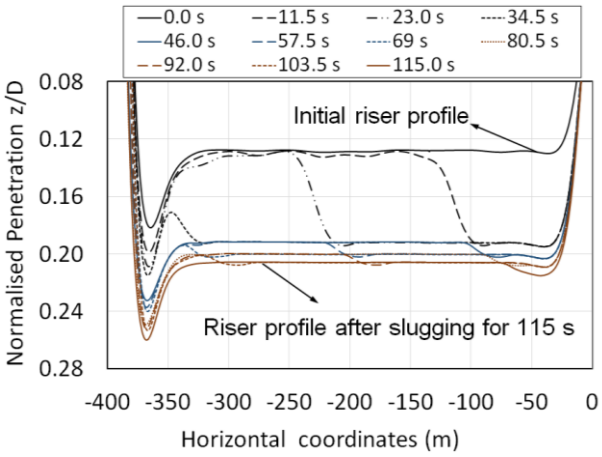

Figure C-16. CS-7.

C.6. Summary and Conclusion

A parametric study was performed using the developed numerical model in Abaqus. Various slug parameters (slug density, length, velocity and frequency) have been fully examined for the SCR laid on non-linear hysteretic seabed with vessel end excited by wave. The key conclusions can ba highlighted as follows:

- The study showed that the fluctuations of SCRs induced by slugging together with non-linear seabed soil degradation might have a significant influence on stress variation distribution along SCRs and decrease the fatigue life.
- Slug-induced oscillation significantly contributes to riser penetration into the seabed when it is coupled with wave-induced oscillation. This shall be further investigated for incorporation in any trench profile model.
- The slug density and length were found to have a significant impact on oscillations.
- It was observed that the slug frequency and velocity affect the oscillation modes particularly when they are combined with wave-frequency vessel motions. This

may be caused by the capability of nonlinear seabed to consider the accumulation of penetration.

- The seabed soil properties showed a significant influence on slug-induced oscillations.
- The study revealed several important trends of SCR response to slug-induced oscillations in the non-linear hysteretic seabed and consequently on accumulated fatigue damage in the TDZ.

C.7. Acknowledgement

The authors gratefully acknowledge the financial support of this research by the Research and Development Corporation (RDC) (now Innovate NL) through the Ignite funding program and Memorial University of Newfoundland through VP start-up funding support.

References

Aubeny, C.P., Biscontin, G. 2009. Seafloor–riser interaction model, Int J Geomechanics, 9: 133-141.

Bordalo, S.N., Morooka, C.K., Cavalcante, C.C.P. 2008. Whipping phenomenon caused by the internal flow momentum on the catenary risers of offshore petroleum fields, in: Proceedings of the ASME 27th International Conference on Offshore Mechanics and Arctic Engineering, Estoril, Portugal, OMAE 2008-57351.

Bordalo, S.N., Morooka, C.K. 2018. Slug flow induced oscillations on subsea petroleum pipelines, Journal of petroleum science and engineering (In press, accepted manuscript).

Bridge, C., Laver, K., Clukey, E., Evans, T. 2004. Steel catenary riser touchdown point vertical interaction models, in: Offshore Technology Conference, OTC16628, Houston, Texas.

Bridge, C., Howells, H. 2007. Observations and modeling of steel catenary riser trenches, in: 17th International Offshore and Polar Engineering Conference, ISOPE2007, Lisbon, Portugal.

Campbell, M. 1999. The complexities of fatigue analysis for deepwater risers, in: Proceedings of the 2nd International Deepwater Pipeline Technology Conference.

Chatjigeorgiou, I.K. 2010a. Three dimensional nonlinear dynamics of submerged, extensible catenary pipes conveying fluid and subjected to end-imposed excitations, International Journal of Non-linear Mechanics, 45: 667-680.

Chatjigeorgiou, I.K. 2010b. On the effect of internal flow on vibrating catenary risers in three dimensions, Engineering structures, 32: 3313-3329.

Chatjigeorgiou, I.K. 2017. Hydroelastic response of marine risers subjected to internal slug-flow, Applied Ocean Research, 62: 1-17.

Clukey, E.C., Aubeny, C.P., Zakeri, A., Randolph, M.F., Sharma, P.P., White, D.J., Sancio, R., Cerkovnik, M. 2017. A Perspective on the state of knowledge regarding soil-pipe interaction for SCR fatigue assessments, in: Offshore Technology Conference, Houston, Texas, OTC27564-MS.

Dong, X., Shiri, H. 2018. Performance of non-linear seabed interaction models for steel catenary risers, part I: Nodal response, Journal of Ocean Engineering, 154: 153-166.

Dong, X., Shiri, H. 2019. Performance of non-linear seabed interaction models for steel catenary Risers, part II: Global response, Applied Ocean Research,82: 158-174.

Elliott, B.J., Zakeri, A., Barrett, J., Hawlader, B., Li, G., Clukey, E.C. 2013. Centrifuge modeling of steel catenary risers at touchdown zone Part II: Assessment of centrifuge test results using kaolin clay, Ocean Engineering, 60: 208-218.

Gundersen, P., Doynov, K., Andersen, T., Haakonsen, R. 2012. Methodology for determining remnant fatigue life of flexible risers subjected to slugging and irregular waves, in: Proceedings of the ASME 2012 31st Int Conf on Ocean, Offshore and Arctic Engineering, OMAE 2012, July 1-6, Rio de Janeiro, Brazil.

Hardin, B.O., Drnevich, V.P. 1972. Shear modulus and damping in soils: Measurement and parameter effects (Terzaghi Lecture). Journal of the Soil Mechanics and Foundations Division; 98 (6): 603-624.

Jiao, Y. 2007. Non-linear load-deflection models for Seafloor Interaction with Steel Catenary Risers. Texas A&M University, College Station, USA. Master of Science, 2007.

Kansao, R., Casanova, E., Blanco, A., Kenyery, F., Rivero, M. 2008. Fatigure life prediction due to slug flow in extra-long submarine gas pipelines, in: Proceedings of the ASME 2008 27th Int Conf on Offshore Mechanics and Arctic Engr, OMAE2008, Estoril, Portugal, 3: 685-692.

Kimiaei, M., Liao, J. 2015. Effects of different loading time histories on fatigue design of steel catenary risers using nonlinear riser-soil interaction models, in: Frontiers in Offshore Geotechnics III, Norway, Trondheim.

Kondner, R.L. 1963. Hyperbolic stress-strain response; cohesive soils. Journal of the Soil Mechanics and Foundations Division; 89 (1): 115-143.

Liu, J., Kimiaei, M., Randolph, M. 2016. A new user defined element for nonlinear riser-soil interaction analysis of steel catenary riser systems. In: ASME 2016 35th International Conference on Ocean, Offshore and Arctic Engineering, OMAE 2016.

Nakhaee, A., Zhang, J. 2008. Effects of the interaction with the seafloor on the fatigue life of a SCR, in: Int Offshore and Polar Engr Conf, Vancouver, BC, Canada.

Nakhaee, A., Zhang, J. 2010. Trenching effects on dynamic behavior of a steel catenary riser, Ocean Engineering, 37(2–3):277–288.

Ortega, A., Rivera, A., Nydal, O.J., Larsen, C.M. 2012. On the dynamic response of flexible risers caused by internal slug flow, in: Proceedings of the ASME 2012 31st Int Conf on Ocean, Offshore and Arctic Engineering, OMAE2012, Rio de Janeiro, Brazil, 5: 647-656.

Ortega, A., Rivera, A., Larsen, C.M. 2013. Flexible riser response induced by combined slug flow and wave loads, in: Proceedings of the ASME 2013 32nd International Conference on Ocean, Offshore and Arctic Engineering, OMAE2013, Jun 9-14, Nantes, France.

Phifer, E.H., Kopp, F., Swanson, R.C., Allen, D.W., Langner, C.G. 1994. Design and installation of Auger steel catenary risers, in: Offshore Technology Conference, OTC7620, Houston, Texas.

Pollio, A., Mossa, M. 2009. A comparison between two simple models of a slug flow in a long flexible marine riser, Thesis.

Randolph, M.F., Quiggin, P. 2009. Non-linear hysteretic seabed model for catenary pipeline contact, in: 28th International Conference on Ocean, Offshore and Arctic Engineering, OMAE 2009, Honolulu, Hawaii, USA.

Randolph, M., Baht, S., Jain, S., Mekha, B. 2013. Modeling the touchdown zone trench and its impact on SCR fatigue life, in: Offshore Technology Conference, Houston, OTC23975.

Shiri, H. 2014. Influence of seabed trench formation on fatigue performance of steel catenary risers in touchdown zone, Journal of Marine Structures, 36: 1-20.

Shiri, H., Randolph, M.F. 2010. Influence of seabed response on fatigue performance of steel catenary risers in touch down area, in: 29th International Conference on Ocean, Offshore and Arctic Engineering, Shanghai, China, 5: 63-72.

Theti, R., Moros, T. 2001. Soil interaction effects on simple-catenary riser response, Pipes and Pipelines Int.; 46 (3): 15-24.